ETHANOL UTILIZATION FOR GENERATION OF ELECTRICITY IN SOLID OXIDE FUEL CELLS

UNIVERSITY OF THESSALIA
DEPARTMENT OF MECHANICAL AND
INDUSTRIAL ENGINEERING

ETHANOL UTILIZATION FOR GENERATION OF ELECTRICITY IN SOLID OXIDE FUEL CELLS

Ph.D. Thesis
by
Savvas L. Douvartzides

Volos - Greece 2004

ΧΡΗΣΗ ΑΙΘΑΝΟΛΗΣ

ΓΙΑ

ΠΑΡΑΓΩΓΗ ΗΛΕΚΤΡΙΚΗΣ ΙΣΧΥΟΣ

ΣΕ

ΗΛΕΚΤΡΟΧΗΜΙΚΑ ΣΤΟΙΧΕΙΑ ΚΑΥΣΙΜΟΥ

ΔΙΑΤΡΙΒΗ ΥΠΟΒΛΗΘΕΙΣΑ ΓΙΑ ΤΗΝ ΑΠΟΚΤΗΣΗ ΔΙΔΑΚΤΟΡΙΚΟΥ ΤΙΤΛΟΥ
ΑΠΟ ΤΟ ΤΜΗΜΑ ΜΗΧΑΝΟΛΟΓΩΝ ΜΗΧΑΝΙΚΩΝ ΒΙΟΜΗΧΑΝΙΑΣ
ΤΟΥ ΠΑΝΕΠΙΣΤΗΜΙΟΥ ΘΕΣΣΑΛΙΑΣ

υπό τον
ΔΟΥΒΑΡΤΖΙΔΗ ΣΑΒΒΑ
του ΛΑΖΑΡΟΥ

ΠΑΝΕΠΙΣΤΗΜΙΟ ΘΕΣΣΑΛΙΑΣ
ΤΜΗΜΑ ΜΗΧΑΝΟΛΟΓΩΝ ΜΗΧΑΝΙΚΩΝ ΒΙΟΜΗΧΑΝΙΑΣ

ΕΡΓΑΣΤΗΡΙΟ ΕΝΑΛΛΑΚΤΙΚΩΝ ΣΥΣΤΗΜΑΤΩΝ
ΜΕΤΑΤΡΟΠΗΣ ΕΝΕΡΓΕΙΑΣ

ΒΟΛΟΣ, 2004

ANNOTATION

Dissertation for the degree of Doctor of Philosophy (Ph.D.) in Mechanical and Industrial Engineering
presented at the University of Thessaly (Volos-Greece) in 2004.
This doctoral work was done in the Laboratory of Alternative Energy Conversion Systems
of the University of Thessalia from 1999 to 2004 under the scientific advice and
supervision of Dr. P. E. Tsiakaras.

U.TH.-DMIE.

EVALUATION COMMITTEE-ΕΞΕΤΑΣΤΙΚΗ ΕΠΙΤΡΟΠΗ

Bontozoglou Vasilios
Associate Professor
Department of Mechanical and Industrial Engineering
University of Thessalia – Volos, Greece

Lois Euripides
Professor
Department of Chemical Engineering
National Technical University of Athens – Greece

Papayianakos Nikolaos
Professor
Department of Chemical Engineering
National Technical University of Athens – Greece

Stoukides Michael
Professor
Department of Chemical Engineering
Aristotle University of Thessaloniki – Greece

Tsiakaras Panagiotis
Assistant Professor
Department of Mechanical and Industrial Engineering
University of Thessalia – Volos, Greece.

Vayenas Constantinos
Professor
Department of Chemical Engineering
University of Patras – Greece

Verykios Xenophon
Professor
Department of Chemical Engineering
University of Patras – Greece

ACKNOWLEDGEMENTS-ΕΥΧΑΡΙΣΤΙΕΣ

Supervisor-Επιβλέπων

Τσιακάρας Παναγιώτης

Evaluation Committee-Εξεταστική επιτροπή

Βαγενάς Κωνσταντίνος
Βερύκιος Ξενοφών
Λόης Ευριπίδης
Μποντόζογλου Βασίλειος
Παπαγιαννάκος Νικόλαος
Στουκίδης Μιχαήλ
Τσιακάρας Παναγιώτης

Scientific Advisors - Επιστημονικοί συνεργάτες

Αθανασίου Κωνσταντίνος
Demin Anatoly
Κουτελιέρης Φραγκίσκος
Kyrillov Svlatoslav
Τζωρτζακάκης Νικόλαος

Institutes and Laboratories - Ινστιτούτα και Εργαστήρια

Institute of High Temperature Electrochemistry, Ekaterinburg- The Ukrane.
Organization for Ionics, Kiel-Germany
Instituto Superior Technico, Lisbon-Portugal
Εργαστήριο Υλικών του ΤΜΜΒ του Π.Θ.
Εργαστήριο Ρευστομηχανικής του ΤΜΜΒ του Π.Θ.
Γραμματεία του ΤΜΜΒ του Π.Θ.
Εκδόσεις TZIOLA, Θεσσαλονίκη (www.tziola.gr)

Personal Thanks -Προσωπικές ευχαριστίες

Στην οικογένειά μου.

CONTENTS

CHAPTER 3:
"PHYSIOLOGY" OF FUEL CELLS:
THERMODYNAMICS AND KINETICS

CHAPTER 4:
FUELS OPTIONS FOR SOFC SYSTEMS:
FIRST LAW ANALYSIS

CHAPTER 5:
ON THE SYSTEMATIC OPTIMIZATION OF SOFC SYSTEMS IN TERMS OF ENERGY AND EXERGY

CHAPTER 6:
CATALYTIC AND ELECTROCATALYTIC OXIDATION OF ETHANOL OVER $La_{0.6}Sr_{0.4}Fe_{0.2}Co_{0.8}O_3$ PEROVSKITE-TYPE CATALYST

CHAPTER 7:
ELECTROCHEMICALLY PROMOTED CATALYSIS :
THE CASE OF ETHANOL OXIDATION OVER PLATINUM

CHAPTER 8
PRELIMIBARY STUDY OF A SOLID OXIDE FUEL CELL
FUELED BY EXTERNAL ETHANOL DECOMPOSITION

APPENDIX $\mathcal{A}$
EXTERNAL REFORMER - SOFC STACK
A THERMODYNAMIC ANALYSIS PROGRAM

APPENDIX $\mathcal{B}$
SIMULATION PROGRAM OF A SOFC POWER PLANT

LIST OF FIGURES

LIST OF TABLES

SYNOPSIS

This doctoral thesis presents new results and information on the utilization of ethanol as a fuel of solid electrolyte electrochemical cells. By recognizing the importance of ethanol as one of the most representative alternative fuels, the basic interest of this work is the examination of ethanol utilization for useful purposes (production of useful chemicals, generation of electrical power etc.) in both electrolytic and galvanic processes in the field of solid state electrochemistry. To meet this challenge, this work was undertaken paying attention in innovative research activities such as the electrochemical promotion of catalysts and the development of the technology of fuel cells.

In a theoretical basis, the thesis in hand emphasizes on the thermodynamic analysis of electricity generation in solid oxide fuel cells (SOFCs). A first approach, assumes various preliminary catalytic processes of ethanol decomposition (steam reforming, dry reforming or partial oxidation) and the subsequent utilization of the decomposition products in a dimensionless reversible SOFC stack. By selecting ethanol steam reforming as the most appropriate preliminary method for SOFC operation, the analysis proceeds in a comparative study with other fuel options (natural gas, gasoline and methanol) to clarify the expectations from the "ethanol scenario". In a second approach, the analysis assumes an integrated power plant comprised by the SOFC and auxiliary equipment (heat exchangers, mixers, burners etc.) and the term "exergy" is introduced to justify design guidelines and optimization methods according to the second law of thermodynamics. As a result, a design strategy is proposed taking into consideration the most important operation parameters, the fuel choice and the plant topology.

Experimentally, the present thesis contributes three independent works on the utilization of ethanol in solid oxygen-conducting yttria stabilized zirconia (YSZ) electrochemical reactors. In the first of these works, the perovskite type catalyst $La_{0.6}Sr_{0.4}Co_{0.8}Fe_{0.2}O_3$ is selected as a working electrode of an YSZ electrolytic cell fed by ethanol. In this work, the preparation and characterization of the catalyst is described and its activity for direct ethanol oxidation is examined. During closed circuit experiments, the mechanism of the reaction revealed purely electrocatalytic response in contrast to the second experimental work of this thesis were the electrochemical promotion of platinum (Pt) catalysts is examined in a similar YSZ reactor. In this work, it is proved that the catalytic rate of ethanol oxidation may be significantly promoted through electrochemical pumping of O^{2-} anions to the working Pt electrode. By application of currents equal to 20 – 80 μA, it is observed that the activation energy of ethanol oxidation may lower up to 70% with respect to the open circuit catalytic value. This phenomenon is described according to the theory of "Non-Faradaic electrochemical modification of catalytic activity" (NEMCA) and is found of significance for the enhancement of the selectivity of the reaction for the production of acetaldehyde. Finally, the last experimental work of this thesis reports preliminary results of ethanol utilization in a tubular SOFC prototype with a Pt anode electrode. In this work, the SOFC is fueled by a H_2+CO+CH_4 gaseous mixture taken by external ethanol reforming and two regimes of operation are recognized depending on temperature. In the first low temperature (660°C) regime, complete oxidation of the gaseous mixture is observed implying the ability for effective power generation. In higher temperatures (800°C), however, the reaction mechanism is found most appropriate for the production of synthesis gas (H_2 + CO).

ΠΡΟΛΟΓΟΣ

Η παρούσα διδακτορική διατριβή παρουσιάζει πρωτότυπα αποτελέσματα και νέες πληροφορίες σχετικά με την εκμετάλλευση της αιθανόλης ως καύσιμο ηλεκτροχημικών στοιχείων στερεού ηλεκτρολύτη. Αναγνωρίζοντας την αιθανόλη ως ένα από τα πλέον αντιπροσωπευτικά εναλλακτικά ή ανανεώσιμα καύσιμα, το βασικό ενδιαφέρον αυτής της διατριβής εστιάζεται στη μελέτη της ως πρώτη ύλη για την επίτευξη ωφέλιμων αποτελεσμάτων (παραγωγή χρήσιμων χημικών προϊόντων, ηλεκτρικής ισχύος κλπ.) μέσω διεργασιών ηλεκτρολυτικής ή γαλβανικής φύσεως στο πεδίο της ηλεκτροχημείας στερεάς καταστάσεως. Για την επίτευξη αυτών των προκλήσεων, η θεματολογία της διατριβής πηγάζει αμέσως από καινοτόμους τομείς της σύγχρονης έρευνας όπως αυτοί της ηλεκτροχημικής προώθησης της ενεργότητας των καταλυτών και της ανάπτυξης της ελπιδοφόρας τεχνολογίας των ηλεκτροχημικών στοιχείων καυσίμου (fuel cells).

Σε θεωρητικό επίπεδο, η κύρια συνιστώσα της παρούσας διατριβής πραγματεύεται τη θερμοδυναμική ανάλυση των διεργασιών παραγωγής ηλεκτρικής ισχύος σε ηλεκτροχημικά στοιχεία ηλεκτρολύτη στερεών οξειδίων (τύπου SOFC). Σε πρώτη προσέγγιση, μελετώνται διαφορετικές καταλυτικές διεργασίες προκαταρκτικής διάσπασης της αιθανόλης (μέσω αναμόρφωσης με υδρατμό ή με διοξείδιο του άνθρακα και μέσω μερικής οξείδωσης) σε συνδυασμό με τη συνακόλουθη τροφοδοσία των μιγμάτων της διασπάσεως σε αδιαστατοποιημένη συστοιχεία στοιχείων SOFC. Στη συνέχεια, επιλέγοντας τη διεργασία της αναμόρφωσης με υδρατμό ως καταλληλότερη για την προκαταρκτική καταλυτική επεξεργασία της αιθανόλης, η ανάλυση προχωρεί στη σύγκριση διαφορετικών σεναρίων επιλογής καυσίμου (φυσικό αέριο, βενζίνη και μεθανόλη) και αποσαφηνίζει τις προσδοκίες για κάθε ένα από αυτά. Σε δεύτερη προσέγγιση, θεωρείται μια ολοκληρωμένη μονάδα παραγωγής ισχύος που απαρτίζεται από το SOFC και τον απαραίτητο βοηθητικό εξοπλισμό (εναλλάκτες θερμότητας, θάλαμοι ανάμιξης, καυστήρες κλπ.) και εισάγεται ο όρος "εξέργεια'' προκειμένου να δικαιολογηθούν σχεδιαστικές κατευθυντήριες υπό την αξιωματική ισχύ του δευτέρου νόμου της θερμοδυναμικής. Αποτέλεσμα αυτής της προσέγγισης είναι η ανάπτυξη στρατηγικών σχεδιασμού και μεθόδων βελτιστοποίησης τόσο των συνθηκών λειτουργίας της μονάδας όσο και ανεξάρτητων επιλογών όπως το είδος του καυσίμου και η τοπολογία της συνολικής διάταξης.

Σε πειραματικό επίπεδο, η διατριβή συνεισφέρει τρεις ανεξάρτητες μελέτες περί της χρήσεως της αιθανόλης σε ηλεκτροχημικούς αντιδραστήρες στερεού ηλεκτρολύτη από ζιρκόνια σταθεροποιημένη με ύττρια (YSZ). Στην πρώτη από αυτές τις μελέτες, επιλέγεται ο περοβσκίτης $La_{0.6}Sr_{0.4}Co_{0.8}Fe_{0.2}O_3$ ως ανοδικός καταλύτης ενός ηλεκτρολυτικού στοιχείου από YSZ που τροφοδοτείται με αιθανόλη. Περιγράφεται η παρασκευή και ο χαρακτηρισμός του υλικού και εξετάζεται η καταλυτική και ηλεκτροκαταλυτική του ενεργότητα κατά την αντίδραση άμεσης οξείδωσης της αιθανόλης. Κατά τη λειτουργία κλειστού κυκλώματος του δεδομένου συστήματος, ο μηχανισμός της αντίδρασης παρουσίασε καθαρά ηλεκτροκαταλυτική απόκριση σε αντίθεση με τη δεύτερη πειραματική μελέτη της διατριβής στην οποία εξετάζεται η ηλεκτροχημική προώθηση του λευκόχρυσου (Pt) σε παρόμοιες συνθήκες. Σε αυτή τη μελέτη, αποδεικνύεται ότι ο καταλυτικός ρυθμός της οξείδωσης της αιθανόλης είναι δυνατό να ενισχυθεί σημαντικά μέσω της ηλεκτροχημικής άντλησης ιόντων O^{2-} από τον ηλεκτρολύτη προς το ηλεκτρόδιο του λευκόχρυσου. Με εφαρμογή ρευμάτων εντάσεως από 20 έως 80 μA, η ενέργεια ενεργοποίησης της οξείδωσης της αιθανόλης παρουσιάζει δραματική μείωση σε ποσοστό έως και 70%. Το συνολικό φαινόμενο αναλύεται σύμφωνα με τη γενικότερη θεωρία του NEMCA (Μη-Φαραντάϊκή ηλεκτροχημική τροποποίηση της καταλυτικής ενεργότητας) και περιγράφεται ως ευνοϊκό για την αύξηση της εκλεκτικότητας της αντίδρασης οξείδωσης της αιθανόλης προς παραγωγή ακεταλδεύδης. Τέλος, η τρίτη πειραματική μελέτη της διατριβής παρουσιάζει προκαταρκτικά αποτελέσματα χρήσης αιθανόλης σε πρωτότυπο κυλινδρικό στοιχείο SOFC με ηλεκτρόδιο ανόδου από λευκόχρυσο (Pt). Η τροφοδοσία του στοιχείου γίνεται με μίγμα αερίων H_2+CO+CH_4 προερχόμενο από την εξωτερική αναμόρφωση της αιθανόλης με υδρατμό και τα πειραματικά αποτελέσματα καταδεικνύουν δύο διαφορετικά καθεστώτα μηχανισμού ανοδικών αντιδράσεων ανάλογα με τη θερμοκρασία. Σε σχετικά χαμηλή θερμοκρασία (660°C) παρατηρείται η πλήρης οξείδωση του μίγματος τροφοδοσίας υποδηλώνοντας την καταλληλότητα των συνθηκών για παραγωγή ηλεκτρικής ισχύος. Παρόλα αυτά, σε υψηλότερη θερμοκρασία (800°C), ο μηχανισμός της αντίδρασης μεταβάλλεται ευνοώντας τη διάσπαση του CH_4 προς αέριο σύνθεσης (H_2 + CO).

Think globally, act locally.

CHAPTER 1

INTRODUCTION - SCOPE

1.1. THE INCENTIVES

Advances in solid state electrochemistry are in evolution *ad infinitum*. Modern ideas are continuously expressed and new applications come into practice. Particularly in the present times, electrochemistry has found significance as a novel and powerful science capable of opening new horizons in engineering. Fuel cell technology and electrochemical promotion techniques are indicative of how engineering will proceed in the future.

Traditional engineering found itself unable to predict its impact on society. This happened mainly because old-fashioned energy strategy refused to compromise with social concerns. Maximization in profit, goods supply and energy consumption brought up the post-industrial era to suffer from the "crisis-management syndrome". Environmental pollution, depletion of mineral sources and energy blackmail are the energy related pieces of this crisis puzzle.

In a global level, the demamd for diversification on energy sources and clean technology development has been officially postulated (*i.e.* Kyoto protocol). Such postulations imply the need for future engineering to reconstruct the energy strategy context imposing upper limits in the emmisions and lower limits in the efficiency of every energy process. In future years, electricity will continue to be the most rapidly growing form of energy consumption. Forecasts show total worldwide electricity consumption rising from 12 trillion kilowatt-hours in 1996 to almost 22 trillion kilowatt-hours in 2020. The strongest growth is expected in developing Asia at an average annual rate of nearly 5%, followed by Central and South America at an average annual rate of over 4%. And by 2020, developing nations are expected to account for 43% of the world's total energy consumption, compared with only 28% in 1996.

In meeting worldwide power needs, fuel cells are applicable to both central powerplant generation and distributed generation scenarios. Their greatest potential, at least in the near term, lies in distributed generation. The first commercial fuel cell on the market, the phosphoric acid fuel cell (PAFC), proved that early entry markets exist to sustain their relatively high initial costs of $3000-4000/kW. These niche markets include premium power applications, such as use in hospitals and computer centers, and opportunity fuel applications where gas from waste materials can be generated in quantity. Regions exceeding ambient air quality standards for pollutants (non-attainment areas) also represent prime market areas. The premium power market in the United States alone is conservatively estimated at $1 billion per year. The U.S. Environmental Protection Agency estimates that the current global market for opportunity fuels is 40-50 gigawatts. Ultimately, for fuel cells to realize their full potential, costs must be competitive with other distributed generation technologies such as gas turbines and reciprocating engines. The incentive to bring costs down is reflected in the size of the global market. The U.S. and European growth and replacement market for distributed generation is expected to approach 10 gigawatts per year for the next decade. Globally, it is expected to be 20 gigawatts per year.

Solid oxide fuel cell technology is currently in the stage of making prototypes. Intensive efforts were devoted on the discovery of appropriate fabrication and operation methods and various fuels have been proposed so as to exploit their unique advantage of their tolerance

in fuel impurities and the feasibility of internal reforming. Accordingly, SOFCs are expanding the list of fuel options offering unique prospects for combined energy policies. On this basis, for example, biomass derived gases are acceptable fuel options for highly efficient SOFC-based electricity scenarios. ***Utilization of domestically produced bio-ethanol in SOFC-oriented electricity industries has been the tacit vision of this thesis, inspired by requirements for upgraded agricultural labour, clean environment and efficient technological innovation.***

1.2. THE STRUCTURE OF THIS THESIS

SOFC technology is new. Furthermore, its combination with the ethanol scenario results in an innovative energy policy. Adopting this starting point, the present doctoral thesis undertook the multiple task;

- to recognize the present relevant research status,
- to examine the theoretical expectations from ethanol utilization in SOFCs,
- to compare the ethanol fed SOFC scenario with those of other fuel options,
- to optimize integrated SOFC systems according to the first and second law of thermodynamics,
- to proceed in the experimental investigation of various catalytic systems for ethanol fed SOFCs,
- to recognize usefull phenomena of industrial or scientific interest as these were observed during its completion, and most importantly
- to manufacture, operate and analyze an ethanol fed SOFC prototype.

Chapters 2 and 3 entitled as "Anatomy of Fuel Cells" and "Physiology of Fuel Cells" respectively, borrowed the terms of medical science in order to attempt a medicine-type recognition firstly of the elementary parts of fuel cells and secondly of the parameters of their operation. Both these chapters have been written as a literature review of the entire fuel cell technology paying specific attention in the technology of SOFCs.

In the following chapters 4 and 5, the theoretical work of this thesis is summarized. Chapter 4 provides the thermodynamic analysis of external steam reformer – SOFC systems fueled by various fuel options (natural gas, methanol, ethanol and gasoline). In this chapter the reader will be informed on the technical prospects from ethanol fed SOFCs. In the fifth chapter, the energy and exergy analysis of a proposed SOFC system will be applied to show the influence of important operational parameters in the first and second law efficiencies of such systems.

Chapters 6 and 7 present experimental studies of ethanol oxidation over two different catalytic systems. In chapter 6, the perovskite-type oxide $LaSrCoFeO_3$ has been studied as an anode catalyst of a CSTR yttria-stabilized-zirconia electrochemical reactor. The behavior of the catalyst during ethanol oxidation has been examined together with electrocatalytic actions. In chapter 7, the electrochemical promotion of platinum catalysts has been studied according to the NEMCA (Non-Faradaic Electrochemical Modification of Catalytic Activity) theory. Finally, chapter 8 presents the preliminary experimental study of ethanol utilization in a SOFC prototype designed and manufactured in the course of this thesis.

"A shock was given which could be felt by five persons joining hands, and which when taken by a single person was painful"
Sir William Grove, Philos. Mag. Ser., **3**, 1839: p. 14

CHAPTER 2

"ANATOMY" OF FUEL CELLS

ABSTRACT

This chapter focuses on the "anatomy" of fuel cells. In other words, it is devoted on the recognition of the basic technical parts of the fuel cells, on their characteristics and their properties, leaving aside the mechanisms that contribute on electricity generation. Then, the classification of fuel cells is provided according to their technical characteristics, and specific mention is given in the technology of Solid Oxide Fuel Cells (SOFCs) that concentrate the basic interests of this thesis. Finally, the chapter provides a brief discussion about the fuels that are considered appropriate for fuel cell applications.

2.1. THE STRUCTURE OF FUEL CELLS

Fuel cells, just like galvanic and electrolytic cells, are comprised of two electrodes and one electrolytic medium. Adopting the very basic classification of conducting materials introduced by Faraday in 1834 [1], the electrodes are conductors of the first kind (electron conductors) and the electrolyte is a conductor of the second kind (ion conductor). The first of the two electrodes is designated as "anode" and the other as "cathode" depending on aspects that will be discussed imminently. The electrodes are applied on the two free surfaces of the electrolyte so that the cell can be symbolically written as,

anode / electrolyte / cathode

where "/" represents an electrode/electrolyte interface .

Fuel cells aim at the conversion of the chemical energy of a fuel into electrical power. For this purpose, one of the electrodes is continously fed by the fuel, the other is exposed to an oxidative medium (most commonly to atmospheric air) and they are both connected to each other through an extrenal electrical circuit.

By reminding the definition of electrical current as "oriented motion of electrons", as well as that the electrolyte is a conductor of the second kind, one can easily observe that the electrical circuit cannot operate without the existence of an appropriate mechanism of charge (electron) transfer through the electrolyte. Virtually, this mechanism corresponds to the migration of ions (charge carriers) from one electrode to other - due to a concentration gradient - which is equivalent of electrical current.

The designation of an electrode as "anode" or "cathode" relies on the direction of the electrical current traversing through the electrode/electrolyte interface. Taking into account that the direction of electricity is, by convention, opposite to the direction of the electronic motion, the current is positive ($I > 0$) and is called "anodic" when it traverses from the electrode to the electrolyte. Therefore, the electrode is designated as "anode" by a positive sign (+) when is traversed from "anodic" current and the other electrode is "cathode" represented with a negative sign (-). This conventional designation is absolutely arbitrary but convenient, since it is the generally adopted in literature [2].

2.2. TYPES AND PROPERTIES OF ELECTROLYTES.

The development and practical application of fuel cells was always inseperably related with the research for the discovery of appropriate electrolytes with desirable properties. Today, the list of available electrolytes has

expanded with representative materials of significantly different nature (liquid solutions, solid mixed oxides, polymer membranes etc.) and properties. Thus, for every technical application, a significantly large list of candidate electrolytes exists.

The specific importance of the electrolyte during designing a fuel cell is so great that their classification is made according to the electrolyte used. This is the "heart element" of the fuel cell affecting almost every design parameter. More precicely, the electrolyte affects on:

- the kind of ions that are allowed to traverse its mass,
- the temperature of cell operation which, in turn, influences on the total field of its applications,
- the magnitude of energy losses due to resistances on the ionic (charge) motion,
- the mechanical integrity of the fuel cell, since it must serve as a substrate for the electrodes and as an unpermeable diaphragm for the gases.

Currently used electrolytes cover a range of applications in the temperature range of 80 - 1500°C and are classified according to their natural state as follows:

- in liguid solutions for applications in low temperature fuel cells,
- in solid polymer membranes for applications in low temperature fuel cells, and
- in solid electrolytes for applications in almost every kind of fuel cell application depending on the case.

The dependence of the feasible application of a fuel cell on the natural state of the electrolyte is either due to the thermal stability of these materials or due to the dependence of their ionic conductivity on temperature.

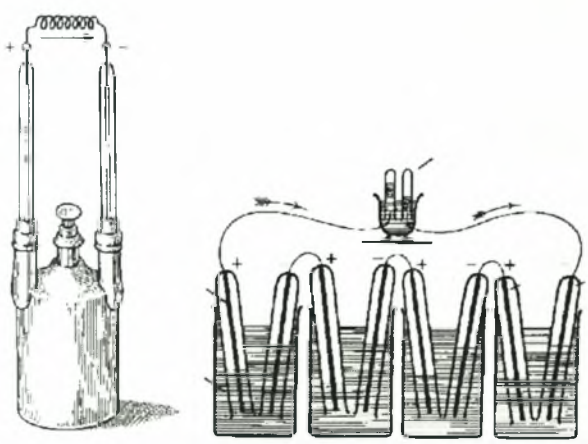

Figure 2.1. The experimental apparatus of W. Grove [3].

Thus, liquid electrolytes are restricted in low temperature applications due to evaporation problems while solid oxide electrolytes have to operate at significantly high temperatures (above 600°C) where ionic conductivity attains values of practical interest.

2.2.1 Liquid electrolytic solutions.

During 1839, the British jurist and amateur physicist W. Grove was the first who discovered the operation principle of fuel cells by using four large cells containing hydrogen and oxygen [3]. During this experiment, Grove was able to produce electrical power which then was consumed for the electrochemical dissociation of liquid water into hydrogen and oxygen in another smaller cell (Figure 2.1). This experiment was based on the principles of liquid phase electrochemistry which were known well before the initiation of the research for solid electrolytes. As a result of this knoweldge, liquid phase electrochemistry borrowed significant experience in the technology of fuel cells among which there are various types operating with alkaline solutions (AFCs) or phosphoric acid (PAFCs).

2.2.2. Polymer electrolyte membranes.

The polymer electrolyte membrane is a solid, organic polymer, usually poly[perfluorosulfonic] acid. A typical membrane material such as Nafion® (produced by DuPont) consists of three regions (Figure 2.2):

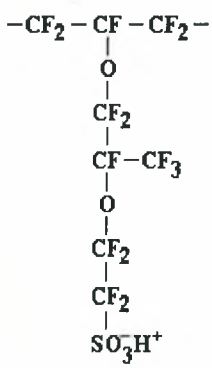

Figure 2.2. The chemical structure of Nafion® (DuPont).

- the Teflon-like, fluorocarbon backbone, consisted of hundred repeating, - $CF_2 - CF - CF_2 -$, units,
- the side chains, - $O - CF_2 - CF - O - CF_2 - CF_2$ -, which connect the molecular backbone to the third region, and
- the ion clusters consisting of sulfonic acid ions: SO_3^- H^+.

The negative ions, SO_3^-, are permanently attached to the side chain and cannot move. However, when the membrane becomes hydrated by absorbing water, the hydrogen ions become mobile. Ion movement occurs by protons, bonded to water molecules, hopping from $SO3^-$ site to $SO3^-$ site within the membrane. Because of this mechanism, the solid hydrated electrolyte is an excellent conductor of hydrogen ions.

Polymer electrolyte membrane fuel cells (PEMFCs) are limited by the temperature range over which water is a liquid. The membrane must contain water so that the hydrogen ions can carry the charge within the membrane. Operating polymer electrolyte membrane fuel cells at temperatures exceeding 100°C is possible under pressurized conditions, required to keep the water in a liquid state, but shortens the life of the cell. Currently, polymer electrolyte membranes cost about $100/square foot. Costs are expected to decrease significantly as the consumer demand for polymer electrolyte membrane fuel cells increases [3].

2.2.3. Solid electrolytes.

The technological development of solid electrolytes caused the transition of the electrochemical research from traditional liquid state to the solid state. The atomical interpretation of ionic conductivity has been promoted initially by the pioneering works of Jost, Frenkel, Wagner and Schottky in the decade of 1920 and in the early 30's [4]. In the ensuing years, the terms "solid electrolytes", "rapid ionic conductors" or even "hyperionic conductors" have beed used widely to describe materials with elecrical conductivity that originates solely or merely due to ionic motion. These combounds comprise a large set of electrolytes including hard refractories such as doped ZrO_2, β''–Al_2O_3 etc.

Six criteria are usually used for the succesful development of a solid electrolyte, by satisfying the following requirements [5] for

- high ionic conductivity (> 10^{-3} S cm^{-1}) which is equivalent with the requirement for minimum energy losses in the cell due to ohmic phenomena,
- numbers of ionic transfer close to unity, i.e.

$$t_i = (\sigma_i/\sigma_{o\lambda}) \approx 1 \qquad (1)$$

where $\sigma_{o\lambda} = (\sigma_e + \Sigma_i \sigma_i)$ is the sum of the conductivities of the specific ion being transfered,

- chemical and mechanical integrity under load and operation,
- low cost,
- long life performance, and
- electronic conductivities near zero to avoid short-circuits.

Solid electrolytes exhibit higher conductivities than semiconductors (10^{-5}-10^{-8} S cm^{-1}) but, obviously, lower than metals (10^{-1}-10^{5} S cm^{-1}). Moreover, their conductivities are often comparable with that of various aqueous electrolytic solutions. The origin of the ionic conductivity in solid electrolytes is due to the existence of point irregularities in their lattice which appear at almost every temperature above 0°C. For most of them, the dependence of their ionic conductivity on temperature can be expressed adequately through the semi-empirical equation,

$$\sigma = (\sigma_o/T)\exp(-E/K_bT) \qquad (2)$$

where σ_o is a function of a) the ionic valence, b) the concentration of mobile ions, c) the attempt frequency and d) the distance of ionic transition. K_b and T stand for Boltzman's constant and temperature, respectively, while the activation energy, E, usually varies between 0.5 and 2 eV.

2.2.3.1. Solid Electrolytes: Historical Development.

Starting in 1800, Davy carried out many investigations into the electrolysis of water and aqueous solutions. Experiments using more and more concentrated solutions of alkali hydroxides led to melting flux electrolysis and in 1807 to the discovery of alkali metals [6]. Davy observed that dried solid alkali compounds were non-conductors but became electrically conducting through just a little moisture. For Faraday it seemed to be an important law that many substances, electrically conducting in the liquid state, lost their conductivity during solidification [7]. In his continuing investigations, Faraday introduced the basic terminology of electrochemistry, and with the aid of many results concerning the concept ``electrolyte" in 1834 he came to the classification of substances into first and second types of conductors [1].

Faraday encountered problems with the classification of silver sulfide, which exhibited conductivities comparable to metals in the high temperature range, but, in contrast to metals, lost its conductivity upon cooling down [7]. Hittorf (1851) devoted himself to this special problem and proved that Ag_2 S is electrolytically decomposable [8]. The generation of a counter voltage (polarisation by chemical precipitation) during the passage of a current was recognised as a characteristic feature of electrolytic conductivity of solids [8, 9], and this led to the discovery of an increasing number of solid conductors of the second class.

A short period before, Gaugain [10] and Becquerel [11] had published experiments on the thermoelectricity between metal contacts on glass and porcelain. Buff

reproduced the results, which turned out very differently depending on the position of the contacts in oxidising or reducing regions of flames, and he interpreted the voltages as a mixture of thermoelectric forces and voltages which he had previously observed between bare platinum wires in flames [12]. But Gaugain investigated his cells, which at first were made of two tubes of glass, platinum wires, air and alcohol vapour, in more detail [13]. He observed their effect on capacitors and their delivery of current, the polarity of the electrodes and their behaviour if the electrode metals or the gas supply were changed. He also noted the large voltage alteration when different gases were mixed with oxygen beyond a certain proportion (known today as the jump at the stoichiometric point k ‹1), and phenomena associated with an iron/air cell which convinced him of the decisive role of oxygen in the electrode reaction. Although restricted by the lack of sensitivity of the available measuring device (a leaf electroscope) so that small voltage differences could not be detected, Gaugain nevertheless found that ``the new source of electricity possesses all the characteristic features of an aqueous-electric cell", and thus he discovered in 1853 galvanic solid electrolyte gas cells.

Towards the end of the 19th century the term ``solid electrolyte" was in use, and many facts were known about the behaviour of these materials. A technological interest in solid ion conductors first arose in connection with the development of electric lighting devices. Early carbon filament lamps manufactured since about 1880 could not compete with the existing gas incandescent light. In 1897, Nernst suggested in a patent [14] that second-class conductors in the form of a thin rod could be made electrically conducting by means of an auxiliary heating appliance and then kept glowing by the passage of an electric current. At first Nernst mentioned only ``lime, magnesia, and those sort of substances" as appropriate conductors. Later investigations stimulated by experiences with gas mantles led to his observation ``that the conductivity of pure oxides rises very slowly with temperature and remains relatively low, whereas mixtures possess an enormously much greater conductivity, a result in complete agreement with the known behaviour of liquid electrolytes" [15]. He pointed out that, for example, the conductivity of pure water and pure common salt is low but that of an aqueous salt solution is high. In a short time many of the mixed oxides which exhibit high conductivity at elevated temperatures, including the particularly favourable composition 85% zirconia and 15% yttria [16], the so-called Nernst mass, were identified. The thesis studies of Reynolds [16] inspired by Nernst, and presented in 1902, were a considerable achievement. These concerned the conductivity in the range 800-1400°C of numerous binary and ternary systems, among others, formed by ZrO_2 with the oxides of the elements La, Ce, Nd, Sm, Ho, Er, Yb, Y, Sc, Mg, Ca, Th and U, including investigations on the role of composition, concentration, direction of temperature alteration (hysteresis) and other phenomena.

Figure 2.4 shows one of the many designs of the Nernst lamp [17, 18]. When the lamp is switched on, the voltage is applied to the Nernst rod, *h*, and to the parallel heating resistor, *i*. Both these components were incorporated in a glass envelope containing air. After sufficient preheating, the current starts flowing through the Nernst rod *h* and through the winding *k* of an electromagnet *b*. At a specified electric current the magnet switches off the heater by opening the contacts between *m* and *l* and then the Nernst rod emits light due to resistive heat generation.

The light effciency of the Nernst lamp exceeded that of the carbon filament lamp by nearly 80%. However there were problems. It was difficult to fabricate reliable contacts to the glower, and the platinum leads and heater made the lamp expensive. The glowers had to be prevented from melting with the aid of special series resistors. It was necessary to wait in darkness for half a minute after switching on the lamp until the light appeared. In view of these and other disadvantages, interest in the Nernst lamp, although considerable for a few years, soon disappeared in 1905 with the introduction of the first tungsten filament lamps, which were much simpler and permitted a substantial increase in the light efficiency by raising the glow temperature. The Nernst glowers were similar to metallic conductors in that decomposition did not occur with the passage of direct current. Nevertheless, Nernst was convinced that his glowers were ionic conductors, and he assumed that in zirconia the oxidic additions were dissociated to some extent and able to provide the necessary charge carriers [15]. He observed evidence of oxygen transport, but believed that metal cations were also deposited by the direct current, and, after immediate oxidation by the surrounding air, the resulting oxides diffused back into the glower. Transference number measurements were not performed on the Nernst mass at that time. It was not until 1943 that Wagner [19] recognised the existence of vacancies in the anion sublattice of mixed oxide solid solutions and thus explained the conduction mechanism of the Nernst glowers. We now know that Nernst glowers are oxide ion conductors and the platinum contacts behaved as air electrodes. It follows that Nernst lamps were the first commercially produced solid electrolyte gas cells.

Electrochemistry was given an important impetus by its connection with thermodynamics, discovered by Helmholtz in 1882 [20]. In 1894 Ostwald illustrated the advantages resulting when energy from coal is produced not with a steam engine but directly with a galvanic cell [21].

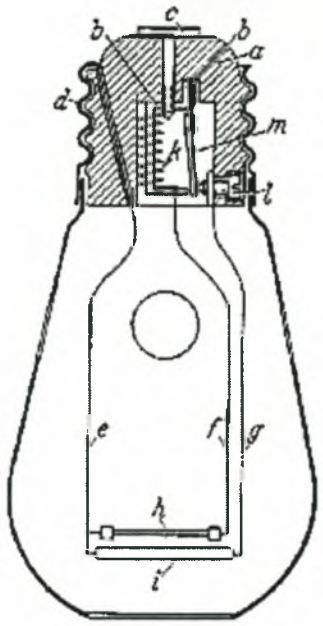

Figure 2.4. Design of Nernst's glower.

The empirical phase of the development of solid electrolyte fuel cells was overcome only after many general advances in research on solids. These included development of X-ray structure analysis, new knowledge on the ion conduction of solids from the measurements of transport numbers by Tubandt, the establishment of the theory of disorders in solids connecte d firstly with the names Frenkel, Schottky, Wagner and Jost, and the development of the methods for the investigation of diffusion processes in solids with stable and unstable isotopes. This technology led to a dramatic increase of studies dealing with solid oxide fuel cells among which the most important are these of Haber (1905), Schottky (1935) and Baur (1937) [4, 22, 23].

Wagner initiated exhaustive investigations of solid oxide fuel cells with his paper of 1943 [19] in Germany and apparently with his paper of 1957 [24] in several other countries. After 1960, a rapidly increasing number of applications for patents were filled and large technological companies such as Westinghouse Electric undertook the effort to continue this work. Already by 1970 the results of investigations on electrical properties and possibilities of the application of solid oxide electrolytes were so numerous as to make them very difficult to survey. A comprehensive review by Etsell and Flengas includes 674 references [25]. Thus, within a relatively short time, the basis was established on which the broad technologically orientated development of solid oxide fuel cells proceeds today.

2.2.3.2. Solid electrolytes: Properties

Oxide materials with oxygen (O^{2-}) ionic and mixed ionic-electronic conductivity have a wide application in high-temperature electrochemical devices such as solid oxide fuel cells (SOFCs), oxygen separation membranes, membrane reactors for hydrocarbon oxidation, and sensors. Therefore the development of oxides having satisfactory properties for electrochemical devices is very important. The main requirements for solid oxide electrolyte materials determining their applicability are high ionic conductivity with negligible electronic conduction, thermodynamic stability under the conditions of the application, and an absence of the degradation of the transport property with time. In known oxide systems based on zirconium dioxide, solid solutions with the cubic fluorite-type structure satisfy these requirements to a large extent [26-28]. Existence of such solid solutions at temperatures below 1000°C is characteristic of the binary oxide systems ZrO_2-M_2O_3 (where M is a rare earth element) and ZrO_2-CaO.

Ranges of formation of the cubic fluorite solid solutions (F-phase) were found for all these systems. There are also fields of tetragonal (T) and monoclinic (M) phases and co-existing phase mixtures in zirconia-rich parts of the phase diagrams. A large number of research projects showed that the conductivity of the fluorite-type solutions has a maximum at 8-10 mol% $MO_{1.5}$ (M = Nd-Lu, Y, Sc) and decreases with further increases in dopant concentration. Therefore a position of the maximum in the conductivity versus composition curves is close to a minimum dopant concentration which provides stabilization of the F-phase at temperatures below 1000°C (low limit of the stabilization). Notice that a) the dopant content corresponding to the conductivity maximum may be somewhat higher compared to the low stabilization limit, and b) both these concentration values depend on the conditions of processing the ceramics. Table 2.1 presents selected data on electrical properties of the zirconia-based solid electrolytes having the highest conductivity prepared by different methods [28].

The solid electrolytes ZrO_2 -Y_2O_3 and ZrO_2 - Sc_2O_3, having the highest conductivity in comparison with other zirconia ceramics, were considered to be most promising electrolyte materials [27]. These materials were subjected to detailed investigations. Phase composition, conductivity, and other properties of the ZrO_2 -Y_2O_3 ceramics containing 8-12 mol% of $YO_{1.5}$ have been reported [29]. The minimum yttria concentration to stabilize the cubic fluorite phase was established to be 10 mol%. Although X-ray diffraction (XRD) of the $Zr_{0.92}$ $Y_{0.08}$ $O_{1.96}$ ceramics did not show the presence of phase

Table 2.1. Electrical conductivity of stabilized zirconia ceramics prepared by different methods†

Electrolyte	Conditions of preparation	Conductivity (S cm^{-1})		Activation energy (eV)	
		800°C	1000°C	T < 900°C	T > 950°C
$Zr_{0.92}Y_{0.08}O_{1.96}$	Co-precipitation and hot pressing (1300°C)	2.5×10^{-2}	8.9×10^{-2}	0.84	0.46
$Zr_{0.90}Y_{0.10}O_{1.95}$	Co-precipitation and hot pressing (1300°C)	4.2×10^{-2}	1.4×10^{-1}	0.84	0.42
$Zr_{0.92}Y_{0.08}O_{1.96}$	Co-precipitation and sintering	3.4×10^{-2}	1.4×10^{-1}	0.80	0.72
$Zr_{0.90}Y_{0.10}O_{1.95}$	Co-precipitation and sintering	2.4×10^{-2}	1.0×10^{-1}	0.80	0.72
$Zr_{0.91}Sc_{0.09}O_{1.96}$	Co-precipitation and hot pressing (1300°C)	1.0×10^{-1}	2.2×10^{-1}	0.79	0.38
$Zr_{0.90}Sc_{0.10}O_{1.95}$	Co-precipitation and hot pressing (1300°C)	8.9×10^{-2}	2.5×10^{-1}	0.75	0.37
$Zr_{0.91}Sc_{0.09}O_{1.96}$	Co-precipitation and sintering	1.1×10^{-1}	3.2×10^{-1}	0.64	0.44
$Zr_{0.90}Sc_{0.10}O_{1.95}$	Co-precipitation and sintering	1.0×10^{-1}	3.0×10^{-1}	0.64	0.46
$Zr_{0.90}Sc_{0.10}O_{1.95}$	Hot pressing (1600°C)	8.3×10^{-2}	2.8×10^{-1}		
$Zr_{0.91}Sc_{0.09}O_{1.96}$	Slip casting	1.1×10^{-1}	3.1×10^{-1}		
$Zr_{0.89}Y_{0.08}Al_{0.03}O_{1.94}$	Hot pressing (1300°C) Hot pressing (1600°C)	1.9×10^{-2} 5.4×10^{-2}	7.9×10^{-2} 1.6×10^{-1}		
$Zr_{0.92}Yb_{0.08}O_{1.96}$	Co-precipitation and sintering	7.9×10^{-2}	2.2×10^{-1}	0.73	0.67
$Zr_{0.90}Yb_{0.10}O_{1.95}$	Co-precipitation and sintering	5.6×10^{-2}	1.9×10^{-1}	0.72	0.63

†[28, and the references therein]

impurities, phase heterogeneity of the material was demonstrated by optical methods. The solid solution $Zr_{0.90}Y_{0.10}O_{1.95}$, which was synthesized before ceramic sintering, exhibited the maximum conductivity [29]. Thermal expansion coefficients (TECs) of the materials are in the range of $(9.7\text{-}10.0)\times10^{-6}$ K^{-1}. For ZrO_2 -Y_2O_3 samples prepared by hot pressing, the cubic fluorite phase stabilization was observed at a yttria content more than 6 mol%, but the conductivity maximum was found to correspond to 10 mol% of yttria [30]. At the same time, the conductivity maximum of the solid electrolytes ZrO_2 -Y_2O_3 produced by thermal decomposition of organometallic compounds and by hydroxide coprecipitation [31] was about 7-7.5 mol% of the stabilizing addition.

The decreasing conductivity of zirconia solid electrolytes with time is determined by the following factors: a) decomposition of a metastable solid solution at reduced temperatures, b) local ordering of the oxygen sublattice of completely stabilized electrolytes with formation of microdomains, c) changing resistance of the ceramic gain boundaries and d) interaction between electrochemical cell materials [27]. The decomposition of metastable cubic phases is characteristic of the electrolytes ZrO_2 -Y_2O_3 and ZrO_2 - Sc_2O_3 containing less than 9 mol% of $MO_{1.5}$ [28, 32] as well as of ZrO_2-CaO ceramics. The degradation of such electrolytes is accompanied by two processes: the increasing concentration of new centers of phase formation and their growth [28, 32]. For a sufficiently long time of annealing, the first process comes to an end. Under the assumption that the conductivity of the starting phase is significantly higher than that of the product phase, the following equations were proposed in order to describe the degradation kinetics [32]:

$$\sigma_\tau = \sigma_o (1 - A\tau) \quad \text{for long periods} \qquad (3)$$

$$\sigma_\tau = \sigma_o (1 - B\tau^{5/3}) \quad \text{for short periods} \qquad (4)$$

where σ_o and σ_τ are the specific electrical conductivities at the start and at the time τ, respectively, and A and B are constants. Selected data on the time degradation of the zirconia electrolytes are given in Table 2.2. The degradation rate of the ZrO_2-Sc_2O_3 and ZrO_2-CaO ceramics is significantly higher than that of YSZ [32]. With regard to this, of interest are results concerning the solid electrolytes of ZrO_2 -Sc_2O_3-Y_2O_3. These materials exhibit a higher conductivity than with YSZ and a much lower rate of degradation than SSZ. So, if the conduvtivity at temperatures of 650-1000 °C before degradation was observed to decrease in the sequence $Zr_{0.905}Sc_{0.095}O_{1.952} > Zr_{0.90}Y_{0.04}Sc_{0.06}O_{1.95} > Zr_{0.93}Y_{0.07}$ - $O_{1.97} > Zr_{0.90}Y_{0.10}O_{1.95}$, the conductivity after annealing at 1020 °C for 650 h follows the relation $Zr_{0.90}Y_{0.04}$ - $Sc_{0.06}O_{1.95} > Zr_{0.905}Sc_{0.095}O_{1.952} > Zr_{0.90}Y_{0.10}O_{1.95} > Zr_{0.93}Y_{0.07}O_{1.97}$ [28, 32].

Table 2.2. Time degradation of conductivity of stabilized zirconia ceramics[†,‡]

Electrolyte	Measurement temperature (°C)	Time and conditions of annealing	$\Delta\rho/\rho$ (%)	$\Delta\rho_b/\rho_b$ (%)	$\Delta\rho_{gb}/\rho_{gb}$ (%)
$Zr_{0.90}\ Y_{0.10}\ O_{1.95}$	1000	2600 h, 1000 °C, air/H_2 gradient	-5	-	-
	1000	2600 h, 1000 °C, H_2	10	-	-
	1000	4300 h, 1000 °C, air	-17	-	-
	1100	4700 h, 1100 °C, air	8	-	-
$Zr_{0.93}\ Y_{0.07}\ O_{1.97}$	500	430 h, 1100 °C, air	88	84	30
$Zr_{0.90}\ Y_{0.10}\ O_{1.95}$	500	430 h, 1100 °C, air	4	1	18
$Zr_{0.92}\ Y_{0.03}\ O_{1.96}$	450	320 h, 830 °C, O_2	18	15	90
	500		20	19	31
$Zr_{0.88}\ Y_{0.12}\ O_{1.94}$	450	320 h, 830 °C, O_2	8	8	12
	500		13	14	4
$Zr_{0.90}\ Y_{0.10}\ O_{1.95}$	1000	100 h, 1000 °C, air	1	-	-
$Zr_{0.867}\ Y_{0.133}\ O_{1.933}$			4	-	-
$Zr_{0.85}\ Y_{0.15}\ O_{1.92}$			10	-	-
$Zr_{0.90}\ Y_{0.10}\ O_{1.95}$	880	1000 h, 880 °C, air	5	-	-
(single crystal)	725	1000 h, 725 °C, air	24	-	-
$Zr_{0.91}\ Y_{0.09}\ O_{1.96}$ + 0.5%MgO	450	100 h, 830 °C, O_2	10	5	24
$Zr_{0.91}\ Sc_{0.09}\ O_{1.96}$	450	120 h, 830 °C, CO	52	59	12
$Zr_{0.91}\ Sc_{0.09}\ O_{1.96}$	900	300 h, 900 °C, air	40	-	-
$Zr_{0.91}\ Sc_{0.09}\ O_{1.96}$	500	430 h, 1100 °C, air	41	46	17
$Zr_{0.905}\ Sc_{0.095}\ O_{1.952}$	500	430 h, 1100 °C, air	55	95	-67
$Zr_{0.90}\ Sc_{0.10}\ O_{1.95}$	1000	2500 h, 1000 °C, air	50	-	-
	1100	4700 h, 1100 °C, air	41	-	-
$Zr_{0.90}\ Y_{0.04}\ Sc_{0.06}\ O_{1.95}$	900	300 h, 900 °C, air	0	-	-
$Zr_{0.90}\ Y_{0.03}\ Sc_{0.07}\ O_{1.95}$			3	-	-
$Zr_{0.92}\ Y_{0.05}\ Sc_{0.06}\ O_{1.95}$			2	-	-
$Zr_{0.90}\ Y_{0.04}\ Sc_{0.06}\ O_{1.95}$	500	430 h, 1100 °C, air	-2	-0.5	-10
$Zr_{0.87}\ Ca_{0.13}\ O_{1.87}$	1000	2500 h, 1000 °C, air	82	-	-
	1100	4700 h, 1100 °C, air	80	-	-
$Zr_{0.88}\ Ca_{0.12}\ O_{1.88}$	1200	100 h, 1200 °C, air	64	-	-
$Zr_{0.85}\ Ca_{0.15}\ O_{1.85}$	1200		30	-	-

† $\Delta\rho/\rho$ is the ratio between the increase of total resistance after annealing and the starting value of the resistance. $\Delta\rho_b/\rho_b$ and $\Delta\rho_{gb}/\rho_{gb}$ are the same quantities for the resistance of the grain bulk and grain boundary, respectively.
‡ [28, and the references therein]

However, a definite degradation in conductivity with time is typical for the $Zr_{0.90}\ Y_{0.04}$ - $Sc_{0.06}\ O_{1.95}$ electrolyte also [32]. The authors demonstrated that diffusion of nickel and cobalt into the bulk of stabilized zirconia at 900-1100 °C for 10000 h did not result in a degradation of the electrolytes. It was also shown that a direct current through a solid electrolyte may lead to redistribution of the stabilizing dopant in the bulk of the electrolyte.

In the cource of the present thesis, the $Zr_{0.92}\ Y_{0.08}\ O_{1.96}$ material has been used during all experiments. Therefore, in the imminent analyses the term "yttria stabilized zirconia" (YSZ) will be considered to reffer to this specific electrolyte.

2.3. TYPES AND PROPERTIES OF ELECTRODES.

Anode and cathode electrodes are the other two important constructive elements of fuel cells, serving to the accomplishment of highly selective processes during operation. Electrodes must be materials of high electronic conductivity (conductors of the first kind) in order to collect and transfer electrons with minimum ohmic losses and minimum impact to the efficiency of the cell. At the same time, electrodes must be able to ease the processes of electroniation (cathode) and de-electroniation (anode) that take place at their interfaces with the electrolyte. As it will be discussed latter, these processes of ion charging and discharging have an extremely important influence to

the perfomance of a fuel cell that depend on the nature of the electrode/electrolyte interfaces.

Selective electroniation of specific atoms in cathode is due to the arrival of a flux of electrons through the external circuit. By reminding the definition of chemical reduction as "process of arithmetic (not absolute) reduction of the valence of a substance", the specific atoms that accept the electrons and become ions in cathode are reduced. Likewise, by reminding the definition of chemical oxidation as "process of arithmetic increase of the valence of a substance", the fuel coming in anode is oxidized releasing electrons that will be collected at the external current. According to the above, it is essential that electrodes must also exhibit adequate catalytic activity during the oxidation or reduction reactions taking place at their surfaces. This requierment is virtually the most important among all others for the selection of appropriate electrode materials, because

- it ensures the collection of elctrodes from anode and
- it reduces the energy gap required to be overcome for the creation of ions in cathode.

The requirement for sufficient cartalytic activity of anode is crucial for the operation of the cell. To better understand it, one must consider that on a catalytically inert anode, oxidation either wont occur or it will happen homogeneously (in gas phase). In the early case no electrons will be released and in the latter electrons will be diffused in the bulk of the fuel feedstream without reaching the electrode surface.

According to the aforementioned discussion, the most crucial requirements for the design of electrodes can be summarized as follows:

- high electronic conductivity
- high catalytic activity
- ability for easy migration of ions in their interfaces with electrolyte (low charge transfer coefficients)
- thermal and mechanical stability during operation
- low cost
- adequate porosity, and
- existence of appropriate techniques for their application on the electrolyte.

Accordingly, the selection of electrodes is closely related with fundamental design parameters of the fuel cell such as the fuel choise, the electrolyte type etc. Therefore, the appropriate electrode must be selected among available taking into account the case in hand.

In practice, the simultaneous fulfilment of all above requirements by one electrode material is a case impossible or rare. A compromise is usually adopted between expensive and highly effective materials such as noble metals and cheap but less active electrodes made of common metals, perovskites or other materials. Some important parameters, however, are usually the operation temperature of the cell and the tolerance to destructive effects such as poisoning. In low temperature fuel cells (such as PEMFCs, AFCs and PAFCs), reaction kinetics requires highly effective electrodes such as Pt. On the other hand, high temperature applications (i.e. in SOFCs) impose relaxed requirements for activity since reaction kinetics is positively influenced.

2.3.1. Noble metal electrodes.

Noble metals are common constructive choise in currently developed fuel cells, despite their disadvantages that can be summarized due to their

- high cost, and
- low thermal stability in high temperature applications (sintering, melting, etc.)

Noble metals exhibit high electronic activity and are considered reliable electrode materials due to their high catalytic activity which has been succesfully exploited in numerous applications (automotive catalytic converters, industrial bed reactors, heterogeneous oxidation or reforming of hydrocarbons etc.). In some cases, such as in low temperature fuel cells, heterogeneous reactions attain rates of practical interest only in presense of a noble metal catalyst. For example, platinum (Pt) is a unique electrode option for hydrogen fed low temperature fuel cells (like PEMFCs) because it is sufficiently reactive in bonding H and O intermediates as required to facilitate the electrode processes, and also capable of effectively releasing the intermediate to form the final product. For example [3, 33], the anode process requires Pt sites to bond H atoms when the H_2 molecule reacts, and these Pt sites next release the H atoms, as $H^+ + e^-$:

$$H_2 + 2Pt \rightarrow 2\ Pt\text{-}H \quad (5)$$

$$2Pt\text{-}H \rightarrow 2Pt + 2H^+ + 2e^-. \quad (6)$$

This requires optimised bonding to H atoms — not too weak and not too strong — and this is the unique feature of a good catalyst. Realizing that the best catalyst for the polymer electrolyte membrane fuel cell is expensive, lowering Pt catalyst levels is an on-going effort. One of the best ways to accomplish this is to construct the catalyst layer with the highest possible surface area. Each electrode consists of porous carbon (C) to which very small Pt particles are bonded. The electrode is somewhat porous so that the gases can diffuse through each electrode to reach the catalyst. Both Pt and C conduct electrons well, so electrons are able to move freely

through the electrode. The small size of the Pt particles, about 2 nanometers in diameter, results in an enormously large total surface area of Pt that is accessible to gas molecules. The total surface presented by this huge number of small particles is very large even when the total mass of Pt used is small. This large Pt surface area allows the electrode reactions to proceed at many Pt surface sites simultaneously. This high dispersion of the catalyst is one key to generating significant electron flow, i.e. current, in a fuel cell.

2.3.2. Common metal electrodes.

Many common metals such as Fe, Ni, Cu, Cr and Ag exhibit adequate activity and are good electrode options at elevated temperature applications. For example, the composite Ni-cermet structure made by appropriate adhesion of Ni films with YSZ electrolytes is one of the most promising for applications in anodes of SOFCs. Due to their low cost, common metals represent a competitive electrode solution against noble metal catalysts but special techniques are usually employed to increase their effectiveness. Another crucial parameter is their independent ability to suppress or expand the range of operation conditions where carbon deposition appears, since this is one of the most important dangers to be avoided during fuel cell operation. In this respect, for example, Cu is generally considered a better choice than other metals such as Ni [33-35].

2.3.3. Perovskite oxides.

The need for independence on precious metals has been an increasing momentum behind research efforts for development of alternative, cheap and durable electrode structures. Perovskite oxides comprise a family of such materials with chemical type ABO_3, where cations A and B are usually transition metals. In these structures, doping of A and B sites by various metals in different stoichiometries, provides hundreds materials that are generally good catalysts [36, 37]. The main advantages of this family are the following:

- In contrast to pure oxides, perovskites exhibit high electronic activity.
- In contrast to metals, perovskites exhibit also good ionic conductivity which provides low charge transfer coefficients at electrode/electrolyte interfaces.
- They exhibit good catalytic activity during various heterogeneous reactions.
- They are cheap, and finally
- they present adequate thermal stability also at very high operation temperatures.

Perovskites are nowadays in use as materials for fuel cells, as membranes for oxygen separation, as catalysts for partial oxidation of hydrocarbons and in the technology of sensors. Specific mention may be given to the structure $La_xSr_{1-x}MnO_3$ which is considered an ideal cathode electrode for SOFCs [33, 35, 37, 38].

2.4. CLASSIFICATION OF FUEL CELLS

The classification of fuel cells is made due to the type of the electrolyte used. Accordingly, Table 2.3 presents the types of fuel cells, their electrolytic medium and the temperature range of their practical application, electrode semi-reactions and some suggested electrocatalysts for each type [39]. The low temperature fuel cells (PEMFC, AFC, PAFC) utilize aqueous electrolytes in which H^+ or OH^- ions are the dominant ionic current carriers. At higher temperatures, CO_3^{2-} ions in the molten salt electrolyte of the MCFCs and O^{2-} ions in the solid electrolyte of the SOFC are the ionic current carriers. The operating temperature has consequences for design, the efficiency of the fuel cell, the choice of other materials needed and the kind of fuel that may be used. For low temperature fuel cells (PEFC, AFC and PAFC), the operating temperature is too low to enable direct oxidation of hydrocarbon fuels like natural gas and, therefore, fuels like hydrogen and methanol are used. Low temperature fuel cells are generally seen as interesting for small scale applications, for example mobile applications like cars (PEMFC), notebooks, phones etc. For high temperature fuel cells (MCFC and SOFC) it is possible to use carbonaceous fuels which can be reformed internally into hydrogen and carbon monoxide (depending on operating temperature a catalyst will be necessary). The high temperature fuel cells, but also PAFC, are interesting for the decentralised generation of heat and power. In the following sections the interest will focus on each fuel cell type and especially in SOFCs because of their importance in the present study.

2.4.1 AFCs.

Alkaline Fuel Cells (AFCs) were the first type of fuel cell developed by W. Grove and also the first type in practical application in the Apollo space programs of NASA. The electrolyte used is an aqueous solution of KOH with concentration dependent on the operating temperature (from 25-35 wt.% at T < 120°C up to 85 wt.% at T~250°C). AFCs exhibit high efficiencies, and low corrosion problems from KOH due to low operating temperatures. However, CO_2 in air usually reacts with KOH lowering the activity and the lifetime of the electrocatalysts.

Table 2.3. Classification of fuel cells

Fuel Cell Type	Acronym	Electrolyte	Operation temperature	Anodic Reaction	Ionic motion	Cathodic reaction	Suggested anode electrode†	Suggested cathode electrode†
Alkaline Fuel Cell	AFC	solution of KOH	50 – 260 °C	$H_2+2OH^-\rightarrow 2H_2O+2e^-$	$\leftarrow OH^-$	$O_2+2H_2O+4e^-\rightarrow 4OH^-$	Pt/Au, Pt, Ag	Pt/Au, Pt, Ag
Phosphoric Acid Fuel Cell	PAFC	H_2PO_3	50 – 200 °C	$H_2\rightarrow 2H^++2e^-$	$H^+\rightarrow$	$O_2+4H^++4e^-\rightarrow 2H_2O$	Pt	Pt/Cr/Co, Pt/Ni
Polymer Electrolyte Membrane Fuel Cell	PEMFC	Nafion	60 – 120 °C	$H_2\rightarrow 2H^++2e^-$	$H^+\rightarrow$	$O_2+4H^++4e^-\rightarrow 2H_2O$	Pt, Pt/Ru	Pt
Direct Methanol Fuel Cell	DMFC	Nafion	50 – 120 °C					
Molten Carbonate Fuel Cell	MCFC	$LiKCO_3$	600 – 650 °C	$H_2+CO^{=}_3\rightarrow H_2O+CO_2+2e^-$ $CO+CO^{=}_3\rightarrow 2CO_2+2e^-$	$\leftarrow CO^{=}_3$	$O_2+2CO_2+4e^-\rightarrow CO^{=}_3$	Ni, Ni/Cr	Li/NiO
Solid Oxide Fuel Cell	SOFC	doped ZrO_2	900 – 1000 °C	$H_2+O^{=}\rightarrow H_2O+2e^-$ $CO+O^{=}\rightarrow CO_2+2e^-$ $CH_4+4O^{=}\rightarrow 2H_2O+CO_2+8e^-$	$\leftarrow O^{=}$	$O_2+4e^-\rightarrow 2O^{=}$	Ni/ZrO_3	$LaSrMnO_3$

† suggested by [39]

2.4.2 PAFCs.

The technological evolution of **P**hosphoric **A**cid **F**uel **C**ells (PAFCs) begun in 1965 by using porous electrodes made by bonds of poly-tertiary-fluoro-ethylene (PTFE) and Pt black with loads equal to about 9mg Pt/cm^2. Pt black was then substituted by Pt/C structures and in the middle 70's the loads of anode and cathode dropped to approximately 0.25mg Pt/cm^2 and 0.5mg Pt/cm^2, respectively. The composite PTFE-Pt/C structure is still under use and the load of anode is currently of the order of 0.1mg Pt/cm^2. In the intervening years, their operating temperature increased significantly with concomitant effect on the acid concentration of the electrolyte. As a result, modern PAFCs operate at about 200°C with 100% H_3PO_4 electrolyte [33, 40].

One of the most important innovations in the technology of PAFCs took place in the late 60's by developing materials from carbon black and graphite that changed previous tantalum structures. Utilization of carbon black with large external surface as Pt substrate significantly reduced the load of Pt and the cost of PAFCs. However, at cell potentials above 0.8V corrosion of carbon and dissolution of Pt become inevitable. As a result, low current density operation at potentials above 0.8V and open circuit operation at high temperatures are avoided.

2.4.3. PEMFCs

Polymer **E**lectrolyte **M**embrane (or ptoton exchange membrane) **F**uel **C**ells (PEMFCs) have grown in recognition as the most appropriate fuel cell technology for vehicular applications due to important characteristics such as the ability for zero-emission application at low temperatures. Operating exclusively with hydrogen (concentration of CO in the feedstream must be lower than 10ppm to prevent poisoning of currently used electrocatalysts) at temperatures between 60 and 120°C, most automotive companies have already adopted the concept for commersialization of PEMFC-powered vehicles in the near future [41].

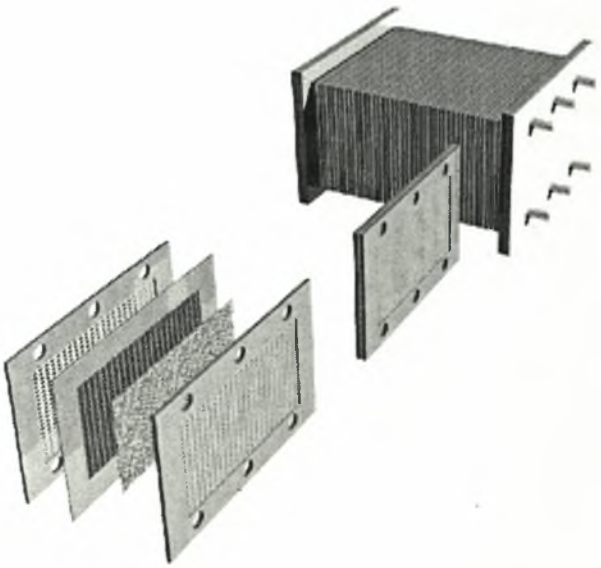

Figure 2.5. PEMFC stack with membrane-electrode-assemblies.

To meet the power demands of an average vehicle, PEMFC stacks of 50 lt volume (or 250-350cm^3 per single cell) are needed. For a cell surface equal to 500cm^2 these volume demands are equivalent for cell widths of the order of 0.5-0.7cm that will envelop the membrane, the electrocatalysts and the separate plates, without impact in the uniformity of the gaseous streams. This is accomplished with development of appropriate membrane-electrode-assemblies (MEAs) of extremely small width without impact on the electrochemical actions or the mechanical integrity of the cell. Pt/C large surface area structures are used as electrodes closely attached with the membrane. Thus, MEAs provide short diffusion paths for gaseous species and high electrolytic conductivities making possible the establishment of high current and power densities. At typical operation (e.g. current density 1A/cm^2 and cell potential 0.7V), a cell of 500cm^2 area can produce approximately (1 x 0.7 x 500) = 350 W. Therefore, the acceleration of an average vehicle to its maximum velocity requires a stack of about 150-200 single cells to provide a total power of approximately 50-65 kW.

2.4.4.DMFCs

Methanol is the only carbonaceous fuel with adequate electrochemical activity on fuel cell electrodes in the temperature range for vehicular applications. Due to this advantage, **D**irect-**M**ethanol **F**uel **C**ells (DMFCs) can be as simple in operation as PEMFCs utilizing an easily stored and cheap fuel. DMFCs attract interest having "anatomy" similar to PEMFCs and methanol is fed in form of vapors. However, they are still in research with production of prototypes because two impediments must overcome. The first is low current densities on operation for automotive applications and the second is the crossover of methanol through the membrane which deteriorates lifetime, performance and efficiency. During the last decade, various alternative designs gave prospects for better future performance. As a result, a great number of PEMFC developing industries are currently differentiating their activities with parallel orientation to DMFCs.

2.4.5. MCFCs

The intermediate temperature (~650°C) technology of **M**olten **C**arbonate **F**uel **C**ells (MCFCs) operates by simultaneous feeding of methane (natural gas) and steam in the anode electrocatalyst (usually Ni) where methane steam reforming takes place for production of CO_2 and H_2. Again, hydrogen is the only gaseous species leading to potential formation. At cathode CO_2 and O_2 form $CO_3^=$ anions and the electrolyte is $CO_3^=$ conducting $LiKCO_3$. The necessity for continuous recycling of CO_2 from anode to cathode for cost –effective operation as well as electrolyte looses by evaporation, creepage and corrosion are their major disadvantages. High-quality waste heat is available for use in cogeneration or in bottoming cycle to increase overall system efficiency. MCFCs are entering the pilot plant technology stage [33, 40].

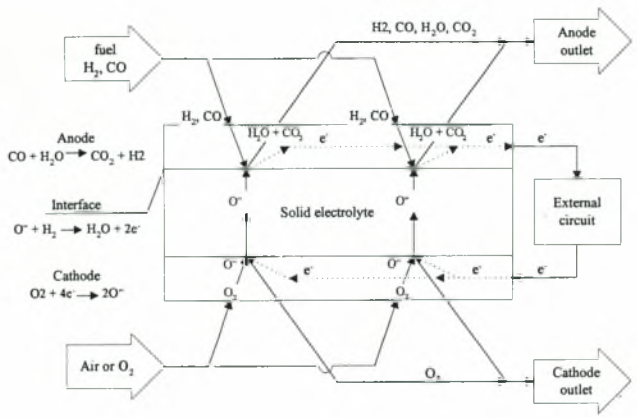

Figure 2.6. Operation principle of SOFCs.

2.4.6. SOFCs

Ceramic fuel cells like **S**olid **O**xide **F**uel **C**ells (SOFCs) operate at elevated temperatures (above 650°C). In the general case, oxygen conducting doped-ZrO_2 electrolytes are used (Figure 2.6) but efforts are made also for the development of proton (H^+) conducting high temperature operating SOFCs. High temperature of operation allows internal reforming, promotes rapid kinetics with non-precious metals and produces high quality byproduct heat for cogeneration or for use in a bottoming cycle, similar to MCFCs. The high operation temperature of the SOFC, however, places stringent requirements on its materials. The development of suitable cheap materials and the low cost fabrication of ceramic structures are presently the key technical challenges facing SOFCs [33, 35, 40]. The solid state character of all SOFC components implies that, in principle, there is no restriction on the cell configuration. Instead, it is possible to shape the cell according to criteria such as overcoming design or application issues.

The tubular SOFC configuration (Figure 2.7) has undergone development at Siemens Westinghouse Co. and its predecessors since the late 1950s. Currently, this configuration is demonstrated in complete power units of nominal 100 kW capacity. The flat plate design is at a much earlier development status.

Table 2.4 provides a brief description of the materials currently used in the various cell components of the more developed tubular SOFC, and those that were considered earlier. Because of the high operating temperatures of present SOFCs (approximately 1000 °C), the materials used in the cell components are limited by chemical stability in oxidizing and reducing environments, chemical stability of contacting materials, conductivity, and thermomechanical compatibility. These limitations

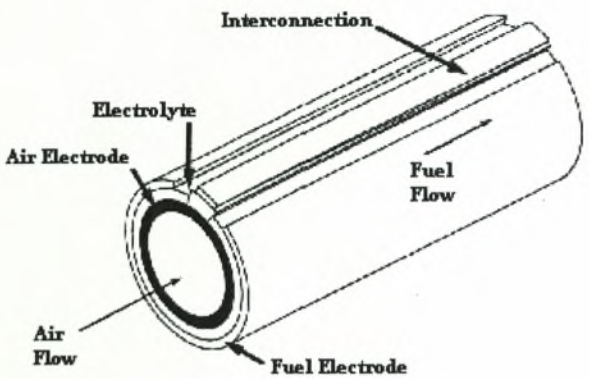

Figure 2.7. Tubular SOFC design.[42]

have prompted investigations of developing cells with compositions of oxide and metals that operate at intermediate temperatures in the range of 600-800 °C.

Present SOFC designs make use of thin film concepts where films of electrode, electrolyte, and interconnect material are deposited one on another and sintered, forming a cell structure (Figure 2.8). The fabrication techniques differ according to the type of cell configuration and developer. For example, an "electrochemical vapour deposition" (EVD) technique has been developed to produce thin layers of refractory oxides suitable for the electrolyte, anode, and interconnection in the Siemens Westinghouse tubular SOFC design (Figure 2.7) [43]. In this technique, the appropriate metal chloride vapour is introduced on one side of the tube surface, and O_2/H_2O is introduced on the other side.

Table 2.4. Technical evolution of materials used in SOFCs

Component	1965	1975	Current status[†]
Electrolyte	• Y_2O_3 stabilized ZrO_2 • 0.5 mm thickness	Y_2O_3 stabilized ZrO_2	• 8%mol Y_2O_3 stabilized ZrO_2 • EVD[‡] • $10.5x10^{-6}$ cm/cm °C thermal expansion from room temperature to 1000 °C
Cell Interconnect	Pt	Mn doped cobalt chromite	• Doped lanthanum chromite • Plasma spray $10x10^{-6}$ cm/cm °C • About 100 μm thickness

[†] Specifications of Siemens Westinghouse SOFC
[‡] Electrochemical vapour deposition

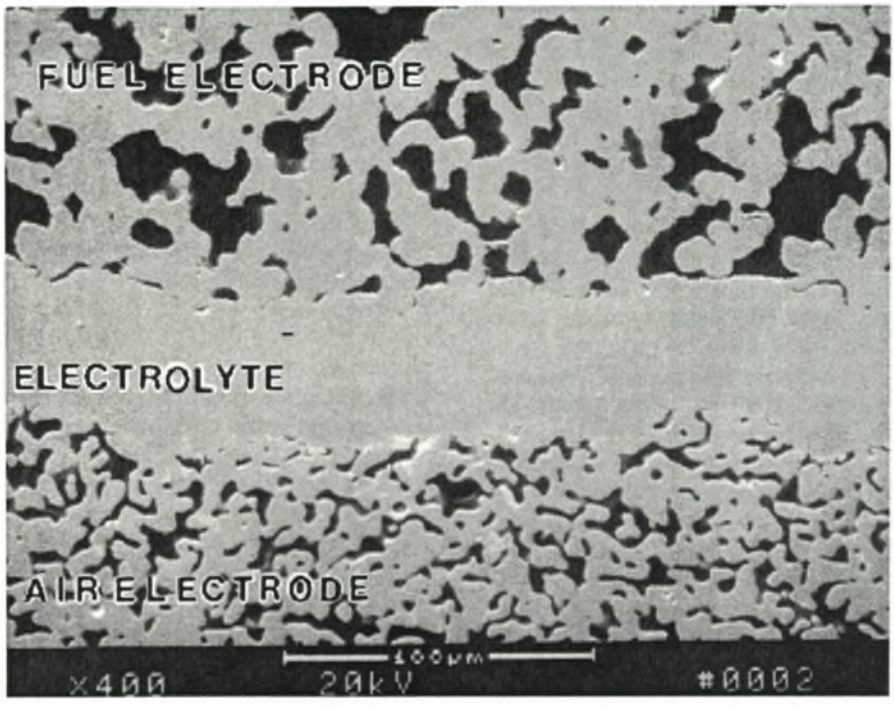

Figure 2.8. Microstructure of a cross section of a Siemens Westinghouse SOFC (Reprinted from [42]).

The gas environments on both sides of the tube act to form two galvanic couples, as demonstrated in Eqs. (7) and (8):

$$MeCl_y + \tfrac{1}{2}yO \rightarrow MeO_{y/2} + \tfrac{1}{2}yCl_2 + ye^- \quad (7)$$

$$\tfrac{1}{2}O_2 + 2e^- \rightarrow O^{2-} \quad (8)$$

$$H_2O + 2e^- \rightarrow H_2 + O^{2-} \quad (9)$$

The net result is the formation of a dense and uniform metal oxide layer in which the deposition rate is controlled by the diffusion rate of ionic species and the concentration of electronic charge carriers. This procedure is used to fabricate the solid electrolyte yttria stabilized zirconia (YSZ).

The solid oxide electrolyte must be free of porosity that permits gas to permeate from one side of the electrolyte layer to the other, and it should be thin enough to minimize ohmic loss. In addition, the electrolyte must have a transport coefficient for O^{2-} as close to unity as possible, and a transport and coefficient for electronic conduction as close to zero as possible. Zirconia-based electrolytes are suitable for SOFCs because they exhibit

pure anionic conductivity over a wide range of O_2 partial pressures (1 to 10^{-20} atmospheres). The other cell components should permit only electronic conduction, and interdiffusion of ionic species in these components at 1000°C (1832°F) should not have a major effect on their electronic conductivity. Other severe restrictions placed on the cell components are that they must be stable in the gaseous environments in the cell and that they must be capable of withstanding thermal cycling. The materials listed in Table 2.4 appear to have the properties for meeting these requirements.

The anode consists of metallic Ni and a Y_2O_3 stabilized ZrO_2 skeleton. The latter serves to inhibit sintering of the metal particles and to provide a thermal expansion coefficient comparable to those of the other cell materials. The anode structure is fabricated with a porosity of 20 to 40% to facilitate mass transport of reactant and product gases. In tubular cells, a 100–150 mm thick layer of Ni /YSZ is applied over the electrolyte by a two-step process. In the first step, nickel slurry is applied over the electrolyte. In the second step, YSZ is grown around the nickel particles by same EVD process as used for depositing electrolyte. Deposition of a Ni–YSZ slurry over the electrolyte followed by sintering has also yielded anodes that are equivalent in performance to those fabricated by the EVD process; use of this non-EVD process will result in a substantial reduction in the cost of manufacturing SOFCs.

Doped lanthanum manganite is most commonly used for the cathode material. Similar to the anode, the cathode is a porous structure that must permit rapid mass transport of reactant and product gases. Lanthanum manganite is a p-type perovskite oxide and shows reversible oxidation–reduction behaviour. The material can have oxygen excess or deficiency depending upon the ambient oxygen partial pressure and temperature. Although, it is stable in air and oxidizing atmospheres, it dissociates at 1000 °C at oxygen pressures lower than 10^{-14} atm. The electronic conductivity of lanthanum manganite is due to hopping of an electron hole between the +3 and +4 valence states of Mn. This conductivity is enhanced by doping with a divalent ion such as calcium or strontium. The defect chemistry, electrical conduction, and cathodic polarization behaviour of doped lanthanum manganites have been studied in detail [44], and alkaline earth doped lanthanum manganite has been found to satisfy all the requirements to be an effective air electrode.

Over 90% of the weight of a tubular SOFC is that of the doped lanthanum manganite air electrode tube. Presently, the air electrode material is using high purity component oxides such as La_2O_3 and MnO_2. Significant reduction in the cost of air electrode material is possible if less expensive, lower purity raw materials are used instead of pure lanthanum compounds to synthesize the air electrode powder. Air electrode material cost can also be reduced by utilizing compositions that have lower rare earth content. Use of such lower cost air electrode materials in fabricating SOFC cathode tubes appears promising.

Interconnection, in the form of a 9-mm-wide strip along the cell length, serves as the electric contact to the air electrode and also protects the air electrode material from the reducing environment of the fuel on the fuel electrode side. The requirements of the interconnection are the most severe of all cell components and include the following.

- Nearly 100% electronic conductivity.
- Stability in both oxidizing and reducing atmospheres at the cell operating temperature since it is exposed to air (or oxygen) on one side and fuel on the other.
- Low permeability for oxygen and hydrogen to minimize direct combination of oxidant and fuel during cell operation.
- A thermal expansion close to that of the air electrode and the electrolyte.

To satisfy these requirements, doped lanthanum chromite is used as the interconnection material. Lanthanum chromite is a p-type conductor; its conductivity is due to small polaron hopping from room temperature to 1400°C at oxygen pressures as low as 10 atm. The conductivity is enhanced as lower valence ions (e.g. Ca, Mg, Sr, etc.) are substituted on either the La or the Cr sites. For the Siemens Westinghouse tubular SOFC, the inter-connection is deposited in the form of an about 85-mm-thick, 9-mm-wide strip along the air electrode tube length by plasma spraying.

The resistivities of typical cell components at 1000°C under fuel cell gaseous environments are (6): 10 ohm^{-1} cm^{-1} (ionic) for the electrolyte (8-10 mol% Y_2O_3 doped ZrO_2), 1 ohm^{-1} cm^{-1} (electronic) for the cell interconnection (doped $LaCrO_3$), 0.01 ohm^{-1} cm^{-1} (electronic) for the cathode (doped $LaMnO_3$), and $3x10^{-6}$ $ohm^{-1}cm^{-1}$ (electronic) for the anode (Ni/ZrO_2 cermet). It is apparent that the solid oxide electrolyte is the least conductive of the cell components, followed by the cell interconnection. Furthermore, an operating temperature of about 1000°C is necessary if the ionic conductivity of the solid electrolyte (i.e., 0.02 $ohm^{-1}cm^{-1}$ at 800°C and 0.1 $ohm^{-1}cm^{-1}$ at 1000°C) is to be within even an order of magnitude of that of aqueous electrolytes. The solid electrolyte in SOFCs must be only about 25-50 μm thick if its ohmic loss at 1000°C is to be comparable to that of the electrolyte in PAFCs. Fortunately, thin electrolyte structures of about 40 μm thickness can be fabricated by EVD, as well as by tape casting and other ceramic processing techniques [33, 35, 40].

2.5. FUELS FOR FUEL CELLS

2.5.1. Hydrogen

Hydrogen is the most attractive fuel for fuel cells having excellent electrochemical reactivity, providing adequate levels of power density in a hydrogen /air system for automobile propulsion, as well as having zero emissions characteristics. Historically, the trend in energy use indicates a slow transition from fuels with high carbon content, beginning with wood, to fuels with more hydrogen. Fossil fuels release varying quantities of carbon dioxide into the atmosphere - coal having the highest carbon content, then petroleum, and finally natural gas - the lowest carbon dioxide emitter per thermal unit. Hydrogen obviously releases no carbon dioxide emissions when burned.

Hydrogen (H_2) is the most abundant element in the universe, although practically all of it is found in combination with other elements, for example, water (H_2O), or fossil fuels such as natural gas (CH_4). Therefore, hydrogen must be manufactured from either fossil fuels or water before it can be used as a fuel. Today, approximately 95% of all hydrogen is produced by "steam reforming" of natural gas, the most energy-efficient, large-scale method of production.

Hydrogen can also be produced by gasification of carbon containing materials such as coal - although this method also produces large amounts of carbon dioxide as a byproduct. Electrolysis of water generates hydrogen and oxygen, as follows:

$$H_2O \rightarrow H_2 + \tfrac{1}{2}O_2 \qquad (10)$$

The electricity required to electrolyze the water could be generated from either fossil fuel combustion or from renewable sources such as hydropower, solar energy or wind energy. In the longer term, hydrogen generation could be based on photobiological or photochemical methods. While there is an existing manufacturing, distribution, and storage infrastructure of hydrogen, it is limited. An expanded system would be required if hydrogen fuel were to be used for automotive and utility applications. While a single hydrogen production/ distribution/storage system may not be appropriate for the diverse applications of fuel cells, it is certainly possible that a combination of technologies could be employed to meet future needs. All of the system components are currently available but cost effective delivery and dispensing of hydrogen fuel is essential. If hydrogen were to become available and affordable, this would reduce the complexity and cost of fuel cell vehicles enhancing the success of the technology. "Hydrogen Economy" is an energy system based upon hydrogen for energy storage, distribution, and utilization. The term, coined at General Motors in 1970, caught the imagination of the popular press. During the oil crisis in the early 70's, the price of crude oil sharply increased, concern over stability of petroleum reserves and the potential lack of a secure energy source grew, and government and industry together developed plans and implementation strategies for the introduction of hydrogen into a world energy system. However, the lessening of tensions in the Middle East led to a lowering of crude oil prices and the resumption of business as usual. Petroleum has continued to be the fuel of choice for the transportation sector worldwide.

Hydrogen fuel has the reputation of being unsafe. However, all fuels are inherently dangerous. Proper engineering, education, and common sense reduce the risk in any potentially explosive situation. A hydrogen vehicle and supporting infrastructure can be engineered to be as safe as existing gasoline systems. Dealing with the perception and reality of safety will be critical to the successful wide introduction of hydrogen into our energy economy [3, 35, 45-48].

2.5.2. Natural gas

Natural gas is composed primarily of methane (CH_4), which remains gaseous unless stored under cryogenic conditions. Due to the high cost of cryogenic storage, compressed natural gas (CNG) is commonly employed. Natural gas has been proposed by many researchers as promising SOFC fuel, since operation temperature of SOFC's allows the catalytic activation of methane dissociation. In this respect, and due to the extensive study on catalysts for methane activation, it was the first fuel that has been experimentally investigated on high temperature operating cells like SOFCs. Research on this field shown that low cost nickel supported catalysts can provide high conversions during methane reforming [47, 49]. Moreover, the thermodynamics of methane steam reforming has also been investigated [47] and results have shown that excess of steam in the reformer feedstream is usually necessary to avoid coke formation. Methane steam reforming is in practice a combination of the following two reactions:

$$CH_4 + H_2O \leftrightarrows CO + 3H_2 \quad \Delta H = +206 \text{ kJ/mol} \qquad (11)$$

$$CO + H_2O \leftrightarrows CO_2 + H_2 \quad \Delta H = -41 \text{ kJ/mol} \qquad (12)$$

where the forward reaction of (1) is favored by high temperature and low pressure. On the other hand, water-gas shift reaction (2) is favored by low temperature but is largely unaffected by changes in pressure. The thermodynamic analysis of methane utilization in SOFCs has been undertaken by Demin et. al. [50] and more recently by Chan and Wang [51] assuming both alternatives of external steam reforming and partial oxidation.

Table 2.5. Physical and chemical properties of various fuel cell fuels

Fuel	Boiling point, °C	Density, g/cm^3	Combustion heat, kJ/g	Viscosity, g/cm s	Specific heat, J/g K	Flammability (in air), % v/v	Autoignition temperature, K	Flash point, K
Natural gas	-161.4	$0.72\ 10^{-3}$	55.68	$1.09\ 10^{-4}{}_{(g)}$	$2.22_{(g)}$	5.0-15.0	811	288.6_{open}, 285.2_{closed}
Methanol	64.7	0.787	22.67	$5.41\ 10^{-3}{}_{(l)}$, $9.68\ 10^{-5}{}_{(v)}$	$2.53_{(l)}$	6.3-39.2	843	85
Ethanol	78.4	0.789	29.81	$1.2\ 10^{-3}{}_{(l)}$	$2.41_{(l)}$	3.5-15.0	698	286_{closed}
Gasoline	125.7	0.703	44.37	$2.92\ 10^{-3}{}_{(l)}$	2.02	1.4-7.6	519	315.92
Hydrogen gas	-252.7	$0.85\ 10^{-4}$	123.17	$8.74\ 10^{-5}{}_{(g)}$	$14.34_{(g)}$	4.0-75.0	833	-

The disadvantages of methane, can be summarized by its high chemical stability and by the high cost involved for its handling and transportation from remote sites. Moreover, high dependency on natural gas imports is an important economical concern for many governments and environmental impact from greenhouse gases of methane combustion is inevitably another disadvantage. Due to these drawbacks, research on the utilization of alternative liquid fuels such as methanol and ethanol, attracted significant interest during the last years.

2.5.3. Methanol

Pure methanol, CH_3OH, is a colorless liquid with boiling point at 65.15°C (at 1atm) and density of 0.7914 g/cm^3 (at 20°C). It is commonly called wood alcohol because it was originally made by pyrolysis of wood. The present manufacture is exclusively by synthesis from an appropriate mixture of carbon monoxide and hydrogen in presence of catalyst at high pressure and temperature:

$$CO + 3H_2 \rightarrow CH_3OH \quad \Delta H = -90.64\ J/mol \qquad (3)$$

Although the carbon monoxide-hydrogen mixture may be derived from many sources, the preferred source is methane through the reaction (1) [52]. Due to this dependence on natural gas reserves, methanol is accompanied by many of the aforementioned disadvantages of natural gas, is more expensive per Joule of energy and contributes also in greenhouse effect. Significant advantage of methanol is easy storage and transportation though it attacks many gasket materials as well as metals and alloys currently used in gasoline fuel tanks. Safety problems are also important due to its high toxicity and also because methanol-air mixtures are explosive over some of the ambient temperature range.

The thermodynamic analysis of methanol steam reforming has been recently undertaken by Ye Lwin et. al. [53]. However, the examined temperature range was between 350-600 K and information has limited practical value for SOFC operation that takes place above 650°C in order the solid electrolyte to be conductive to oxygen ions. The most widely used catalysts for methanol steam reforming are copper containing, since copper has been found to be highly active and selective for hydrogen [54, 55].

2.5.3. Ethanol

Pure ethanol, C_2H_5OH, is a colorless liquid with a boiling point at 78°C (at 1atm) and density of 0.789 g/cm^3 (at 20°C) [56]. It is readily manufactured either chemically from ethylene or biochemically from biomass. Indeed, as raw matter for ethanol manufacture may be considered every cellulosic material containing sugar or starch (i.e. sugar canes, sugar beets, sorghum, corn etc.). Manufacture technology of ethanol from biomatter is practically unchanged for years and relies on the microbial fermentation of the sugars or on the hydrolysis of the starch-containing compounds to the corresponding sugar-containing [57-60]. Due to the natural availability of bioethanol, it is considered an

Table 2.6. Qualitative evaluation of potential fuels for fuel cells

Fuel	Production	Storage	Safety	Distribution infrastructure	Environmental attributes
Natural gas	Abundant domestic or imported feedstock.	Stored in compressed gas cylinders.	• Low flashpoint. • Non-carcinogenic • Dissipates into the air in open areas. • Adequate training recquired to operate safely.	Limited infrastructure.	• Non-renewable. • Possible increase in nitrogen oxide emissions.
Methanol	Abundant domestic or imported natural gas feedstock	Requires special storage because fuel can be corrosive to rubber, plastic and some metals.	• Toxic and can be absorbed through the skin. • Wide flammability limit. • No visible flame. • Adequate training required to operate safely.	Infrastructure needs to be expanded .	High greenhouse gas emissions when manufactured from coal.
Ethanol	Made from domestic renewable sources: wood, rice, straw, sugar beets, sugar canes etc.	Requires special storage because fuel can be corrosive to rubber, plastic and some metals.	• Less toxic than methanol and gasoline. • Adequate training required to operate safely.	Nearly no infrastructure.	Zero net carbon dioxide accumulation in atmosphere when manufactured from residues.
Gasoline	• Large existing production operation from imported feedstocks. • No energy security or trade balance benefits.	Conventional storage tanks.	• Low flashpoint. • Narrow flammability limits. • Potentially carcinogenic when inhaled.	Existing infrastructure and distribution network.	• Greenhouse gases. • Hydrocarbon, sulfur oxide and nitrogen oxide emissions.

alternative fuel with positive impact both on economy [61] and environment. Ethanol combustion produces just the products required by nature to recompose ethanol molecules through photosynthesis, and therefore net CO_2 contribution in atmosphere can be negligible.

Although ethanol steam reforming has been investigated for hydrogen production in various reports [62-64], the analysis of ethanol utilization in SOFCs was undertaken only by Tsiakaras et. al. [65]. In this work, ethanol steam reforming was recognized as the most appropriate external process allowing SOFC efficiencies of the order of 90%. Finally, it must be stressed that when ethanol steam reforming is employed to feed a SOFC system, azeotropic or impure (containing water) ethanol derived directly from biomass may be used avoiding the distillery cost.

2.5.4. Gasoline

Gasoline utilization in Otto internal combustion engines has been the most salient technological choice in the sector of transportation during the second half of the 20th century. Gasoline is a depletable energy source of variable composition but in calculations can be well represented by n-octane. Although gasoline utilization in fuel cells is currently quite controversial due to economical, environmental and governmental issues, existing infrastructure for handling and dispensing fuel gasoline includes it also between the fuels available for fuel cells. Reforming of gasoline has been thermodynamically examined by Docter and Lamm [66] and Thomas et. al. [67] for fuel cell vehicle applications. However, gasoline utilization in SOFCs was examined scarcely.

REFERENCES

1. Faraday M., *Experimental-Untersunchugen uber Electrizitat, VII. Reihe. Von der electrochemischen Zersetzung.* 1834, in *Ostwalds Klassiker der exakten Naturwissenchaften*, Ostwald. A. von, Editor: Liepzig 1897. p. 39-106.
2. Vetter K. J., *Electrochemical Kinetics*, 1967: Academic Press, New York.
3. Thomas S. and Zalbowitz. M., *Fuel Cells: Green Power*. 1999, Los Alamos National Laboratory: New Mexico, USA.
4. Schottky W., *Uber stromliefernde Prozesse im Konzentrationsgefalle fester Electrolyyte.* Wiss Veroff Siemens-Werke, 1935. **14**(2): p. 1-19.
5. Tsiakaras P. E., Ph.D. Thesis, 1993. University of Patras: Patras-Greece.
6. Davy H., *Electrochemische Untersuchungen, Vorlesung am 19.11.1807, Verfahrensarten, um die feuerbestandingen Alkalien zu zersetzen*, 1807, in *Ostwalds Klassiker der exakten Naturwissenchaften*, Ostwald. W, Editor: Liepzig 1893. p. 52-55.
7. Faraday M., *Experimental-Untersuchungen uber Elektrizitat, IV. Reihe. Uber eine neues Gesetz der Elektrizitatsleitung.*, 1833, in *Ostwalds Klassiker der exakten Naturwissenchaften*, Ostwald .A. von, Editor: Leipzig 1897. p. 39-55.
8. Hirtoff W., *Uber das elektrische Leitungsvermogen des Schwefelsilbers und Halbschwefelkupfers.* Ann Physik u Chem, 1851. **84**: p. 1-28.
9. Buff H., *Uber die Zersetzung des Wassers durch sehr schwache elektrische Strome, insbesondere durch die Maschinen-Elektrizitat.* Ann Chem Pharm, 1855. **96**: p. 257-286.
10. Gaugain J-M., *Note sur les signes electriques attribues au mouvement de la chaleur.* C R Seances Acad Sciences, 1853. **37**: p. 82-84.
11. Becquerel AC., *Note sur la production des courants pyroelectriques.* C R Seances Acad Sciences, 1854. **38**: p. 905-910.
12. Buff H., *Uber die elektrische Beschaffenheit der Flamme.* Ann Chem Pharm, 1851. **80**: p. 1-16.
13. Gaugain J-M., *Note sur une classe nouvelle de couples gazeux.* C R Seances Acad Sciences, 1853. **37**: p. 584-588.
14. Nernst W., *Verfahren zur Erzeugung von elektrischem Gluhlicht.*. 1899, DRP 104 872, filed 6.7.1897.
15. Nernst W., *Uber die elektrolytische Leitung fester Korper bei sehr hohen Temperaturen.* Z Electrochem, 1899. **6**: p. 41-43.
16. Nernst W., *Material for electric lamp glowers.* 1901, US-P 685 730, filed 24.8.1899.
17. Bartel H-G., Scholz G., and Scholz F., *Die Nernst-Lampe und ihr Erfinder.* Z Chem, 1983. **23**: p. 277-287.
18. Mobius H-H., *On the history of solid electrolyte fuel cells.* Journal of Solid State Electrochemistry, 1997. **1**: p. 2-16.
19. Wagner C., *Uber den Mechanismus der elektrischen Stromleitung im Nernststiff.* Naturwissenschaften, 1943. **31**: p. 265-268.
20. von Helmholtz H., *Die Thermodynamik chemischer Vorgange I, II, III. Sitzungsber Akad Wiss Berlin 2.2.1882, 27.7.1882, 31.5.1883*, in *Wiss Abhandlungen, Ambrosius Barth,* Leipzig, **2** (1883): pp. 958-978, 979-992 and **3** (1895): pp.92-114.
21. Ostwald W., *Die wissenschaftliche Elektrochemie der Gegenwart und die technische der Zukunft.* Z Electrochem, 1894. **1**: p. 81-84, 122-125.
22. Haber F. and Moser A., *Das Generatorgas - und das Kohlenelement.* Z Electrochem, 1905. **11**: p. 593-609.
23. Baur E. and Brunner R., *Uber die Eisenoxyd-Kathode in der Kohle-Luft-Kette.* Z Electrochem, 1937. **43**: p. 725-727.
24. Kiukkola K. and Wagner C., *Measurements on Galvanic Cells Involving Solid Electrolytes.* J. Electrochem Soc., 1957. **104**: p. 379-387.
25. Etsell T.H. and Flengas S.N., *The electrical properties of solid oxide electrolytes.* Chem Rev, 1970. **70**: p. 339-376.
26. Chebotin M.V. and Perfilyev M.V., *Electrochemistry of solid electrolytes.* 1978: Moscow -Khimiya.
27. Perfilyev M.V., Demin A.K., and Kuzin B.L., *High-temperature electrolysis of gases.* 1988: Moscow - Nauka.
28. Kharton V. V., Naumovich E. N., and V.A. A., *Research on the electrochemistry of oxygen ion conductors in the former Soviet Union. I. ZrO^2-based ceramic materials.* Journal of Solid State Electrochemistry, 1999. **3**: p. 61-81.
29. Ezersky M.L., et al., Neorg Mater, 1968. **4**(1599).
30. Lipilin A.S., Neuimin A.D., and Palguev S.F., Tr Inst Electrochim Ural Akad Nauk SSSR, 1976. **24**: p. 72-77.
31. Palguev S.F., Gorelov V.P., and Volchenkova Z.S., Tr Inst Electrochim Ural Akad Nauk SSSR, 1973. **20**: p. 140-144.
32. Perfilyev M.V., Inozemtsev M.V., and Vlasov A.N., Elektrokhimiya, 1982. **18**: p. 1230.

33. Hirschenhofer J. H., et al., *Fuel Cell Handbook.* 4th Edition ed. 1997, Orinda, USA.: Business/Technology Books.
34. de Boer B., *SOFC Anode: Hydrogen oxidation at porous nickel and nickel/yttria-stabilised zirconia cermet electrodes.* 1998: Proefschrift Technische Universiteit of Twente, Enshcede - The Netherland.
35. Minh N. Q. and Takahashi T., *Science and technology of ceramic fuel cells.* 1995: Amsterdam - The Netherlands. Elsevier Science B.V.
36. Seiyama T., *Total oxidation of hydrocarbons on perovskite oxides.* Catal. Rev.-Sci. Eng., 1992. **34**(4): p. 281-300.
37. Kharton V. V., Yaremchenko A. A., and Naumovic E.N., *Research on the electrochemistry of oxygen ion conductors in the former Soviet Union. II. Perovskite-related oxides.* Journal of Solid State Electrochemistry, 1999. **3**: p. 303-326.
38. van Heuveln F., *Characterization of porous cathodes for application in Solid Oxide Fuel Cells.* 1997: Proefschrift Technische Universiteit of Twente, Enschede - The Netherlands.
39. Acres G. J. K., et al., *Electrocatalysts for fuel cells.* Catalysis Today, 1997. **38**: p. 393-400.
40. Benjamin T.G., Camara E.H., and Marianowski L.G., *Handbook of Fuel Cell Performance.* May 1980: Institute of Gas Technology, Chicago-Illinois.
41. Kalhammer F. R., et al., *Status and prospects of fuel cells as automobile engines.* 1998: Fuel Cell Technical Advisory Panel. Sacramento-California, USA.
42. Singhal S. C., *Advances in solid oxide fuel cell technology.* Solid State Ionics, 2000. **135**: p. 305-313.
43. Isenberg A.O. in *Symposium on electrode materials and processes for energy conversion and storage.* 1977: Pennington-New Jersey, The Electrochemical Society, Inc.
44. Yamamoto O., et al., Solid State Ionics, 1987. **22**: p. 241.
45. Bockris J.O'M., *Hydrogen economy in the future.* International Journal of Hydrogen Energy, 1999. **24**: p. 1-15.
46. Armor J. N., *The multiple roles for catalysis in the production of H2.* Applied Catalysis A: General, 1999. **176**: p. 159.
47. Ridler D. E. and Twigg M. V., *Steam reforming*, in *Catalyst Handbook*, Twigg M. V., Editor. 1996, Chapter 5: Manson Publishing Ltd, London-England.
48. *Fuel cells: Opening new frontiers in power generation.* November 1999: U.S. Department of Energy, Office of Fossil Energy, Federal Energy Technology Center.
49. Clarke S. H., et al., *Catalytic aspects of the steam reforming of hydrocarbons in internal reforming fuel cells.* Catalysis Today, 1997. **38**: p. 411-423.
50. Demin A. K., et al., *Thermodynamic Analysis of Methane Fueled Solid Oxide Fuel Cell System.* Int. J. Hydrogen Energy, 1992. **17**(6): p. 451-458.
51. Chan S. H. and Wang H. M., *Thermodynamic analysis of natural-gas fuel processing for fuel cell applications.* International Journal of Hydrogen Energy, 2000. **25**: p. 441-449.
52. Bridger G. W. and Spencer M. S., *Methanol Synthesis*, in *Catalyst Handbook*, Twigg M. V., Editor, 1996, p. 441-468: Manson Publishing Ltd., London-England.
53. Ye Lwin, et al., *Hydrogen Production from Steam-Methanol Reforming: Thermodynamic Analysis.* International Journal of Hydrogen Energy, 2000. **25**: p. 47-53.
54. Kobayashi H., Takezawa N., and Minochi C., *Methanol reforming reaction over copper containing mixed oxides.* Chemical Letters, 1976: p. 1347.
55. Amphlett J. C., Mann R. F., and Weir R. D., *Hydrogen production by the catalytic steam reforming of methanol. Part 3: Kinetics of methanol decomposition using C18HC catalyst.* Canadian Journal of Chemical Engineering, 1988. **66**: p. 950.
56. *Guidebook for handling, storing & dispensing fuel ethanol.* 1998: U.S. Department of Energy, Center for Transportation Research, Argonne National Laboratory, U.S.A.
57. Margiloff I. B., Reid A. J., and O'Sullivan T. J., *Ethanol: Manufacture and Applications*, in *Monohydric Alcohols.* 1981, p. 441-468: Washington D. C.
58. McMillan J. D., *Bioethanol production: status and prospects.* Renewable Energy, 1997. **10**(2/3): p. 295-302.
59. Prince R. G. H. *The outlook for liquid fuels from biomass.* in *3rd World Congress of Chemical Engineering.* 1986: Tokyo- Japan.
60. Wyman C. E., *Applications of cellulose conversion technology to ethanol production from corn.* 1994: Alternative Fuel Division, National Renewable Energy Laboratory: Colorado, U.S.A.

61. Evans M. K. *The economic impact of the demand for ethanol.* in *Midwestern Governors' Conference.* 1997: Lombard-Illinois, U.S.A.
62. Garcia E. Y. and Laborde M. A., *Hydrogen production by the steam reforming of ethanol: thermodynamic analysis.* International Journal of Hydrogen Ennergy, 1991. **16**(5): p. 307-312.
63. Vasudeva K., et al., *Steam reforming of ethanol for hydrogen production: Thermodynamic analysis.* International Journal of Hydrogen Energy, 1996. **21**(1): p. 13-18.
64. Fishtik I., et al., *A thermodynamic analysis of hydrogen production by steam reforming of ethanol via response reactions.* International Journal of Hydrogen Energy, 2000. **25**: p. 31-45.
65. Tsiakaras P., et al., *Ethanol Utilization in Solid Oxide Fuel Cells: A Thermodynamic Approach.* Ionics, 1999. **5**: p. 206-212.
66. Docter A. and Lamm A., *Gasoline fuel cell systems.* Journal of Power Sources, 1999. **84**: p. 194-200.
67. Thomas C. E., et al., *Fuel options for the fuel cell vehicle: hydrogen, methanol or gasoline?* International Journal of Hydrogen Energy, 2000. **25**: p. 551-567.

CHAPTER 3

"PHYSIOLOGY" OF FUEL CELLS: THERMODYNAMICS AND KINETICS

ABSTRACT

This chapter describes the deduction of information about the operational characteristics of fuel cells in a mathematical basis. Thermodynamic and kinetic principles are revisited under the concept of fuel cell operation. Therefore, a fundamental distinction is made between chemical and electrochemical processes and an insight is accomplished to the differences between ideal and real fuel cells. Again, the interest is concentrated in SOFCs. Finally, a comparative discussion clarifies the advantages of fuel cells towards conventional energy conversion systems.

3.1. INTRODUCTION

Thermodynamics is concerned with the relations between the observable properties of macroscopic pieces of matter. It is essentially an empirical science based on accumulated experience of the behavior of real systems. According to thermodynamics, measurable macroscopic properties can be explained and interrelated simply and axiomatically. Therefore, it is the starting point for the analysis of every engineering system in which interactions of matter and energy take place. It examines each process according to the macroscopic properties of the initial and final states, taking into account the magnitude of driving forces for each property change. Therefore, an equilibrium state is a state where no driving forces for such changes exist.

Due to macroscopic considerations, thermodynamics generally ignores the microscopic mechanisms which comprise a process. Therefore, it is only capable to answer the "if"-type questions about the accomplishment of a process and is generally in a weak position to estimate "when", "how" and "how quickly" the process will proceed. This weakness is profound in the case of catalytic reactions where, in principle, the presence of a catalyst cannot be taken into account thermodynamically. To overcome these impediments, experimental data of reaction kinetics are necessary. Thus, reaction kinetics is generally an experimental analysis method leading to information about the rates and mechanisms of reactions. In other words, kinetics focuses on the microscopic actions and mechanisms that compose the overall macroscopic process.

During fuel cell operation, both chemical and electrochemical phenomena are involved. Chemical reactions on the electrocatalysts and charge transfer processes in electrode/electrolyte interfaces are representative processes of chemical and electrochemical nature, respectively. Hence, both thermodynamic and kinetic approaches should be adopted for both types of reactions. Formation of equilibrium potential differences is equivalent with the establishment of chemical equilibrium, in the sense that thermodynamics can lead to conclusions. On the other hand, the study of overpotentials in the electrode/electrolyte interfaces is equivalent with the study of the rates of chemical

reactions, since both require a microscopic kinetic analysis.

3.2. THERMODYNAMICS

3.2.1. Chemical Reactions

The heat of a reaction is defined as the energy absorbed by the system of reaction when the products are kept at the temperature of reactants. To strictly define the thermodynamic states of the reactants and products, their pressure must be stated. In the case were the reactants and products are at the same pressure, the heat of the reaction is equal to the enthalpy change:

$$\Delta H = H_{reactants} - H_{products.} \quad (1)$$

Thus, the heat of every reaction can be calculated from the heats of formation or the heats of combustion of the reactants and products. Data for these calculations can be found at almost every book of thermodynamics [1, 2].

In absence of experimental data, various methods for calculation of the heat of a reaction can be followed. Reid, Prausnitz and Poling [3] described the most reliable method that is applicable to combounds of carbon, hydrogen, oxygen, nitrogen and alogons. The change of the heat of reaction with temperature depends on the differences of the molecular thermal capacities of reactants and products. Therefore,

$$\Delta H_T = \Delta H_{T_0} + \int_{T_0}^{T} \Delta c_p dT \quad (2)$$

where

$$\Delta c_p = \sum \left(N_i c_{p_i}\right)_{products} - \sum \left(N_i c_{p_i}\right)_{reactants},$$

and N_i, c_{p_i} are the numbers of moles and the thermal capacity under constant pressure of the species i, respectively. For known average thermal capacities $\overline{c_p}$ of the species involved in the temperature range between T_0 and T, Eq. (2) can be simplified as

$$\Delta H_T = \Delta H_{T_0} + (T - T_0)\left(\sum \left(N_i \overline{c_{p_i}}\right)_{products} - \sum \left(N_i \overline{c_{p_i}}\right)_{reactants}\right) \quad (3).$$

Details about the methods used to determine the effect of temperature and pressure on the heat of reactions are also available in literature [1].

When a reaction takes place in equilibrium, temperature and pressure are constant and the change in free energy is zero ($\Delta G=0$). These restrictions can lead to the following expression for the change of standard free energy ΔG° and the equilibrium constant of the reaction K:

$$\Delta G^\circ = -R_g T \ln K \quad (4)$$

where R_g is the gas constant. ΔG° expresses the difference between the free energies of the reactants and products when they are both in the standard state which, for ideal gases, corresponds at the 298K and 1atm. On the other hand, for a single reaction between ideal gases in the scheme

$$\alpha A + \beta B \rightleftarrows \gamma \Gamma + \delta \Delta, \quad (5)$$

the equilibrium constant K is expressed as

$$K = \frac{P_\Gamma^\gamma P_\Delta^\delta}{P_A^\alpha P_B^\beta}, \quad (6)$$

where, for example the partial pressure P_A of the gas A is in relation with the total pressure P_t through the molar fraction y_A of the gas in its mixture, as follows

$$P_A = P_t \, y_A. \quad (7)$$

It is therefore evident that, the knowelege of K allows the estimation of the equilibrium composition. In the case where two or more reactions take place simoultanously, the method of Langrange's multipliers may be considered as most applicable for the solution of such thermodynamic problems [2].

3.2.2. Electrochemical Reactions – Ideal Cell Potential.

The maximum electrical work obtainable from a fuel cell (W_{el}) under isothermal and isobaric operation is the change of the free energy due to the overall electrochemical reaction, i.e.,

$$W_{el} = \Delta G = -nFE \quad (8)$$

where n represents the number of electrons involved in the overall electrochemical reaction, F is Faraday's constant and E is the potential of the cell. In the case where both reactants and products are in the standard state, it is

$$\Delta G^\circ = -nFE^\circ \quad (9)$$

Table 3.1. Fuel cell reactions and corresponding Nernst equations

Overall Cell Reaction	Nernst Equation
$H_2 + ½\ O_2 \rightarrow H_2O$	$E = E^\circ + \left(\frac{RT}{2F}\right)\ln\left[\frac{P_{H_2}}{P_{H_2O}}\right] + \left(\frac{RT}{2F}\right)\ln\left[P_{O_2}^{1/2}\right]$
$H_2 + ½\ O_2 + CO_{2(c)} \rightarrow H_2O + CO_{2(a)}$	$E = E^\circ + \left(\frac{RT}{2F}\right)\ln\left[\frac{P_{H_2}}{P_{H_2O}\left(P_{CO_2}\right)_{(a)}}\right] + \left(\frac{RT}{2F}\right)\ln\left[P_{O_2}^{1/2}\left(P_{CO_2}\right)_{(c)}\right]$
$CO + ½\ O_2 \rightarrow CO_2$	$E = E^\circ + \left(\frac{RT}{2F}\right)\ln\left[\frac{P_{CO}}{P_{CO_2}}\right] + \left(\frac{RT}{2F}\right)\ln\left[P_{O_2}^{1/2}\right]$
$CH_4 + 2O_2 \rightarrow 2H_2O + CO_2$	$E = E^\circ + \left(\frac{RT}{8F}\right)\ln\left[\frac{P_{CH_4}}{P_{H_2O}^2 P_{CO_2}}\right] + \left(\frac{RT}{8F}\right)\ln\left[P_{O_2}^2\right]$

where the superscript "°" indicates the standard state (298K, 1atm).

From the above it is evident that, in the case of fuel cells, the maximum available work that can be derived from a fuel source is related with the free energy of the reaction, in contrast to thermal engines were the maximum available work is related with the enthalpy change, given as

$$\Delta G = \Delta H - T\Delta S. \qquad (10)$$

The entropy change, ΔS, is manifested in changes in the degrees of freedom for the chemical system being considered. The maximum available electrical work is ΔG, as mentioned above, and the total thermal energy available is ΔH. The amount of heat that is produced by a reversibly operating fuel cell is $T\Delta S$. Reactions in fuel cells that have negative entropy change generate heat, while those with positive entropy change may extract heat from their surroundings, if the reversible generation of heat is smaller than the reversible absorption of heat.

By differentiating Eq. (10) with respect to temperature or pressure, and substituting into Eq. (8), it is obtained that

$$\left(\frac{\partial E}{\partial T}\right)_P = \frac{\Delta S}{nF} \qquad (11)$$

or

$$\left(\frac{\partial E}{\partial P}\right)_T = \frac{-\Delta V}{nF}. \qquad (12)$$

These equation express the effect of temperature and pressure on the ideal potential, E, of the fuel cell. Morerover, since,

$$\Delta H_T = \Delta H^\circ + \int_{298}^{T} \Delta C_p dT \qquad (13)$$

and

$$\Delta S_T = \Delta S^\circ + \int_{298}^{T} \frac{\Delta C_p}{T} dT, \qquad (14)$$

the ideal potential of the cell at a given temperature T can be calculated by using ΔS° and ΔH° values for the reaction at the standard temperature of 298K taking into account the variation of c_{p_i} with temperature. Finally, for the general reaction (5), Eqs. (4) and (6) give,

$$\Delta G = \Delta G^\circ + RT \ln \frac{[\Gamma]^\gamma [\Delta]^\delta}{[A]^\alpha [B]^\beta}. \qquad (15)$$

By substituting Eqs. (8) and (9) in Eq. (15), it is

$$E = E^\circ + \frac{RT}{nF} \ln \frac{[A]^\alpha [B]^\beta}{[\Gamma]^\gamma [\Delta]^\delta} \qquad (16)$$

or,

$$E = E^{\circ} + \frac{RT}{nF} \ln \frac{\prod_i a_i}{\prod_j a_j} \qquad (17)$$

which is the generalized expression of Nernst's equation. Obviously, the potential of the cell increases with the activity (concentration), a_i, of the reactants and decreases with the activity, a_j, of products. Changes in temperature affect also the potential of the cell depending on the the overall cell reaction. The reactions and the corresponding Nernst equation of the fuel cell reactions discussed in Chapter 2 are presented in Table 3.1.

3.3. KINETICS

From an engineering point of view, reaction kinetics has the following principal functions:

- establishing the chemical mechanism of a reaction,
- obtaining experimental rate data,
- correlating rate data by equations or other means,
- designing suitable reactors, and
- specifying operation conditions, control methods, and auxiliary equipment to meet the technological and economic needs of the reaction process.

3.3.1. Chemical Kinetics

The term "rate of reaction" denotes the rate of decomposition of a reacting substance A per unit volume,

$$r_A = -\frac{1}{V}\frac{dn_A}{dt} \quad \text{mol/(unit time)(unit volume)} \qquad (18)$$

$$= \frac{n_{A0}}{V}\frac{dx_A}{dt}, \quad n_0 = n_{A0}(1 - x_A) \qquad (19)$$

where x_A is the fractional conversion of substance A. Similarly, the rate of a reaction may be expresses with respect the rate of the formation of a product. Hence, the negative sign in Eqs. (18) and (19) is required for the rate of decomposition to be a positive number. When the volume is constant, the rate of decomposition may be expressed as

$$r_A = -\frac{dC_A}{dt}. \qquad (20)$$

The effect of concentration on the rate is isolated through the "law of mass action", as

$$r_A = kf(C_A, C_B, \ldots)$$

where the specific rate k is independent on concentration but depends on temperature, catalyst, and other factors. The law of mass action states that the rate of the reaction is proportional to the concentration of the reactants. For the reaction,

$$\nu_A A + \nu_B B + \nu_\Gamma \Gamma + \ldots \rightarrow \nu_\Lambda \Lambda + \nu_M M + \ldots \qquad (21)$$

the rate equation is

$$r_A = -\frac{1}{V}\frac{dn_A}{dt} = kC_A^p C_B^q C_\Gamma^r \ldots. \qquad (22)$$

$$\Rightarrow -\frac{dC_A}{dt} \quad \text{at constant volume.} \qquad (23)$$

The exponents (p, q, r, ...) are empirical, but they are identical with the stoichiometric coefficients ($\nu_A, \nu_B, \nu_\Gamma, \ldots$) when the stoichiometric equation truly represents the mechanism of reaction. The first group of exponents identifies the "order" of the reaction and the stoichiometric coefficients the "molecularity" of the reaction.

Depending on the conditions, the rate of a chemical reaction may be controlled by different mechanisms of chemical or physical nature. For example, ethylene oxidation over MnO_2 catalysts has been found being controlled by the rate of the reaction at low temperatures, by internal diffusion of reactants in the porous catalyst at intermediate temperatures and by external diffusion of reactants to the catalyst surface at high temperatures [4]. This dependence of the overall rate of a process on the rate of a step of the overall mechanism is due to the determing role of the slower step at the conditions of the experiment. The "rate determining step" of the process imposes the rate for the overall process.

The accomplishment of a natural phenomenon (chemical or physical) may be spontaneous ($\Delta G<0$), impossible ($\Delta G>0$) or forced. Forced accomplishment implies that the phenomenon may proceed to completion only in case an energy barrier be overcome. For example, a reaction which is in rest at certain conditions may proceed rapidly in completion by increasing temperature (absorbing heat energy), intervening a catalyst (addition of surface energy) or both. The energy amount required to be given in a mole of a reactant to transform into product is termed "activation energy" of the reaction (Figure 3.1).

The Arrhenius equation interelates the specific rate with the absolute temperature,

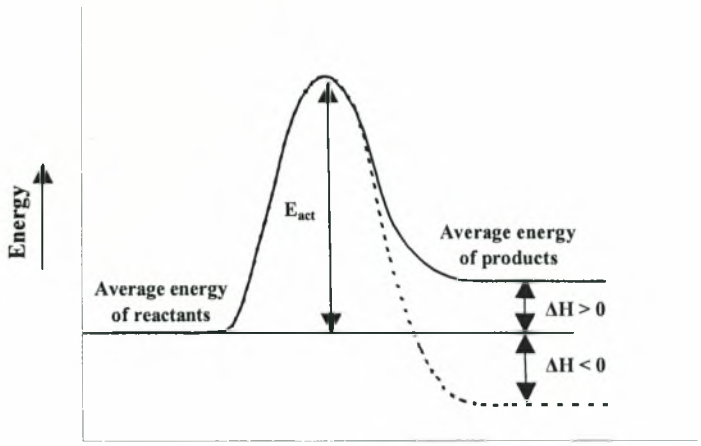

Figure 3.1. Indicative illustration of activation energy, E_{act}, in exothermic ($\Delta H<0$) and endothermic ($\Delta H>0$) reactions.

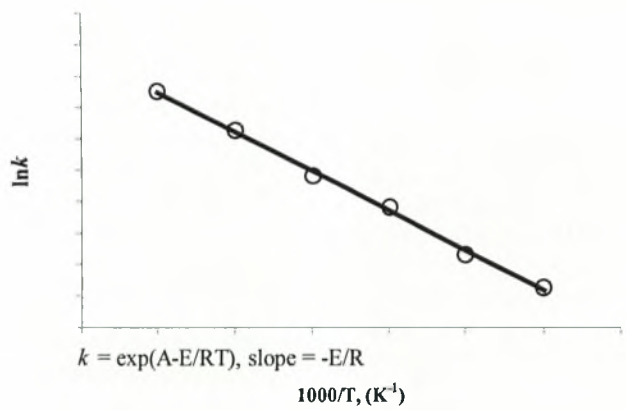

Figure 3.2. Typical Arrhenius plot for chemical reactions.

$$k = k_0 \exp\left(\frac{-E_{act.}}{RT}\right) \quad (24)$$

or

$$\ln\frac{k}{k_0} = \frac{-E_{act.}}{RT}, \quad (25)$$

where k_0 is the "pre-exponential factor". As a result, Arrhenius equation allows for the estimation of the activation energy of the reaction when accurate data are available for the rate of the reaction at different temperatures, since it forecasts a linear $\ln k = f(T^{-1})$ behavior. Such a behavior is shown in Figure 3.2 as a typical case of many real reactions. According to the Arrhenius plot, the activation energy of the reaction can be calculated from the slope, $(-E_{act.}/R)$ of the linear $\ln k = f(T^{-1})$ dependence. When presumably accurate data deviate from Eq. (25), the reaction is supposed to be controlled by a more complex mechanism.

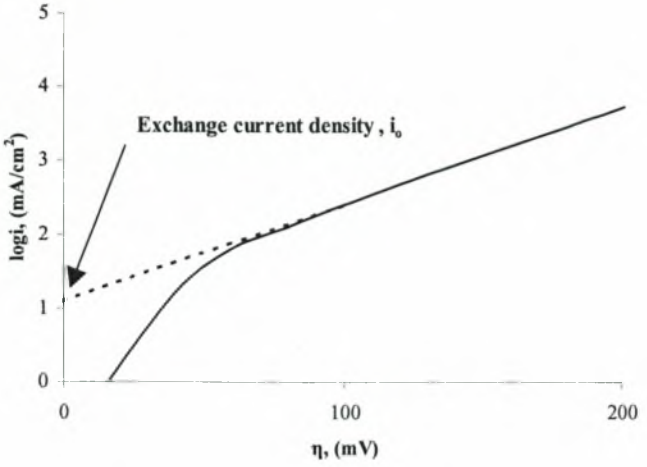

Figure 3.3. Typical Tafel plot.

3.3.2. Electrohemical Kinetics and Overpotentials.

Thermodynamics defines the maximum equilibrium potential established in a fuel cell according to the Nernst equation. However, kinetic analysis of the processes of charge transfer taking place at the gas/electrode or electrode/electrolyte interfaces reveals potential losses that render Nernst potential unattainable in practice. These potential losses, usually termed as "overpotentials", are classified as follows [5, 6]:

- activation overpotential (η_{act}) – due to slow charge transfer processes in the interfaces,
- ohmic overpotential (η_{ohm}) – equal to the product of the current intensity, I, and the overall ohmic resistance, R, of the cell, and
- concentration overpotential, (η_{conc}) – due to the concentration gradient of the reactants and products on the catalytic surfaces.

3.3.2.1. Activation Overpotential

Activation overpotential appears when the rate of the electrochemical (charge transfer) reaction which takes place on an electrode is controlled by sluggish electrode kinetics. In other words, activation overpotential is closely related with the rates of electrochemical reactions. Chemical and electrochemical reactions are rather similar in the fact that they are both equally characterized by their activation energies. In the case of an electrochemical reaction with $\eta_{act} > 50$-100 mV, η_{act} is described by a semi-empirical equation, called "Tafel equation". Activation polarization is expressed as

$$\eta_{act} = \frac{RT}{\alpha n F} \ln \frac{i}{i_o}, \qquad (25)$$

where α is the electron transfer coefficient of the reaction at the electrode being addressed, and i_o is the exchange current density. Tafel plots provide a visual understanding of the activation polarization of a fuel cell. They are used to measure the exchange current density [given by the extrapolated intercept at $\eta_{act} = 0$ which is a measure of the maximum current that can be extracted at negligible polarization] and the transfer coefficient (from the slope).

The usual form of the Tafel equation that can be easily expressed by a Tafel Plot is

$$\eta_{act} = a + b \log i \qquad (26)$$

where $a = (-2.3RT/\alpha nF) \log i_o$ and $b = 2.3RT/\alpha nF$. The term b is called "the Tafel slope", and is obtained by the slope of a plot of η_{act} as a function of log i. The Tafel slope for an electrochemical reaction is about 100 mV/decade (log current density) at room temperature. Thus, a tenfold increase in current density causes a 100 mV increase in the activation polarization. Conversely, if the Tafel slope is only 50 mV/decade, then the same increase in current density produces a 50 mV increase in activation polarization. Clearly, there exists a strong

incentive to develop electrocatalysts that yield a lower Tafel slope for electrochemical reactions.

3.3.2.2. Ohmic Overpotential

Ohmic losses occur because of resistances to the flow of ions in the electrolyte and the flow of electrons through the electrode materials. The dominant ohmic losses through the electrolyte, are reduced by decreasing the electrode separation and enhancing the ionic conductivity of the electrolyte. Because both the electrolyte and fuel cell electrodes obey Ohm's law, the ohmic losses can be expressed as

$$\eta_{ohm} = iR \qquad (27)$$

where i is the current flowing through the cell, and R is the total cell resistance, which includes electronic, ionic and contact resistance.

3.3.2.3. Concentration Overpotential

As a reactant is consumed at the electrode by electrochemical reaction, there is a loss of potential due to the inability of the surrounding material to maintain the initial concentration of the bulk phase where a concentration gradient is formed. Several processes may contribute to the concentration polarization; slow diffusion in the gas phase in the electrode pores, solution/dissolution of reactants/products into/out of the electrolyte, or diffusion of reactants/products through the electrolyte to/from the electrochemical reaction site. The rate of mass transport to an electrode surface in many cases can be described by Fick's first law of diffusion:

$$i = \frac{n F D (C_B - C_S)}{\delta} \qquad (28)$$

where D is the diffusion coefficient of the reacting species, C_B is its bulk concentration, C_S is its surface concentration, and δ is the thickness of the diffusion layer. The limiting current (i_L) is a measure of the maximum rate at which a reactant can be supplied to an electrode, and occurs when $C_S = 0$, i.e.,

$$i_L = \frac{n F D C_B}{\delta} \qquad (29)$$

By appropriately manipulating Eqs (28) and (29), it is

$$\frac{C_S}{C_B} = 1 - \frac{i}{i_L} \qquad (30)$$

The Nernst equation for the reactant species at equilibrium conditions, or when no current is flowing, is

$$E_{i=0} = E^\circ + \frac{RT}{nF} \ln C_B \qquad (31)$$

When current is flowing, the surface concentration becomes less than the bulk concentration, and the Nernst equation becomes

$$E_{i=0} = E^\circ + \frac{RT}{nF} \ln C_S \qquad (32)$$

The potential difference (ΔE) produced by a concentration change at the electrode is called the concentration polarization:

$$\Delta E = \eta_{conc} = \frac{RT}{nF} \ln \frac{C_S}{C_B} \qquad (33)$$

or (Eq. (30)),

$$\eta_{conc} = \frac{RT}{n F} \ln\left(1 - \frac{i}{i_L}\right) \qquad (34)$$

where i_L is the limiting current. For practically useful values of current densities, slow transport of reactants/products to/from the electrochemical reaction site is a major contributor to concentration polarization.

3.3.2.4. Overall Overpotential

Activation and concentration polarization can exist at both the positive (cathode) and negative (anode) electrodes in fuel cells. The total polarization at these electrodes (designated by subscripts "c" and "a" respectively) is the sum of η_{act} and η_{conc}, or

$$\eta_{anode} = \eta_{act,\,a} + \eta_{conc,\,a} \qquad (35a)$$

and

$$\eta_{cathode} = \eta_{act,\,c} + \eta_{conc,\,c} \qquad (35b)$$

The effect of polarization is to shift the potential of the electrode ($E_{electrode}$) to a new value ($V_{electrode}$):

$$V_{electrode} = E_{electrode} \pm |\eta_{electrode}|. \qquad (36)$$

where the positive sign is valid for anode and negative for cathode. The net result of current flow in a fuel cell is a decrease of the cell voltage due to the increment of the

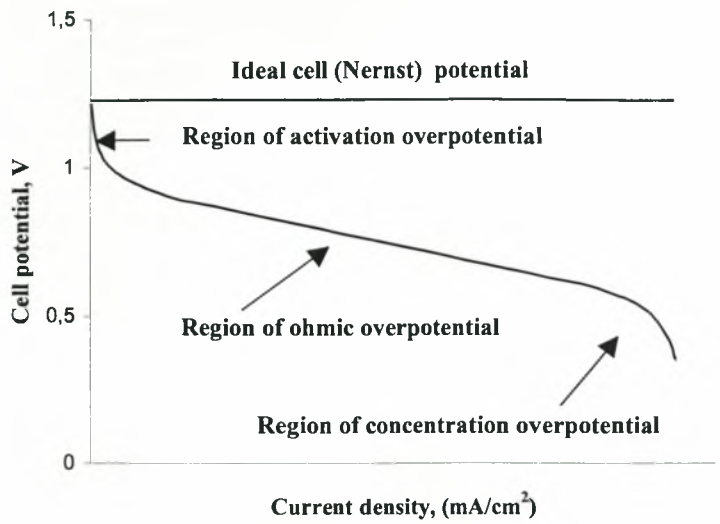

Figure 3.4. Ideal and actual fuel cell voltage/current characteristics.

anode potential and the decrement of the cathode potential.

3.4. ACTUAL FUEL CELL PERFORMANCE

The cell voltage includes the contribution of the anode and cathode potentials and ohmic polarization:

$$V_{cell} = V_{cathode} - V_{anode} - iR. \quad (37)$$

When Eqs. (35a), (35b) and (36) are substituted in Eq. (37),

$$V_{cell} = E_{cathode} - |\eta_{cathode}| - (E_{anode} - |\eta_{anode}|) - iR \quad (38)$$

or

$$V_{cell} = \Delta E_e - |\eta_{cathode}| - |\eta_{anode}| - iR \quad (39)$$

where $\Delta E_e = E_{cathode} - E_{anode}$. Eq. (39) shows that current flow in a fuel cell results a decrease in the cell voltage because of losses by electrode and ohmic polarizations. These losses result a cell voltage (V) for the fuel cell that is less than its ideal potential, E (V = E - Losses).

Useful work (electrical energy) is obtained from a fuel cell only when a reasonable current is drawn, but the actual cell potential decreases from its equilibrium potential because of irreversible losses as shown in Figure 3.4. The activation polarization loss is dominant at low current density. At this point, electronic barriers have to be overcome prior to current and ion flow. Activation losses show some increase as current increases. Ohmic polarization (loss) varies directly with current, increasing over the whole range of current because cell resistance remains essentially constant. Gas transport losses occur over the entire range of current density, but these losses become prominent at high limiting currents where it becomes difficult to provide enough reactant flow to the cell reaction sites.

The goal of fuel cell developers is to minimize the polarization in order for V_{cell} to approach ΔE_e. This goal is approached by modifications to fuel cell design (improvement in electrode structures, better electrocatalysts, more conductive electrolyte, thinner cell components, etc.). For a given cell design, it is possible to improve the cell performance by modifying the operating conditions (e.g., higher gas pressure, higher temperature, change in gas composition to lower the gas impurity concentration). However, for any fuel cell, compromises exist between achieving higher performance by operating at higher temperature or pressure and the problems associated with the stability/durability of cell components encountered at the more severe conditions.

Large, complex computer models are used to characterize the actual operation of fuel cells based on minute details of cell component design (physical dimensions, materials, etc.) along with physical considerations (transport phenomena, electrochemistry, etc.). These codes, often proprietary, are needed in the design and development of fuel cells, but would be cumbersome and time consuming for use in system analysis. Simpler approaches are normally used for

system studies. One approach, for example, would be to conduct tests at every condition expected to be analyzed in the system; this would, however, be very costly. Instead, it is prudent to develop correlations based on thermodynamic modeling that depict cell performance as various cell operating conditions are changed, such as temperature, pressure, and gas constituents. Thermodynamic modeling is used to depict the equations so that only a limited number of tests are needed to define design constants within the equation. Adjustments can be applied to a reference performance at known operating conditions to achieve the performance at the desired operating conditions.

3.4. FUEL CELL EFFICIENCY

3.4.1. Thermodynamic efficiency

In an fuel cell the free enthalpy change of the cell reaction, ΔG, may be totally converted to electrical energy. Thus a fuel cell has an intrinsic (maximum) thermodynamic efficiency given by,

$$\eta_T = \frac{\Delta G}{\Delta H} = 1 - \frac{T\Delta S}{\Delta H}. \quad (40)$$

3.4.2. Heating efficiency

The heating efficiency must be considered in cases where the fuel contains inert gases, impurities and other combustibles in addition to the electrochemically active species. The heating value efficiency, η_H, is defined as:

$$\eta_H = \frac{\Delta H^0}{\Delta H_{com}} \quad (41)$$

where ΔH^0 represents the amount of enthalpy of fuel species available in the fuel cell to generate electricity and ΔH_{com} represents the amount of enthalpy included in all combustible species in the fuel gases fed to the fuel cell.

3.4.3. Voltage efficiency

In an operating fuel cell the cell voltage is always less than the reversible voltage. As the current is drawn from the fuel cell, the cell voltage is reduced due to overpotentials. The reduction in the cell voltage under current load depends on current density and several factors such as temperature, pressure, gas flow rate, gas combustion and cell material. The voltage efficiency, η_V, is defined as the ratio of the operating cell voltage under load, V_{cell}, to the equilibrium cell voltage, E^0, and is given as

$$\eta_V = \frac{V_{cell}}{E^0}. \quad (42)$$

3.4.4. Current efficiency

The efficiency of a SOFC drops in the case where not all of the reactants are converted to reaction products. For 100% conversion of a fuel, the amount of current density produced, i_F, is given as (Faraday's law)

$$i_F = nF\frac{df}{dt} \quad (43)$$

where *df/dt* is the molar flow rate of the fuel. For the amount of fuel actually consumed, the current density produced is given by

$$i = nF\left(\frac{df}{dt}\right)_{consumed} \quad (44)$$

The current efficiency, η_J, is the ratio of the actual current produced to the current available from complete electrochemical conversion of the fuel

$$\eta_J = \frac{i}{i_F} \quad (45)$$

In the case of fuel cells, the current efficiency is commonly expressed as fuel utilisation.

3.4.5. Overall cell efficiency

The overall efficiency of a fuel cell, η_{cell}, is the product of the electrochemical efficiency, η_E, times the heating efficiency, η_H. The electrochemical efficiency is the product of the thermodynamic efficiency, η_T, the voltage efficiency, η_V, and the Faradaic or current efficiency, η_J, of the fuel cell. Thus,

$$\eta_{cell} = \eta_E\eta_H = \eta_T\eta_V\eta_J\eta_H. \quad (46)$$

3.5. COMPARISON OF FUEL CELLS AND HEAT ENGINES.

3.5.1. Ideal fuel cells and Carnot limitations

It is commonly and misleadingly said or written that fuel cells exhibit higher efficiencies than heat engines because they are not subjected to the limitations of Carnot. Fuel cells are "non-Carnot limited" in that their

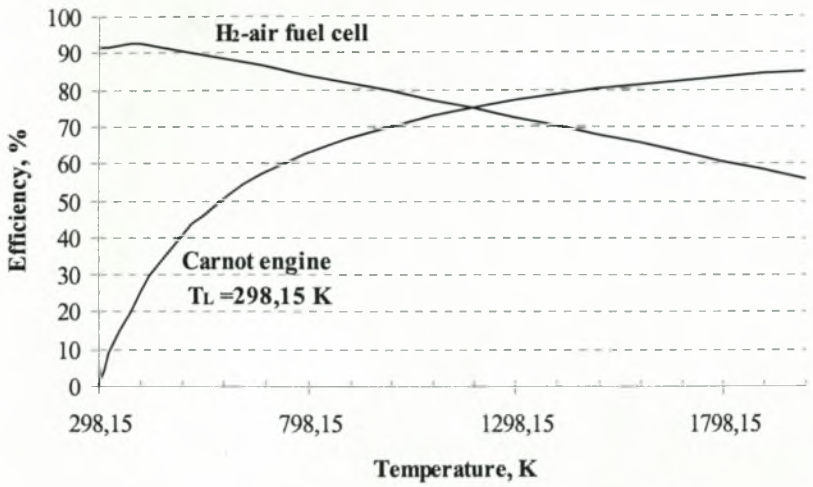

Figure 3.5. Effect of temperature on the thermodynamic efficiency of an ideal H_2-air fuel cell and a Carnot heat engine.

operation is not a function of temperature reservoirs, but one must be careful not to conclude that an ideal fuel cell is a better energy converter than is a Carnot cycle. Both units are perfect energy conversion devices that conserve the supply of *exergy* received by them.

As it will be discussed in Chapter 5 of this thesis, a figure of merit of an energy system is how well it conserves the exergy supplied to it or, in other words, the magnitude of exergy desrtuction that accompanies the operation of the system due to irreversibilities. Exergy is the part of the amount of energy that is transformable into useful work and, for all actual systems, although energy is conserved, exergy degrades.

By comparing an ideal fuel cell and an externally reversible heat engine, a difference exists in that the exergy supply of the ideal fuel cell is due to supply of a *chemical fuel* while the exergy supply of the ideal heat engine is due to supply of *heat*. Under the assumption that both ideal systems receive energy flows containing the same exergy amount, one may writte the equality

$$\sum_i \left(\dot{n}_i e_i \right)_{\text{inlet, fuel cell}} = \left[1 - \frac{T_0}{T_H} \right] \dot{Q}_H \qquad (47)$$

where the term on left hand side represents the chemical exergy input of the ideal fuel cell and the right hand side represents the thermal exergy input of the ideal engine. Since both systems are ideal, their efficiency is maximum, all exergy received by them is converted and the output product of both devices has zero exergy. Therefore, by considering both devices as reversible thermodynamic "black boxes", they are both exhibiting the same productivity and they are both providing the same work output.

Most references which state that fuel cells have better performance than Carnot cycles are making the comparison in regard to both systems being fed by the same chemical reactants. This type of comparison, however, forces an indirect link between Carnot cycles and combustion irreversibilty. Since externally reversible heat engines do not generate entropy while combustion is highly irreversible, this link between combustion processes and Carnot efficiency is inappropriate [7]. Although the comparison made in the previous paragraph is thermodynamically sound, a more practical comparison in terms of the same chemical exergy input would require the comparison of a fuel cell system with a combustion power system. In this case, the lack of combustion irreversibilty is the primary reason for the higher efficiencies of fuel cell systems, as it will be discussed in Chapter 5.

3.5.2. Effect of temperature on thermodynamic efficiency

As mentioned, the thermodynamic efficiency of ideal fuel cells is given by Eq. (40). This intrinsic thermodynamic efficiency depends on the fuel used for the cell reaction. Further, a significant parameter is the operation temperature of the cell. For H_2-air and CO-air fuel cells (this is also the case for fuel cells receiving the products of external reforming), an increase of the operation temperature reflects in a decrement of ΔG without significant change in ΔH. Hence, in these cases the efficiency decreases with temperature increment.

A comparison between the thermodynamic efficiency of an ideal H_2-air fuel cell with that of a heat engine as a function of temperature is given in Figure 3.5. Obviously, the thermodynamic efficiency of an ideal heat engine is the Carnot efficiency given as

$$\eta_{HE}=\frac{T_H-T_L}{T_H}=1-\frac{T_L}{T_H} \qquad (48)$$

where T_H and T_L represent the absolute temperatures of the high and low temperature reservoirs of the heat engine, respectively. Under the assumption of T_L=298.15K, Figure 3.5 illustrates that the higher is the temperature T_H of the heating source of the engine the higher is the Carnot efficiency. On the other hand, for an ideal H_2-air fuel cell, efficiency decreases with temperature as was discussed.

Figure 3.5 clearly shows that electrochemical conversion of chemical energy into work in a fuel cell does not depend as strongly by temperature as for heat engines. The issue is that fuel cells may efficiently produce electricity even when their operation temperature is near the temperature of the environment while heat engines require a heat source of high temperature. Therefore, the "non-Carnot limited" label for fuel cells in this case, is appropriate in that their efficiency is not subjected to temperature limitations as highly as heat engines.

As it will be discussed in Chapter 5, the thermodynamic efficiencies of fuel cells being fed directly (without external reforming) by hydrocarbons, are considerably higher than the efficiencies of H_2-air and CO-air fuel cells. Especially for hydrocarbon-air fuel cells operating above 100°C which involve steam generation in vapor phase, the change of Gibbs free energy ΔG which is associated to the cell oxidation reaction is higher than ΔH because changes in entropy ΔS are positive [8]. This causes the thermodynamic efficiencies of hydrocarbon-air fuel cells to be greater than 100%. This occurrence implies that, theoretically, hydrocarbon-air fuel cells are able to overcome the barrier of 100% thermodynamic efficiency but practically significant difficulties arise due to carbon formation and high overpotential problems. If sufficient advances in electrocatalysis could be made to reduce the overpotentials and inhibit carbon formation on anode electrocatalysts of these fuel cells (mainly SOFCs), especially high efficiencies could be attained.

Finally, an important misconception must be avoided during the analysis of high temperature fuel cells, such as MCFCs and SOFCs. Given that high temperature fuel cells produce electrical work due to electrochemical oxidation reaction and a heat flux at the elevated temperature of cell operation, T_{cell}, the estimation of the maximum work obtainable from such a device must consider also a Carnot heat engine receiving the heat flux and operating between the temperature levels of T_{cell} and T_0=298.15K. This encounter allows the assumption of maximum exergy exploitation and approximates the reversible ideal cell operation. Equivalently, such an analysis may proceed assuming an adiabatic SOFC operation as in this case all exergy loss associated with the heat flux is considered to remain as part of the exergy of the SOFC eflluents. In either case, the ideal fuel cell efficiency may be accurately stated as follows [7]:

$$\eta_{ideal}=\frac{-\Delta G+\left(1-T_0/T_{cell}\right)\dot{Q}_{rejected}}{-\Delta H} \qquad (49)$$

3.5.3. Fuel flexibility and safety

When a power system is designed for peak efficiency at the lowest lifetime cost, tradeoffs are usually encountered that force the system to operate in a certain control parameter space. In addition, only one fuel can be used to achieve this peak efficiency. Employing other secondary fuels normally results in greatly reduced efficiency, reliability and operating range. For fuel cell systems, however, the development of a reliable, fuel-flexible system can be accomplished with relatively little effort during the design stage. The designer will simply be required to account for any new thermal demands/dissipations due to the variation in fuel, and ensure that the reformer and fuel cell continue to operate effectively. Clearly, each fuel type will result in its own performance curve, and some fuels will be able to provide higher current and/or efficiency than others, but the risk of entering an unstable/dangerous mode of operation is very small.

This stability feature of fuel cells is largely attributed to the fact that the distribution of flow over the many cells prevents the entire mass of flow to experience coherent (high energy) instability, and the fact that the major fuel cell processes (reactant gas delivery and electrochemical conversion) are sufficiently decoupled. That is, the electrochemical rates may depend on gas delivery rates, but gas delivery rates do not depend much on the electrochemical rates. This is not the case for other power technologies, such as IC engines or gas turbines, in which chemical reactions and flow dynamics/turbulence are integrally linked, or where distinct flow features have similar time scales and can become mutually excited/enforced (e.g. vortex mixing and acoustics) [9].

REFERENCES

1. Smith J. M., Van Ness H. C., and Abbott M. M., *Introduction to chemical engineering thermodynamics*. 1996: McGraw-Hill, Inc.
2. Perry R. H., Green D. W., and M.J. O., Editors. *Perry's Chemical Engineers' Handbook*. 7th ed. 1997, Chapter 4, p. 33-34: McGraw-Hill, Inc.
3. Reid R.C., Prausnitz J.M., and Poling B.E., *The properties of gases and liquids*, 4th Edition., 1988: International Edition, McGrraw-Hill Books-Co., Singapore.
4. Smith J. M., *Chemical Engineering Kinetics*. 1981: McGraw-Hill.
5. Bockris J'O.M. and Reddy A.K.N., *Modern Electrochemistry*. 1977: Plenum/Rosetta edition, New York.
6. Hirschenhofer J. H., et al., *Fuel Cell Handbook*. 4th Edition. 1997: Business/Technology Books, Orinda-USA.
7. Haynes C., *Clarifying reversible efficiency misconceptions of high temperature fuel cells in relation to reversible heat engines*. Journal of Power Sources. **92**, 2001: p. 199-203.
8. Kordesch K., and Simader G., *Fuel Cells and Their Applications*. 1997, p. 42-47: VCH Verlagsgesellschaft, Weinheim-Germany.
9. Richards G. A., McMillian M. M, Gemmen R. S., Rogers W. A. and Cully S. R., *Issues for low-emission, fuel-flexible power systems*, Progress in Energy and Combustion Science, **27**, 2001: p. 141-169.

Journal of Ionics, 5, 1999: p. 206-212
and AIChE Journal, 49(1), 2003: p. 248-257

CHAPTER 4

FUEL OPTIONS FOR SOFC SYSTEMS: FIRST LAW ANALYSIS

ABSTRACT

The eligibility of natural gas (methane), methanol, ethanol and gasoline as fuels for generation of electrical power in Solid Oxide Fuel Cells (SOFCs) is discussed by means of an analysis according to the first law of thermodynamics. Initially, the case of ethanol is examined assuming three different methods of external processing; a) steam reforming, b) carbon dioxide (dry) reforming and c) partial oxidation. The equilibrium mixture of each of these processes was assumed as a feedstream of a multi-cell SOFC stack. The analysis was carried out assuming carbon-free operation conditions at atmospheric pressure and in the temperature range of 800-1200 K. It was found that the preliminary process of the steam reforming of ethanol is advantageous in that it is able to provide higher overall efficiencies than dry reforming and partial oxidation. As a consequence, the external steam reformer – SOFC stack system is taken under consideration and a comparison between the most important fuel candidates for SOFC applications is presented. Results were obtained in terms of both electromotive force (emf) output and efficiency. It was found that methane seems to be the most appropriate fuel option with a SOFC system efficiency value close to 96%. Furthermore, methanol and ethanol were found to be very promising alternative options (90.3% and 93.5%, respectively), while gasoline (83.06%) utilization requires special reforming conditions.

4.1. INTRODUCTION

Solid oxide fuel cells (SOFCs) seem to be very promising for the direct conversion of chemical energy into electricity attaining significantly higher efficiencies with respect to other conventional systems such as gas turbines, internal combustion engines etc. Various fuel options are considered feasible for SOFC operation especially after an appropriate external process in order to obtain a gas mixture rich in hydrogen such as steam reforming. The electrochemically combustible species are usually H_2, CO and CH_4, but, it is common system analysis practice to assume that only H_2 contributes to power generation while CO and CH_4 are consumed through *in-situ* steam reforming providing additional amounts of H_2 [1, 2].

Methane, methanol, ethanol and gasoline are currently regarded as the most probable SOFC fuels due to a number of considerations dealing with their accessibility and their physical properties [3, 4]. Methane was the first fuel that has been investigated on high temperature operating cells both experimentally [5, 6] and theoretically [7, 8]. Gasoline has also been thermodynamically examined [9, 10] for fuel cell vehicle applications. It is a depletable energy source of variable composition but in calculations can be well represented by n-octane.

It is well known that both methane and gasoline are *mineral* fuels and that their deposits are limited enough to be considered as an appropriate long-term global solution for the energy problem. Furthermore, these fuels have a significant influence to the surcharge of the environmental pollution, mainly due to their high impact to the 'greenhouse effect'. These drawbacks have led researchers to pay significant interest on the utilization of alternative, renewable and environmental-friendly liquid fuels such as methanol and ethanol. Methanol is manufactured exclusively by a mixture of carbon monoxide and hydrogen most commonly derived by methane steam reforming [11]. The thermodynamic analysis of methanol steam reforming has been recently discussed [12] while a lot of experimental investigations have been presented during the last thirty years [13, 14]. Ethanol can be considered as a very promising and reliable fuel option for fuel cells because it can be alternatively produced biochemically from biomass [15-18]. Due to the natural availability of bioethanol, it is considered an alternative fuel with positive impact both on economy [19] and environment. Although ethanol steam reforming has been variously investigated for hydrogen production [20-22], the analysis of ethanol utilization in SOFCs was undertaken by Tsiakaras et. al. [23].

In the present work, a comparison of the eligibility of methane, methanol, ethanol and gasoline as fuels for generation of electrical power in SOFCs is presented in terms of both electromotive force (emf) output and system efficiency. A mathematical model has been developed in order to adequately estimate, according to the method of the direct minimization of Gibbs free energy, the spatial variance of the molar fractions of the components that are involved to the chemical reactions taking place within the SOFC system.

4.2. MODEL DEVELOPMENT

Independently of the fuel used in a SOFC with an oxygen-ion-conducting electrolyte, its operation principle relies on the continuous supply of fuel, H_2, CO and CH_4 at the anode compartment while cathode is exposed at atmospheric air. According to this operation regime, the following reaction takes place at the cathode

$$\tfrac{1}{2}\, O_{2\,(c)} + 2e^- \rightarrow O^{=}_{(e)} \qquad (1)$$

where the subscripts (*c*) and (*e*) represent the states at the cathode and in the electrolyte, respectively. At the anode, the reaction of electrochemical hydrogen oxidation occurs as

$$H_{2\,(a)} + O^{=}_{(e)} \rightarrow H_2O_{(a)} + 2e^-, \qquad (2)$$

where the subscript (*a*) represents the state at the anode [24]. The overall cell reaction is the sum of eqs. (1) and (2) and the reversible electromotive force is given by the Nernst equation

$$E = \frac{RT}{4F} \ln \frac{P_{O_2,(c)}}{P_{O_2,(a)}}, \qquad (3)$$

where R is the gas constant, T is the temperature, F is the Faraday constant and P_{O_2} is the partial pressure of oxygen on the electrode. Oxygen partial pressure at the anode is calculated taking into account that oxygen is in equilibrium with hydrogen and steam according to reaction

$$H_2 + \tfrac{1}{2}\, O_2 \rightleftarrows H_2O \qquad (4)$$

and, therefore, is equal to

$$P_{O_2,(a)} = \left(\frac{P_{H_2O,(a)}}{K P_{H_2,(a)}} \right) \qquad (5)$$

where K is the equilibrium constant of the reaction (4).

In the frame of this consideration it is assumed that oxygen utilization from air fed to the cathode is negligible, so that oxygen partial pressure at the cathode is constant to $P_{O_2,(c)} = 0.209$. Therefore, the value of E depends on the partial pressure of the oxygen in the anode, i.e. on the fuel type and composition fed to the anode. Thus, SOFC power output depends both on the fuel choice and on the preliminary method of fuel processing.

The overall reaction of the steam reforming of a fuel represented as $C_aH_bO_c$, can be expressed generally as

$$C_aH_bO_c + mH_2O \rightarrow \sum_i n_i A_i \qquad (6)$$

or, equivalently, as

$$C_aH_bO_c + mH_2O \rightarrow n_{CO}\, CO + n_{CO2}\, CO_2 + n_{H2}\, H_2 + n_{H2O}\, H_2O + n_{CH4}\, CH_4 \qquad (7)$$

where *m* is the reforming factor. In the right hand of eq. (5), only the species that are allowed to exist in equilibrium with noticeable concentrations have been considered, as follows from previous works [6, 9, 12, 21]. Therefore, the composition of the equilibrium mixture derived by eq. (5) for each fuel can be calculated according to thermodynamical methods.

Equations and formulation of the method of direct minimization of Gibbs free energy

The initial 10x10 system

$$(\Delta G^f_{fuel}/RT)_T + \ln y_{fuel} + a\,\lambda_C + b\,\lambda_H + c\,\lambda_O = 0 \quad (8)$$

$$(\Delta G^f_{H2O}/RT)_T + \ln y_{H2O} + 2\,\lambda_H + \lambda_O = 0 \quad (9)$$

$$(\Delta G^f_{CO}/RT)_T + \ln y_{CO} + \lambda_C + \lambda_O = 0 \quad (10)$$

$$(\Delta G^f_{CO2}/RT)_T + \ln y_{CO2} + \lambda_C + 2\,\lambda_O = 0 \quad (11)$$

$$(\Delta G^f_{CH4}/RT)_T + \ln y_{CH4} + \lambda_C + 4\,\lambda_H = 0 \quad (12)$$

$$\ln y_{H2} + 2\,\lambda_H = 0 \quad (13)$$

$$a\,y_{fuel} + y_{CO} + y_{CO2} + y_{CH4} = b_C / n \quad (14)$$

$$b\,y_{fuel} + 2\,y_{H2O} + 4\,y_{CH4} + 2\,y_{H2} = b_H / n \quad (15)$$

$$c\,y_{fuel} + y_{H2O} + y_{CO} + 2\,y_{CO2} = b_O / n \quad (16)$$

$$y_{fuel} + y_{H2O} + y_{CO} + y_{CO2} + y_{CH4} + y_{H2} = 1 \quad (17)$$

The modified 3x3 system

$$\left[a-c\left(\frac{b_C}{b_O}\right)\right]K y^c_{H2O} y^a_{CH4} y^{4-c+b-2a}_{H2} - \left(\frac{b_C}{b_O}\right) y_{H2O} y^4_{H2} + \left[1-\left(\frac{b_C}{b_O}\right)\right] L y_{H2O} y_{CH4} y_{H2} + \left[1-2\left(\frac{b_C}{b_O}\right)\right] M y^2_{H2O} y_{CH4} + y_{CH4} y^4_{H2} = 0 \quad (18)$$

$$\left[b-c\left(\frac{b_H}{b_O}\right)\right]K y^c_{H2O} y^a_{CH4} y^{4-c+b-2a}_{H2} + \left[2-\left(\frac{b_H}{b_O}\right)\right] y_{H2O} y^4_{H2} - \left(\frac{b_H}{b_O}\right) L y_{H2O} y_{CH4} y_{H2} - 2\left(\frac{b_H}{b_O}\right) M y^2_{H2O} y_{CH4} + 4 y_{CH4} y^4_{H2} + 5 y^5_{H2} = 0 \quad (19)$$

$$K y^c_{H2O} y^a_{CH4} y^{4-c+b-2a}_{H2} + y_{H2O} y^4_{H2} + L y_{H2O} y_{CH4} y_{H2} + M y^2_{H2O} y_{CH4} + y_{CH4} y^4_{H2} + y^5_{H2} - y^4_{H2} = 0 \quad (20)$$

where

$$K = e^{(-\Delta G^f_{fuel} + \Delta G^f_{H2O} + 2\Delta G^f_{CH4})/RT} \quad (21)$$

$$L = e^{(\Delta G^f_{H2O} - \Delta G^f_{CO} + \Delta G^f_{CH4})/RT} \quad (22)$$

$$M = e^{(2\Delta G^f_{H2O} - \Delta G^f_{CO2} + \Delta G^f_{CH4})/RT} \quad (23)$$

The independent equations

$$\frac{y_{fuel} y^{(c-b+2a)}_{H2}}{y^c_{H2O} y^a_{CH4}} = K \quad (24)$$

$$\frac{y_{CO} y^3_{H2}}{y_{H2O} y_{CH4}} = L \quad (25)$$

$$\frac{y_{CO2} y^4_{H2}}{y^2_{H2O} y_{CH4}} = M \quad (26)$$

In the present analysis, equilibrium compositions were calculated according to the method of the direct minimization of Gibbs free energy [25]. Therefore, for each initial system of (Fuel + mH_2O), the system of nonlinear algebraic Eqs. (8)-(17) was considered. In this system, R represents the universal gas constant, $y_i = n_i / \sum_i n_i$ is the molar fraction of the i^{th} chemical species present in thermodynamic equilibrium, b_j are the numbers of the j atoms in the initial (Fuel + mH_2O) system, and λ_j are Langrange's multipliers used as scalar parameters.

According to simple analytical manipulations, the above system can be written as a 3x3 system of non-linear algebraic equations (Eqs. 18-20) and three separate equations solved independently (Eqs. 24-26). The non-linear system of Eqs. (18)-(20) was solved for y_{H2O}, y_{CH4} and y_{H2} by using a complicated Newton's iterative method [26], while a lot of effort has been paid in order to ensoure the independence of the solution on the arbitrary initial values. Furthermore, y_{fuel}, y_{CO} and y_{CO2} are obtained just by substituting y_{H2O}, y_{CH4} and y_{H2} from Eqs. (18)-(20) into Eqs. (24)-(26).

Considering that carbon formation on the SOFC anode deteriorates its operation lifetime and performance [5], the posibillity of carbon deposition in the gaseous equilibrium system was examined assuming the Boudouard reaction

$$2CO \leftrightarrows CO_2 + C \qquad (27)$$

For this purpose, the limiting reforming factors above which carbon deposition is thermodynamically impossible were calculated using the carbonization criterion

$$\alpha_C = K_{25} \frac{P_{CO}^2}{P_{CO_2}} \geq 1 \qquad (28)$$

where K_{25} is the equilibrium constant of Eq. (25). The locus of points corresponding to these minimum reforming factors will be now on described as "boundary of carbonization" (BC). Moreover, all conditions of SOFC operation have been selected to correspond above this boundary, where carbon deposition on the anode electrocatalyst to be thermodynamically impossible.

The equilibrium gas mixture coming from the reformer reacts in the anode compartment of the SOFC with oxygen ions coming from cathode, according to the general reaction

$$\sum_i n_i A_i + kO^{=} \rightarrow \sum_i n_i' A_i \qquad (29)$$

where k is equal to 4, 3, 6 and 25 for methane, methanol, ethanol and gasoline, respectively, and n_i' is the number of moles of the i^{th} component in SOFC anode outlet mixture. This equation is the sum of the following simultaneous reactions

$$CH_4 + H_2O \rightarrow CO + 3H_2 \qquad (30)$$

and

$$CO + H_2O \rightarrow CO_2 + H_2. \qquad (31)$$

and reaction (2).

It was shown that the SOFC stack has higher efficiency than a single cell. Therefore, in the present case it is assumed that the electrochemical section represents a multi-cell stack. Oxygen flux through the solid electrolyte was assumed uniform and the anode mixture composition in any point x of the channel can be therefore calculated by using Eq. (29) and substituting instead of k the following value

$$k_{(x)} = (1-\alpha)k, \qquad (32)$$

where $\alpha = x/L$ represents a dimensionless relative channel length.

After the calculation of the anode gas mixture distribution along the channel by using Eqs. (29) and (32), the oxygen partial pressure distribution was found by using Eq. (5) and, finally, the electromotive force distribution was calculated by using Eq. (3). An average electromotive force, $\bar{E}$, was calculated by means of numerical integration of E distribution along the cell channel. Thus,

$$\bar{E} = \int_0^L E(\alpha) d\alpha \qquad (33)$$

Finally, the maximum SOFC efficiency was calculated as

$$\eta = \frac{q\bar{E}}{-\Delta H^\circ}, \qquad (34)$$

where $-\Delta H^\circ$ is the lower heating value (LHV) of the fuel at the standard conditions and q is the electrical charge passing through the electrolyte, which has been set equal to q = 8F, 6F, 12F and 50F for methane, methanol, ethanol and gasoline, respectively. Maximum efficiency represents the upper limit for the efficiency of a SOFC runnning under zero-load conditions. The real SOFC runs under non-equilibrium conditions, i.e. the average cell voltage is less than $\bar{E}$. The actual SOFC efficiency can be obtained as [27]

$$\eta_{actual}=0.5\eta(1+\sqrt{1-p_r}). \quad (35)$$

where p_r is a relative power equal to a ratio of the current power to the maximum one at a definite temperature.

4.3. RESULTS

4.3.1. Comparison of preliminary methods of ethanol processing

The first step of the thermodynamic approach concerned the selection of the partial reactions that can well represent the processes of ethanol oxidation with steam, carbon dioxide and oxygen. Then, the full transformation of the system ethanol-oxidant can be expressed as follows:

$$\text{Ethanol} + \text{Ox} \rightarrow n_{CO}\,CO + n_{CO2}\,CO_2 + n_{H2}\,H_2 + n_{H2O}\,H_2O + n_{CH4}\,CH_4 \quad (36)$$

where Ox represents anyone of possible oxidants or their mixture.

The most accessible oxidants for ethanol oxidation are steam, carbon dioxide and oxygen. Initially, three systems were considered:

$$\text{system A: Ethanol} + r_1H_2O \quad (37)$$

$$\text{system B: Ethanol} + r_2CO_2 \quad (38)$$

$$\text{system C: Ethanol} + r_3O_2 \quad (39)$$

Then, taking into account that in practice it is senseless to use absolute ethanol as a fuel and pure oxygen as an oxidant, the following systems were also considered:

$$\text{system B}': \text{Ethanol} + r_{1a}H_2O + r_2CO_2 \quad (40)$$

$$\text{system C}': \text{Ethanol} + r_{1a}H_2O + r_3O_2 + r_4N^* \quad (41)$$

were r_{1a} represents the water/ethanol mole ratio in azeotropic ethanol alcohol and N^* all air components except oxygen. Taking into account that the azeotropic ethanol alcohol contains 96 vol% of ethanol and that the oxygen mole fraction in air is 0.209, one can obtain that $r_{1a} = 0.135$ and $N^* = 3.785$.

The calculation of the thermodynamic equilibrium composition that results from ethanol reaction with steam, CO_2 or O_2 was accomplished using the method of the direct minimization of the free energy, that has been discussed in detail previously. All calculations concerning SOFC electromotive force and efficiency were done for systems A, B′ and C′. A solid oxide fuel cell was supposed fed by the equilibrium mixture associated with each oxidant/ethanol feed ratio at each temperature value. Under this consideration the distribution of the molar fractions of the equilibrium species along the anode was also encountered. For each temperature, it was assumed that an inlet gas to the SOFC channel is an equilibrium mixture at or above the boundary of carbonization. When this mixture is passing along the anode the fuel components are gradually oxidizing electrochemically by oxygen spontaneously supplied through the electrolyte and the concentration of oxidizing components increases. The inlet gases, and especially those derived from the system A, contain some amount of methane. The latter does not take part in the reaction of electrochemical oxidation. Nevertheless methane concentration reduces in the inlet part of the channel due to its reforming by arising oxidants. Within the rest part of the channel, methane concentration is negligible and only electrochemical oxidation takes place. To the end of the channel, the fuel components disappear at all and only oxidants (and "nitrogen" for the systems C and C′) remain.

As it was previously demonstrated, fuel components can be, in principal, completely utilized in SOFC. Oxidation of the fuel components in the products of one ethanol mole reforming requires 3 oxygen moles. Therefore for the cases A, B and B′ it is $q = 12F$. The products of one ethanol mole partial oxidation contain fewer amounts of fuel components and only $(3 - r_3)$ moles of oxygen are required for their electrochemical oxidation. Therefore for the cases C and C′, it is

$$q = (12 - 4r_3)F. \quad (42)$$

Maximum efficiency was calculated using Eq. (34)

Figure 4.1a illustrates the carbonization boundaries associated with each oxidant for the cases of utilization of absolutely dry (dashed lines) and azeotropic ethanol (solid lines). In Figure 4.1a, the temperature dependencies of the mole ratios of the main oxidants to ethanol are plotted. The main oxidants are CO_2 and oxygen in cases B′ and C′, respectively. As one can observe, the region of the temperature and initial system conditions where carbon deposition is thermodynamically impossible increases from the case of partial oxidation to the case of CO_2 reforming. The different behavior can be reasonably explained by the oxidative force of each oxidant and by the contribution of the carbon from the CO_2. It is clear that for azeotropic ethanol which contains 4 vol% water, the amount of the main oxidant (CO_2 or oxygen) at the boundary of carbonization is less than for absolute ethanol. That is why the dashed lines for systems B′ (azeotropic ethanol + cabon dioxide) and C′ (azeotropic ethanol + oxygen) lie significantly lower with respect to the solid lines of the corresponding systems.

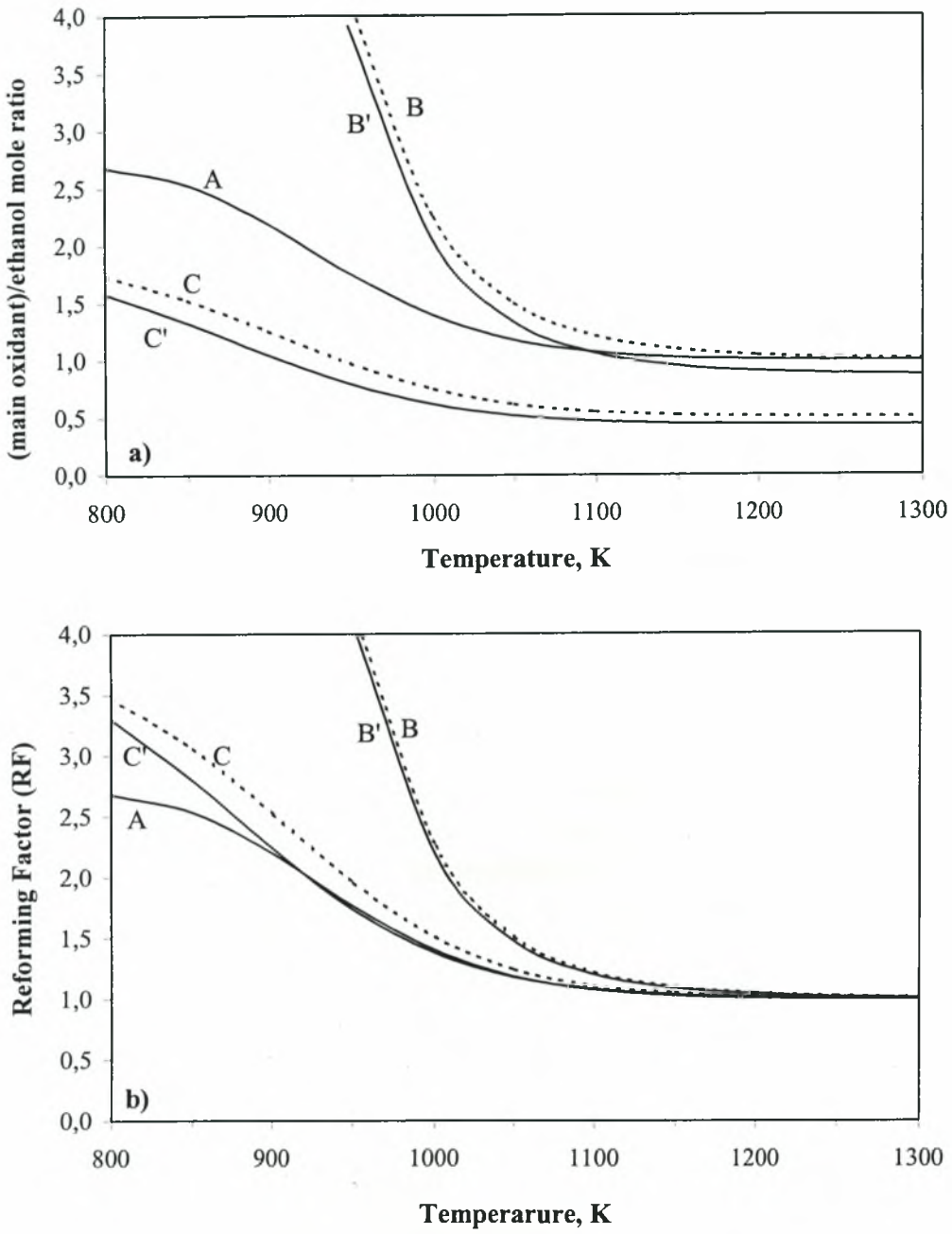

Figure 4.1. Effect of temperature on the boundary of carbonization expressed with a) main oxidant/ethanol mole ratio and b) reforming factor (RF).

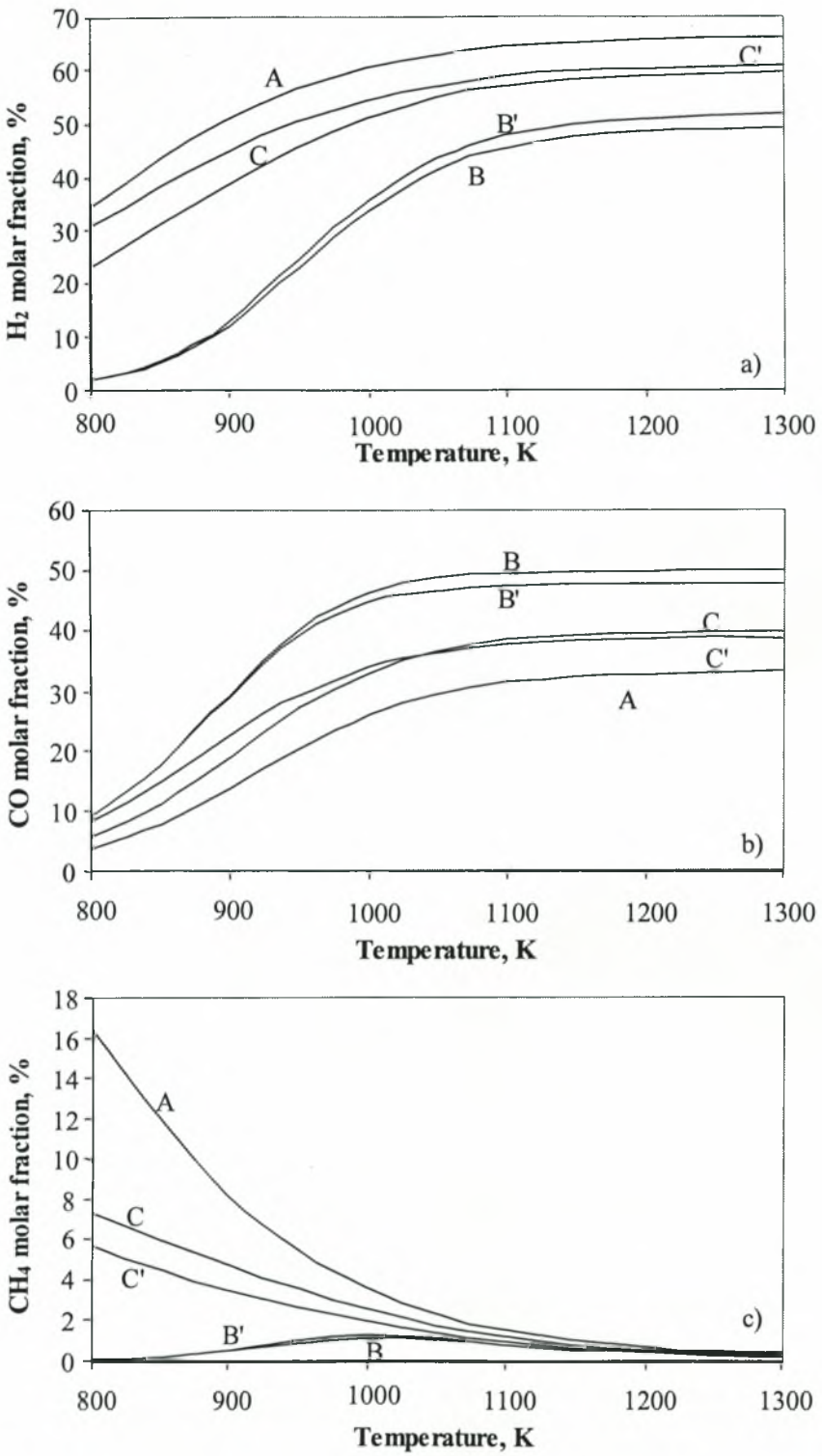

Figure 4.2. Effect of temperature on the equilibrium molar fractions of a) hydrogen b) carbon monoxide and c) methane.

For unification, it is very convenient to introduce a term called "reforming factor" (RF). This value is equal to the number of oxygen atoms of the oxidant that are able to oxidize ethanol. It is obvious that an oxygen molecule contains two of such atoms and a steam molecule contains just one. Although a carbon dioxide molecule contains two oxygen atoms, only one of them is able for ethanol oxidation. The reforming factor is given by the following expression:

$$RF = r_1 + r_2 + 2r_3 \qquad (43)$$

In Figure 4.1b is shown that at temperature values higher than 1150 K the reforming factors of all considered systems at the boundary of carbonization are practically the same. The reforming factors at the boundary of carbonization for the systems B and B′ are very close in all the examined temperature region. However, at temperature values less than 1100 K, they are significantly higher than those for other systems. If oxidant does not contain carbon, the reforming factors of the systems A, C and C′ at the boundary of carbonization and temperature values higher than 1050 K are almost identical. It is very interesting to point out that the reforming factors of the systems A and C′ at the boundary of carbonization are indistinguishable at temperature values higher than 900 K. Figures 4.2a, 4.2b and 4.2c illustrate the selectivity values (molar fractions) of H_2, CO and CH_4 respectively at equilibrium for the systems A, B′ and C′ and for conditions at the boundary of carbonization.

Figures 4.3a to 4.3c illustrate the emf distribution along the SOFC length for the systems A, B′ and C′, respectively. For all systems it is assumed that the inlet mixture is at the boundary of carbonization. Some reasonable limitations were done as concern the reforming factors. It is senseless to consider the system B′ if its reforming factor is more than 10. It is also clear that there is of no use to consider the system C' when its reforming factor is more then 2 because in this case one third of ethanol is loosing due to non-electrochemical combustion. Taking into account these two circumstances, the lower temperature selected for the systems B′ and C′ was 900K. For these systems this choice seems quite logical also because the molar fractions of the fuel components at low temperature for these systems are very low: around 10% for B′, less than 20% for C′ comparing with about 40% for A (see Figure 4.2).

On the whole, the emf does not change as strongly at the low temperature values as at the high temperatures. At low temperature values, emf changes significantly only the region close to the channel outlet, whereas at high temperature values it changes drastically both at the inlet and at the outlet of the channel. Within the wide

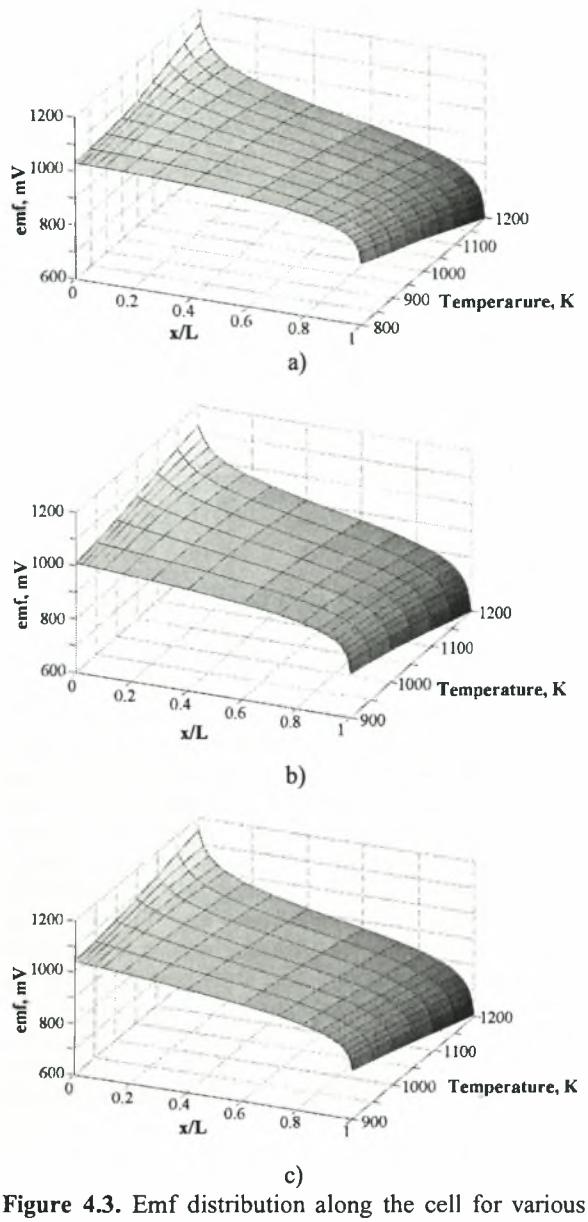

Figure 4.3. Emf distribution along the cell for various temperature values for the systems a) A, b) B′ and c) C′.

middle part of the channel, emf changes very slowly for all temperature values.

The temperature dependence of the maximum efficiency of the ethanol fueled SOFC system is illustrated in figure 4. For systems A and B' at the boundary of carbonization, the maximum SOFC system efficiency is very high in the entire temperature region and increases as the temperature decreases. On the whole,

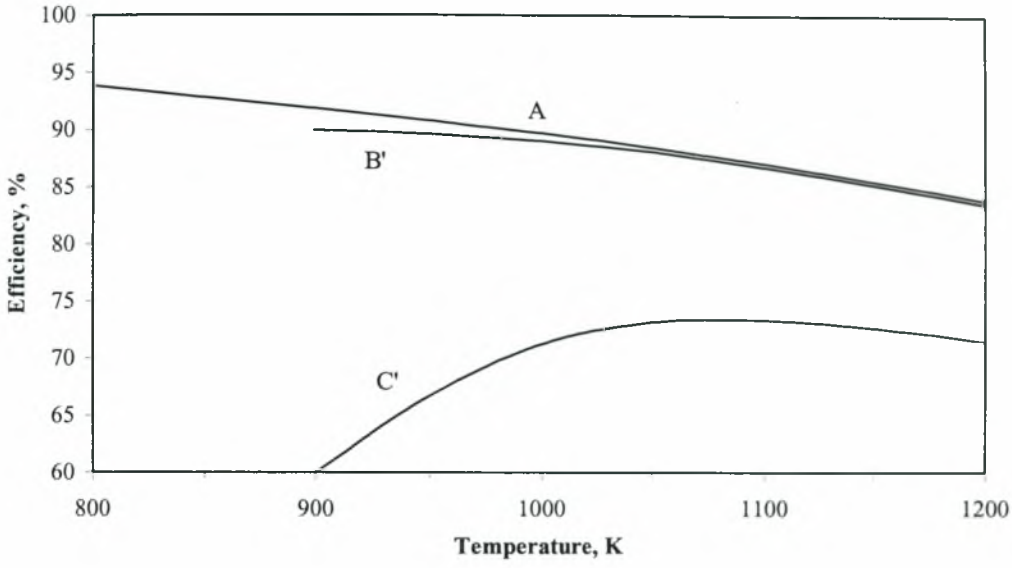

Figure 4.4. Dependence of SOFC theoretical efficiency on temperature for the systems A, B´ and C´.

the SOFC system efficiency in the case of ethanol steam reforming is higher than in the case of ethanol CO_2 reforming and exceeds 93% at 800 K, whereas the efficiency in the latter case doesn't exceed 90%. As to the efficiency in the case of ethanol partial oxidation, it is significantly less than in the previous cases. The temperature dependence of the efficiency in this case presents a maximum at about 1060 K and decreases strongly especially as the temperature decreases. The low SOFC system efficiency in this case is connected with a waste of significant amount of fuel due to non-electrochemical combustion of ethanol which becomes more important with increasing temperature.

It is clear that in practice it is necessary to use gas compositions above the boundary of carbonization. Figure 5a represents the dependence of maximum thermodynamic efficiency on the reforming factor for the SOFC system fueled by azeotropic ethanol for systems A (solid lines) and B' (dashed lines) while Figure 5b represents the same dependence for system C'. As it was mentioned above, it was assumed that the RF is less than 5 for systems A and B' and less than 2.4 for system C'.

As one can observe in figure 4.5a, the SOFC system efficiency for the systems A and B' is very high in all temperature regions and increases with decreasing both temperature and reforming factor. It can be seen, that within temperature interval 950 – 1100 K and reforming factors above the boundary of carbon deposition, the efficiency in the case of ethanol CO_2 reforming is higher than in the case of ethanol steam reforming, while under other conditions the SOFC system efficiency is higher in the latter case.

As it is shown in Fig. 4.5b, the SOFC system efficiency in the case of system C' (ethanol-oxygen feed) is significantly lower compared to the other systems. The temperature dependence of the efficiency in this case exhibits a maximum at ~ 1060 K, and the efficiency strongly decreases with decreasing temperature. It should be finally stressed out that the results of SOFC efficiency with the systems A and B are based on the assumption of heat transfer from the SOFC to the reforming section to account for the endothermicity of the reforming step. Such an assumption is not necessary for system C, which is generally exothermic because of the use of oxygen as an oxidant. Due to these obsrevations, the following paragraphs are concerned with the eligibility of natural gas, methanol, ethanol and gasoline for application in steam reformer – SOFC stack systems.

4.3.2. Comparison of methane, methanol, ethanol and gasoline fuel options

The conditions conducive for carbon formation in the equilibrium mixture of steam reforming for the cases of methane, methanol, ethanol and gasoline were determined calculating the carbonization boundaries (BC) of Figure 4.6. These boundaries represent the limiting steam/fuel ratios above which carbon deposition is thermodynamically impossible. As shown, the higher is the carbon content in the mole of a fuel, the higher should be the reforming factor (at a given temperature) in

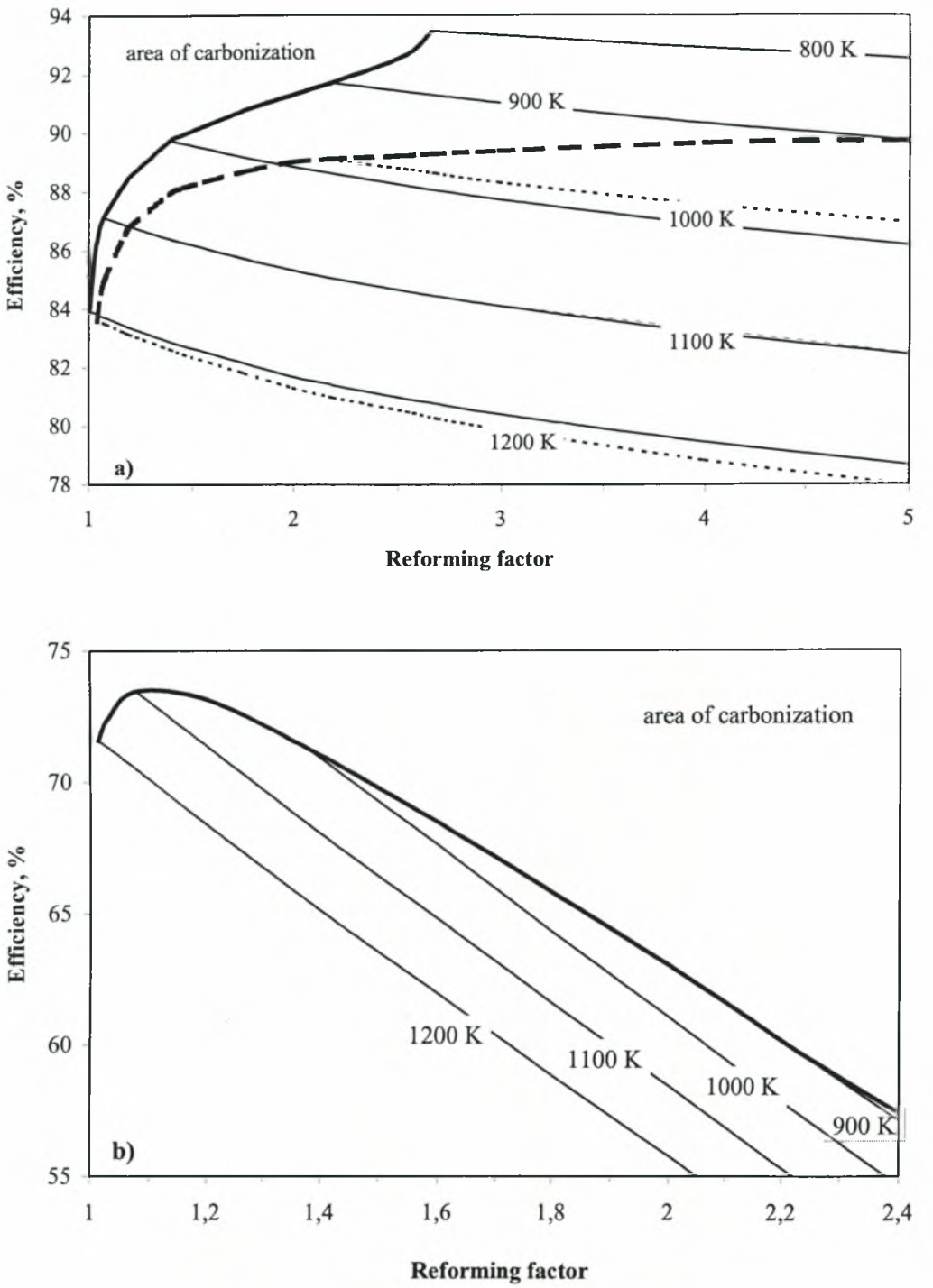

Figure 4.5 Dependence of the maximum thermodynamic efficiency of the ethanol fueled SOFC on the reforming factor for systems: a) A (solid lines) and B' (dashed lines), b) C'. (The thick dashed line represents the boundary of carbonization for system B').

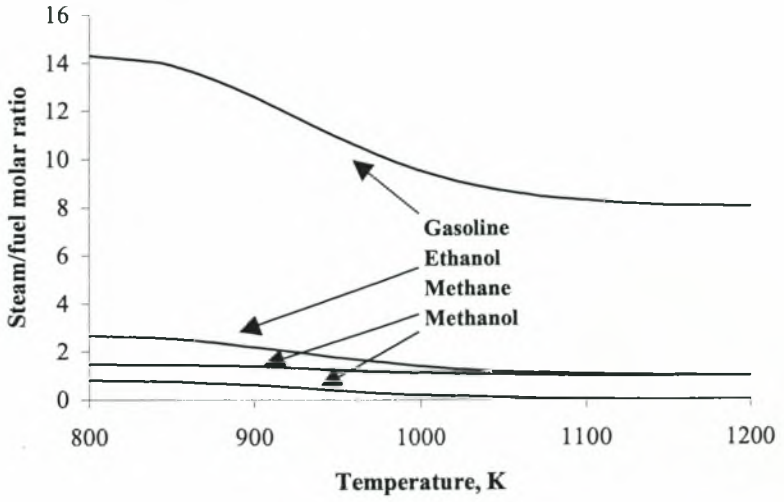

Figure 4.6. Boundaries of carbonization for methane, methanol, ethanol and gasoline.

order carbon deposition to be avoided. BC of gasoline lies much higher than the others, while methane requires lower reforming factors than ethanol at low temperatures (< 1100 K) and almost the same at higher temperatures. Finally, methanol has the smaller area of carbonization than all other cases. For any fuel, the limiting values at the BC decrease as temperature increases. Furthermore, for the cases of methane and ethanol, a critical value of temperature exists (~1100 K) where both fuels present identical values for steam/fuel molar ratio. It is obvious that the overall behaviour of these fuels is expected to be similar for T ≥1100 K due to the thermodynamics and this is confirmed by the imminent analysis (see Figure 4.3 and the respective discussion).

The equilibrium compositions of all external reforming processes were calculated by solving the mixed system of Eqs. (18)-(20) and (24)-(26) and are presented in Figure 4.7. The reforming factors wereselected near the boundary of carbon formation of each fuel since higher values of m would result in undesirable high percentages of steam in the SOFC feedstream (reforming equilibrium composition). As shown in Figure 4.7, an increment of the reforming factor results mainly in increases of the molar fractions of steam and carbon dioxide and in decreases of the molar fractions of hydrogen, carbon monoxide, and methane. The last three are the only species that contribute to the generation of electricity in the SOFC. The equilibrium percentages of hydrogen and carbon monoxide icrease as the temperature increases while methane's concentration is practically diminished at high temperatures. The analysis employed for the estimation of the distribution of emf along the cell channel revealed that the optimum conditions for the operation of the SOFC system correspond at conditions (T, m) at the boundary of carbon formation of each fuel option. This observation is reasonably explained as these optimum conditions of steam reforming provide the maximum possible ratio of combustibles/oxidants in the SOFC feedstream. Therefore, Figures 4.8 and 4.9 present the maximum emf distribution and the correspnding average emf, $\overline{E}$ (obtained by Eq. (33)) respectively, at the optimum conditions at the BC of each fuel option. Methanol, ethanol and gasoline present similar optimum emf outputs, which decrease linearly to the temperature increment.

Figure 4.10 presents the overall efficiency, obtained by Eq. (34), for any fuel, which has been set at optimal conditions. Temperature is an unfavourable parameter for the efficiency as it decreases with temperature increment. This behavior is expected due to the linear dependence of efficiency on average emf (see Figure 4.8). Furthermore, as was expected, maximum efficiency is presented while reforming factors are very close to the boundary of carbon formation of each fuel due to the aforementioned effect of m on the total percentage of the combustible species in the SOFC feedstream.

The dependency of maximum efficiency in optimal conditions for each fuel on the temperature variation is clarified in Figure 4.11, where a comparison of maximum efficiency for each fuel choice is presented. An almost linear decrement of maximum efficiency as temperature values become higher has been observed. Moreover, it is worth noticing that the worst efficiency

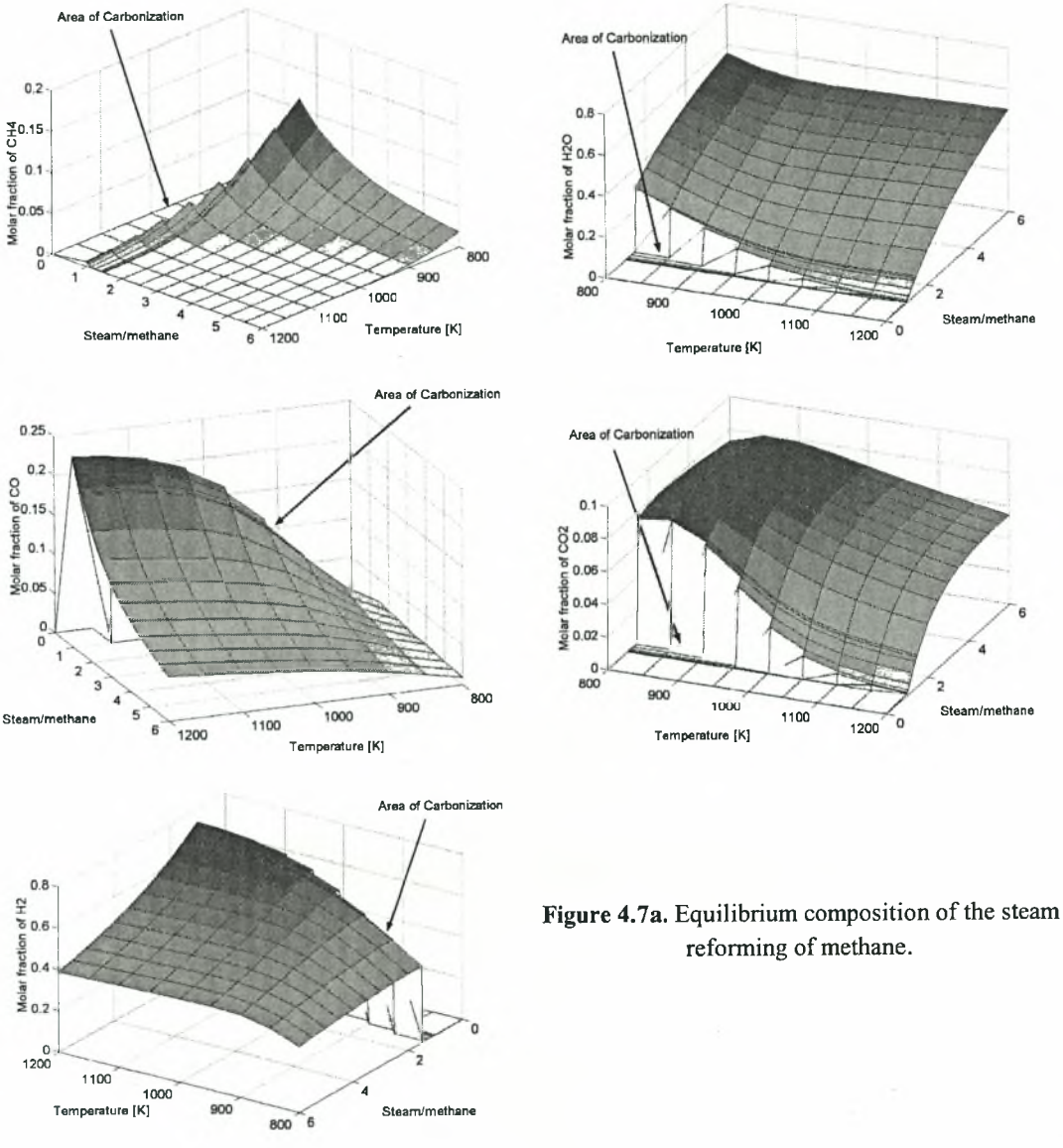

Figure 4.7a. Equilibrium composition of the steam reforming of methane.

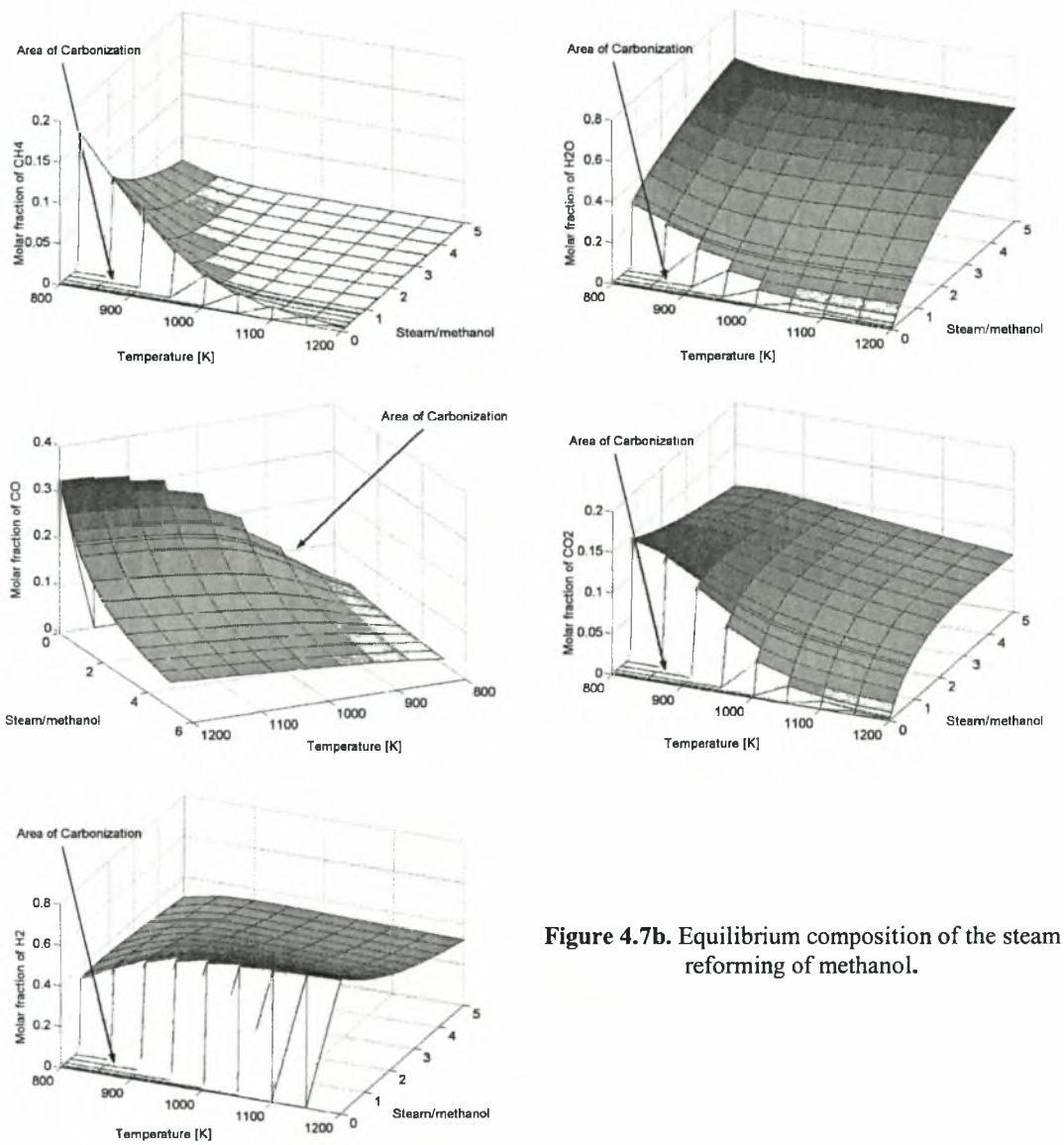

Figure 4.7b. Equilibrium composition of the steam reforming of methanol.

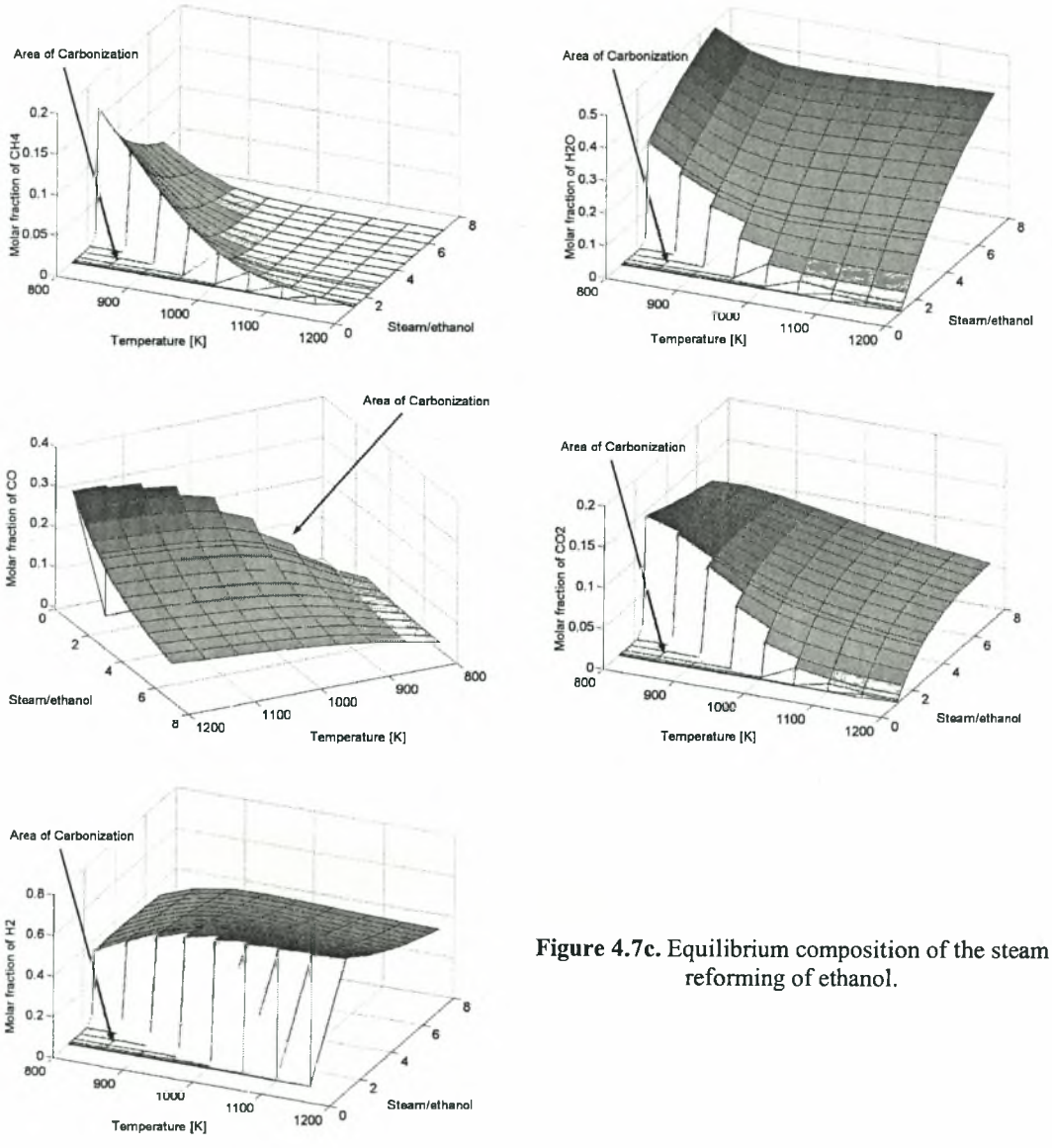

Figure 4.7c. Equilibrium composition of the steam reforming of ethanol.

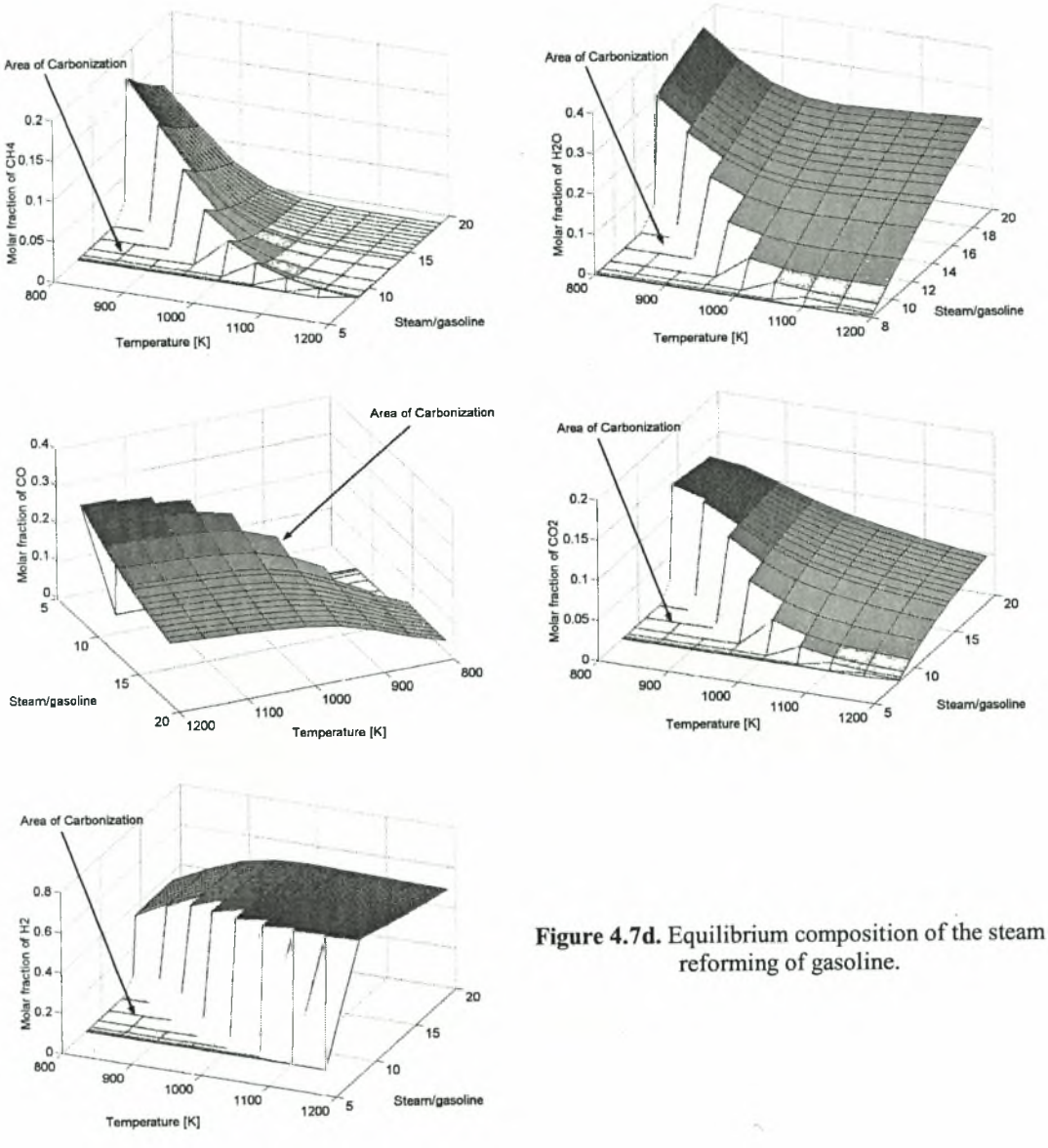

Figure 4.7d. Equilibrium composition of the steam reforming of gasoline.

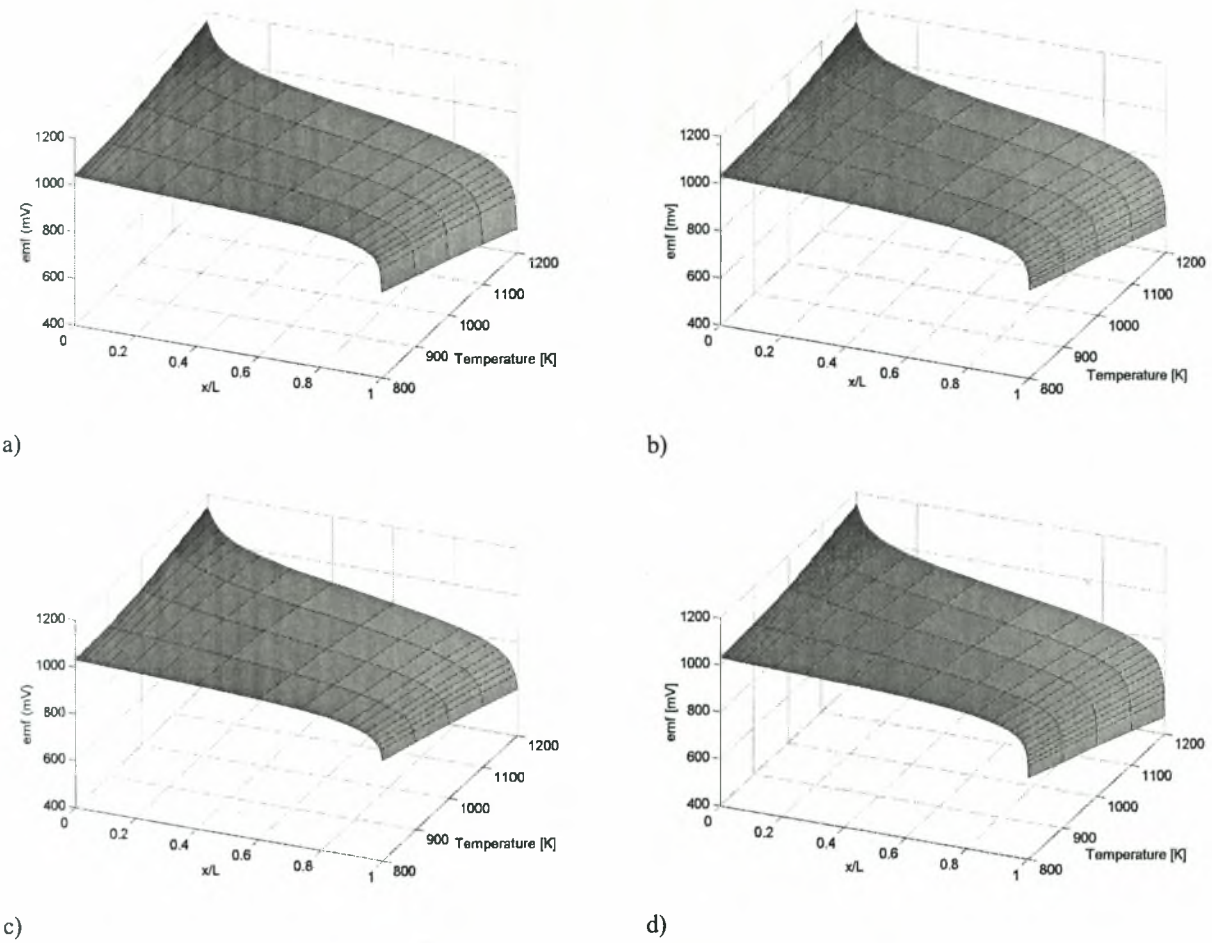

Figure 4.8. Emf distribution along a multi-cell stack fed by a) methane, b) metnanol, c) ethanol and d) gasoline (fuel utilization is fixed 99.99% at all cases).

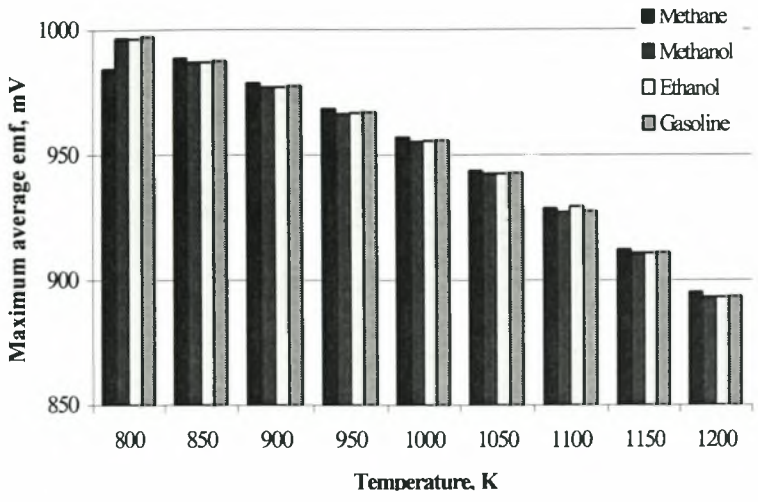

Figure 4.9. Maximum average emf for any fuel selected in its most suitable conditions.

value for any fuel and temperature is high enough (>80%) for almost any practical use and almost two times higher than the efficiency of every actual power cycle currently used for electricity generation. Figure 4.12 illustrates the dependence of the actual SOFC efficiency on the relative power for all fuel options in optimal conditions. It is also supposed that T = 1100 K. As it follows from Eq. (35), the fuel cell efficiency is the half of the maximum efficiency when the fuel cell runs at full power. The fuel classification produced by the comparison of maximum efficiencies (see Figure 4.10) remains unchanged.

4.4. DISCUSSION

Selection of the most appropriate SOFC fuel is a multi-criteria task involving both quantitative and qualitative parameters. The analysis made before, shown that all fuels have similar potential for generation of electricity with respect the expected emf output and the efficiency of the SOFC system. Methane was found as the optimum fuel that provides the higher feasible emf distribution and system efficiency, methanol and ethanol were found as promising alternative options and gasoline utilization was found to require special reforming conditions (high reforming factors) so as carbon formation to be avoided. Thus, quantitative evaluation seems to be weak in order to accurate a definitively valid decision of an optimal fuel choice. Thus, some fundamental qualitative and quantitative parameters, which are characteristic for each fuel, should be examined. These parameters can be the existed infrastructure, the production costs as well as the environmental impact. Furthermore, some relative parameters like the self-sufficiency in energy resources and the agricultural assistantship in national level should also be considered. Further, as it will be discussed in Chapter 5, the actual classification of fuels must take into account specific operational parameters of the integrated SOFC power plant which is designed for practical application. In this respect, the analysis presented previously must be considered as the first step for the thermodynamic analysis of indivindual SOFC stacks operating under the constraints imposed from the overall plant design.

4.5. SUMMARY

Thermodynamic analysis of the eligibility of methane, methanol, ethanol and gasoline as fuels for generation of electrical power in SOFCs is presented here. A mathematical model has been developed in order to adequately represent, according to the method of direct minimization of Gibbs free energy, the spatial variance of the molar fractions of the components that are involved to the chemical reactions taking place within the steam reformer/SOFC system. The above model has also minimized the influence of the arbitrary initial values needed for the iterative solution of the non-linear system. All the fuels presented almost equal maximum average electromotive force (emf) output for optimal conditions. Furthermore, the overall system efficiency obtained by the model presented the following sequence for each fuel option: $\eta_{methane} > \eta_{ethanol} > \eta_{methanol} > \eta_{gasoline}$. Thus, methane seems to be the most appropriate fuel option to feed a steam reformer/SOFC system while methanol and ethanol were found as promising alternative options and gasoline utilization was found to require special reforming conditions. The above classification remains unchanged even when the fuel cell runs at full power. For that case, it was found that the fuel cell efficiency for each fuel option is almost the half of the maximum efficiency

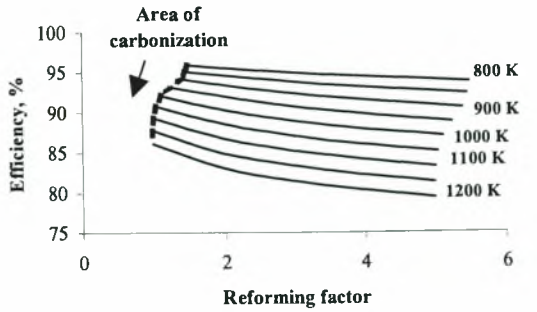

a)

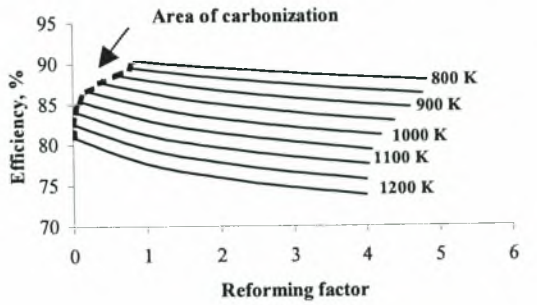

b)

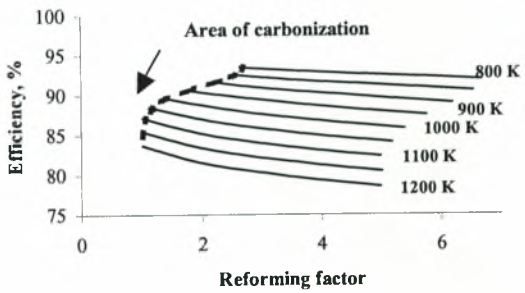

c)

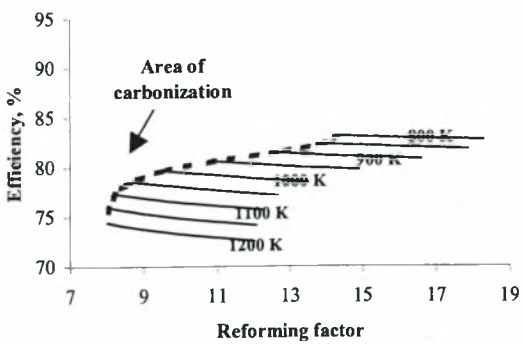

d)

Figure 4.10. Overall efficiency distribution for (a) methane (b) methanol (c) ethanol and (d) gasoline fed SOFC system.

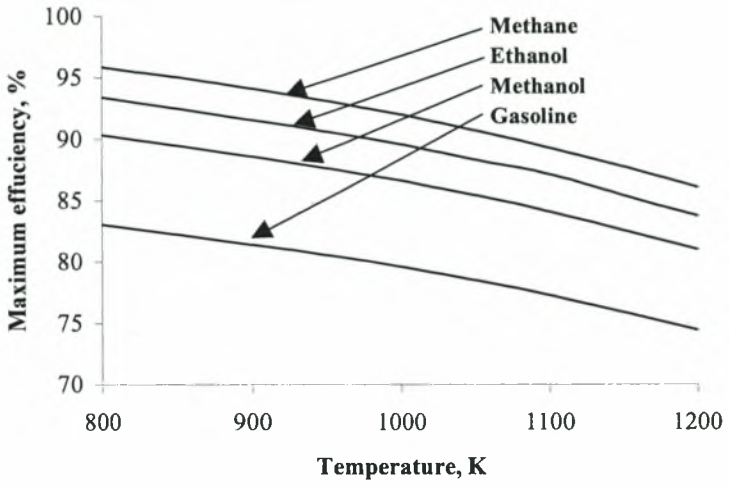

Figure 4.11. Maximum overall efficiency.

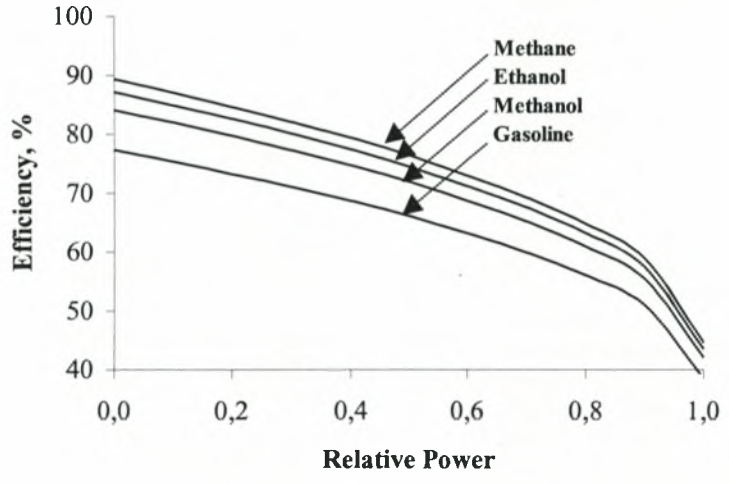

Figure 4.12. Dependence of the efficiency of SOFC on the relative SOFC power for any fuel option (T = 1100 K).

REFERENCES

1. Hirschenhofer J. H., Stauffer D. B., Engleman R. R., and Klett M. G., *Fuel Cell Handbook*. 4th Edition, 1997: Business/Technology Books, Orinda-USA.
2. Benjamin T. G., Camara E. H., and Marianowski L. G., *Handbook of fuel cell performance,* May 1980: Institute of Gas Technology, Chicago-Illinois, USA.
3. Thomas S. and Zalbowitz M., *Fuel Cells: Green Power*., 1999: Los Alamos National Laboratory, New Mexico -USA.
4. Pimentel D., et. al., *Renewable energy: Economic and environmental issues*. BioScience, 1994. **44**(8).
5. Clarke S. H., et. al.., *Catalytic aspects of the steam reforming of hydrocarbons in internal reforming fuel cells*. Catalysis Today, 1997. **38**: p. 411-423.
6. Ridler D. E. and Twigg M. V., *Steam reforming*, in *Catalyst Handbook*, Twigg M. V., Editor, 1996, Chapter 5: Manson Publishing Ltd., London-England.
7. Demin A. K., et. al., *Thermodynamic analysis of methane fueled solid oxide fuel cell system.* International Journal of Hydrogen Energy, 1992. **17**(6): p. 451-458.
8. Chan S. H., and Wang H. M., *Thermodynamic analysis of natural-gas fuel processing for fuel cell applications*. International Journal of Hydrogen Energy, 2000. **25**: p. 441-449.
9. Docter A., and Lamm A., *Gasoline fuel cell systems*. Journal of Power Sources, 1999. **84**: p. 194-200.
10. Thomas C. E., et. al., *Fuel options for the fuel cell vehicle: hydrogen, methanol or gasoline?* International Journal of Hydrogen Energy, 2000. **25**: p. 551-567.
11. Bridger G. W., and Spencer M. S., *Methanol synthesis*, in *Catalyst Handbook*, Twigg M. V., Editor, 1996, p.441-468: Manson Publishing Ltd., London-England.
12. Lwin Y., et. al., *Hydrogen production from steam-methanol reforming*, International Journal of Hydrogen Energy, 2000. **25**: p. 47-53.
13. Kobayashi H., Takezawa N., and Minochi C., *Methanol reforming reaction over copper containing mixed oxides*, Chemical Letters, 1976: p. 1347.
14. Amphlett J. C., Mann R. F., and Weir R. D., *Hydrogen production by the catalytic steam reforming of methanol. Part 3: Kinetics of methanol decomposition using C_{18}HC catalyst*, Canadian Journal of Chemical Engineering, 1988. **66**: p. 950.
15. Margiloff I. B., Reid A. J., and O'Sullivan T. J., *Ethanol: Manufacture and applications*, in *Monohydric alcohols*, 1981, Vol. 159: p. 47-54: ACS Symposium Series, Whasington D.C.-USA.
16. McMillan J. D., *Bioethanol production : Status and prospects*, Renewable Energy, **10**(2/3): p. 295-302.
17. Prince R. G. H., *The outlook for liquid fuels from biomass*, Proc. of 3rd Word Congress on Chemical Engineering, Tokyo, Japan, 1986.
18. Wyman C. E., *Applcations of cellulose conversion technology to ethanol production from corn*, 1994: Alternative Fuel Division, National Renewable Energy Laboratory. Colorado-USA.
19. Evans M. K., *The economic impact of the demand for ethanol*, 1997: Midwestern Covernors' Conference, Lombard-Illinois, USA.
20. Garcia E. Y., and Laborde M. A., *Hydrogen production by the steam reforming of ethanol: Thermodynamic analysis*, International Journal of Hydrogen Energy, 1991. **16**(5): p. 307-312.
21. Vasudeva K., et. al., *Steam reforming of ethanol for hydrogen production*, International Journal of Hydrogen Energy, 1996. **21**(1): p. 13-18.
22. Fishtik I., et. al., *A thermodynamic analysis of hydrogen production by steam reforming of ethanol via response reactions*, 2000. **25**: p. 31-45.
23. Tsiakaras P., et. al., *Ethanol utilization in solid oxide fuel cells : A thermodynamic approach*, Ionics. **5**: p. 206-212.
24. Minh N. Q., and Takahashi T., *Science and technology of ceramic fuel cells*, 1995: Elsevier Science B. V., The Netherlands.
25. Smith J. M., Van Ness H. C., and Abbott M. M., *Introduction to Chemical Engineering Thermodynamics*, 1996: McGraw-Hill, Inc.
26. Burden R. L., and Faires D. J., *Numerical analysis*, 1989, p. 536-540: PWS-Kent Publishing Company, Boston-USA.
27. Demin A.K., and Tsiakaras P.E., *Thermodynamic analysis of a hydrogen fed SOFC based on proton conductor*, International Journal of Hydrogen Energy, **26**(10), 2001: p. 1103-1108.

S. L. Douvartzides, Ethanol utilization for generation of electricity in Solid Oxide Fuel Cells.

Journal of Power Sources, 114(2), 2003: p. 203-212

CHAPTER 5

ON THE SYSTEMATIC OPTIMIZATION OF SOFC SYSTEMS IN TERMS OF ENERGY AND EXERGY

ABSTRACT

A systematic procedure for the optimization of solid oxide fuel cell (SOFC) power plants according to the first and second law of thermodynamics is described in detail. As a case study, a certain plant topology is contemplated being comprised of a SOFC, an external steam reformer, an afterburner, two heat exchangers, a vaporizer and a mixer. The analysis employs parameters such as the extent of the steam reforming reaction, ε, and hydrogen utilization in the SOFC, U, and proves that the appropriate adjustment of the plant performance can be achieved by simply interrelating them to control the energy losses to environment and the participation of combustion processes in the power cycle. Energy losses from the SOFC stack are found also of negative impact to plant efficiency and are minimized through an appropriate thermal management between the mixtures incoming and outgoing the stack, attaining the adiabatic regime of SOFC operation. The strategy proceeds in the estimation and allocation of exergy destruction rates (irreversibilities) inside the indivindual units of the autonomous plant, indicating design optima unconceivable by first law. Assuming a general fuel $C_xH_yO_z$, it is shown that the proposed optimization strategy provides the optimal temperatures and the optimal catalytic activities for the reactions in the reformer and the SOFC. Then, a parametric analysis is provided to illustrate guidelines for parctical improvements. The effect of fuel type and plant topology is also under discussion and useful information is deduced by comparative considerations.

5.1. INTRODUCTION

From the very beginning of the systematic development of actual electricity generating systems based on fuel cells, research was guided by endeavors to approximate their optimal theoretical patterns of operation as dictated by the first law of thermodynamics. Given that the first law (energy) analysis has been generally regarded as capable and sufficient to determine real design optima, the analysis according to the second law was usually underestimated. In fact, it was not until the term "exergy" became a synonym of monetary value when the second law aquired practical significance in the oprtimization of energy systems [1]. Since this had happened, the "exergy analysis" has been accepted as a sound method for the interpretation of the axiomatic role of the second law in the design and optimization of energy systems in terms of both efficiency and cost, and as a supplementary tool to aid in decision making about the parameters and criteria that may lead to optimality in terms of the impact of a process to the environment [1, 2].

Ordinary power generation systems transform the chemical energy of a fuel into useful work (i.e. electricity) by passing through the intermediade stage of production of thermal power that is most commonly achieved by processes of combustion. This route of energy conversion results in significant losses of potential energy that could otherwise be useful in work form, because of extremely irreversible mechanisms of energy exhange between the molecules in the combustion chamber [3, 4]. These mechanisms involve transfer of momentum and heat from the combustion products to the

surrounding immotionless species inside the chamber, being responsible for almost 70% of the entropy generation in it [3-6]. On the other hand, solid oxide fuel cells (SOFCs) are electrochemical devices operating at high temperatures (above 800 K) that allow the conversion of the chemical energy of a fuel directly into electrcity. Comprised of an oxygen ion (O^{2-}) conducting electrolyte and two electrodes in cathodic and anodic roles, SOFCs allow the exploitation of various fuels for generation of electricity with efficiencies unattainable by all other conventional systems [7-9]. Energy conversion takes place electrochemically through controlled migration of O^{2-} ions from air exposed cathode to fuel fed anode and therefore oxidation becomes more controllable and less ireversible than in ordinary combustion systems. Energy conversion and management is more rational and entropy generation is substantially lower [3, 10, 11].

To realize its full potential, utilization of SOFCs for practical power generation requires optimization to reflect on the maximization of the efficiency of the fuel exploitation and on their cost competitiveness to turbines and reciprocal engines [10, 12, 13]. Succesful design presupposes that optimization criteria must be based not only on the oftenly misleading quantitative considerations of the first law of the thermodynamics, but also on the evaluation of the qualitative availabilty of energy for transformation into usefull work according to "exergy analysis" [14, 15]. In this respect and for a given SOFC plant configuration, it would be useful to create a strategy to which features of operation conditions and used materials (catalysts) could be indexed according to their effect on the deviation or convergence to optimality. Some previous work on exergy analyses of high temperature fuel cells such as molten carbonate (MCFCs) and solid oxide (SOFCs) is outlined in references [3, 11-13, 16, 17].

In the present study, it will be shown that SOFC power systems may be easily adjusted to optimum -or at standard quality- operation depending on the available technical infrastructure (SOFC catalysts, reforming catalysts etc.). It is necessary to have in mind that the search for appropriate conditions in a power plant is the leading force in research for materials and catalysts. As it will be indicated, in a SOFC plant designed to operate at certain temperatures, the real independent variable is not the individual activity of the catalysts for reforming or SOFC anode but their combination. The analysis will provide a set of criteria that allow the recognition of the parameters for modification in actual SOFC systems as well as useful information on the effect of fuel type and plant architecture.

5.2. THEORY

5.2.1. Energy, Exergy and Anergy

Rant [18] grouped energy in two categories: transformable and non-transformable energy. Transformable energy (ordered energy) can be converted fully to work, and work can be converted to any other energy form. Non-transformable energy (disordered energy) cannot be converted to any other form. Transformable energy is called "exergy" while non-transformable energy is "anergy". Exergy is then the part of energy which can be converted to any other form, and anergy is the rest.

Fratzcher and Gruhn [19] define exergy as the maximum obtainable work a substance can yield when it is brought reversibly to equilibrium with the environment. Kotas [15] defines exergy as the maximum work which can be obtained from a given form of energy using the environmental parameters as the reference state. In accord, exergy analysis cannot be carried out without relating to the environment. Exergy is a thermodynamic property depended on the states of both the system and its environment that must be clearly stated.

5.2.1. Energy and Exergy Balances of Open Systems

Exergy is the thermodynamic property that describes the "useful energy" content, or the "work producing potential" of a system at a cetrain state. Accordingly, it is a property depended on both the states of the system and its environment that can be calculated assuming the reversible thermal, mechanical and chemical transition of the system to a state in equilibrium with its environment. A clarification of the exergy concept can be presented by considering an one inlet – one outlet device (a control volume) as a system, with a flow of a mixture of *i* chemical species of known composition at elevated temperature and high pressure. The energy balance for this system, ignoring the changes in kinetic and potential energy, may be expressed as

$$\sum_j \dot{Q}_j - \dot{W} = \left(\sum_i \dot{m}_i h_i \right)_{inlet} - \left(\sum_i \dot{m}_i h_i \right)_{exit} \qquad (1)$$

where heat flux $\dot{Q}_j$ is conventionally positive when absorbed by the system and work $\dot{W}$ is positive when it is produced by the system. On the other hand, the exergy balance for this system is,

$$\dot{E}_D = \left(\sum_i \dot{m}_i e_i\right)_{inlet} - \left(\sum_i \dot{m}_i e_i\right)_{exit} + \sum_j \left(1 - \frac{T_0}{T_j}\right)\dot{Q}_j - \dot{W} \quad (2)$$

where $\dot{E}_D = T_0 S_{gen}$ (the Gouy-Stondola theorem) is the rate of exergy destruction into the device due to irreversibilites and e_i is the total exergy of each chemical species i. In fact, $e = \sum_i \dot{m}_i e_i$ is the sum of the physical and chemical exergy components that are associated with the physical and chemical properties of the stream of matter, respectively [14]. Physical exergy, e_i^{PH}, expresses the useful work that the chemical component i can produce if it is brought reversibly from the state of the system to the "restricted dead state" that is a state in thermal and mechanical equilibrium with the environment. Therefore, physical exergy can be expressed as,

$$e_i^{PH} = (h - h_0)_i - T_0 (s - s_0)_i \quad (4)$$

where

$$(h - h_0)_i = \int_{T_0}^{T} (C_P)_i \, dT \quad (5)$$

and

$$(s - s_0)_i = \int_{T_0}^{T} \frac{(C_P)_i}{T} dT - R \ln \frac{p_i}{p_0}. \quad (6)$$

On the other hand, chemical exergy, e_i^{CH}, expresses the useful work that the chemical species i can produce if it is brought reversibly from the "restricted dead state" in chemical equilibrium with the environment ("dead state"). For this estimation, it is essential that the chemical species comprising the system should be refered to the properties of a suitable selected set of environmental substances. Accordingly, an appropriate "exergy reference environment" is usually used in order to estimate the standard chemical exergy e_i^{CH} according to the relation [14, 15, 20],

$$e_i^{CH} = -RT_0 \ln \frac{x_i^e p_0}{p_0} \quad (7)$$

where x_i^e is the molar fraction of the component i in the standard reference environment. For combounds that do not form the environmental composition, the chemical exergy is estimated according to a standard procedure described elsewhere [14]. To simulate the environment, all standard chemical exergies have been selected from literature [20] assuming an environmental composition of 75.67% N_2, 20.35% O_2, 0.03% CO_2, 3.03% $H_2O_{(g)}$ and 0.92% Ar in volume basis, at T_0 = 298.15 K and p_0 =1.013 bar.

5.3. DESCRIPTION OF THE SOFC PLANT

As a case study, a SOFC system with the configuration of Figure 5. 1 will be contemplated. It is common practice to feed the SOFC with hydrogen produced by the steam reforming of hydrocarbons or alcohols [7-9, 21-26]. In the general case of a fuel $C_xH_yO_z$, the reaction of the steam reforming can be written thermochemically as,

$$C_xH_yO + (2x\text{-}z)\,H_2O \rightarrow xCO_2 + \left(\frac{y}{2} + 2x\text{-}z\right)H_2 \qquad \Delta H_{ref} > 0 \quad (8)$$

Steam reforming is an endothermic reaction imposing the necessity for adequate heat supply from a thermal source. For most compounds, it attains rates of practical interest at relatively high temperatures (500-1000K) depending on the heterogeneous regime of reaction. Due to this role of catalysis, a general theoretical encounter of the steam reforming process can take place assuming the temperature and the extent of reforming, ε, as independent variables despite the phenomenal falsehood of the assumption. This will allow the engineer to encounter each specific problem on the basis of the available knoweledge and recearch status. Finally, it should be stressed that the reforming factor (the steam/fuel reacting molar ratio) must always be sufficiently high to prevent the equipment from fouling of channels or breakdown of catalysts due to carbon deposition.

The reformate enters in the anode compartment of the SOFC, where hydrogen reacts with O^{2-} ions supplied from cathode through the solid electrolyte as follows

$$H_2 + O^{2-} \rightarrow H_2O + 2e^- \qquad \Delta H_{H2} = -248818 \text{J/mol } H_2 \quad (9)$$

producing electricity and heat. Although hydrogen oxidation is the primary reaction leading to electricity

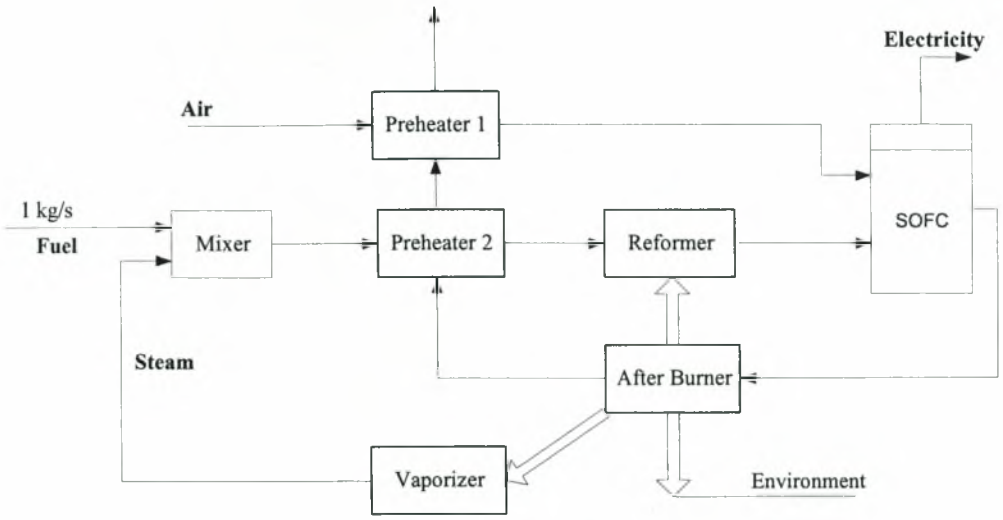

Figure 5. 1. Schematic representation of the SOFC power plant.

generation, in practice CO and CH_4 reformate components react also in the SOFC anode with steam serving as sources for secondary hydrogen. In the present analysis, it was assumed that in the SOFC only reaction (9) takes place while a portion of unreformed fuel is passing through the SOFC as inert gas. Accordingly, the amount of secondary hydrogen produced by CO and CH_4 was supposed as being directly fed to the SOFC inlet and was considered as parameter involving extent of reforming ε. Moreover, it was supposed that reaction (9) takes place in an extend below 100% by employing the factor of hydrogen utilization, U. In practice, a portion of hydrogen must remain as an unreactant component in the SOFC outlet to avoid losses in the potential (emf) of the SOFC. This can be explained by the well known Nernst equation,

$$\mathrm{emf} = \frac{RT}{4F} \ln \frac{p_{O_2(c)} p^2_{H_2(a)}}{p^2_{H_2O(a)}} \qquad (10)$$

where the subsripts (*a*) and (*c*) represent states at anode and cathode, respectively. It is apparent that the electromotive force (emf) of the SOFC deteriorates significantly when hydrogen partial pressure at anode tends to zero. On the other hand, a fraction of the hydrogen entering in the SOFC must be allowed to reach the afterburner in order to support the heat demands of the reformer and the vaporizer. Heat required by the reformer was set equal to

$$\dot{Q}_{ref} = \left(\Delta H_{ref} \frac{\mathrm{J}}{\text{mol of fuel}} \right) \varepsilon ,$$

and that from vaporizer was calculated as

$$\Delta H_{vap} = \left(2442310 \frac{\mathrm{J}}{\text{kg of } H_2O_{(g)}} \right) \dot{m}_{H_2O_{(g)}} ,$$

where the latent heat of water was taken, with negligible error, to correspond for vaporization at 298.15K. These demands should be met by the heat produced from the afterburner by means of complete combustion of unreacted fuel and hydrogen according to the thermochemical reaction,

$$C_xH_yO_z + \left(\frac{y}{4} - \frac{z}{2} + x \right) O_2 \rightarrow x CO_2 + \frac{y}{2} H_2O \qquad \Delta H_{fuel}, \Delta H_{H2} < 0 \qquad (11)$$

where, apparently, the hydrogen reaction is derived for x = z = 0, y = 2. Finally, as shown in Figure 5. 1, two preheaters (heat exchangers) were used to contribute in the thermal management of the plant, the one to increase the thermal content of air before the SOFC, and the other to do the same for the steam/fuel mixture before the reformer. In order to calculate the exact temperature in each branch of the power cycle, an iterative method has

been employed taking into account the variation of the thermal capacities, $(C_P)_i$, with temperature [27].

5.4. OPTIMIZATION

A mathematical model has been developed in order to simulate the processes involved in the plant of Figure 5.1. This simulation program was able to calculate the flow rate, the temperature, the energy and the exergy in every stream line of the plant as well as the irriversibilities appearing in the individual units. The overall exergetic efficiency of the plant as percentange of the standard chemical exergy of the fuel and the energy efficiency of the plant as percentange of the standard chemical energy (LHV) of the fuel were also calculated. The influence of the indepentent variables (namely: reforming factor, extend of reforming, hydrogen utilization, air excess, temperature of reforming and the temperature of fuel cell) to the final efficiency of the system was recognized and optimized. On the basis of results from this model, the following optimization strategy was recognized.

5.4.1. Optimization Strategy

The optimization strategy for the configuration of Figure 5.1 will comprise of the following stages:

- *Minimization of energy (exergy) losses from the heating source (afterburner) to environment.* This initial stage is carried out, exclusively, under application of the first law of thermodynamics on the control volume of the afterburner, providing a) the relations between the participations (extents) of the chemical reactions in the plant operation and b) their effect on the efficiency of energy conversion. It is important that maximization of parameters ε and U, under the demand of the above constraint, is equivalent to the minimization of exergy destruction due to spontaneous combustion, which is inherently highly irreversible.

- *Direct minimization of exergy losses from the SOFC.* From an energetic point of view, this stage of analysis is equivalent to minimization of heat waste from the SOFC to environment. Accordingly, the optimal temperature difference between the mixtures outgoing and incoming the SOFC device is specified and an adiabatic regime of SOFC operation is established. Coupled with the first stage of optimization, the establishment of adiabatic SOFC operation completes the optimization of the efficiency of the plant. From exergetic point of view, both these stages of analysis are of great importance when the plant is designed to operate autonomously without interactions with other work producing devices (gas turbines, heat engines, etc.)

- *Allocation of exergy costs (destructions or losses) in the indivindual units or stream lines of the plant.* This stage of optimization starts with the recognition of the equivalent parameters of the operative schemes of the plant in terms of efficiency. By contemplating these equivalently efficient regimes, the optimum design is finally specified though allocating the exergy costs in the indivindual operation units. This stage of analysis is capable to specify parameters such as the temperatures of reforming and air preheating.

5.4.1.1. Energy optimization strategy

Depending on the operational conditions of the plant, the heat demand of the reformer and the vaporizer will be higher, lower or equal to the heat supplied from the afterburner. In the first case, the plant will not operate at the prescribed conditions and in the second a portion of the amount of energy produced in the afterburner will be rejected unexploitedly to the environment. Obviously, the optimum case of operation is expected at the third case and the demand for positive energy balance can be expressed generally, as follows:

$$(1-\varepsilon)\Delta H_{fuel}+A\varepsilon(1-U)\geq \varepsilon\Delta H_{ref}+\Delta H_{vap}$$

$$\Rightarrow \Delta H_{fuel}-\Delta H_{vap}\geq \varepsilon(\Delta H_{fuel}+\Delta H_{ref}-A\Delta H_{H2}+A\Delta H_{H2}U)$$

$$\Rightarrow B\geq \varepsilon(C+U)$$

$$\Rightarrow B-\Delta H_{loss}=\varepsilon(C+U) \qquad (12)$$

where

$$A=\left(\frac{y}{2}+2x-z\right),$$

$$B=(\Delta H_{fuel}-\Delta H_{vap})/A\Delta H_{H2},$$

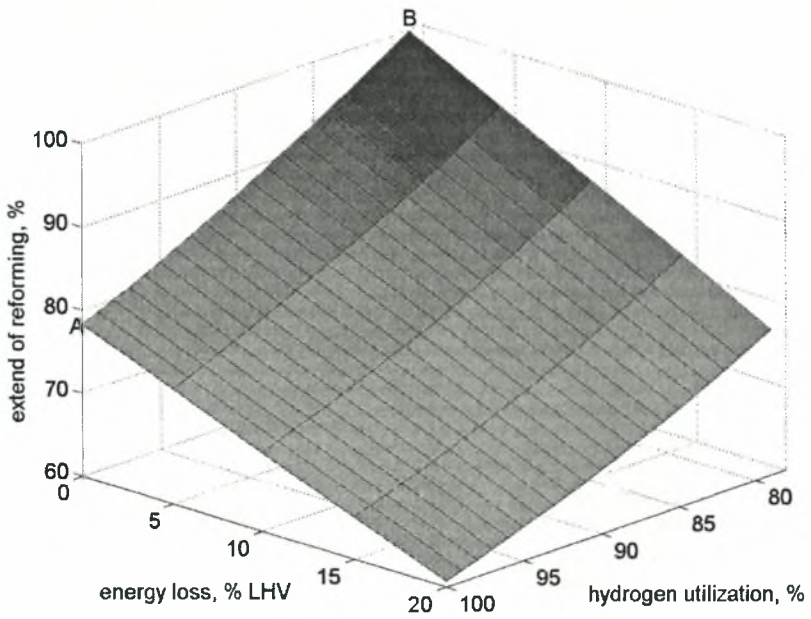

Figure 5.2. Dependence of the energy balance of the burner on the extent of the reforming, ε, and hydrogen utilization in the SOFC device, U. (Fuel = ethanol, RF=3). The locus AB defines the optimal pairs of ε_0 and U_0 for which energy losses from burner balance become zero.

$$C=\left(\Delta H_{fuel}+\Delta H_{ref}-A\Delta H_{H2}\right)/A\Delta H_{H2},$$

and ΔH_{loss} is the possible waste of energy from afterburner to the environment which may be expressed as percentage of the ΔH_{fuel}=LHV. Eq. (12) shows that at exact combinations of ε and U there are standard losses of energy. In other words, if ΔH_{loss}=0, one can easily estimate all pairs of ε_0 and U_0 that correspond to optimal thermal management of burner operation. The influence of ε and U on the energy losses of the burner is illustrated in Figure 5.2 for a plant fueled by ethanol with reforming factor RF=3. As shown, the optimal values of ε_0 and U_0 for which ΔH_{loss}=0 correspond on the locus A-B.

The product of the extent of reforming with the hydrogen utilization may be termed as "absolute hydrogen utilization", AHU=(ε U)/1000, expressing the percentage of the hydrogen content per mole of fuel that is exploited for generation of electricity in the SOFC. Therefore, AHU is partially a measure of the maximum work the SOFC can produce at reversible operation. By application of Eq. (12) for a given fuel, it is proved that AHU depends only on the the reforming factor, RF, and the losses of energy from the burner, ΔH_{loss}. Further, for a given RF and ΔH_{loss}, it is proved that AHU is practically independent on the specific values of ε and U. Therefore, the optimal operation conditions correspond at maximum AHU values attainable from all the pairs, (ε_0, U_0), of the zero-loss locus of Figure 5.2, since for all these conditions it is AHU=78.95%. To estimate the interrelations of ε and U for other saturated hydrocarbons and alcohols the required values of ΔH are given in Table 1. Parameters A, B and C may be used directly to specify the interrelation between ε_0 and U_0.

In the case of a general fuel with formula $C_xH_yO_z$, the reversible electrical energy that may be produced (per mole of fuel) may be estimated as

$$W_{el,rev}=A10^{-3}(\varepsilon U)\left(\Delta G_{H2}\right)_T=A(AHU)\left(\Delta G_{H2}\right)_T \quad (13)$$

and the heat released from the SOFC reaction will be

$$Q=A10^{-3}(\varepsilon U)\left[\left(\Delta H_{H2}\right)_T-\left(\Delta G_{H2}\right)_T\right]=$$

$$=A(AHU)\left[\left(\Delta H_{H2}\right)_T-\left(\Delta G_{H2}\right)_T\right] \quad (14)$$

where $\left(\Delta H_{H2}\right)_T$ and $\left(\Delta G_{H2}\right)_T$ are the changes of enthalpy and Gibbs free energy of hydrogen oxidation at the average temperature of SOFC operation. The enthalpy change of hydrogen oxidation is practically unaffected by

temperature variations and the corresponded change of Gibbs free energy decreases by temperature increment. Hence, the work produced per mol of hydrogen decreases with temperature increment and a clear incentive is justified for low temperature SOFC operating systems.

5.4.1.2. Direct minimization of exergy loss due to heat transfer from SOFC to environment

Since energy contains exergy, it is obvious that every waste of energy has impact on both the energetic and exergetic efficiencies of the plant. Hence, an optimization constraint is imposed also for the other device of the plant in thermal interaction with the environment which is the SOFC. By considering a desired temperature for the products of the SOFC device and standard AHU provided by given RF and zero-loss burner balance, minimization of heat waste from the SOFC to environment (adiabatic SOFC operation) may be established only if the heat released from hydrogen oxidation is exactly equal to the heat absorbed by the gaseous stream flowing inside the SOFC. In light of this and in absense of cooling media as it is the case of Figure 5.1, the average temperature of the SOFC inlet must be at an appropriately lower value than the prescribed temperature of the products. In this respect, an iterative calculation may be employed as follows

$$Q = \left(T_{\text{sofc, out}} - \frac{T_{\text{sofc, out}} - \Delta T_{\text{sofc}}}{2} \right) \sum_i m_i C_{p,i} \qquad (15)$$

where Q is given by Eq. (14), $T_{\text{sofc, out}}$ is the desired temperature of the SOFC effluents and ΔT_{sofc} is the uknown optimal temperature difference between the mixture outgoing and incoming the SOFC unit. As follows by Eq. (15), SOFC operation (*i.e.* hydrogen oxidation) is considered for simplicity to take place in the average temperature between the mixtures downstream and upstream the SOFC.

Following the iterative scheme of Eq. (15), direct minimization of exergy losses due to heat waste from SOFC to environment may be achieved by specifying the optimal temperature difference ΔT_{sofc}, as shown in Figure 5.3. Under the assumption of the operation of the ethanol fed plant with RF=3, $T_{\text{sofc, out}}$=1200K and zero-loss burner operation, it is shown that exergy losses due to heat waste decrease with the increment of ΔT_{sofc} and an optimal temperature difference is specified at 332K. At this optimal case, the heat released by hydrogen oxidation is equal to the heat absorbed by the gaseous mixture in the SOFC and, therefore, thermal impact to environment is eliminated. For a given reforming factor and zero-loss burner balance, this method of "direct minimization of exergy losses" from the SOFC, provides the higher possible exergetic efficiency of the plant, as shown in Figure 5.4. As observed, by attaining the optimal temperature difference of ΔT_{sofc}=332K, exergetic efficiency tends to maximize at 66.5% due to reduction of the average temperature of hydrogen oxidation in the SOFC stack.

5.4.1.3. Allocation of exergy costs

In the two previous sections, a strategy of decicion making for the optimization of the overall exergetic efficiency of the plant of Figure 5.1 has been provided according to considerations of the first law of thermodynamics. Here, the crucial role of "exergy analysis" will be provided by contemplating all possible equivalent regimes of the above analysis and specifying the optimal one according to objective criteria such as cost-effectiveness and thermodynamic feasibility.

On the assumption of ideal thermal exchange between the air and reformate streams incoming the SOFC unit, there are infinite temperature combinations of these streams given by equation

$$T_{\text{ref}} = T_{\text{sofc, in}} + \frac{\dot{m}_{\text{air}} \sum_i x_i^e \left(C_p^e\right)_i}{\dot{m}_{\text{ref}} \sum_i x_i^r \left(C_p^r\right)_i} \left(T_{\text{air}} - T_{\text{sofc, in}}\right) \qquad (16)$$

that are providing the same work output (efficiency). Accordingly, the first law analysis is unable to specify an optimal operative scheme regarding the temperatures of the reforming reaction and air preheating. To overcome this weakness, the "exergy analysis" may be apllied as shown in Figure 5.5 for the example of ethanol under consideration. In this case, the design parameters of the temperatures of the reformate, T_{ref}, and air preheating, T_{air}, may be specified according to the necessity for cost-effective plant operation, allocating the exergy costs of the indivindual units of the plant. Although the overall exergy destruction rate is constant (about 31% of the standard chemical exergy of ethanol), different equivalent scenarios of Figure 5.5 result in different allocations of exergy costs in the devices of the plant.

Independently on the type of the specific devices that comprise a plant, it has been proved (see reference [14], p.436) that avoidable exergy destruction in a device of a plant that is close to the product (i.e. electrical power) has greater impact on the system efficiency and cost of electricity than avoidable exergy destruction of the same magnitude in a device close to the inputs (fuel, air, steam). Since the major devices that contribute on electricity generation are the reformer and the SOFC, a scenario of low exergy costs in these units is preferable than a scenario involving low exergy costs in devices

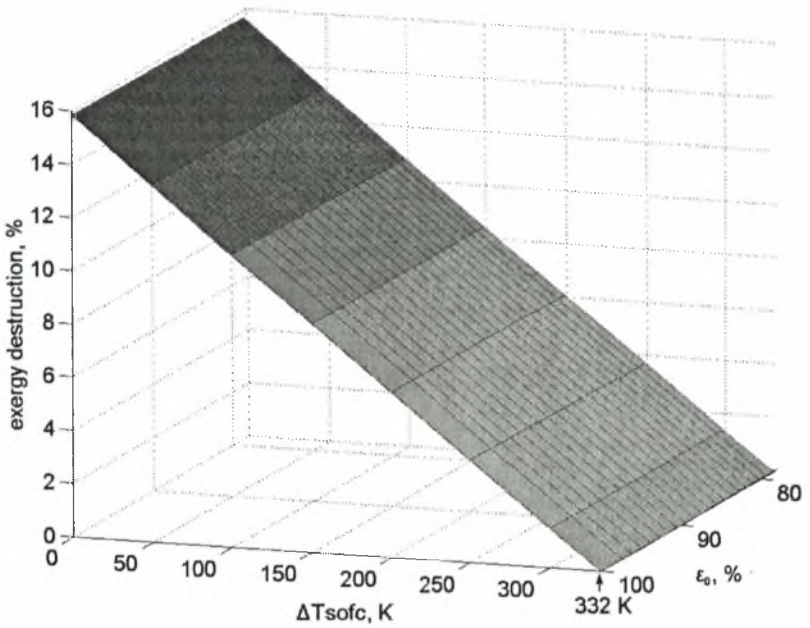

Figure 5.3. Direct minimization of the exergy destruction due to heat waste from the SOFC to environment at zero-loss burner conditions.

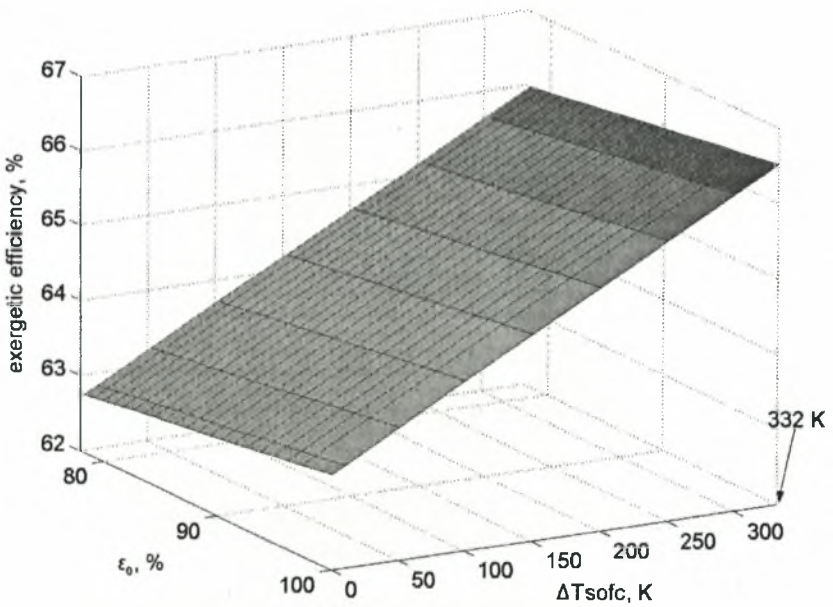

Figure 5.4. Second law efficiency optimization at zero-loss burner balance and zero thermal dissipation from the SOFC.

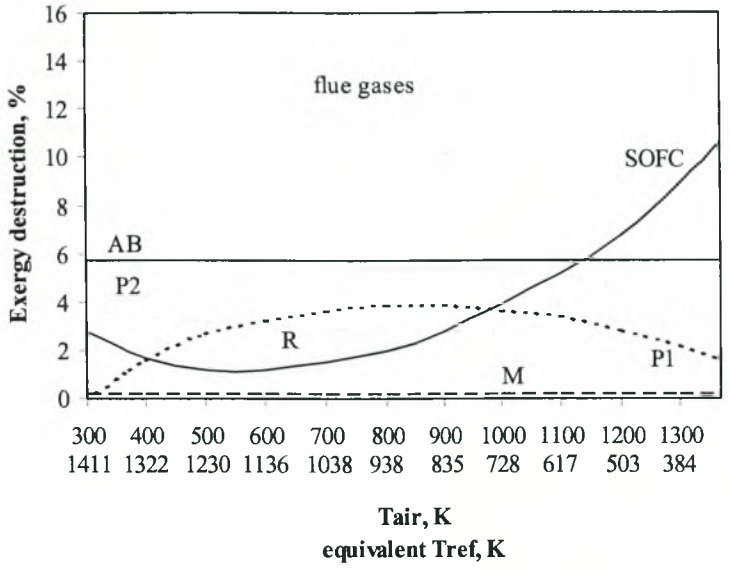

Figure 5.5. Allocation of exergy costs in the units of the optimally designed ethanol fueled SOFC plant (RF=3, 100% theoretical air, $T_{sofc,\,out}$=1200K, ΔT_{sofc}=332, ε_0=100%, U_0=78.95%, η_{II}=66.5%, M=Mixer, P1=Preheater 1, P2=Preheater 2, AB=After Burner, R=Reformer) at all equivalent schemes for temperatures of preheated air and reformate.

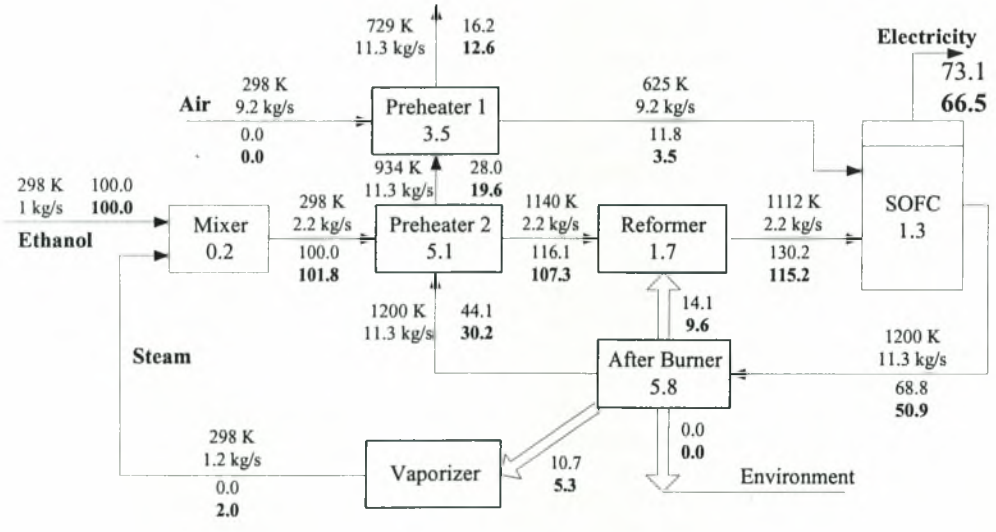

Figure 5.6. Optimal configuration of the ethanol fueled SOFC plant. (RF=3, 100% theoretical air, ε_0=100%, U_0=78.95% (Plain text stands for energy values while bold stands for exergy ones).

close to the plant inputs. In this respect, the region of minimal exergy destruction in the SOFC unit may be considered as optimal in terms of cost efectiveness, temperatures (about 600 K) [28-34], it is here proved that the plant design should aim at the desired value of extent of reforming ε_0 at this specified temperature interval.

To better justify the decicion of this optimal region of temperatures, another reason may also be stated as follows. Figure 5.5 implies that minimization of exergy destruction in the SOFC is mainly compensated by an increment of the exergy loss accompanying the flue gases. Although exergy destruction due to dissipative phenomena (friction, chemical reactions, heat transfer, ohmic losses, etc.) is irreversibly lost, exergy losses may be considered exploitable by an appropriate engine (gas turbines, heat engines, etc.) or usefull for practical purposes (heating rooms, water, etc.). As a result, the conditions mentioned above of minimum exergy destruction in the SOFC are justified again as optimal.

Figure 5.6 provides the optimal configuration of the ethanol fueled plant (RF=3, $T_{sofc,\ out}$=1200K) in terms of both energy and exergy efficiency, its impact to environment and its cost-effectiveness. As observed, the stream of the exhaust gases contains 12.6% of the standard chemical exergy of ethanol and obviously may be usefull for practical purposes as mentioned previously. Further, the major exergy sink of the plant is found to be the afterburner with exergy destruction rate equal to 5.8% due to highly irreversible mechanisms that are accompanying all spontaneous combustion processes. However, it is important to notice that this rate of exergy destruction in the burner is the minimum possible for the example under consideration, since AHU maximization according to Section 5.4.1.1 is practically equivalent to minimization of the participation of combustion in the plant. Finally, the demand for high temperatures of steam reforming reflects into an appreciably high rate of exergy destruction (5.1%) in preheater 1 which is attributed to increased stream-to-stream heat transfer through a finite temperature difference.

5.4.2. Parametric Analysis

The description of the optimization strategy in Section 5.4.2 assumed the example of ethanol with RF=3 and $T_{sofc,\ out}$=1200K. The dependence of the attainable energetic and exergetic efficiencies of the ethanol fueled plant mentioned above on the burner balance and the reforming factor may be clarified by the nomograph of Figure 5.7. An increment of the heat losses from the afterburner reduces the upper limit of the AHU value and concomitantly has the same effect on both the efficiencies. Similarly, an increase of the reforming factor is also unfavourable in terms of efficiency. Thus, the lower possible limit imposed either by the stoichiometry of the reforming reaction or the impying moderate air preheating at 500-650K and reformate production at 1100-1230K. Although ethanol reforming has been found feasible at significantly lower carbonization boundary of the given fuel is recommended. Results of Figure 5.7 have been derived according to the optimization strategy mentioned above for ε = 100% when RF>3. For RF<3 there exist a maximum $\varepsilon = \varepsilon_{max}$ due to the stoichiometricity of the reforming reaction (i.e. for RF=2.68 it is ε_{max}=89.33%).

For the cases presented in Figure 5.7, specification of optimal ΔT_{sofc} provides the diagram of Figure 5.8. Optimal temperature difference decreases as both reforming factor and burner losses tend to increase. An increment of the reforming factor, obviously increases the thermal capacity of the stream of matter flowing inside the device and thus lowers ΔT_{sofc}. Instead, losses from burner balance decrease the AHU values as showed in Figure 5.7 and concomitantly the absolute heat amount produced by hydrogen reaction. Therefore, although a non-linear dependence of ΔT_{sofc} on RF is presented, the dependence on burner losses follows a normal linear behavior.

By reminding the allocation of exergy costs according to Figure 5.5, it would be useful to recognize the effect of the reforming factor on the equivalent temperatures of the reformate and air together with its effect on the indivindual exergy costs of each unit. Figure 5.9 provides the effect of the reforming factor on the equivalence of the temperatures of the reformate, T_{ref}, and preheated air, T_{air}. Since an increment of the reforming factor induces higher energy requirements from the vaporizer, the zero-loss burner balance (Eq. 12) provides lower possible AHU values and concomitantly lower plant efficiency. However, the important information from Figure 5.9 is that an increment of the reforming factor reduces the slope of Eq. (16) and therefore it also reduces the list of materials that can be considered appropriate catalysts for reforming. Especially for the cases of combounds exhibiting high reactivity for reforming at low temperatures (such as ethanol), it is here proved that an increment of the reforming factor is unfavorable, not only due to its effect on efficiency, but also due to suppressing of the range of feasible temperatures for reforming.

Figure 5.10 illustrates that an increment of ΔH_{loss} causes the transition of the curve, equivalent $T_{ref} = f(T_{air})$, to higher temperatures with approximately the same slope. However, the effect of the burner balance on the equivalent temperatures is not so dramatic as the effect of the reforming factor and, in general, no deductions can be made about the role of a change of ΔH_{loss} on the selection of ethanol reforming catalysts, since the transition may be attributed to the decrement of ΔT_{sofc}, as was discussed in Figure 5.8. In order to complete the pattern of the effect of the plant parameters on the electrical efficiency

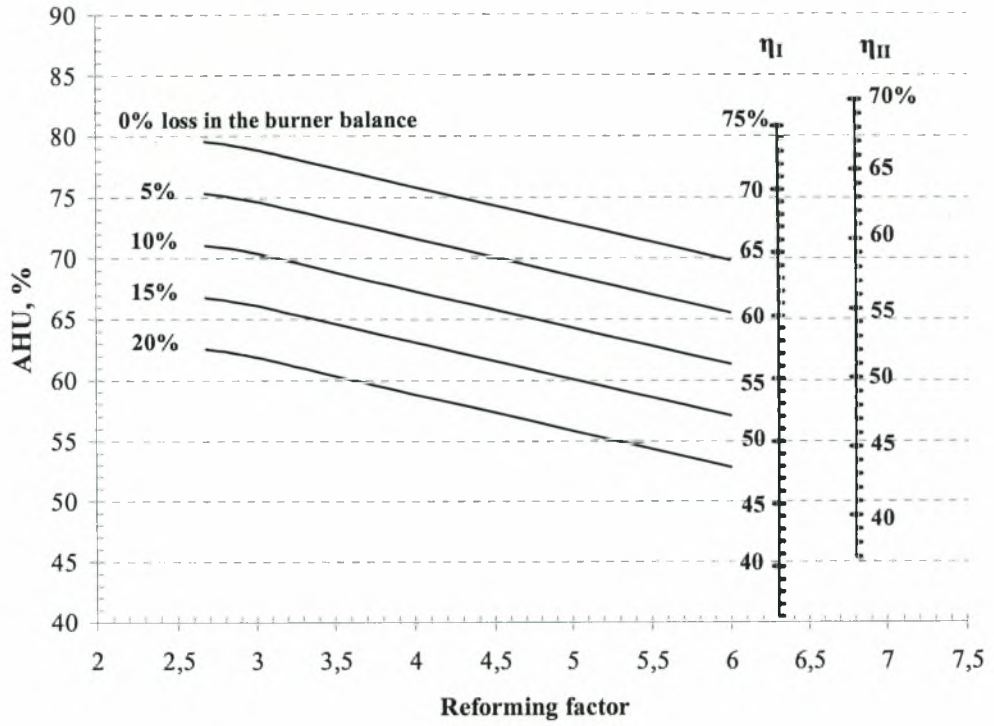

Figure 5.7. Nomograph of the first and second law efficiencies for various reforming factors and burner balances (Fuel = ethanol, $\varepsilon = \varepsilon_{max}$, optimum ΔT_{sofc}, $T_{sofc,\,out} = 1200K$).

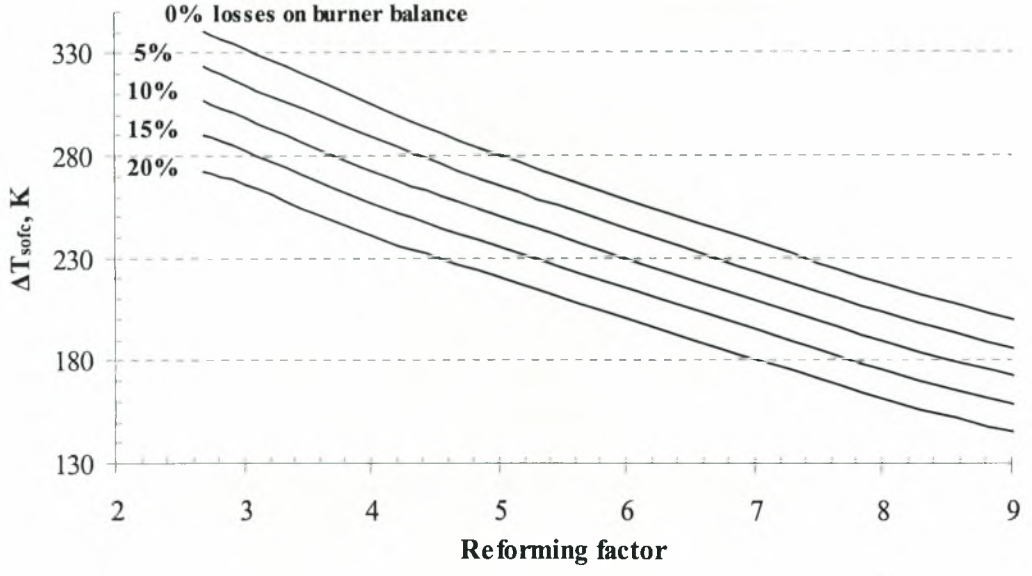

Figure 5.8. Effect of the reforming factor and burner balance on the optimal temperature difference ΔT_{sofc} required for adiabatic SOFC operation (Fuel = ethanol, $T_{sofc,\,out}$=1200K, $\varepsilon=\varepsilon_{max}$)

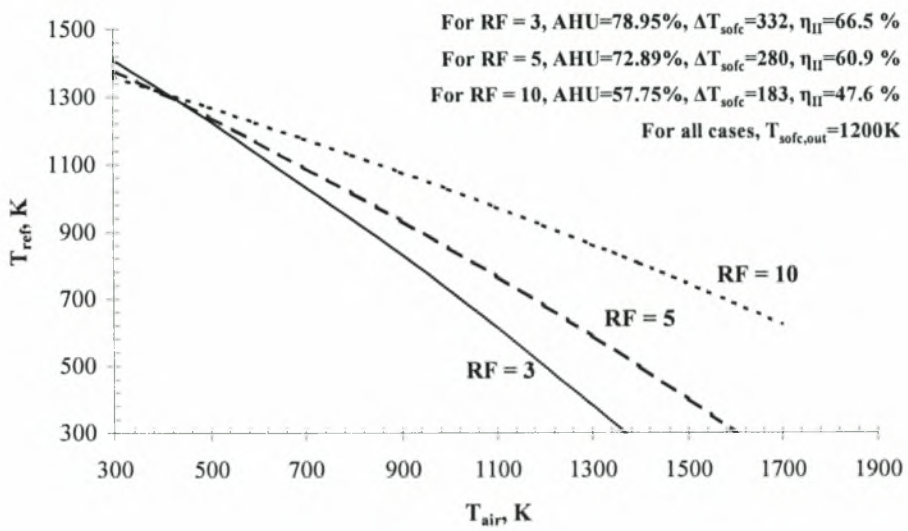

Figure 5.9. Effect of the reforming factor on the equivalence of the temperatures of the reformate and the preheated air for the ethanol fueled SOFC plant.

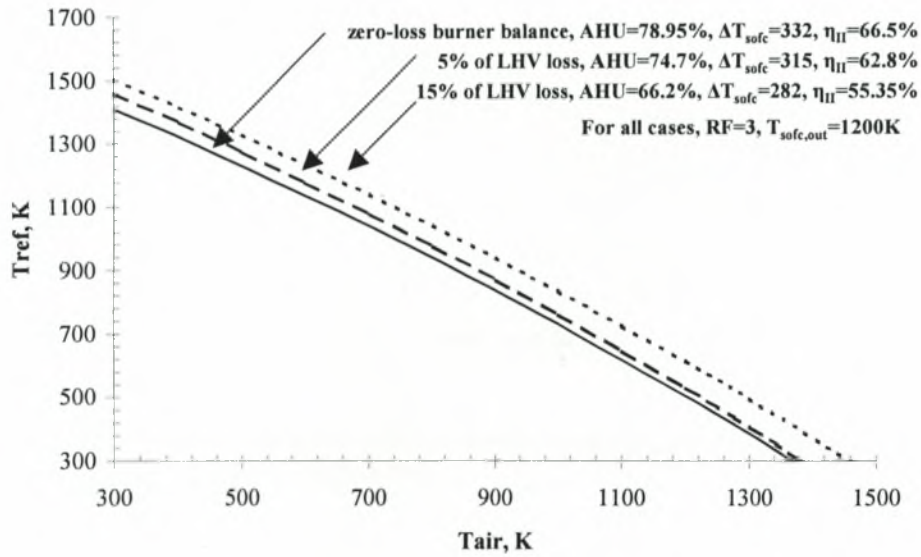

Figure 5.10. Effect of burner-to-environment energy losses on the equivalence of the temperatures of the reformate and the preheated air for the ethanol fueled SOFC plant.

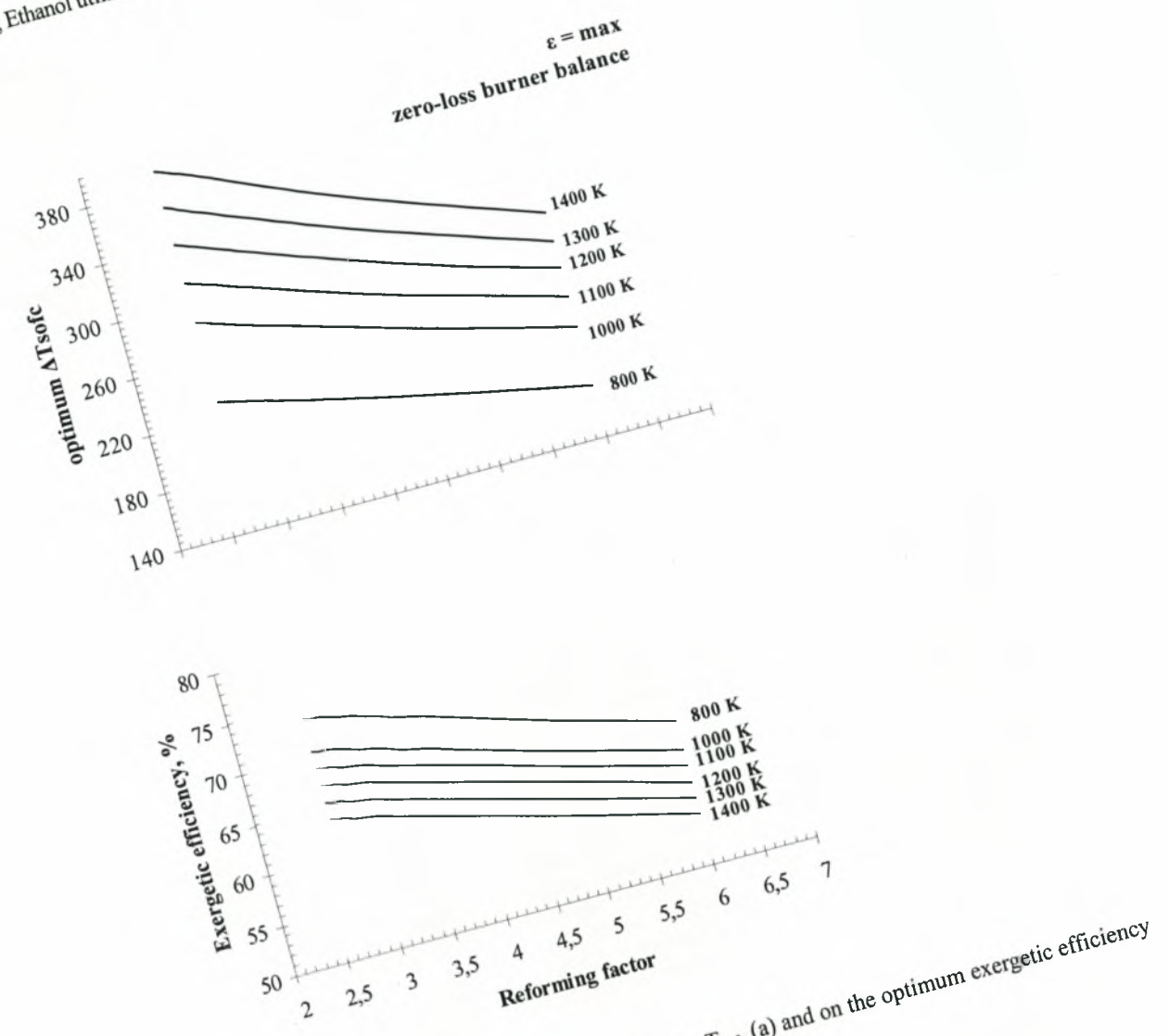

Figure 5.11. Effect of the temperature of the SOFC effluents on the optimum ΔT_{sofc} (a) and on the optimum exergetic efficiency (b) of the ethanol fueled plant for various reforming factors.

of the plant that is described in Figure 5.7, Figures 5.11a and 11b show the influences of the reforming factor and the desired temperature of SOFC products on the optimal temperature differences ΔT_{sofc} and the optimal exergetic efficiencies of the plant, respectively. As one can observe, the optimal temperature differences, ΔT_{sofc}, decrease at lower temperatures of SOFC operation due to the dependence of thermal capacities on temperature. Further, the higher is the temperature of SOFC operation the lower is the efficiency as was theoretically justified in section 5.5.1.1.

5.4.3. Deviation from optimality and its effect on irreversibility

Decision making in engineering of actual systems usually requires some compromises dictated by available materials, technical infrastructure, difficulties for optimal control and monitoring of units, etc. For the ethanol fueled SOFC plant described above, a deviation from the optimal regime of Figure 5.6 either may be required by the designer or may appear as the confluence of undesirable changes in one or more parameters. In both cases, it is important to assess the effect of each deviating reason on the irreversibilities appearing inside the plant so as to recognize appropriate modifications for improvements.

5.5.2.1. Non-adiabatic SOFC operation.

The optimization strategy developed in this Chapter, showed that the initial design parameter may be taken as the desired temperature of the SOFC effluents. Moreover, with the help of Figures 5.3 and 5.4 it was enunciated that depending on this initial parameter there exists an optimal temperature difference, ΔT_{sofc} (between the mixtures downstream and upstream the SOFC device) at which an adiabatic SOFC operation is attained, eliminating the exergy cost due to unnecessary heat waste. This stage of optimization, has been found crucial for the maximization of the plant performance (Figure 5.4) as it benefits both the energy and exergy balance of the most important unit for electricity generation. Futher, it is evident that this condition may be easily controlled by appropriate measuring of temperatures and therefore it is one of the most easily established. For this reason, the analysis of all other effects leading to deviation from optimality will be provided on the assumption of adiabatic SOFC operation.

5.5.2.2. Deviation from optimality due to requirements for high reforming factors.

The role of the reforming factor on the design and optimization of the SOFC power plant has been summarized by the discussion of Figures 5.5 and 5.6 assuming the fuel case of ethanol. However, by reminding the allocation of exergy costs according to Figure 5.5, it would be useful to recognize the effect of the reforming factor on the indivindual exergy costs of each unit.

In terms of exergy, the effect of the reforming factor can be presented by Figures 5.12a,b which provide the allocation of exergy costs in the indivindual units of the plant of Figure 5.1 for RF=5 and RF=10, respectively. By comparing these allocations with the optimal allocation of Figure 5.5, one can observe that the major influence of the increment of the reforming factor corresponds to a significant increment of the exergy destruction inside the burner. In fact, this is an indirect effect of the reforming factor that must be attributed on its effect on lowering the AHU value which forces the system to operate with higher participation of combustion in the burner. Further, one can observe that an increase of RF increases also the rates of exergy destruction in the reformer, due to friction and higher demand of heat supply, and in preheater 2 due to friction and higher driving forces of heat transfer. Exergy loss within the flue gases increases, due to the increment of their thermal capacity caused by addition of steam, and irreversibilities in the SOFC tend to increase (in absolute value). Finally, it is important to notice that the exergy analysis has all the respect provided by the axiomatic role of the second law of thermodynamics, indicating those cases and those operation regimes that are allowed or not. Under this respect, all cases at which one or more devices are characterized by negative exergy destruction rate (negative irreversibility) are implying direct violation of the second law of thermodynamics and are not feasible in practice. For example, it may be stated that those equivalent regimes of Figures 5.12a,b for which the exergy destruction in preheater 1 are negative are not allowed.

5.5.2.3. Deviation from optimality due to heat waste from the afterburner.

Heat waste from the afterburner to the environment has been recognized as a parameter of negative impact on plant performance as was showed in Figure 5.5. Due to the direct relation of ΔH_{loss} with the extend of reforming, ε, and hydrogen utilization, U it was proved (see Eq. 12) that such a heat waste reduces the AHU value and the efficiency of the plant. Here, the discussion will be focused on the effect of ΔH_{loss} on the relation of equivalence between the temperatures of the reformate and the preheated air as well as on its effect to the indivindual exergy destructions of the devices comprising the plant.

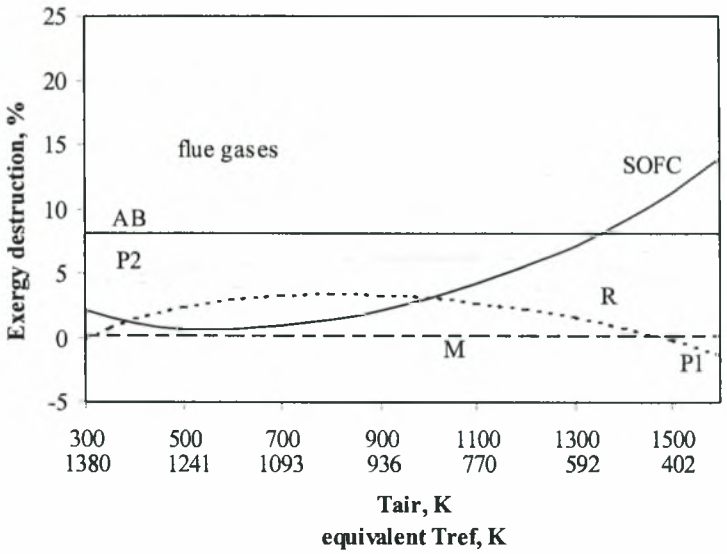

a) RF=5, ε_0=100%, U_0=72.89%, ΔT_{sofc}=280, η_{II}=60.9%, $T_{sofc,out}$=1200K

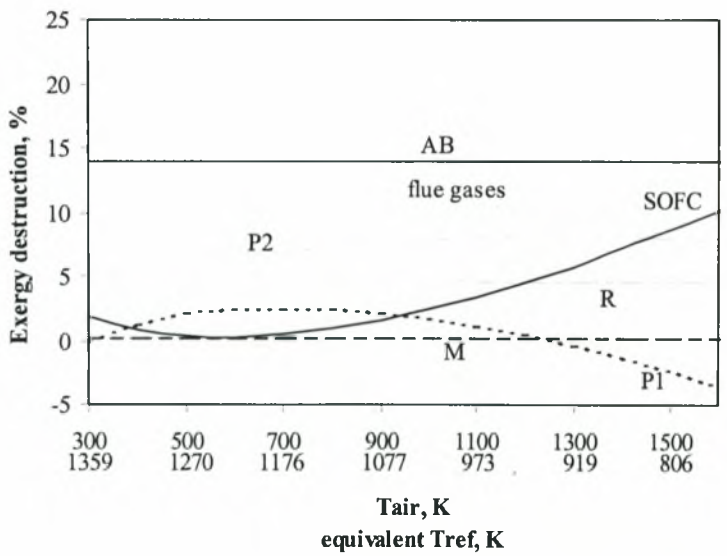

b) RF=10, ε_0=100%, U_0=57.75%, ΔT_{sofc}=183, η_{II}=47.6%, $T_{sofc,out}$=1200K

Figure 5.12. Allocation of exergy destruction rates in th ethanol fueled plant with RF=5 (a) and RF=10 (b).

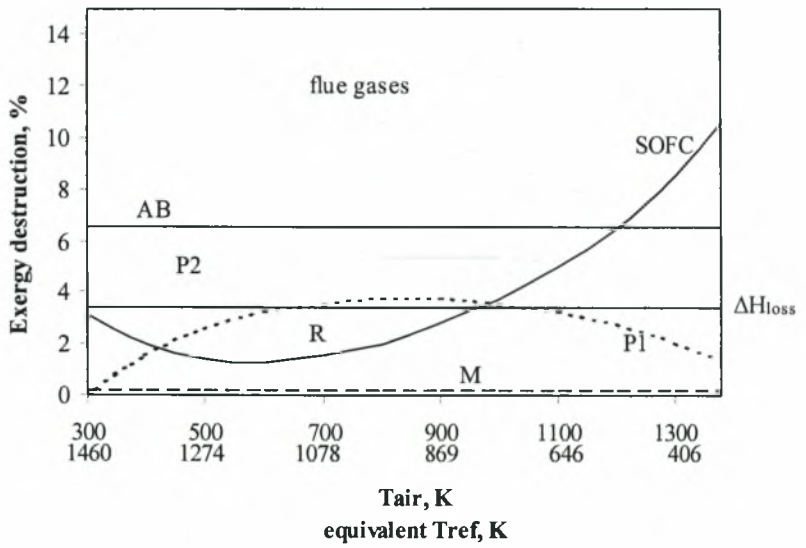

a) RF=3, ε=100%, U=74.7%, ΔT_{sofc}=315, η_{II}=62.8%, $T_{sofc,out}$=1200K

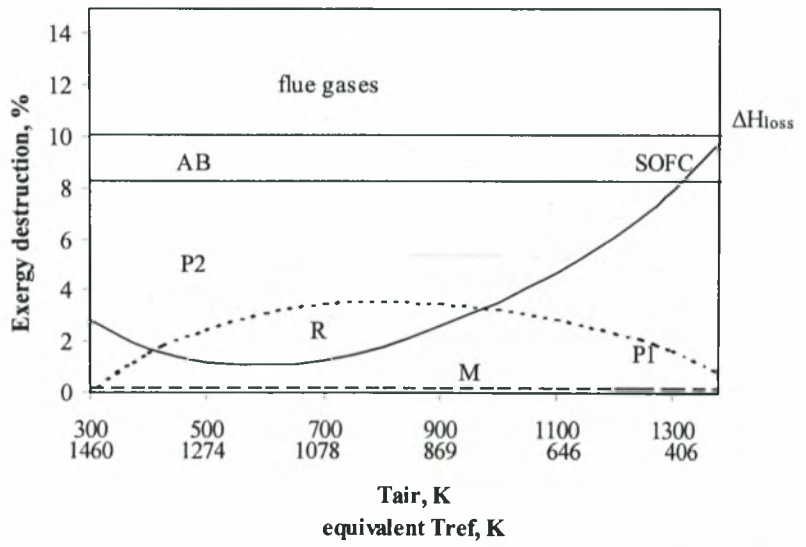

b) RF=3, ε=100%, U_0=66.2%, ΔT_{sofc}=282, η_{II}=55.35%, $T_{sofc,out}$=1200K

Figure 5.13. Allocation of exergy destruction rates in the ethanol fueled plant with ΔH_{loss}= 5% (a) and ΔH_{loss}= 15% (b) of LHV energy loss from afterburner to environment.

In terms of exergy, Figures 5.13a,b illustrate the allocation of the rates of exergy destruction in the devices of the plant when the burner operates with 5% and 15%LHV losses, respectively. Again, the higher is the energy loss the lower is AHU for electricity generation and the higher are the losses of exergy due to combustion in the burner. A significant observation, in comparison to Figure 5.7, is the appearance of the extra exergy sink due to ΔH_{loss} from burner to environment.

5.6. EFFECT OF FUEL TYPE

Table 5.1 provides the required parameters for the optimization of the plant when it operates with selected saturated hydrocarbons or alcohols. In order to specify the lower limit of steam/fuel ratios below which carbon deposition is thermodynamically possible, the values LRF were calculated assuming the Boudouard reaction of carbon monoxide disproportionation. As shown, the higher is the carbon content of the molecule of the fuel, the higher must be the minimum reforming factor (LRF) to avoid carbonization. Moreover, depending also on the heats of the combustion and reforming of each fuel, the constants B and C are calculated. Thus, the zero-loss locus (ε_0, U_0) may be specified.

As mentioned, the lower is the reforming factor the higher will be the efficiency of the plant. The lowest possible reforming factor may be imposed either by the limiting reforming factor above which carbon formation is possible (LRF) or by an appropriately higher value MRF for which Eq. (12) is valid. For example, in the case of methane, the extend of reforming must always be lower than (1.486/2)x100=74.3% when the LRF is used. For such low values of ε, the system cannot operate at zero-loss conditions. The same effect is valid for methanol as well. For all other fuels of Table 5.1, the optimization for the cases of LRF takes place at conditions near the above-mentioned upper limit. When the stoichiometric reforming factor SRF value is selected, the extend of reforming can attain 100% and so for all cases except ethane the maximum will correspond at ε =100%. As shown, the utilization of the LRF provides higher efficiencies than the utilization of SRF since generally LRF<SRF.

Moreover, it is evident that the lowest is the homologue in the series of the saturated hydrocarbons or alcohols the highest is the expected maximum exergetic efficiency. This can be explained by the relative ratio of hydrogen/carbon atoms in the mole of each fuel that is the highest in the case of methane (equal to 4) and decreases for higher homologues. Finally, it is observed that the higher homoloques impose lower optimal temperature differences, ΔT_{sofc}, for adiabatic SOFC operation.

Up to this point, the example of ethanol has been used to clarify the indivindual effect of the parameters of the SOFC plant on the optimization. However, as it will be discussed, the significance of the effect of these operative parameters on the plant efficiency is different for different fuels. For this reason, a more detailed analysis of selected hydrocarbons and alcohols is provided.

5.6.1. The case of methane

By assuming the plant of Figure 5.1 being fueled by methane and by following the optimization strategy mentioned in section 5.5.1, the effect of the reforming factor and the effect of the burner balance on the overall efficiency is provided in the nomograph of Figure 5.14.

Similarly to Figure 5.7, Figure 5.17 depicts the effect of the temperature of the SOFC effluents on the optimal temperature difference ΔT_{sofc} and the optimal exergetic efficiency of the plant fueled by methane. It can be said that for a given RF the effect of $T_{sofc,out}$ on the exergetic efficiency is similar to that of the ethanol plant.

Further, Figure 5.18 illustrates the equivalent solutions and the allocation of the exergy costs for an optimally designed plant using methane with RF=2.2. It is interesting to observe that the dependence of the indivindual exergy costs on T_{air} and the equivalent T_{ref} differs significantly from those obtained for the ethanol plant (Figure 5.7). Indeed, a significantly large region of solutions is found to violate the second law by means of negative exergy destruction rates in the reformer and the preheater 2. This seems plausible by observing that low temperatures of air preheating require extremely high equivalent temperatures for reforming. As a consequence, air must be preheated above 800 K and the reformate must be produced at temperatures lower than 1150 K in order the plant to perform optimally. Minimization of exergy destruction in the SOFC device is found to correspond at even higher temperatures of T_{air} but a significant constraint arises by the technical impediments in accomplishing methane reforming at temperatures below 1100 K. Therefore, the optimality may be considered in this case to correspond at T_{air}=800 K and T_{ref}=1150 K, as shown in Figure 5.19. In terms of exergy, a comparison of the cases of methane and ethanol is provided for their optimal designs by the Grassman (exergy flow) diagrams of Figure 5.20.

5.6.2. Comparison of fuels

Despite the fact that methane optimization according to the parameters of Table 5.1 provides higher efficiencies than ethanol, a comparison between Figure 5.14 and Figure 5.5 clearly shows that the effect of the reforming factor on the optimal efficiency is more dramatic in the case of methane than in the case of

Table 5.1. Parameters of optimization for selected saturated hydrocarbons and alcohols*

	RF†	LHV (J/mol)	ΔH_{ref} (J/mol)	Standard chemical exergy (J/mol)	B	C	A	U_0‡ (%)	ε_0‡ (%)	ΔT_{opt}, K	η_{II}* (%)
Saturated hydrocarbons											
CH_4	LRF=1.486	802600	164627	831650	0.76190	-0.000357	4	-	-	-	-
	MRF=1.54				0.759901	-0.000357		99	76.74	**346**	**69.93**
	SRF=2				0.73854	-0.000357		73.9	100	**323**	**67.78**
C_2H_6	LRF=3.26	1428600	268074	1495840	0.759299	-0.002332	7	93	81.44	**338**	**67.63**
	SRF=4				0.7400806	-0.002332		99	74.57	**321**	**65.77**
C_3H_8	LRF=5.1	2043100	375061	2150400	0.752175	-7.86×10^{-6}	10	88.5	84.99	**332**	**66.69**
	SRF=6				0.735813	-7.86×10^{-6}		73.59	100	**315**	**65.07**
C_4H_{10}	LRF=6.95	2657300	486298	2805800	0.748104	-1.15×10^{-5}	13	86.2	86.78	**328**	**66.04**
	SRF=8				0.733421	-1.15×10^{-5}		73.35	100	**313**	**64.60**
$C_5H_{12(l)}$	LRF=8.8	3244900	$597395_{(g)}$	3461800	0.738685	-0.006925	16	84.7	87.93	**326**	**65.57**
	SRF=10				0.7250505	-0.006925		73.2	100	**312**	**64.31**
$C_8H_{18(l)}$	LRF=14.3	5074200	$929766_{(g)}$	5413100	0.7353545	-0.006862	25	82.97	89.36	**322**	**65.19**
	SRF=16				0.7229924	-0.006862		72.99	100	**310**	**64.06**
Alcohols											
$CH_4O_{(l)}$	LRF=0.825	638200	$48969_{(g)}$	718000	0.829731	-0.052774	3	-	-	-	-
	MRF=0.882				0.8268223	-0.052774		99	88.16	**369**	**69.90**
	SRF=1				0.8191262	-0.052774		87.2	100	**363**	**69.77**
$C_2H_6O_{(l)}$	LRF=2.68	1235000	$173536_{(g)}$	1357700	0.7699888	-0.029204	6	89.15	89.29	**341**	**67.16**
	SRF=3				0.760293	-0.029204		78.95	100	**332**	**66.52**

†LRF=limiting reforming factor for carbonization at 800K,
MRF=minimum possible reforming factor for oprimization according to zero-loss burner balance,
SRF=stoichiometric reforming factor
‡calculated for zero energy loss from the burner according to Eq. (12)
*for $T_{SOFC,\,out}$ = 1200K

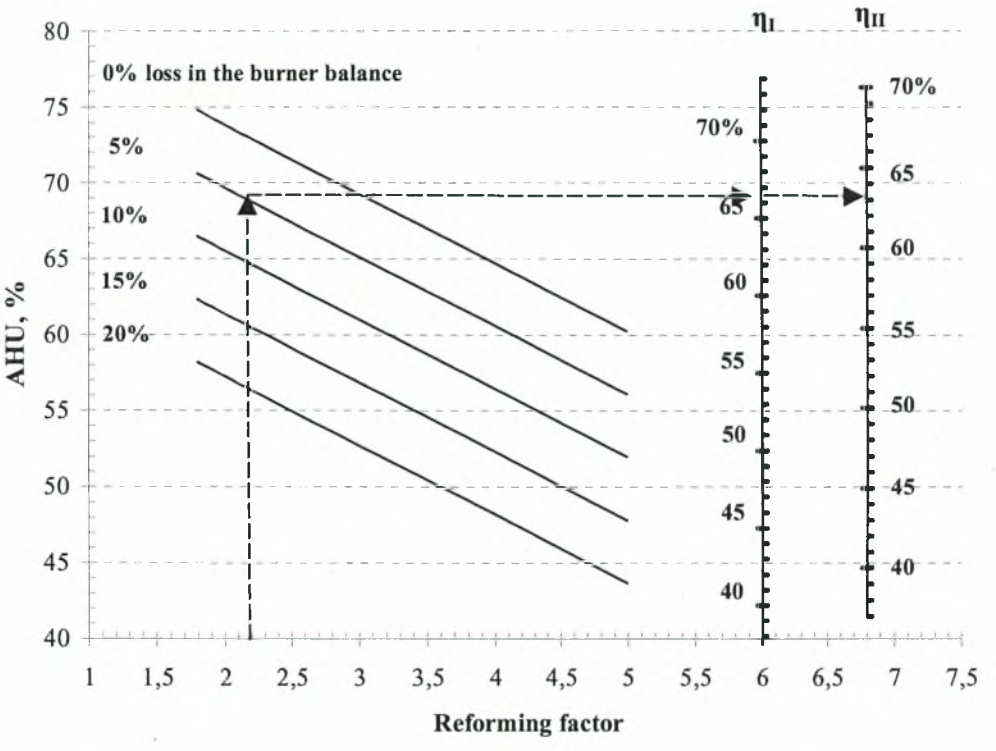

Figure 5.14. Nomograph of the first and second law efficiencies of the methane fueled SOFC plant for various reforming factors and burner balances ($\varepsilon = \varepsilon_{max}$, optimum ΔT_{sofc}, $T_{sofc,\,out}$ = 1200K). The example corresponds to results published in [11].

ethanol. Indeed, one can observe that every additional mole steam of steam per mole of fuel incopropates a decrease of the exergetic efficiency of the plant by almost 4.67% in the case of methane and by approximately 2.67% in the case of ethanol. Hence, Table 5.1 does not imply a "global" rule for the expectations by each fuel choice but only their relative classification at conditions providing the maximum possible efficiency for each of them. At conditions that deviate from optimality with approximately the same way, it is possible that utilization of ethanol be preferable than utilization of methane in terms of theoretical efficiency. The same effect may also become more profound due to deviation from the optimal burner balance; however both ethanol and methane are providing quite similar dependence from it (approximately 3.5% and 4% efficiency decrease per 5% increment of energy loss).

In order to assess the influence of the reforming factor and burner balance on the relative classification of fuels according to expected efficiency, Figure 5.21 illustrates this dependence for the plant of Figure 5.1, assuming it is fed by selected hydrocarbons such as methane, ethane, butane and n-octane. It is considered that the reforming factor for each fuel increases up to 6 units higher from its corresponding minimum value (LRF or MRF, see Table 5.1), and three cases of burner balance corresponding to 0, 5 and 10% of LHV losses are presented. As shown, at the minimum values of reforming factors LRF or MRF, the eligibility of all fuels for efficient plant operation decreases from lighter to heavier hydrocarbons regardless of the burner balance. However, by keeping the same fuel input and adding the same amount of steam in the feedstream of the reformer, a new classification of the fuels is taken.

The decrement of the expected exergetic efficiency of the plant of Figure 5.1 due to supply of additional amount of steam in the reformer, is more dramatic the lighter is the hydrocarbon fuel. Thus, as one can observe, the relative classification of all saturated hydrocarbons at high reforming factors is expected to be exactly the opossite of the one described in Table 1 when a standard burner balance is assumed. Indeed, this effect of the reforming factor is so crucial in selecting the fuel for utilization, as it can be observed by a comparison

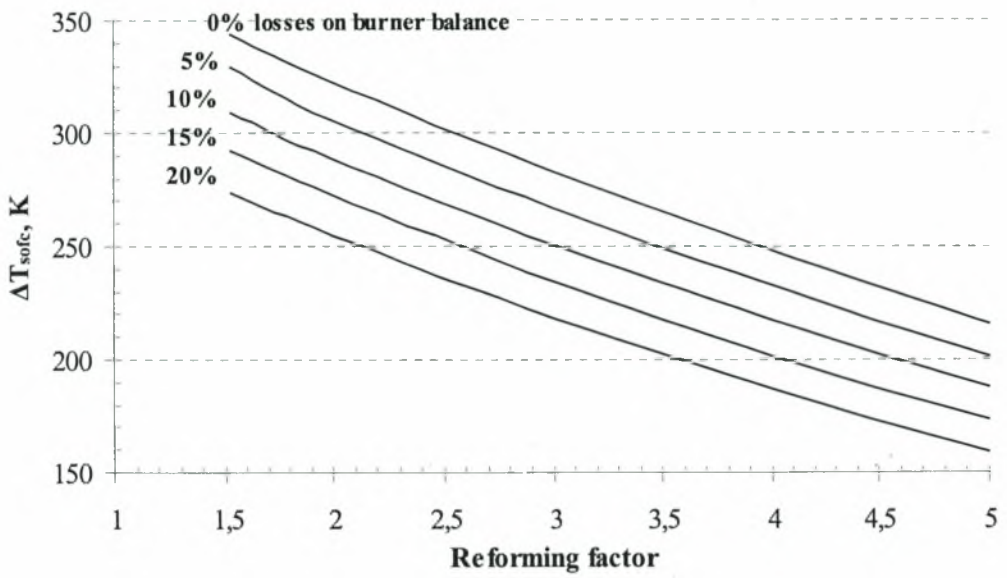

Figure 5.15. Effect of the burner balance and reforming factor on the optimal temperature difference ΔT_{sofc} for the methane fueled plant ($T_{sofc,\,out}$=1200K).

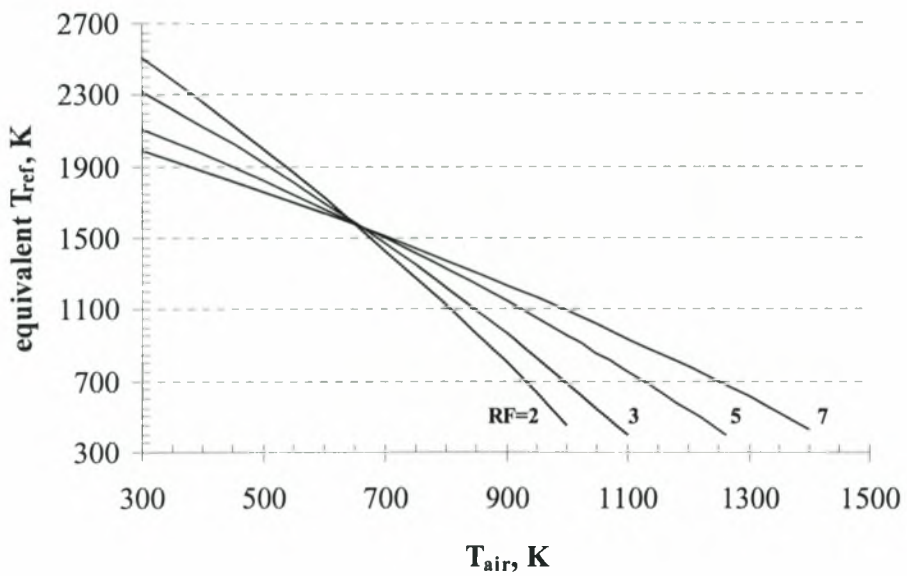

Figure 5.16. Effect of the reforming factor on the equivalent temperatures of the reformate and preheated air for the methane fueled plant ($T_{sofc,\,out}$=1200K, ΔT_{sofc}=optimum).

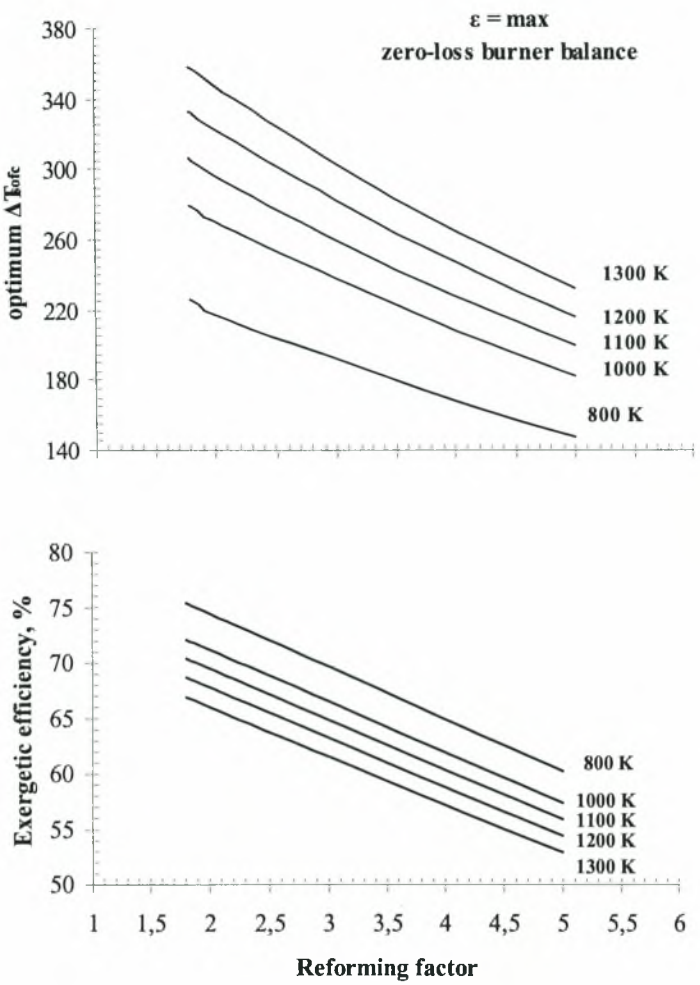

Figure 5.17. Effect of the temperature of the SOFC effluents on the optimum ΔT_{sofc} (a) and on the optimum exergetic efficiency (b) of the methane fueled plant for various reforming factors.

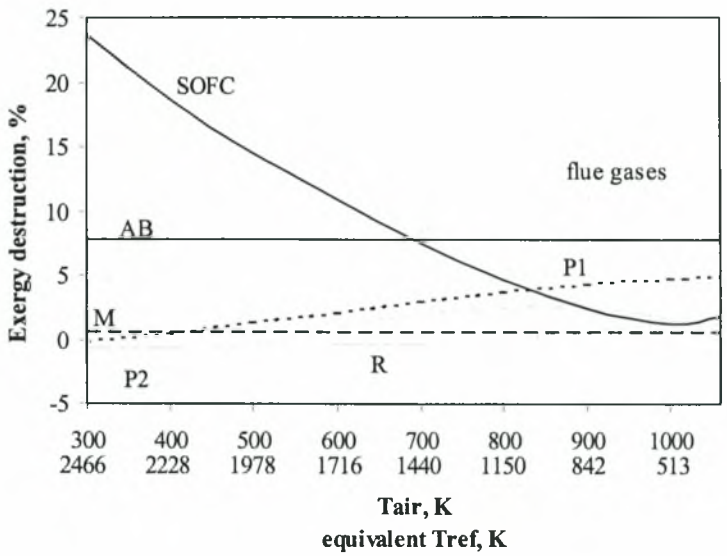

Figure 5.18. Allocation of exergy costs in the units of the optimally designed methane fueled SOFC plant (RF=2.2, $T_{sofc,out}$=1200K, ΔT_{sofc}=315, ε_0=100%, U_0=72.98, η_{II}=66.9%, M=Mixer, P1=Preheater 1, P2=Preheater 2, AB=After Burner, R=Reformer) at all equivalent schemes for temperatures of preheated air and reformate.

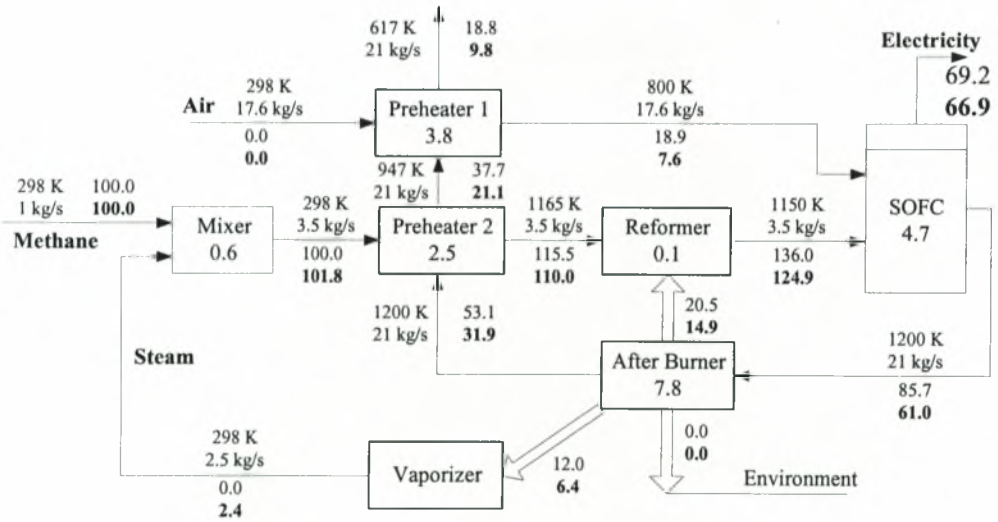

Figure 5.19 Optimal configuration of the methane fueled SOFC plant. (RF=2.2, 100% theoretical air, ε_0=100%, U_0=72.98% (plain text stands for energy values while bold stands for exergy ones).

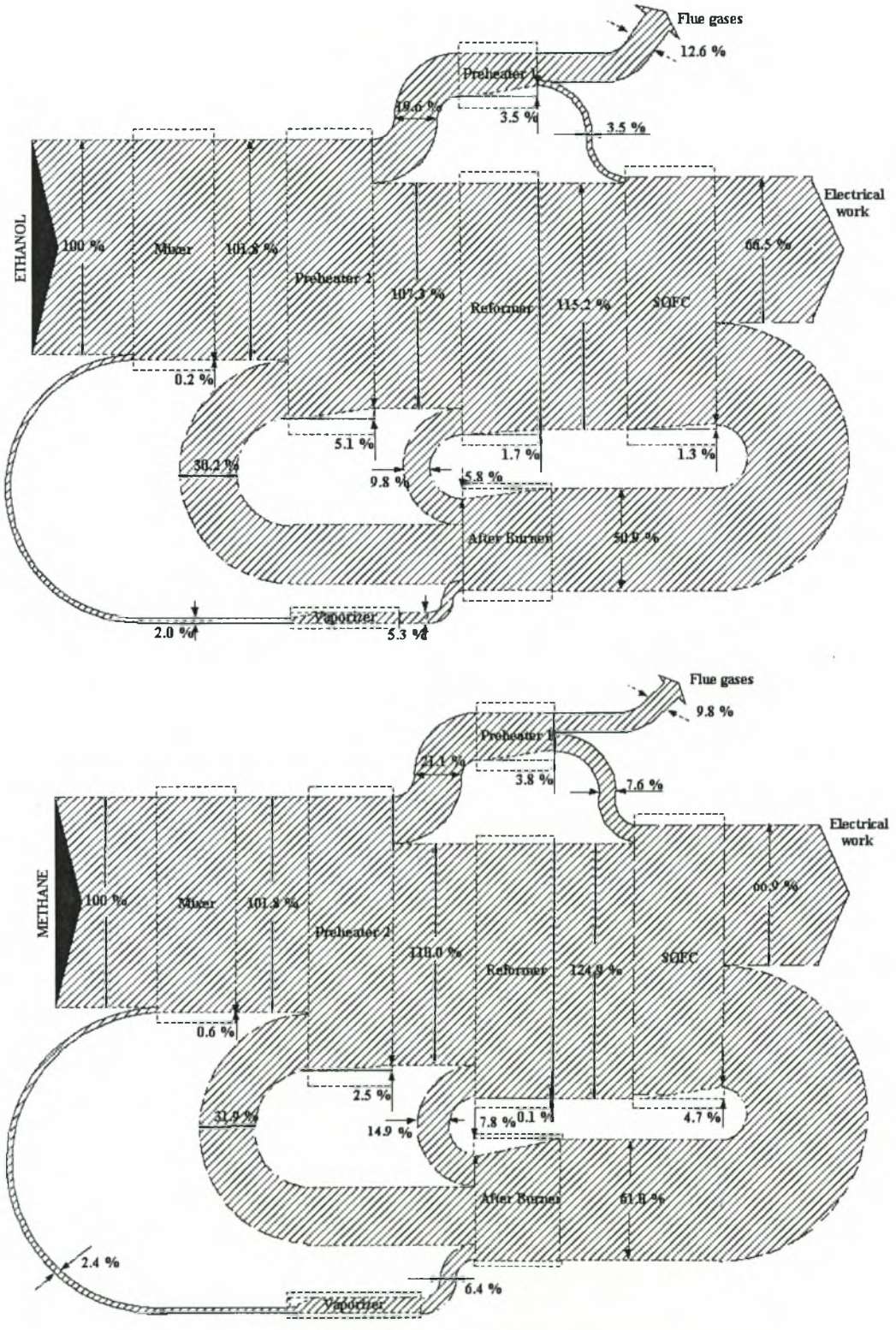

Figure 5.20. Grassman diagrams of ethanol and methane fueled SOFC plants (comparison of optimal designs).

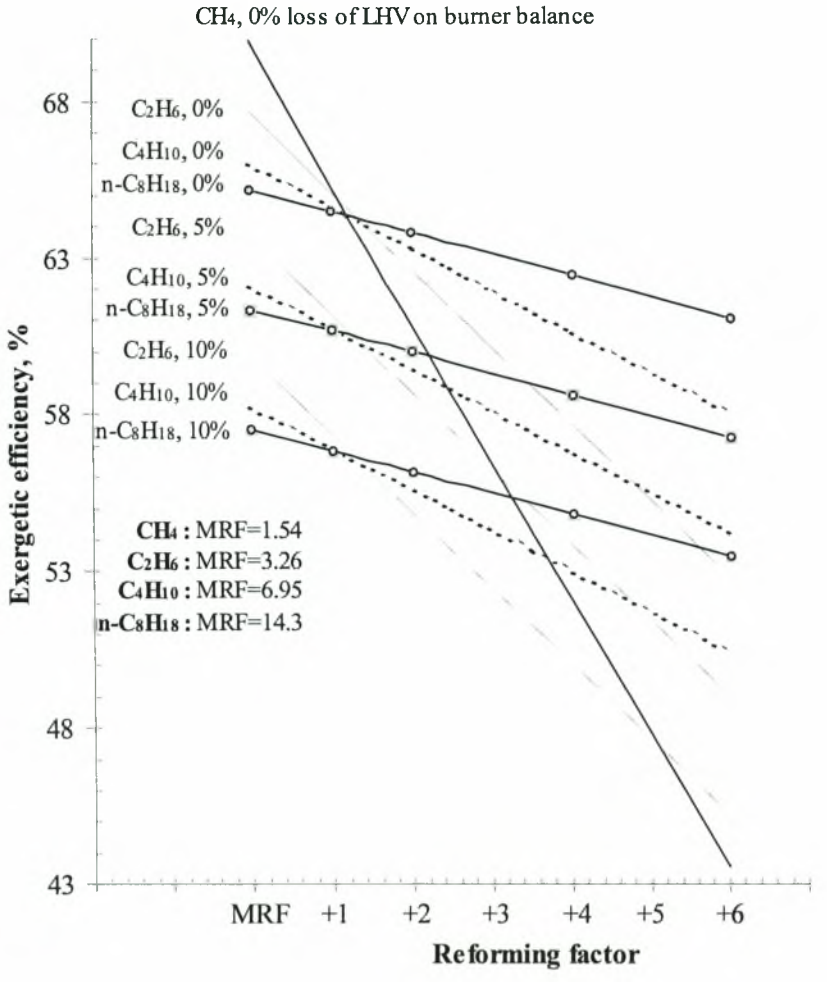

Figure 5.21. Effect of the increment of the reforming factor and burner losses on the relative classification of selected saturated hydrocarbons (methane, ethane, butane and n-octane) in terms of the overall exergetic efficiency of the plant of Figure 5.1 ($T_{sofc,\,out}$ = 1200 K, ΔT_{sofc}=optimal).

between methane and n-octane. Since methane and gasoline (n-octane) have been found to be the best and worse fuel options respectively with respect the maximum expected efficiency after optimization (see Table 5.1), a lack of the awareness of the results of Figure 5.21 could lead to the misleading assumption that this is also the case at higher reforming factors or even at higher losses from the burner. Figure 5.21 clearly shows that the expected efficiency in the case of n-octane drops from 65.19% at the 0% loss and LRF=14.3 regime, into about 61.07% at 0% loss with RF=20.3 and into about 53.5% in the worse case examined with 10% loss and RF=20.3. In contrast, expected exergetic efficiency from methane utilization only in the optimal case of 0% losses from the burner, becomes lower than 60% at RF>3.5 and lower than 53.5% at RF>5.2.

A similar comparison between saturated hydrocarbons and selected alcohols (methanol and ethanol) is presented in Figure 5.22. In this case only the respective saturated hydrocarbons (i.e. methane and ethane) are presented. As shown, higher alcohols (ethanol) are less depended from a change of the reforming factor than lower (methanol), in a similar way to saturated hydrocarbons. In general, alcohols are found to exhibit similar behavior with their corresponding saturated hydrocarbon (i.e. ethanol with ethane) with slightly higher dependencies on the reforming factor. In

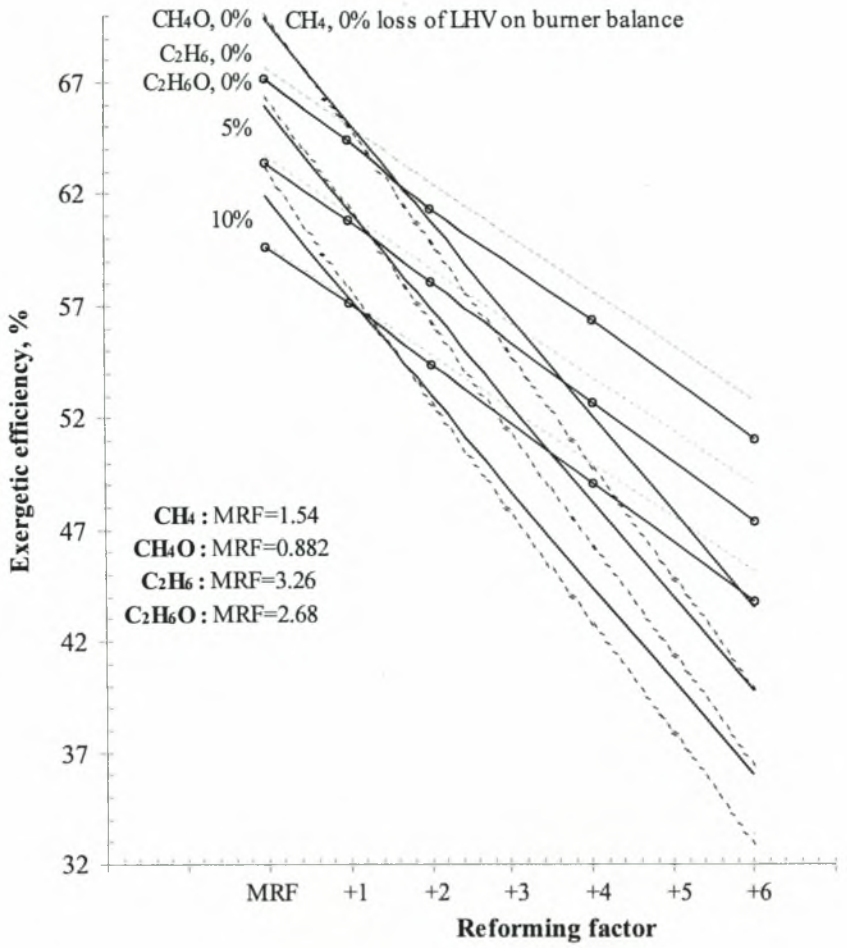

Figure 5.22. Effect of the increment of the reforming factor and burner losses on the relative classification of selected saturated hydrocarbons (methane, ethane) and alcohols (methanol, ethanol) in terms of the overall exergetic efficiency of the plant of Figure 5. 1 ($T_{sofc,\,out}$ = 1200 K, ΔT_{sofc}=optimal).

factors, as the losses of the burner balance increase, alcohols tend to surmount the efficiency barrier of their corresponding hydrocarbon. This effect is presented in Figure 5.22 between methanol and methane and is clear for their MRF values at 10% losses. Therefore, at an approximately same deviation from the optimal burner balance, methanol fed SOFC may be considered preferable to methane fed. It is worth noticing that this effect tend to appear also so as to change the relative classification of ethane and ethanol at low reforming factors and burner losses higher than 10% of their low heating values.

5.7. TOPOLOGY MODIFICATIONS

Modeling, analysis and optimization of energy systems usually begin by assuming a certain architecture and topology. Then, a simulation of the operative regime of the system provides a mathematical description of its performance and the conditions that are most favorable for optimization in terms of one or more objective criretia (maximum efficiency, minimum cost etc.). However, the search for optimal design is considerable more challenging than optimizizing the operation of an assumed configuration [35]. Topology is the major

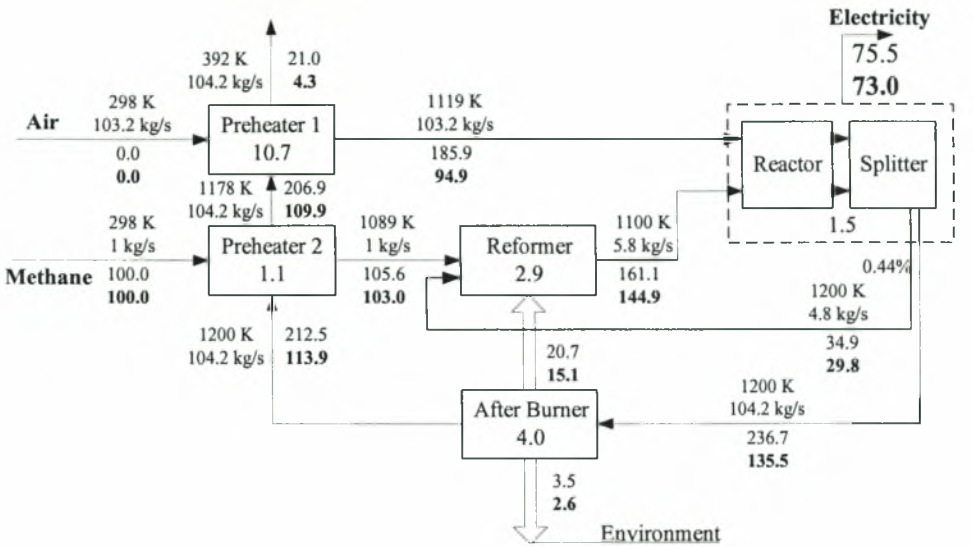

Figure 5.23. Nearly optimal configuration of a methane fueled SOFC plant proposed by Bedringas et. al. [10, 11]. RF=2.2, 600% theoretical air, ε =90%, U=75%, Splitting fraction =0.44%. (plain text stands for energy values while bold stands for exergy ones).

unknown in engineering design and methods for improvement of performance by rational architectural modifications could be extremely helpful in meeting high standards and overcoming obstacles in practice.

The principle that generates geometric structure is the pursuit of a global objective subject to specified global and local constraints [36]. For example, SOFC-based systems, like that of Figure 5.1, may be modified in topology with global objective the maximization of the thermodynamic performance or the minimization of thermodynamic irrversibility, under the constraints imposed by required engineering integrity and theoretical limitations.

For the plant configuration of Figure 5.1, Eq. (12) provides the condition

$$AHU = B - \Delta H_{loss} - \varepsilon C \qquad (16)$$

indicating that, at standard burner balance, AHU maximization (and thus work output maximization according to Eq. (14)) requires topology modifications to induce an increase of parameter B, a decrease of parameter C, or both. On this basis, two topological modifications can be discussed as done in the following two sections.

5.7.1. Elimination of the vaporization requirements.

For a given fuel, the parameter C is constant indepedently on the reforming factor, while B increases by decreasing $\Delta H_{vap.}$ Therefore, the work output may increase either by keeping the topology of Figure 5.1 and lowering the reforming factor - as was discussed in detail previously - or by completely eliminating the requirement for vaporization by means of a change in the architectural design. This approach was followed by Bedringas *et. al.* [10, 11] for the modification of the methane fueled plant of Figure 5.19, by splitting a fraction of the steam containing stream of the effluents of the SOFC device to support the reforming reaction without external water supply. Indeed, by keeping the same reforming factor (RF=2.2), it was found that the overall exergetic efficiency of the plant may increase from 66.9% (Figure 5.19) up to 73.0% (Figure 5.23) even when the burner balance corresponds to ΔH_{loss} = 3.5 % of LHV and air excess is 600% (obviously, an adiabatic burner operation and stoichiometric air utilization would have a more positive impact). According to these results [10, 11], a fraction equal to 0.44% of the stream outcoming from the SOFC anode is required to be recycled and routed as input of the reformer unit.

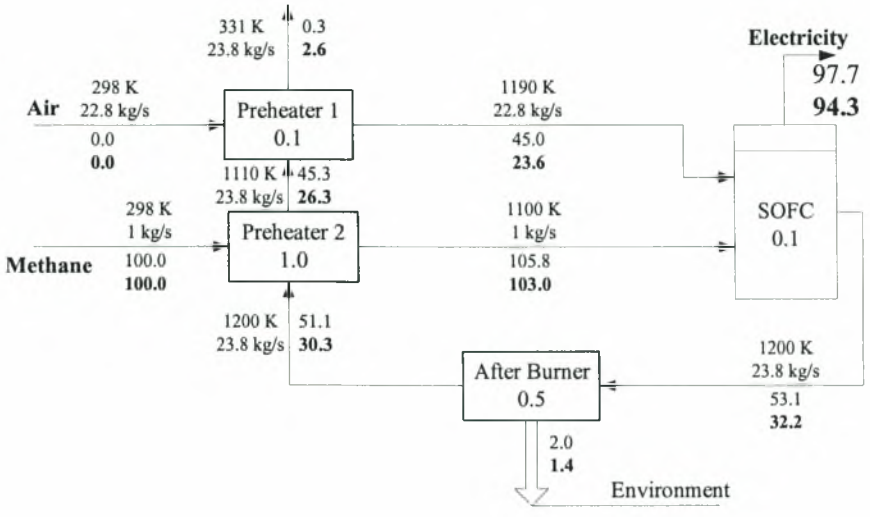

Figure 5.24. Nearly optimal configuration of a direct-methane SOFC plant. 130% theoretical air, U_{CH4}=98%. (plain text stands for energy values while bold stands for exergy ones)

5.7.2.Elimination of steam reforming - Direct oxidation of hydrocarbons in the SOFC.

Even higher efficiencies might be achieved by topology modifications in the direction of extracting both the vaporizer and the reformer from the plant of Figure 5.1. In fact, such a modification corresponds to the design and development of a plant that should be able to directly oxidize the fuel in the SOFC unit.

Direct oxidation of hydrocarbons in SOFCs, though theoretically feasible due to high operating temperatures and presence of O^{2-} anions on the SOFC anode (in contrast to all other fuel cell types), is technologically prevented by the tendency of currently used anodes (most commonly Ni-based ytrria (Y_2O_3) cermets) to catalyze carbon formation. To overcome this obstacle, addition of steam in the SOFC input (internal reforming) or, even better, steam reforming of carbonacous fuels in a separate reactor (external reforming) was found as appropriate remedy during the last years.

Recent work in the direction of anode development for direct oxidation of hydrocarbons in SOFCs, revealed two methods in facing the problem of carbon formation: a) selection of appropriate anodes (mixed perovskite oxides do not catalyze C-C bond formation and are therefore resistant to carbon formation) and operation of SOFC with methane at a narrow range of operating temperatures (500 – 700 °C) were carbon deposition is not favored [37-39], and b) utilization of metal cermet catalysts like Ni-cermets, where the conducive in carbon deposition Ni metal is being solely substituted by another metal (such as Cu) that does not force carbon formation reaction in equilibrium [40, 41]. Both these resently developed methods, give prospects for future development and operation of direct-hydrocarbon and especially direct-methane SOFCs. Therefore it would be interesting to examine the effect of maximization of constant B (elimination of vaporization) together with the minimization of constant C (elimination of reforming) on the performance of a plant fueled by methane.

Figure 5.24 illustrates a direct-methane SOFC operating with U_{CH4}=98 % and 130% theoretical air. Due to large allowable fuel utilization, the overall efficiency can attain extremely high values such as 94.3% of the chemical exergy of methane. The overall topology is significantly simplified and the burner can also be eliminated assuming that the associated exergy loss and exergy destruction are carried to environment within the flue gases. The optimal difference between the mixtures incoming and outcomming the SOFC is now of the order of ΔT_{sofc}=4 and may vary significantly without serious impact of the SOFC balance (an increment to ΔT_{sofc} = 100 does not affect efficiency and requires only 5% of LHV additional heat in the SOFC to establish the required temperatures).

From the example of Figure 5.24, one may conclude that direct oxidation of hydrocarbons in the SOFC provides the upper limit of efficiencies that can be expected by any topology modification. Further, since virtually no limit is imposed in fuel utilization, the maximum expected efficiency will tend to equalize the intrinsic theoretical efficiency of the fuel used, as it can be expressed by the ratio

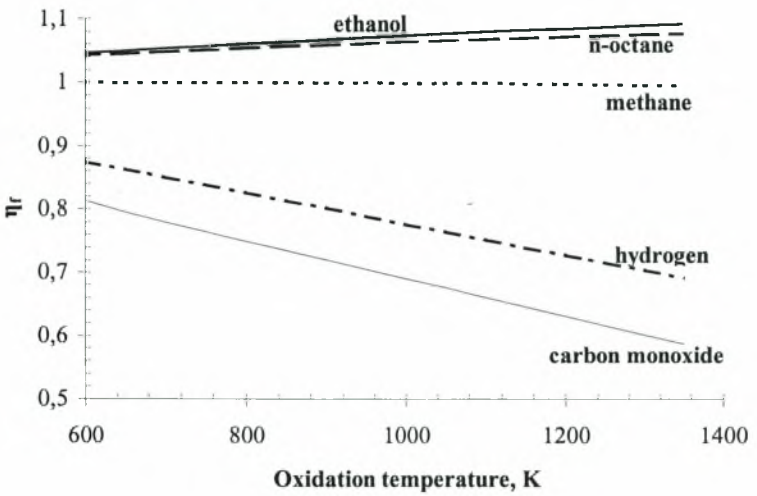

Figure 5.25. Expected maximum theoretical efficiency from direct oxidation of selected hydrocarbons, hydrogen and carbon monoxide at various temperatures of SOFC operation (results obtained by methodology and data presented in [27]).

$\eta_f = (\Delta G)_T/\Delta H^o$

that is presented for selected fuels in Figure 5.25. As one can distinguish, efficiencies from direct oxidation of hydrocarbons is theoretically less dependent on temperature variations than efficiencies from oxidation of hydrogen or carbon monoxide derived by reforming. Further, it is shown that carbonaceous fuels such as ethanol and n-octane have even higher tendency for efficient application than methane. Technically, however, these fuels present higher conducivities for carbon deposition and they are not considered appropriate for direct SOFC applications. Finally, Figure 5.25 illustrates that direct oxidation of fuels such as ethanol and gasoline may provide theoretical efficiencies above 100%. Indeed, hydrocarbon-air fuel cells operating above 100°C (at 1atm) produce water from the SOFC reaction in vapor phase and, thus, the entropy change of the reaction is positive. As a result, if sufficient advances in electrocatalysis could be made to avoid carbon formation and reduce overpotentials, it would be possible to attain efficiencies above 100%.

5.10. CONCLUSIONS

In Chapter 5, the design guidelines for integrated SOFC power plants were discussed. Based on first and second law considerations, an optimization strategy and a thorough parametric analysis was presented indicating methods and techniques for optimal plant operation. The strategy proposed was applied for different topologies and fuel options providing usefull information and criteria for practical decision making. The axiomatic value of exergy analysis in the design and optimization of SOFC systems was clarified and its specific role was explained.

REFERNCES

1. Sciubba E., *Beyond thermoeconomics? The concept of extended exergy accounting and its application to the analysis and design of thermal systems.* Exergy Int. J., 2001. **1**(2): p. 68-84.
2. Rosen M. A. and Dincer I., *Exergy as the confluence of energy, environment and sustainable development.* Exergy Int. J., 2001. **1**(1): p. 3-13.
3. Dunbar W. R., Lior N., and Gaggioli R. A, *Combining fuel cells with fuel-fired power plants for improved exergy efficiency.* Energy, 1991. **16**: p. 1259-1274.
4. Dunbar W. R. and Lior N., *Sources of combustion irreversibility.* Combust. Sci. Technol., 1994. **103**: p. 41-61.
5. Caton J. A., *On the destruction of availability (exergy) due to combustion processes - with specific application to internal combustion engines.* Energy, 2000. **25**: p. 1097-1117.

6. Petela R., *Apllication of exergy analysis to the hydrodynamic theory of detonation in gases.* Fuel Processing Technology, 2000. **67**: p. 131-145.
7. Hirschenhofer J. H., et al., *Fuel Cell Handbook.* 4th Edition ed. 1997: Business/Technology Books, Orinda-USA.
8. Benjamin T. G., Camara E. H., and Marianowski L. G., *Handbook of Fuel Cell Performance.* May 1980: Institute of Gas Technology, Chicago-Illinois.
9. Minh N. Q. and Takahashi T., *Science and technology of ceramic fuel cells.* 1995: Elsevier Science B.V. Amsterdam-The Netherlands.
10. Bedringas Kai W., *The exergy concept in simulation of power systems*, in *Department of thermodynamics*. 1993: Norwegian Institute of Technology, University of Trondheim, Trondheim-Norway.
11. Bedringas Kai W., et al., *Exergy analysis of Solid-Oxide-Fuel-Cell (SOFC) systems.* Energy, 1997. **22**(4): p. 403-412.
12. van der Oosterkamp P. F., Goorse A. A., and Blomen L. J. M. J., *Review of an energy and exergy analysis of a fuel cell system.* J. Power Sources, 1993. **41**: p. 239-252.
13. Cownden R., Nahon M., and Rosen M. A., *Exergy analysis of a fuel cell power system for transportation applications.* Exergy Int. J., 2001. **1**(2): p. 112-121.
14. Bejan A., Tsatsaronis G., and Moran M., *Thermal design and optimization.* 1996: John Wiley & Sons, Inc.
15. Kotas T. J., *The exergy method of thermal plant analysis.* 1985: Butterworths, London-England.
16. Gaggioli R. A. and Dunbar W. R., *EMF, maximum power and efficiency of fuel cells*, in *Fundamentals of Thermodynamics and Exergy Analysis*, Tsatsaronis G. et. al., Editor. 1990, p. 7-11: ASME, New York.
17. Ratkje S. K. and Moller-Holst S., *Exergy efficiency and local heat production in solid oxide fuel cells.* Electrochimica Acta, 1993. **38**(2/3): p. 447-453.
18. Rant Z., *Die heiztechnik und der zweite hauptsatz der thermodynamik.* Gaswarme, 1963. **12**: p. 31-48.
19. Fratzcher W. and Gruhn G., *Die bedeutung und bestimmung des umgebungszustands fur exergetische untersuchungen.* Brennstoff-Warme-Kraft, 1965. **17**(337-341).
20. Szargut J., Morris D. R., and Steward F. R., *Exergy analysis of thermal, chemical and metallurgical processes.* 1988, p. 297-309: Hemisphere, New York.
21. Kalhammer F. R., et al., *Status and prospects of fuel cells as automobile engines*. 1998: Fuel Cell Technical Advisory Panel, Sacramento-California, USA.
22. Vasudeva K., et al., *Steam reforming of ethanol for hydrogen production: Thermodynamic analysis.* International Journal of Hydrogen Energy, 1996. **21**(1): p. 13-18.
23. Ridler D. E. and Twigg M. V., *Steam reforming*, in *Catalyst Handbook*, Twigg M. V., Editor. 1996, Chapter 5: Manson Publishing Ltd., London-England.
24. Ye Lwin, et al., *Hydrogen Production from Steam-Methanol Reforming: Thermodynamic Analysis.* International Journal of Hydrogen Energy, 2000. **25**: p. 47-53.
25. Garcia E. Y. and Laborde M. A., *Hydrogen production by the steam reforming of ethanol: thermodynamic analysis.* International Journal of Hydrogen Ennergy, 1991. **16**(5): p. 307-312.
26. Tsiakaras P., et al., *Ethanol Utilization in Solid Oxide Fuel Cells: A Thermodynamic Approach.* Ionics, 1999. **5**: p. 206-212.
27. Smith J. M., Van Ness H. C., and Abbott M. M., *Introduction to chemical engineering thermodynamics.* 1996: McGraw-Hill, Inc.
28. Cavallaro S. and Freni S., *Ethanol steam reforming in a molten carbonate fuel cell. A preliminary kinetic investigation.* International Journal of Hydrogen Energy, 1996. **21**(6): p. 465-469.
29. Fatsikostas A. N., Kontarides D. I., and Verykios X. E., *Steam reforming of biomass-derived ethanol for the production of hydrogen for fuel cell applications.* Chemical Communications, 2001: p. 851-852.
30. Freni S., *Rh based catalysts for indirect internal reforming ethanol applications in molten carbonate fuel cells.* J. Power Sources, 2001. **94**: p. 14-19.
31. Freni S., et al., *Steam reforming of ethanol on Ni/MgO catalysts: H2 production for MCFC.* J. Power Sources, 2002. **4704**: p. 1-5 (article in press).
32. Freni S., et al., *Hydrogen production by steam reforming of ethanol: A two step process.* React. Kinet. Catal. Lett., 2000. **71**(1): p. 143-152.
33. Galvita V. V., et al., *Synthesis gas production by steam reforming of ethanol.* Applied Catalysis A: General, 2001. **220**(1-2): p. 123-127.
34. Marino F. J., et al., *Hydrogen from steam reforming of ethanol. Characterization and performance of copper-nickel supported catalysts.* International Journal of Hydrogen Energy, 1998. **23**: p. 1095.

35. Bejan A., *Thermodynamic optimization of geometry in engineering flow systems.* Exergy Int. J., 2001. **1**(4): p. 269-277.
36. Bejan A., *Shape and structure, from engineering to nature.* 2000: Campridge Univ. Press, Cambridge-UK.
37. Murray E. P., Tsai T., and Barnett S. A., *A direct-methane fuel cell with ceria-based anode.* Nature, 1999. **400**: p. 649-651.
38. Steele B. C. H., *Running on natural gas.* Nature, 1999. **400**: p. 619-621.
39. Doshi R., et al., *Carbon monoxide and methane oxidation properties of oxide solid solution catalysts.* J. Catalysis, 1993. **140**: p. 557-563.
40. Park S., Vohs J. M., and Gorte R. J., *Direct oxidation of hydrocarbons in a solid oxide fuel cell.* Nature, 2000. **404**: p. 265-267.
41. Gorte R. J., Kim H., and Vohs J. M., *Novel SOFC anodes for the direct electrochemical oxidation of hydrocarbon.* J. Power Sources, 2002. **4639**: p. 1-6 (article in press).

Solid State Ionics, 136-137, 2000: p. 849-855

CHAPTER 6

CATALYTIC AND ELECTROCATALYTIC OXIDATION OF ETHANOL OVER $La_{0.6}Sr_{0.4}Co_{0.8}Fe_{0.2}O_3$ PEROVSKITE-TYPE CATALYST

ABSTRACT

The catalytic and electrocatalytic behavior of the perovskite-type $La_{0.6}Sr_{0.4}Co_{0.8}Fe_{0.2}O_3$ catalyst was investigated during the reaction of ethanol oxidation. Experiments were carried out at atmospheric pressure in a fully Yttria-Stabilized-Zirconia (YSZ) continuous stirred tank reactor (CSTR) in the temperature range between 300-750°C with fuel-rich reactant mixtures (P_{O2} = 2 kPa, $P_{ethanol}$ = 10 kPa). It was found that oxygen-nitrogen streams saturated with ethanol (at 25°C and 1 atm) lead mainly to the formation of formaldehyde and acetaldehyde. For the aforementioned reaction conditions, gas phase oxidation becomes predominant at temperature values higher than 650°C and in combination with the heterogeneous phenomena leads to 100% ethanol conversion and high acetaldehyde yields (75%) at about 750°C. The electrochemical supply of oxygen anions affects mainly the formation rates of CO and CO_2. Due to the high operation temperatures, direct electrocatalysis and homogeneous reactions, more than NEMCA ($\Lambda_{max}\approx3$), affect the overall kinetic behavior.

Keywords: Ethanol oxidation, perovskite oxides, electrocatalysis

6.1. INTRODUCTION

Ethanol has been recognized as a quality motor fuel since the design of the first combustion engines because of its high octane and British thermal unit content. Despite the fact that it is currently used only as a component of light-duty vehicle fuels, it is also possible to be used in fuel cells for the production of electrical power with efficiencies attaining 50 to 65%.

The operation of the Solid Oxide Fuel Cells (SOFCs) relies on the high ionic conductivity of solid $ZrO\text{-}Y_2O_3$ (YSZ) to carry O^{2-} ions between the two electrodes of the cell. Under this operation principle, during the last decades, SOFCs have been widely examined for the electrochemical production of electricity using fuels such as hydrogen, carbon monoxide, methane and other hydrocarbons [1]. As a result, SOFCs were found to have significant advantages such as high energy-conversion efficiency, the ability to operate at temperatures at which reaction rates attain values of practical interest [2] and the feasibility of chemical cogeneration [3].

On the other hand, perovskite type oxides containing transitional metals are attracting great attention as catalysts for the combustion of fuels as well as for oxygen electrochemical reduction [4, 5]. Moreover, their thermal stability in correlation with their low cost provides them a competitive position against noble metal catalysts.

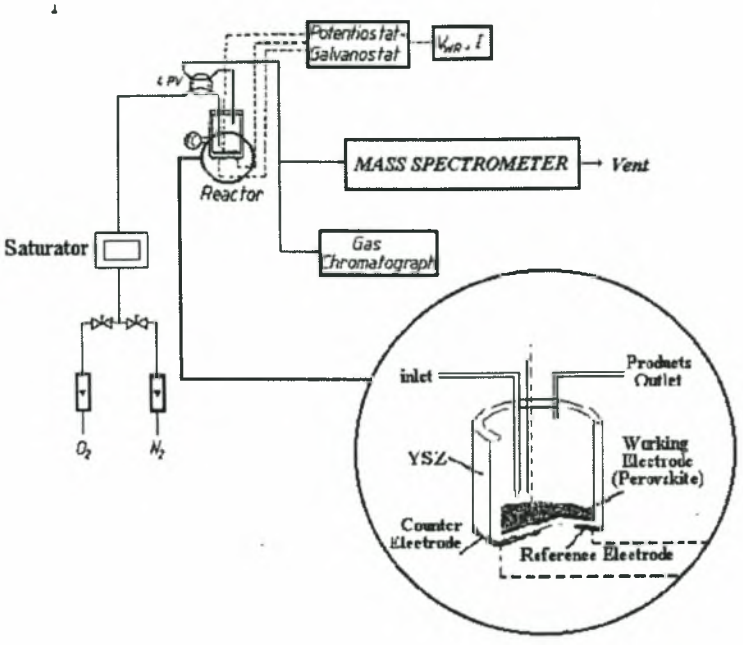

Figure 6.1. Schematic illustration of the experimental setup.

In the present study, the perovskite type oxide $La_{0.6}Sr_{0.4}Co_{0.8}Fe_{0.2}O_3$ (LSCF) was tested in the reaction of ethanol oxidation. Catalytic and electrocatalytic measurements have been taken in order to determine the pattern of the catalytic activity of LSCF at very low oxygen concentrations. The same perovskite material has been adequately examined in previous works where was found to exhibit high catalytic activity during different reactions such as methane and carbon monoxide combustion [6-8].

6.2. EXPERIMENTAL

6.2.1. Preparation and characterization of the perovskite electrode

The LSCF powder was prepared by the EDTA method as described previously [6, 7, 9]. Nitrates of the constituent metals (Merck, p.a. quality) were dissolved separately in Q_2 water and their concentrations were determined by titration with EDTA. Stoichiometric amounts of the solutions were taken and mixed. A solution of ammonia/EDTA was added to the mixed metal solution, the final concentration of EDTA being 1.5 times the total metal cation concentration. The pH of the solution was adjusted to 8-9 by using ammonia. The solution was mixed for several hours under moderate heating to complete complexation and then pyrolysed in a stove at 500K. The resulting powder was milled for several hours in a planetary mill in acetone and after drying calcined at 1200 K in stagnant air for 12 hours. Calcination at lower temperatures also resulted in perovskite formation but in these cases XRD revealed traces of $SrCO_3$.

Sample characterization was performed by taking XRD spectra (Philips PW1710) from crushed sintered membranes uisng graphite-filtered $CuK\alpha_1$ (1.5406 Å) radiation. LaB_6 was added as an internal standard and the samples were measured with 2θ scan from 20° to 140° with steps of 0.018°. The intensity was measured during 5-10 seconds. The membrane surface morphology was examined by HR-SEM (Hitachi S-800 field emission microscope). Phases present at the surface were determined by XRD. The spectra of powders obtained from crushed membranes showed a single-phase perovskite. All peacks could be indexed on the basis of a rombohedrally distorted cubic cell with lattice parameters a=5.4450(9) Å and c=13.2553(3) Å (hexagonal setting).

Then, the perovskite powder was mixed with ethyl glycol ether and the mixture was heated until half of the volume was evaporated. The resulting viscous suspension was deposited on the inside bottom wall of the zirconia tube by painting. The tube was then heated at 1200°C. The heating rate was kept at about 200°C/hr. The low heating rate is necessary in order to avoid up to a certain degree both blistering of the electrode surface and LSCF interfusion through the YSZ. The perovskite electrode, thus formed, had a superficial surface area of 2 cm^2 and a thickness of about 20 μm. The total calculated surface area

was found to be approximately 800 cm^2, by using SEM data. The perovskite unit cells exposed at the catalyst surface were estimated about $1.53x10^{-7}$ mol [7].

For the preparation of the counter and the reference electrodes silver paste (GC Electronics, 22-202) was used. In the same way, as in the case of the perovskite, two similar silver films were deposited on the outside bottom wall of the YSZ tube, which was exposed to ambient air (Figure 6.1). The superficial surface area of the Ag electrodes were 1 cm^2 and 0.2 cm^2 respectively for the counter and the reference electrodes. The distance between the above two electrodes was about 0.5 cm. Further details for the preparation of Ag electrodes can be found in previous communications [10]. In the course of the close circuit experiments both the galvanostatic and the potentiostatic operation modes were used. In the first mode, a constant current I is applied between the catalyst and counter electrodes while monitoring the Ohmic drop free potential V_{WR} between the catalyst and the reference air/Ag electrode [13]. In the second, a constant potential V_{WR} is applied between the catalyst and the reference electrode while monitoring the current I between the catalyst and the counter electrode.

The apparatus used for the electrochemical and catalytic measurements was also previously described in details [6, 7, 10]. A schematic diagram of the solid electrolyte electrochemical cell-reactor is shown in Figure 1. It consists of an Yttria-Stabilized-Zirconia (YSZ) tube (19mm OD, 16mm ID, 15cm long), closed flat at the bottom end. The cell was placed in an oven with maximum operating temperature of 1200°C. A mixture of oxygen and nitrogen was saturated with ethanol in a saturator at atmospheric conditions (25°C, 1bar) and then was fed in the cell. Constant currents were applied between the working (anode) and the counter electrodes by using a fully computerized AMEL System 5000 potentiostat-galvanostat. Currents and voltages were measured by means of a BarGraph HC-737 digital multimeter.

The analysis of the reactants and products was carried out by means of a Baltzers-Omnistar mass spectrometer and a Perkin Elmer (Sigma 300, FID/HWD) gas chromatograph with a Carbopack B/6.6% Carbowax 20M packed column.

6.3. RESULTS AND DISCUSSION

6.3.1. Open circuit measurements

A set of blank experiments was initially performed, in absence of the LSCF catalyst, in a temperature range between 300 and 750°C by feeding a mixture of 10% ethanol and 2% oxygen diluted in nitrogen. The results revealed that for temperature values less than 650°C, both YSZ catalytic effect and gas phase (homogeneous) phenomena were negligible. Over that temperature homogeneous ethanol oxidation rates were observed. In the same temperature range and by feeding the same reactant mixture, ethanol oxidation experiments were conducted in the presence of a thin LSCF catalytic film. Figure 6.2a, shows the effect of temperature on the total ethanol conversion. The onset of the reaction (conversion>1%) was observed at 300°C and the maximum ethanol conversion (98%) was attained at 750°C. The apparent activation energy was calculated equal to 10±0,5 kcal/mole from rate data in the kinetically controlled region of the reaction (conversions < 20%). As it was observed, the production and destruction of formaldehyde and acetaldehyde significantly controlled ethanol conversion.

Figure 6.2b shows the effect of temperature on the formation rates of the reaction products and on the consumption rate of ethanol. The overall reaction behavior most probably can be described by the following sequence

$$CH_3CH_2OH \xrightarrow{Ox} CH_3CHO \xrightarrow{Ox} HCHO \xrightarrow{Ox} CO_X, H_2O, H_2 \qquad (1)$$

At low temperatures, it was observed that ethanol consumption results to significant formation rates of formaldehyde and carbon dioxide. This behavior can e attributed to the existence of adequate oxygen concentration that allows the destruction of acetaldehyde until the production of formaldehyde and CO_2. Above 700°C, lack of oxygen leads in the increase of acetaldehyde and CO formation rates. In all these cases, the mass balance of carbon was conserved within an error range of about ± 6%. The same behavior is presented in Figure 6.2c in terms of the selectivity of the products.

6.3.2. Current-potential behavior

As reported in previous works [6] the fundamental electrochemical reaction, taking place at the LSCF/YSZ interface, is the oxygen exchange between the gas phase and the electrolyte:

$$O_2 + 4e^- + 2\ddot{U}_o = 2O_o \qquad (2)$$

This overall reaction can be broken down into a number of sequential reaction steps [11]. Each of these reaction steps contributes to the overall electrode polarization behavior. For every reaction, the electrode kinetics can be expressed by the Butler-Volmer equation [6]:

$$I = I_o[\exp(\alpha_a F\eta/RT) - \exp(\alpha_c F\eta/RT)] \qquad (3)$$

where α_a and α_c represent the anodic and the cathodic charge transfer coefficients respectively, F is the Faraday's constant, R is the ideal gas constant and I_o is the

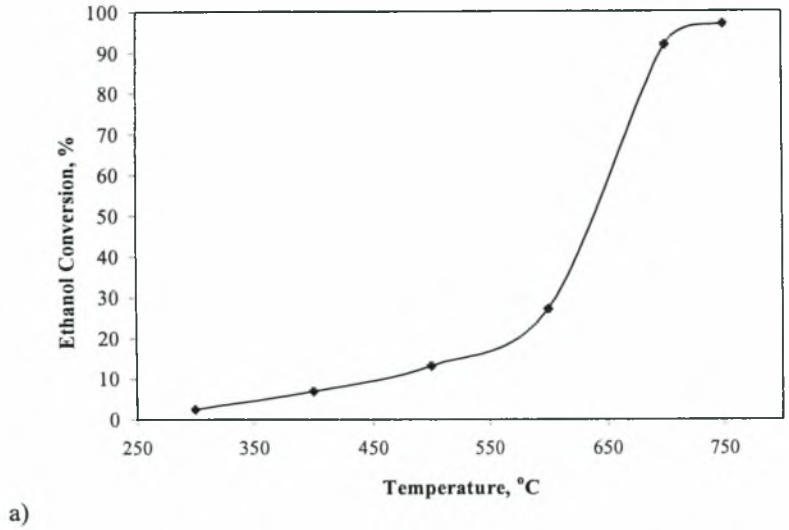

a)

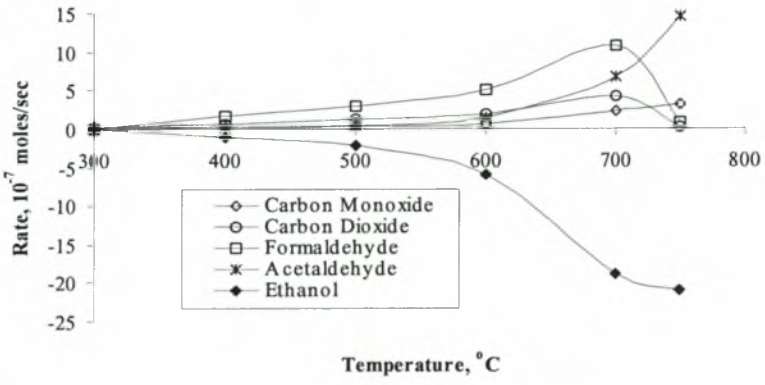

b)

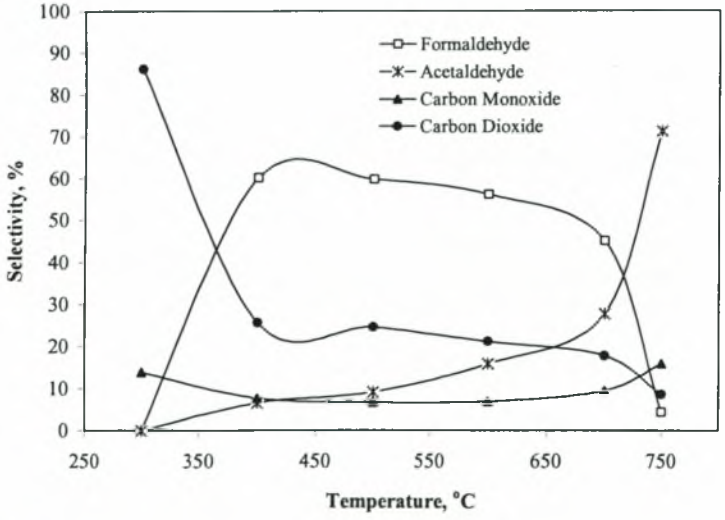

c)

Figure 6.2. a) Effect of temperature on ethanol conversion. b) Effect of temperature on the formation rates of the products of the reaction and on the consumption rate of ethanol. c) Effect of temperature on the selectivity of the products.

Table 6.1. The values of the exchange currents and charge transfer coefficients for the anodic and cathodic operation.

T, °C	$I_{0,anodic}$, μA	$I_{0,cathodic}$, μA	α_a	α_c
400	6,5	3,5	0,25	0,27
450	14,2	15,9	0,26	0.23
500	47,5	31,1	0,26	0,32
550	152,6	41,6	0,33	0,34

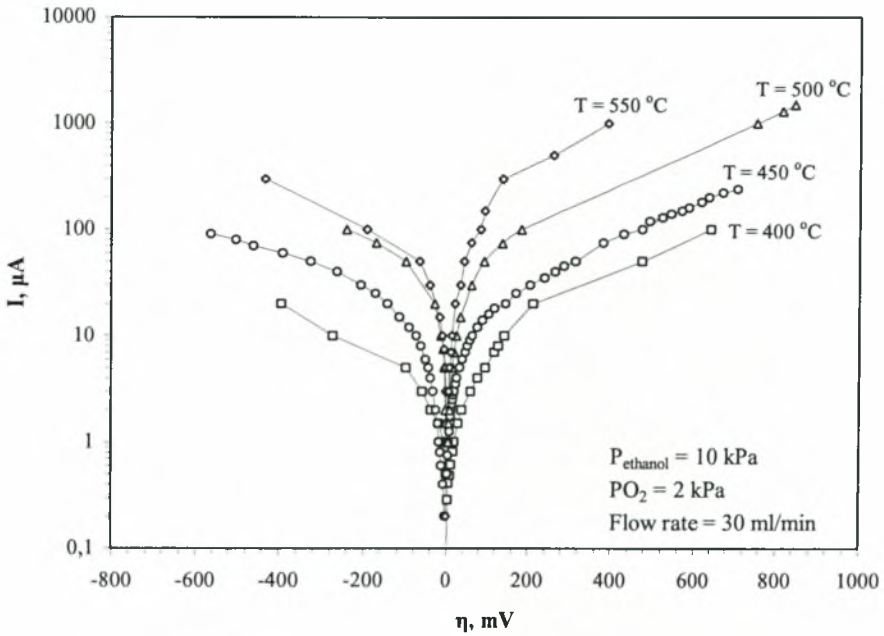

Figure 6.3. Tafel plots of anodic and cathodic overpotentials at various temperatures.

exchange current density, as it is shown in table 6.1.

Figure 6.3 shows a typical relation between the overpotential η and the current density I for the LSCF/YSZ interface, in the presence of the reaction mixture. The overpotential is defined as :

$$\eta = V_{WR} - V^{o}_{WR} \quad (4)$$

where V^{o}_{WR} is the open circuit catalyst potential relative to the reference electrode. This figure shows the effect of the activation overpotential on the electrical current. Positive overpotential ($\eta > 0$) causes an exponential increase in current. This exponential (Tafel) dependence, is in good agreement with the high field approximation of the Butler-Volmer equation [3, 6], i.e. with:

$$\ln (I/I_o) = \alpha_a F\eta/RT \quad (5)$$

where I_o is the exchange current density of the perovskite - solid electrolyte interface. Negative currents ($\eta < 0$) do not lead to a limiting current, despite the low oxygen partial pressure. The values of the apparent charge transfer coefficients were calculated from the slope of the curves and are reported in Table 6.1. These values are

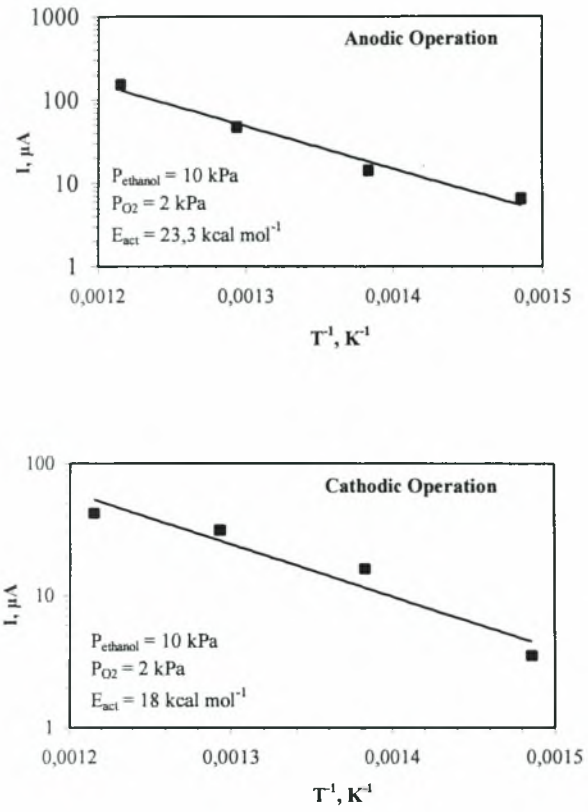

Figure 6.4. Arrhenius plots of the charge transfer processes during cathodic and anodic operation.

essentially unaffected by temperature. Exchange current density I_o increases with the increase of temperature at both anodic and cathodic polarization. The measured apparent activation energy values were about 23.3xchange current density, as it shown in Table 6. 1.

6.3.2. Closed circuit measurements.

Closed circuit measurements ($I \neq 0$) were carried out in the electrochemical device of Figure 6.1 in presence of the reactant mixture at the feedstream. Previous studies with such solid electrolyte cells reported that, under certain conditions, the increase of the rate of oxygen consumption is not equal with the rate of the O^{2-} ions that are electrochemically pumpedthrough the electrolyte [12, 13]. Vayenas and co-workers [13] defined the dimensionless rate enhancement factor Λ as:

$$\Lambda = \Delta r / (I/2F) \qquad (6)$$

where $\Delta r = r - r_o$ is the increase in the catalytic rate of oxygen consumption and I/2F is the reported flux of O^{2-} ions that are electrochemically pumped through the electrolyte. In the present case Λ is defined as:

$$\Lambda = (\Delta r_{CO2} + \Delta r_{CO} + \Delta r_{Formaldehyde} + \Delta r_{Acetaldehyde}) / (I/2F) \quad (7)$$

Electrochemically supplied oxygen leads mainly to the increase of the formation rates of CO_2 and CO and to a slight decrease of the formation rate of formaldehyde. As a result, the rate changes $\Delta r_{Formaldehyde}$ and $\Delta r_{Acetaldehyde}$ can be considered negligible and Λ can now be defined as:

$$\Lambda = (\Delta r_{CO2} + \Delta r_{CO}) / (I/2F) \qquad (8)$$

Figure 6.5 illustrates typical galvanostatic rate transients for anodic operation (I>0), i.e. it depicts the effect of constant applied current between the $La_{0.6}Sr_{0.4}Co_{0.8}Fe_{0.2}O_3$ catalyst and the Ag counter electrode on the formation rates of CO and CO_2. At 550°C (Figure 5a) the circuit is initially open (I = 0) and the corresponding global steady-state catalytic rate r_o for the reaction of ethanol consumption towards the formation of HCHO, CH_3CHO, CO and CO_2 is r_o= 7,4x10^{-7} gr-atom O/sec.

The catalyst potential V^o_{WR} was initially equal to –1128 mV (open circuit value). At time t = 0, the galvanostat is used to apply a constant current I = 5mA (Figure 4), so that O^{2-} ions are supplied to the catalyst at a steady state rate I/2F = 2.59x10^{-8} gr-atom O/sec. This causes a 10% increase in the rate of ethanol consumption. The potential V_{WR} reaches a value of –220 mV. The increase $\Delta r = (\Delta r_{CO2} + \Delta r_{CO})$ is equal to 8x10^{-8} gr-atom O/sec, thus $\Lambda = \Delta r/(I/2F) = 3$. Subsequently, (Figure 6.5a), the circuit is opened (I = 0) and the global rate r is restored in its initial value r_o= 7,4x10^{-7} gr-atom O/sec indicating the reversibility of the processes.

The procedure is then repeated at 600°C with I = 10mA (Figure 6.5b). In this case, the open circuit consumption rate of ethanol is 13,8x10^{-7} gr-atom O/sec, and the steady-state rate I/2F of O^{2-} ions supply is 5.182x10^{-8} gr-atom O/sec. The close circuit operation causes again an increase of about 10% in the rate of ethanol consumption (mainly due to the increase of the formation rates of CO_2 and CO). The rate increase $\Delta r = (\Delta r_{CO2} + \Delta r_{CO})$ is equal to 14x10^{-8} gr-atom O sec^{-1}, thus $\Lambda = \Delta r/(I/2F) = 2.7$. Considering that Λ takes values between 2 and 3, the observed phenomena are purely Faradaic compared with other catalytic oxidation reactions presenting very high Λ values [13, 14] (see also chapter 7).

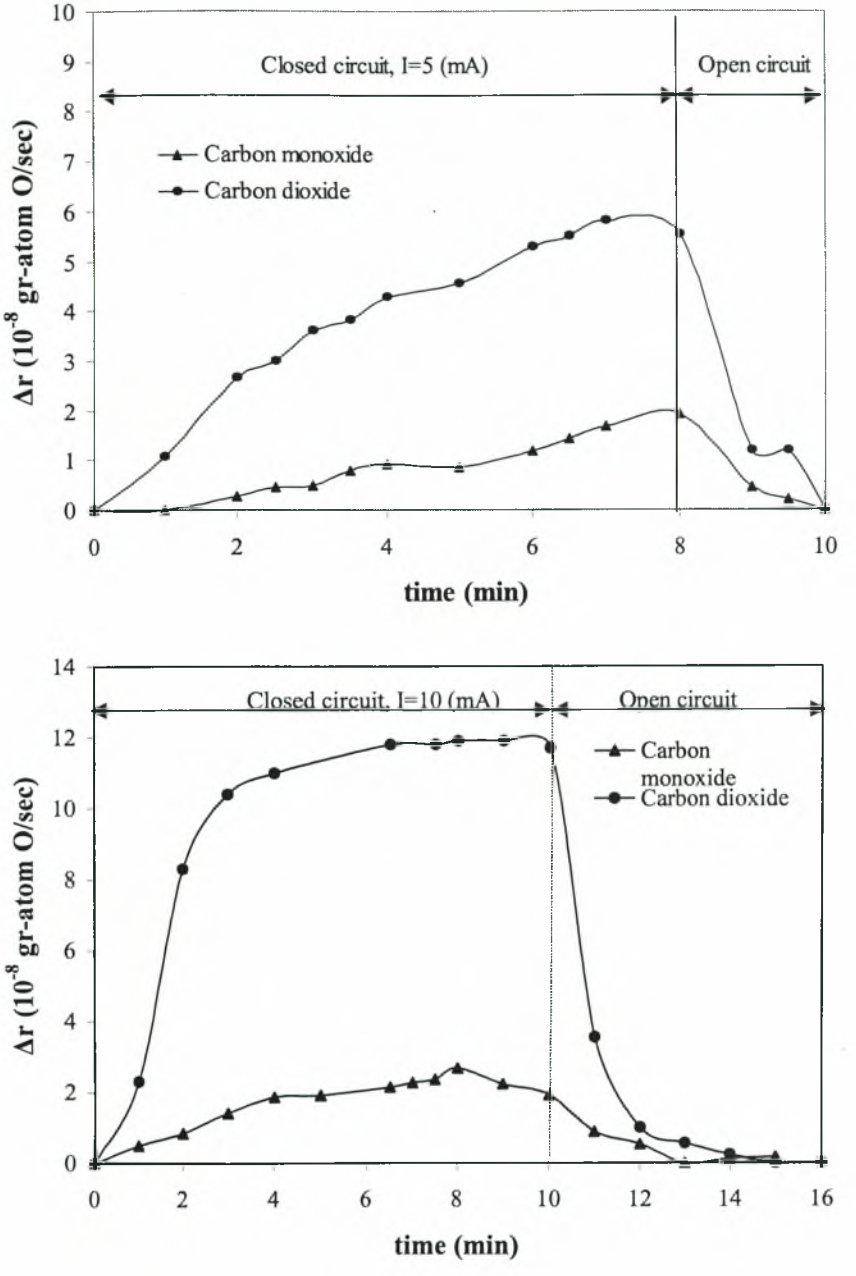

Figure 6.5. Transient change of the formation rates of COand CO_2 during close circuit operation a) at 550°C($P_{ethanol}$ = 10 kPa, P_{O2} = 2 kPa, P_{N2} = 88 kPa, Flow rate 30 ml/min, G = I/2F = 2,59x10^{-8} g-atom O/sec) and b) at 600°C($P_{ethanol}$ = 10 kPa, P_{O2} = 2 kPa, P_{N2} = 88 kPa, Flow rate 30 ml/min, G = I/2F = 2,59x10^{-8} g-atom O/sec).

6.4. CONCLUSIONS

The results obtained show that the $La_{0.6}Sr_{0.4}Co_{0.8}Fe_{0.2}O_3$ catalyst behaves as a relatively effective catalyst for ethanol oxidation. Total ethanol conversion was attained at about 750°C leading mainly to acetaldehyde. Due to the high operation temperatures, direct electrocatalysis and homogeneous reactions, more than NEMCA (Λ_{max} = 3), affect the overall kinetic behavior. However, there are indications that higher Λ values can be achieved during ethanol oxidation at lower temperatures and in different electrode-catalyst materials.

REFERENCES

1. E. C. Subbarao, in "Solid Electrolytes and their Application", 1980: Plenum Press, New York.
2. M. Stoukides, *Applications of solid electrolytes in heterogeneous catalysis*, Ind. Eng. Chem. Res., 1988, **27**: p. 1745
3. C. G. Vayenas, *Catalytic and electrocatalytic reactions in solid oxide fuel cells*, Solid State Ionics, 1988, **28**: p. 1521
4. R. J. H. Voorhove, et. al., *Rare earth oxides of Manganese and Cobalt rival Platinum for treatment of carbon monoxide in auto exhaust*, Science, 1972, **177**: p. 353
5. T. Seiyama, *Total oxidation of hydrocarbons on perovskite oxides*, Catal. Rev.-Sci. Eng., 1992, **34**: p. 281
6. P. Tsiakaras, et. al., *Electrode polarization and electrical properties of the $La_{0.6}Sr_{0.4}Co_{0.8}Fe_{0.2}O_{3-\delta}$, O_2/yttria stabilized zirconia inreface: Effect of gas phase composition and temperature*, Solid State Ionics, 1996, **86**: p. 1451
7. P. Tsiakaras, et. al., *Methane activation on a $La_{0.6}Sr_{0.4}Co_{0.8}Fe_{0.2}O_3$ perovskite : catalytic and electrocatalytic results*, Applied Catalysis A: General, 1998, **169**(2): p. 247
8. S. Douvartzidis, G. Dimoulas and P. Tsiakaras, *Catalytic and electrocatalytic oxidation of methane over perovskite-type oxides*, Studies in Surface Science and Catalysis, 1998, **119**, p. 93
9. J. E. ten Elsoff, Ph.D Thesis, 1997: University of Twente, The Netherlands
10. P. Tsiakaras and C. G. Vayenas, *Non-Faradaic electrochemical modification of catalytic activity: VII. The case of methane oxidation on platinum*, Journal of Catalysis, 1993, **144**: p. 333
11. D. Y. Wang and A. S. Nowick, *Diffusion-controlled polarization of Pt, Ag and Au electrodes with doped ceria electrolyte*, J. Electrochem. Soc., 1981, **128**: p. 55
12. M. Stoukides, *Electrochemical studies of methane activation*, J. Appl. Electroch., 1995, **25**: p. 899
13. C. G. Vayenas, et. al., in "Modern Aspects in Electrochemistry", J.O.M. Bockris et. al. Editors, 1996, Vol 29: Plenum Press, New York
14. C. G. Vayenas, et. al., *Non-Faradaic electrochemical modification of catalytic activity: A status report*, Catalysis Today, 1992, **11**(3): p. 303

Journal of Catalysis, 211(2), 2002: p. 521-529

CHAPTER 7

ELECTROCHEMICALLY PROMOTED CATALYSIS: THE CASE OF ETHANOL OXIDATION OVER PLATINUM

ABSTRACT

Ethanol oxidation was investigated over polycrystalline Pt films deposited on 8 mol% Y_2O_3-stabilized-ZrO_2 (YSZ) in the temperature range of 300 – 350 °C. It was found that electrochemical supply of oxygen anions (O^{2-}) to the Pt-catalyst results in significant changes both in the rate of ethanol consumption and in the yield of acetaldehyde. Electrochemical supply of O^{2-} anions induces an enhancement of the reaction rate that was found typically 10^3 - 10^4 times larger than the Faradaic rate of O^{2-} supply and an almost 7-fold increase on the reaction yield to acetaldehyde. In the range of the applied currents, it was found that the catalytic avtivation energies of ethanol consumption and acetaldehyde formation can be lowered by 70 and 80% respectively, with respect to the regular (open circuit) values. The observed behavior is discussed and explained on the basis of the theory of NEMCA.

Keywords: Electrochemical promotion, NEMCA, Ethanol oxidation, Acetaldehyde production, Platinum catalyst.

1 INTRODUCTION

During the last decades, the terms "electrochemical promotion" and "non-Faradaic electrochemical modification of catalytic activity" (NEMCA) have been considered as the most appropriate to describe those cases in which electrochemistry serves as an activator of catalysis. More specifically, it was observed that the catalytic behavior of metals interfaced with solid electrolytes can be altered dramatically and reversibly upon polarizing the metal/solid electrolyte interface (Figure 7.1). This effect has been successfully explained theoretically in terms of modifications induced in the work function of metal catalysts due to changes on the catalyst (electrode) overpotential. Results of numerous studies for various heterogeneous reactions are summarized in recent reviews or as chapters in books of solid state electrochemistry [1-5].

It has been shown that electrochemical supply or removal of oxygen anions (O^{2-}) to or from the catalyst through the solid electrolyte can enhance dramatically the rate of catalytic reactions and tune their selectivity on useful chemicals (see Figure 7.2). The main features that were found common in all NEMCA studies can be summarized as follows:

I. Over a wide range of experimental conditions catalytic rates of heterogeneous reactions depend exponentially on the Ohmic-drop-free catalyst potential ,V_{WR}, with respect to the reference electrode, according to the expression:

$$\ln(r/r_o) = aF(V_{WR} - V^*_{WR})/RT \qquad (1)$$

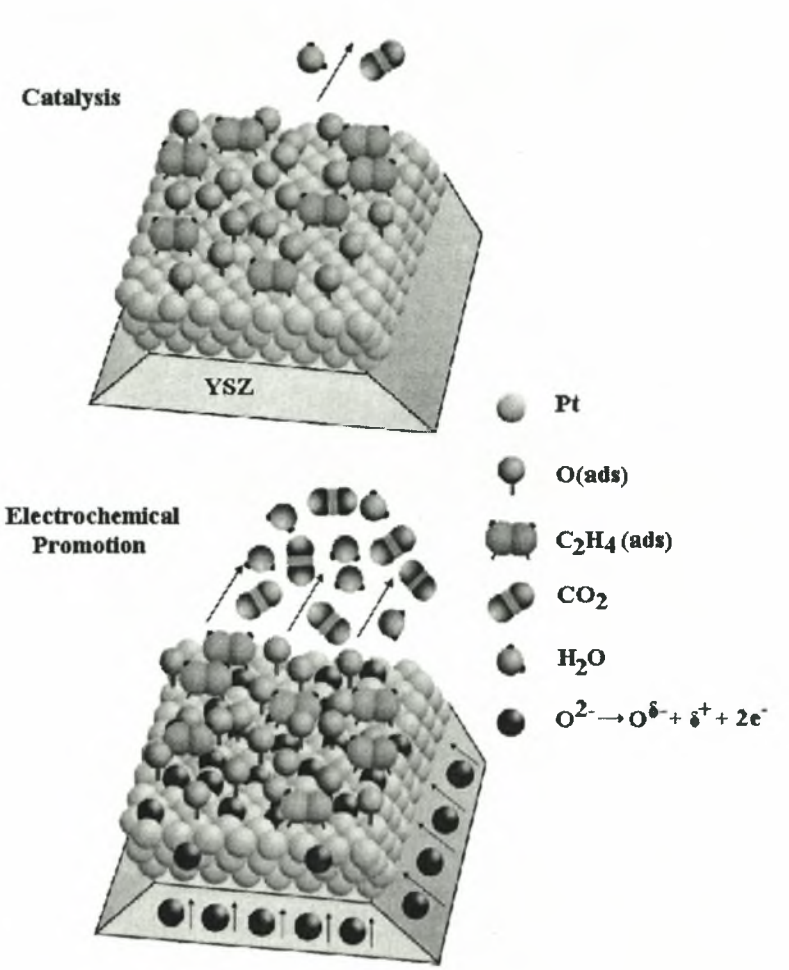

Figure 7.1. Atomic visualization of electrochemical promotion (NEMCA) when using and O^{2-} conductor (YSZ) during C_2H_4 oxidation on Pt. The O^{2-} ions form $O^{\delta-}$-δ^+ backspillover dipoles which migrate (backspillover) at the Pt/gas interface, forming an effective double layer which weakens the Pt=O bond and strengthens the Pt-C_2H_4 bond, thus enhancing catalytic activity. The lifetime of $O^{\delta-}$-δ^+ on the catalyst surface is Λ times shorter than the lifetime of Pt=O (Reprinted from: Vayenas C. G., Brosda S., and Pliangos C., Journal of Catalysis, **203**, 2001: p. 332).

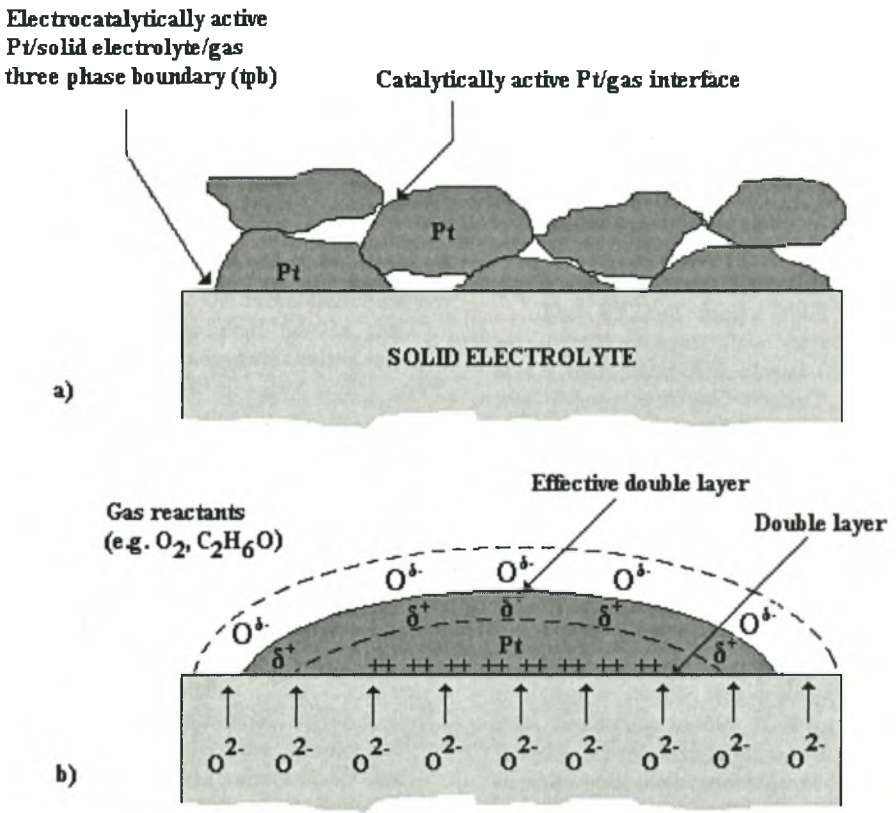

Figure 7.2. Schematic representation of a Pt electrode deposited on O^{2-} conducting YSZ solid electrolyte; a) Microscopical representation of the arrangement of the Pt crystallites on the YSZ, showing the catalytically active Pt/gas interface and the three phase (Pt/YSZ/gas) boundary, b) illustration of the classical metal-electrode double layer and of the effective double layer created at the Pt/gas interface due to potential (or current) controlled ion migration (back spillover).

where r_o is the regular (i.e., open circuit) catalytic rate and α and V^*_{WR} are catalyst and reaction specific constants. The parameter α typically takes values between −1 and 1. Depending on the sign of this parameter, catalytic reactions can be classified as electrophobic ($\alpha > 0$) or electrophilic ($\alpha < 0$).

Moreover, it has been shown that the electromotive force (emf) of the solid electrolyte cells with metal electrodes provides a direct measure of the difference in work function of the catalyst and reference electrode gas-exposed surfaces. Thus, when the catalyst potential is changed by ΔV_{WR}, either by changing the composition of the gas in contact with the catalyst or by polarizing the catalyst/solid electrolyte interface, the average catalyst surface work function $e\Phi$, changes by

$$\Delta e\Phi = \xi e \Delta V_{WR} . \qquad (2)$$

where $\xi \leq 1$ depends upon operating conditions and electrode morphology. Important information about the thermodynamic considerations leading to this conclusion as well as on the exploitation of Eq. (2) for the prediction of the extent of the modification of the rate of a heterogeneous reaction can be found *inter allia* in recent literature [5-7].

II. The order of magnitude (typically between 1 and 10^5) of the absolute value $|\Lambda|$ of the enhancement factor Λ defined as:

$$\Lambda = \frac{\Delta r}{I/2F} \qquad (3)$$

where Δr is the change in catalytic reaction rate and I/2F is the rate of supply (I>0) or removal (I<0) of O^{2-} to or from the catalyst, can be estimated from the expression:

$$|\Lambda| = \frac{2Fr_o}{I_o}, \quad (4)$$

where I_o is the exchange current of the catalyst/solid electrolyte interface. Therefore, in order to observe a strong non-Faradaic enhancement, i.e., $|\Lambda| >> 1$, highly polarizable, i.e., low I_o catalyst/solid electrolyte interfaces are required.

III. During galvanostatic transients, the relaxation time constant, τ, defined as the time required for the rate change to reach 63% of its steady-state value, are typically of the order of,

$$\tau = \frac{2FN}{I}, \quad (5)$$

where N, expressed in g-atom, is the total gas-exposed catalyst film surface area. This shows that electrochemical promotion changes the catalytic properties of the entire catalyst surface and is not restricted to the vicinity of the three-phase boundaries (tpb) gas/catalyst/solid electrolyte. The above observations have been interpreted semiquantitatively on the basis of the changes induced in the strength of chemisorptive bonds of reactants and intermediates due to an electrochemically induced and controlled ion spillover with consequent change in catalyst work function.

The results presented in this work are concerned with the electrochemical promotion of a Pt catalyst during the reaction of ethanol oxidation using 8 mol % Y_2O_3-stabilized-ZrO_2 (YSZ), an O^{2-} conductor, as solid electrolyte. Because of the high cost of noble Pt catalysts, the optimization of the design and the amount of Pt used in practice via appropriate promotion is of significant interest. The unexamined case of the reaction of ethanol oxidation was selected because of the possible utilization of ethanol for generation of electricity in fuel cells as well as because of the feasibility of generation of useful chemicals of increased value such as acetaldehyde. Acetaldehyde is a highly reactive compound and widely used as an indermediate in industrial organic synthesis. It can be produced by hydration of acetylene, vapor-phase oxidation of butane, and oxidation or dehydrogenation of ethanol [8, 9]. Based on these interests, the present study focuses on the existence, the extent and the results of the *in-situ* electrochemical promotion of Pt-catalysed ethanol oxidation.

2. EXPERIMENTAL

The apparatus used in the course of this study has been described in detail in previous works [10]. It consisted of the feeding unit, the oven/YSZ-reactor system and the system of analysis. The mixture of the reactants was formed by feeding streams of 5.5 (or 21) vol % O_2 diluted in N_2 and pure N_2 (99.999 vol%) in a saturator containing pure ethanol at 25°C and 1bar. Gas flow rates before the saturator were continuously monitored by digital mass flow controllers (Brooks series 5800).

The YSZ (8 mol% Y_2O_3 in ZrO_2) atmospheric pressure, continuous flow stirred tank reactor (CSTR) was a cylindrical tube closed flat at the bottom end of total volume of 30 cm^3 (Figure 7.3). On the inside bottom wall of the tube, the porous Pt catalyst film was deposited by applying a thin coating of Engelhard A1121 Pt paste. Two similar Pt films were deposited on the outside bottom wall of the YSZ tube which was exposed to ambient air and served as counter and reference electrodes, respectively. Previously, in order to remove possible impurities of the YSZ tube, it was slowly heated to 900 °C and then cooled, also slowly, to 25 °C and bathed in acetone. After the application of the Pt paste, the ceramic reactor was dried at 120 °C for 30 min and then heated up to 500 °C in a furnace with slow air feeding. At this temperature, the reactor remained for 2h in order both the evaporation of the paste solvent and the adhesion of Pt crystallites at the YSZ surface to take place. Then, the temperature was increased at 850 °C causing partial sintering of the Pt and formation of coarse Pt crystallites. Coarse Pt stucture was desired for the reduction of the extension of the three phase boundary (Pt/YSZ/gas) and therefore for the reduction of the magnitude of the exhange current, I_o. The reactor remained at 850 °C for 30 min. Through all these stages, increase of temperature was done with slow rates of the order of 200 °C/h, to avoid fracture of YSZ as well as blistering of electrodes. The thickness of the Pt catalyst film was of the order of 5-10 μm. The superficial area was 2 cm^2 and the true surface area was of the order of 50 cm^2 as measured by a surface titration technique utilizing O_2 and C_2H_4 described previously [11]. In this way, the total exposed catalyst film surface area was estimated equal to about $N = 4 \times 10^{-8}$ g-atom of Pt.

In the course of the experiments, a potentiostat/galvanostat (AMEL system 5000) was used to apply currents between the catalyst and the counter electrode while monitoring the Ohmic-drop-free potential, V_{WR}, between the catalyst and the reference electrode. The analysis of reactants and products was carried out by utilizing a mass spectrometer (Balzers Omnistar), an FID gas chromatograph (Shimadzu GC 14B) and a series of on-line gas analysers (Hartmann & Braun Braun Advance Optima). By making a set of

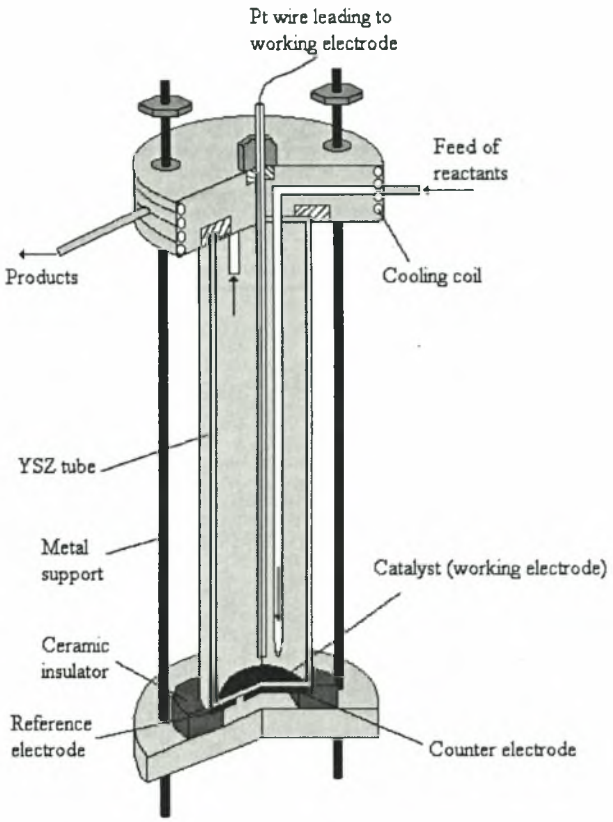

Figure 7.3. Schematic illustration of the YSZ reactor.

preliminary measurements at different flowrates in the range of 20-160 ml/min STP and the same reactants composition the apparent reaction rate was found constant demonstrating the absense of external mass transfer phenomena. Further, internal diffusion of gaseous reactants in the porous catalyst was considered negligible due to the small thickness of the Pt film.

3. RESULTS AND DISCUSSION

3.1 The electrocatalytic activity of the three phase boundary.

It is well known [2-5] that the estimation of the magnitude of the purely electrochemically promoted catalytic modifications (resulted by the application of current or potential) requires the estimation of the electrocatalytic activity of the *tpb* formed by the interfaces of the catalyst crystallites, the solid electrolyte and the gas phase. This magnitude mainly refers on the intenseness of the electrocatalytic actions taking place on the *tpb* that cause transfer of electrical charge. A measure of the electrocatalytic activity of the *tpb* is the value of the exchange current, I_o, or the exchange current density i_o given as,

$$i_o = \frac{I_o}{A} \qquad (6)$$

where A represents the superficial catalyst surface area (in cm^2). The calculation of I_o is accomplished according to the low field approximation of the Butler-Volmer equation, which can be written as,

$$I = I_o\,[\exp(\alpha_a F\eta_{act,j}/RT) - \exp(\alpha_c F\eta_{act,j}/RT)]. \qquad (7)$$

This equation allows for the calculation of the exhange current density, I_o, and the charge transfer coefficients α_a and α_c.

Figure 7.4 illustrates the effect of the overpotential, η, on the logarithm of the current, I, for both positive and negative currents under constant gas composition ($P_{ethanol}$ = 34.8 kPa, P_{O2} = 8 kPa at the reactor outlet) at various temperatures. The overpotential, η, is defined as,

Table 7.1. Exchange currents and charge transfer coefficients during anodic (I > 0) and cathodic (I < 0) operation

Temperature (°C)	$I_{o,\,anodic}$ (μA)	$I_{o,\,cathodic}$ (μA)	α_{anodic}	$\alpha_{cathodic}$
300	2.5	1	0.1	0.12
325	7	1.7	0.11	0.13
350	12	3	0.14	0.16

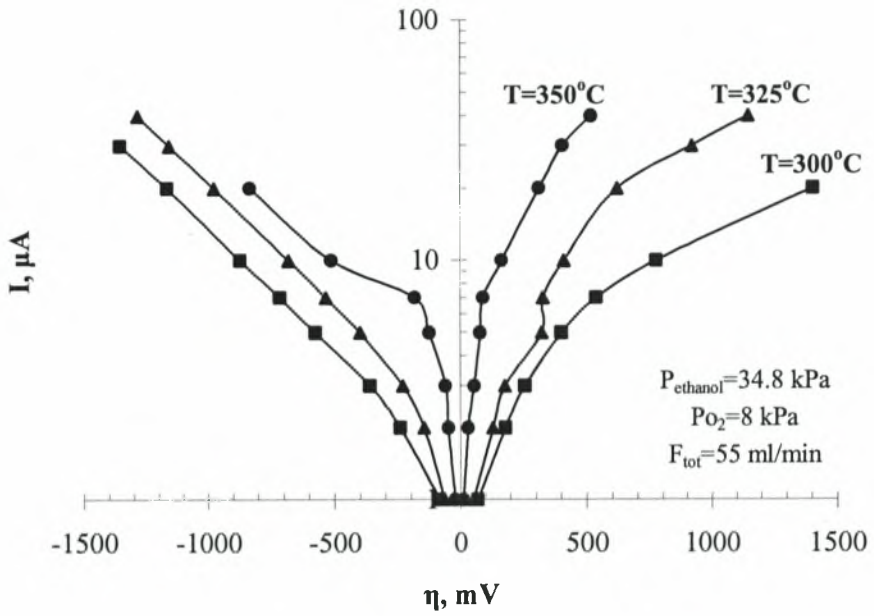

Figure 7.4. Effect of overpotential, η, on the current I (Tafel plots) ($V^{o}_{WR} \approx$ -440 mV).

$$\eta = V_{WR} - IR - V^{o}_{WR} \qquad (8)$$

where V^{o}_{WR} is the catalyst potential, V_{WR}, during open circuit conditions (I = 0). Due to the low operating temperatures of 300-350 °C, relatively high values of ohmic-drop IR were expected. The standard current interruption technique [12] was followed to quantify this parasitic effect and IR-drop values were measured to be typically of the order of 20-50% of the corresponding overpotential values. The charge transfer coefficients, α_a and α_c, were calculated from the slopes of the linear parts (Tafel region) of the curves of Figure 7.4 that correspond at low overpotential values, and are given in Table 7.1. As shown, both anodic and cathodic transfer coefficients are similar indicating the same dominant electrocatalytic reactions during both modes of operation. Moreover, Table 7.1 presents also the values of the anodic and cathodic exchange currents calculated by extrapolating the linear (Tafel) regions of the curves of Figure 7.4 at η = 0. In this case it is shown that Pt/YSZ interface can be considered highly polarizable as it is characterized by very low values of I_o (of the order of 1-10μm).

Figure 7.5 illustrates the dependence of the exhange current on temperature. The apparent activation energy during cathodic operation was calculated equal to about E_{act} = 15.6 kcal/mole, while at anodic operation it was found approximately equal with E_{act} = 22.3 kcal/mole. In practice, these values express the energy required for charge transfer to occur through cathode/YSZ and anode/YSZ interfaces, respectively. Given that previous studies on oxygen adsorption on platinum suggest an apparent activation energy of about 45 kcal/mole when

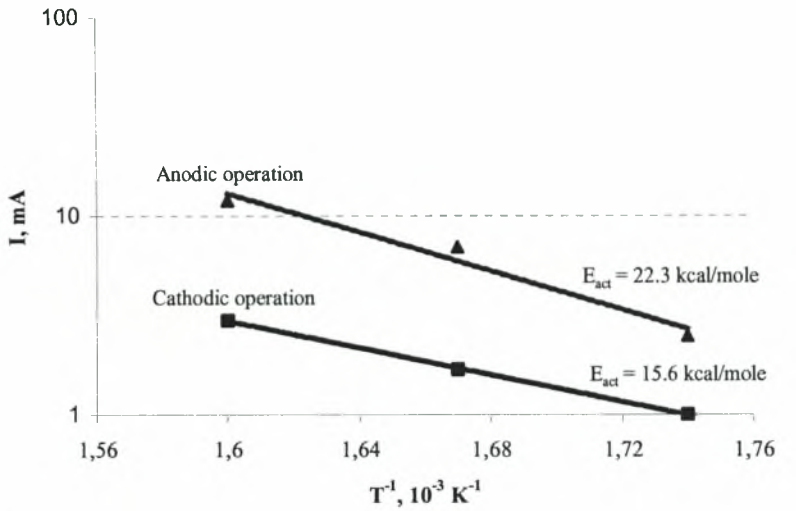

Figure 7.5. Effect of temperature on exhange current (Arrhenious plots).

oxygen anion de-electronation is the only electrocatalytic reaction in the *tpb* [13-14], it is likely that the lower values measured here must me due to other elementary steps involving ethanol adsorbed on the catalytically active sites of the Pt film. From the view point of electrochemical promotion, the exact determination of this complex mechanism of charge transfer steps is not crucial, as the only parameter of practical importance is the exchange current, I_o, which determines the expected magnitude of the dimensioneless factor of rate enhancement through Eq. (4).

3.2 Galvanostatic transients.

The application of small positive currents between the catalyst and the counter electrode was found to induce significant changes on the rate of ethanol oxidation in a reversible manner. Experiments were conducted in the temperature range of 300-350°C at atmosheric pressure, at conditions where ethanol dehydrogenation to acetaldehyde was found to be the primary reaction step. Indeed, under the examined conditions, acetaldehyde, carbon dioxide and steam were the main products, probably due to the following reaction sequence:

$$CH_3CH_2OH \xrightarrow{0.5\,O_2} CH_3CHO + H_2O \longrightarrow CO + CH_4 + H_2O \quad (9)$$

$$3\,O_2 \searrow \qquad \swarrow 2.5\,O_2$$

$$2CO_2 + 3H_2O$$

Taking into account the presence of traces of formaldehyde, one might also consider the following reaction:

$$CH_3CHO \xrightarrow{1/2\,O_2} 2HCHO \quad (10)$$

and the subsequent reaction of formaldehyde decomposition:

$$HCHO \longrightarrow CO + H_2 \quad (11)$$

The above reaction steps justify also the amounts of HCHO, CO, CH_4 and H_2 detected by mass spectrometry in very low quantities (less than 0.3 vol%).

Constant current (I > 0) application (galvanostatic operation) between the catalyst and the counter electrode results in steady state supply of O^{2-} to the catalyst through the YSZ electrolyte with Faradaic rate equal to I/2F (in g-atom O/s where F is Faraday's constant). Electrochemical pumping of O^{2-} anions was found to alter significantly the rate of ethanol oxidation. Figures 7.6a and b illustrate transient responses of the consumption rates of ethanol and oxygen upon the sequential application of positive currents equal to I = 20 μA and 40 μA respectively. As shown in Figure 7.6, at time t = 0 the circuit is closed by applying a constant current I = 20 μA. Electrochemical supply of O^{2-} anions to the catalyst results in gradual increases on the consumption rates of both reactants (Figures 4a and 4b). More specifically, the consumption rate of ethanol increases from the initial (open-circuit) value of r_o = 2.6×10^{-7} g-atom O/s to a new value, r = 7.1×10^{-7} g-atom

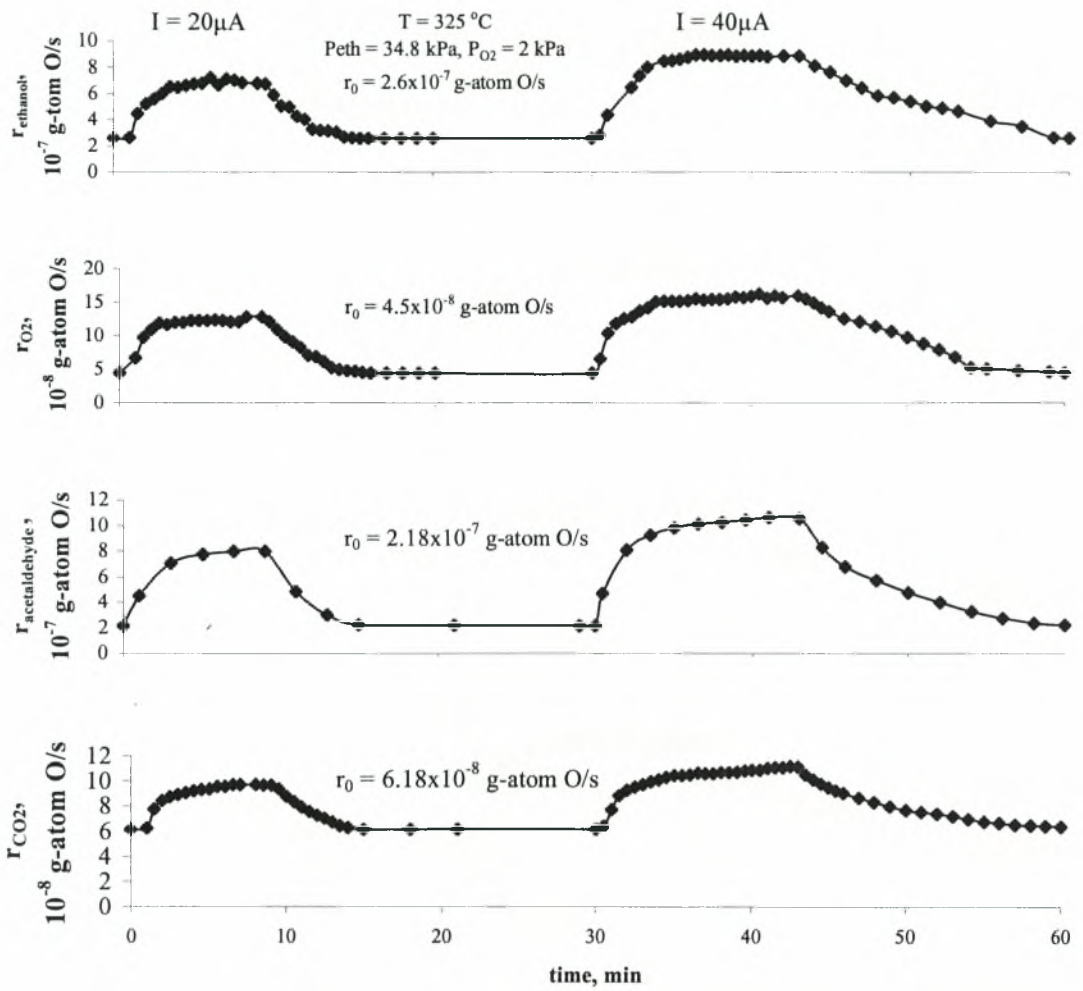

Figure 7.6. Transient behavior of the rates of a) ethanol consumption, b) oxygen consumption, c) acetaldehyde formation and d) carbon dioxide formation after the sequential application of currents equal to I = 20 μA and I = 40 μA ($P_{ethanol}$ = 34.8 kPa, P_{O2} = 2 kPa, T = 325 °C).

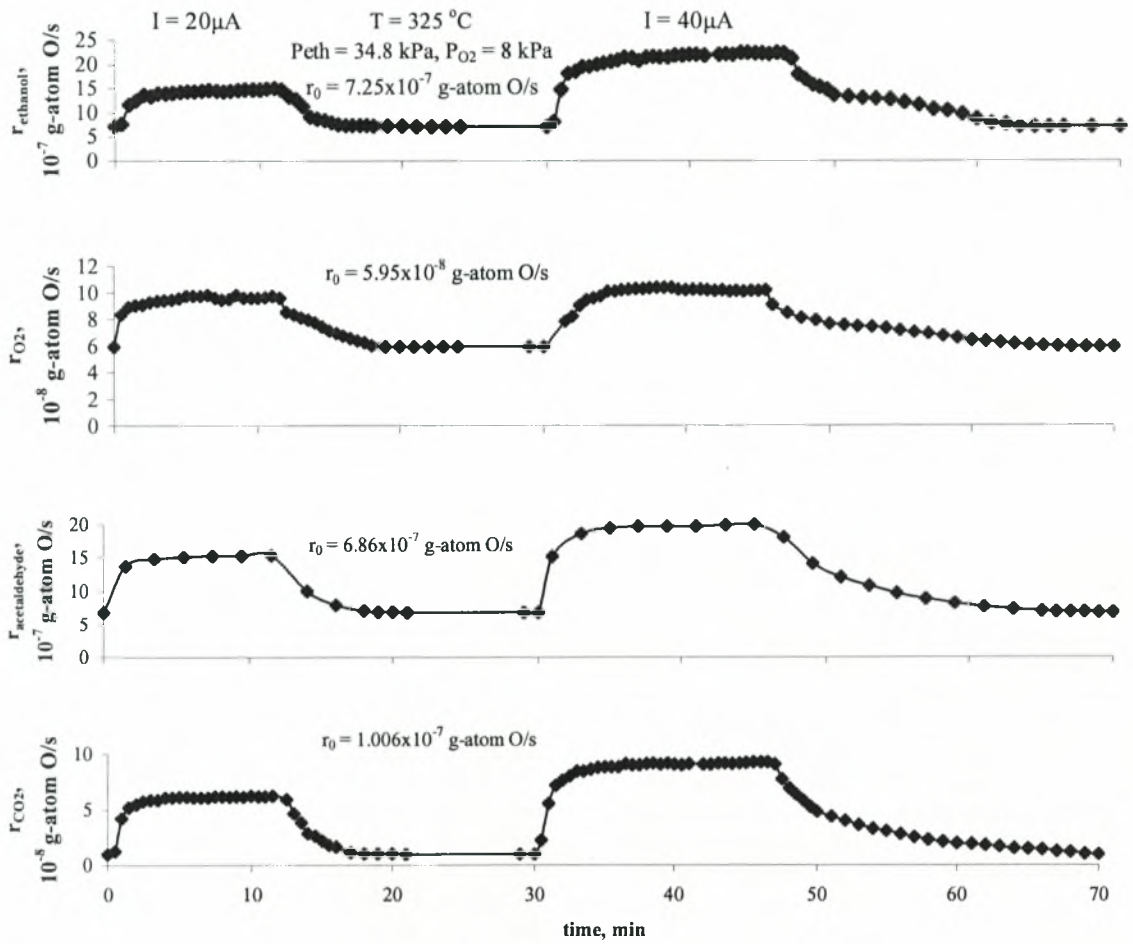

Figure 7.7. Transient behavior of the rates of a) ethanol consumption, b) oxygen consumption, c) acetaldehyde formation and d) carbon dioxide formation after the sequential application of currents equal to I = 20 μA and I = 40 μA ($P_{ethanol}$ = 34.8 kPa, P_{O2} = 8 kPa, T = 325 °C).

Table 7.2. Comparison between calculated and experimental relaxation time constants

Applied current, I (μA)	Oxygen partial pressure (kPa)	Experimental time constant (min)	Theoretical time constant (min)
20	**2**	2.8	6.4
20	**8**	1.3	6.4
40	**2**	2	3.2
40	**8**	1.3	3.2

O/s at the steady state closed-circuit condition. Similarly, the consumption rate of oxygen increases also from r_o = $4.5x10^{-8}$ g-atom O/s up to about $12.7x10^{-8}$ g-atom O/s. Note that electrochemical O^{2-} supply to the catalyst causes a *decrease* in oxygen concentration at the exit of the reactor. Figure 7.6b, shows the essence of the appearance of the effect of NEMCA which is the activation of previously (under open-circuit conditions) more inert chemisorbed oxygen atoms due to supply of partially charged $O^{\delta-}$ anions [15]. After the establishment of the new (closed-circuit) steady state condition, the circuit is opened again at time t = 9 min and all rates are observed to restore their regular, r_o, (open circuit) values, indicating the reversibilty of the observed phenomenon.

The behavior described above for the reactants is naturally compensated by increases in the formation rates of the products. Thus, Figures 7.6c and 7.6d show the galvanostatic transient responces of the major reaction products (i.e., acetaldehyde and carbon dioxide) upon the sequential application of currents (I = 20 μA and I = 40 μA), at the same conditions ($P_{ethanol}$ = 34.8 kPa, P_{O2} = 2kPa and T = 325 °C). For I = 20 μA, the formation rate of acetaldehyde changes from $r_o = 2.18x10^{-7}$ g-atom O/s up to about $7.98x10^{-7}$ g-atom O/s and the formation rate of carbon dioxides from $r_o = 6.18x10^{-8}$ g-atom O/s up to about $9.64x10^{-8}$ g-atom O/s. As shown, an increase of the intensity of the applied current, further increases the formation rates of the products. Similarly, these increases are also higher when the oxygen partial pressure is higher as shown in Figure 7.7 for P_{O2} = 8 kPa.

As mentioned, the relaxation time constant of the catalytic rate of ethanol oxidation was expected to be of the same order of magnitude with the values given by Eq. (5). In fact, the calculated values obtained by Eq. (5) represent the time period required for the formation of a monolayer of O^{2-} ions in a catalytic surface of N active centers. In the cases of the transient changes described above, the experimental values of the relaxation time constants were found to be in close qualitative agreement with those expected theoretically, as shown in Table 7.2.

3.3 The extent of electrochemical promotion.

On the basis of previous NEMCA studies and their conclusions that lay the foundation of the relevant theory today, the quantification of the extent of the promotion can be made using the dimensionless rate enhancement factor, Λ, given by Eq. (3). For the case of this study, the total change of the rate of the reaction of ethanol oxidation, Δr, can be expressed either as the the steady-state increase of the consumption rates of ethanol and oxygen or as the sum of the steady-state increases of the formation rates of the products (CO_2, CH_3CHO). Figures 7.8 and 7.9 illustrate the dependence of the change of the formation rates of acetaldehyde and carbon dioxide on the rate of electrochemical supply of O^{2-} anions through the YSZ at three temperatures and constant oxygen partial pressure equal to P_{O2} = 8 kPa. Straight dashed lines represent Λ = *const.* curves derived by Eq. (3). As shown in Figure 7.8, electrochemical promotion of Pt enhances the rate of ethanol dehydrogenation into acetaldehyde by a factor, Λ, of the order between 10^3 and 10^4 depending on the operation temperature. Λ values are of the order of 10^4 at low temperatures when high polarization of the Pt/YSZ interface is achieved by application of low positive currents (10-30 μA). At higher temperatures (325-350°C) the extent of the promotion decreases with Λ values between $3x10^3$ and $7x10^3$. The same temperature dependence is also evident in Figure 7.9 for the case of carbon dioxide, but Λ values in this case are lower than 10^3. The fact that I_0 increases exponentially with temperature in conjuction with the fact that Λ is proportional to I_0^{-1} (Eq. (4)) explains why most NEMCA studies are restricted to low temperatures (typically lower than 600 °C) [3].

The dependence of the enhancement factor on the partial pressure of oxygen is shown in Figures 7.10 and 7.11 for acetaldehyde and carbon dioxide respectively, at constant temperature T = 325 °C. For both products the extent of the NEMCA effect is higher at higher oxygen partial presssures and this observation is more profound at high rates of electrochemical oxygen pumping where the intenseness of the activation of the chemisorbed oxygen atoms is higher. A comparison between these two

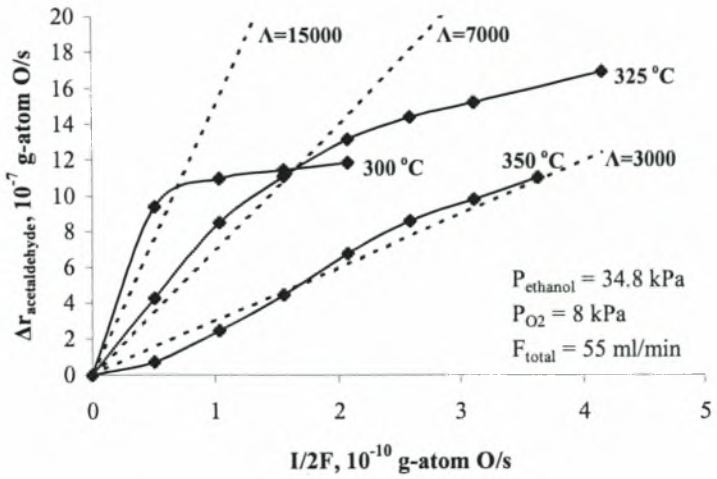

Figure 7.8. Steady-state effect of current on the enhancement of the formation rate of acetaldehyde at different temperatures.

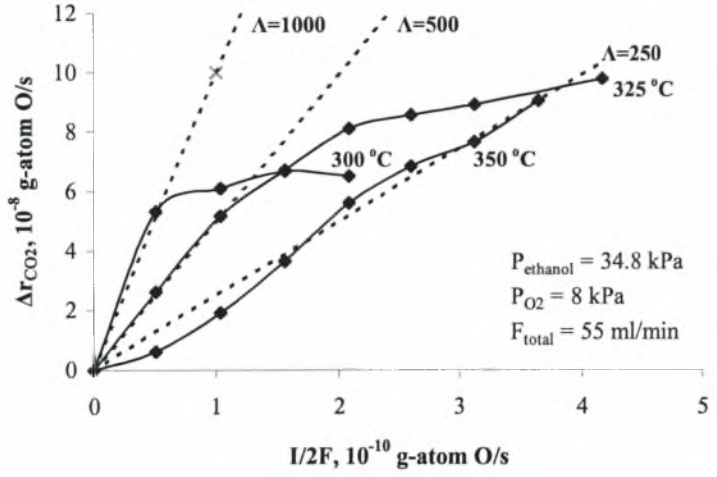

Figure 7.9. Steady-state effect of current on the enhancement of the formation rate of carbon dioxide at different temperatures.

Figures (7.10 and 7.11) shows that current application affects mainly the formation rate of acetaldehyde. More presicely, the ratios $\rho = r/r_o$ taken after the establishment of the steady-state closed circuit operation were calculated at all cases for acetaldehyde in the range,

$$1 < \rho_{acetaldehyde} < 5.5 \qquad (12)$$

and for carbon dioxide in the range,

$$1 < \rho_{carbon\ dioxide} < 2. \qquad (13)$$

These observations show that electrochemical O^{2-} supply to the catalyst surface enhances the oxidative dehydrogenation of acetaldehyde more strongly than the consequtive oxidation of acetaldehyde, CO and CH_4 to CO_2. An interpretation of this preferential rate enhancement in terms of the NEMCA theory can be as follows. Oxide ions O^{2-} arriving at the three phase boundaries form backspillover oxygen ions:

$$O^{2-} \longrightarrow (O^{\delta-} - q^{\delta+}) + 2e^- \qquad (14)$$

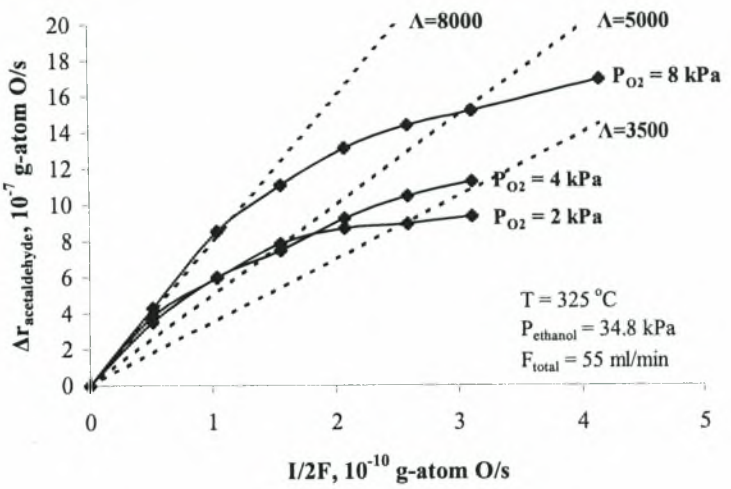

Figure 7.10. Effect of steady-state current on the enhancement of the formation rate of acetaldehyde at different partial pressures of oxygen.

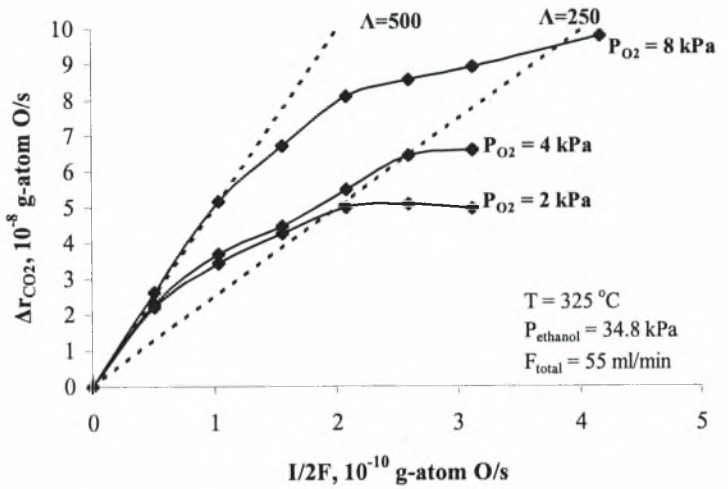

Figure 7.11. Effect of steady-state current on the enhancement of the formation rate of carbon dioxide at different partial pressures of oxygen.

which are less reactive (in fact Λ times less reactive) than absorbed oxygen produced by gaseous oxygen adsorption:

$$O^{2-} \longrightarrow O_{(ads)} + 2e^{-}. \qquad (15)$$

Reaction (15) produces adsorbed atomic oxygen $O_{(ads)}$ which reacts rapidly with other adsorbed species. On the other hand, spillover oxide ions which are formed according to recation (14) spread over the catalyst surface and increase substantially the catalyst work function, thus weakening the $O_{(ads)}$ chemisorptive bond (see Figures 7.1 and 7.2) [2-5]. This, in turn, results in significant lowering of the activation energy of the oxidation reactions (9) which determine the overall rate of ethanol consumption. Indeed, a significant decrease was observed in both the catalytic activation energies of ethanol consumption and acetaldehyde formation, which are given in Table 7.3. As shown, under NEMCA conditions the activation energy of acetaldehyde production becomes megligible (about 2 kcal/mole) indicating that the weakening in the chemisorptive bond of $O_{(ads)}$

Table 7.3. Changes in the catalytic activation energy due to the electrochemical promotion.

Current I (μA)	Measured overpotential η (V)	Activation Energy (kcal/mole) Acetaldehyde formation	Ethanol consumption
0	0	14.3	27.7
10	0.2	2.3	10.1
20	0.3	2.3	8.3
30	0.35	2.3	7.9

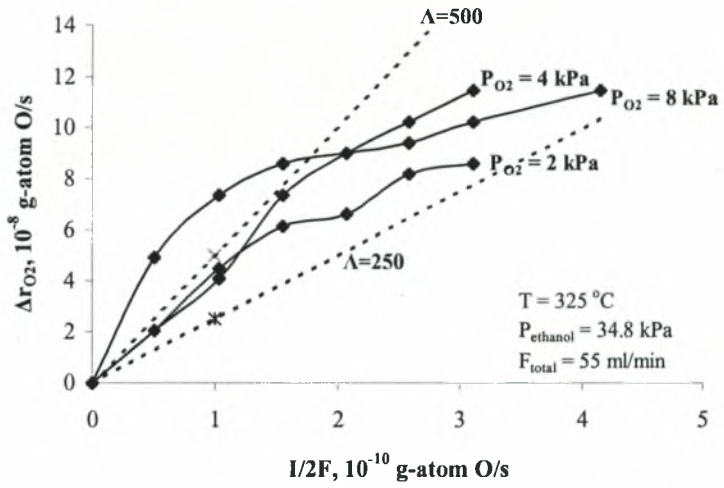

Figure 7.12. Steady-state effect of current on the enhancement of the consumption rate of oxygen at different oxygen partial pressures.

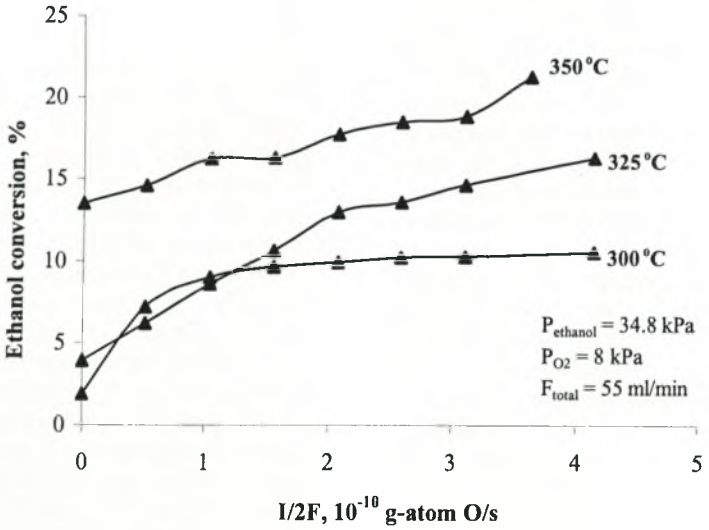

Figure 7.13. Steady-state effect of current on ethanol conversion.

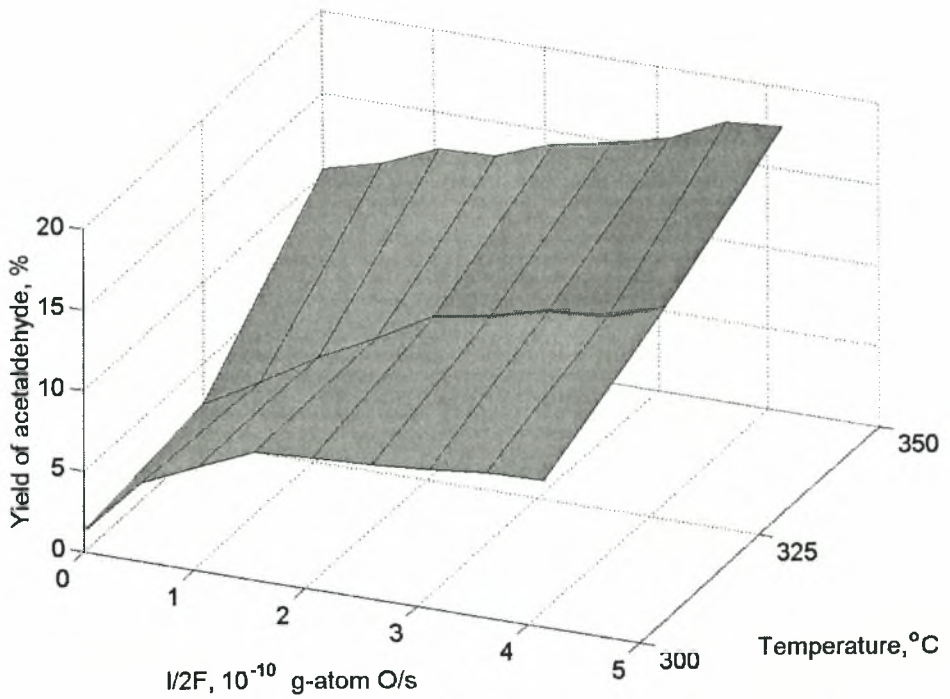

Figure 7.14. Effect of electrochemical promotion on the reaction yield to acetaldehyde ($P_{ethanol,\,in}$ = 36.3 kPa, P_{O2} = 8 kPa).

enhances preferentially the ethanol oxidative dehydrogenation step rather than the complete oxxidation step to CO_2. A similar enhancement in the selectivity to partial oxidation products has been found during C_2H_4 and C_3H_6 oxidation in Ag [2-5].

The spillover mechanism of reactions (14) and (15) may be illustrated by Figure 7.12 which indicates the enhancement of the consumption rate of surface oxygen due to the electrochemical supply of O^{2-} anions through the YSZ electrolyte. It is shown that the number of previously (under open circuit conditions) inert activated oxygen atoms is typically 2-3 orders of magnitude higher than the number of the electrochemically supplied O^{2-} ions. Figure 7.13 shows the steady-state effect of currrent, I, (expressed as the rate of O^{2-} supply, I/2F) on the conversion of ethanol, at three temperatures for P_{O2} = 8 kPa. As expected, conversion of ethanol is higher at higher temperatures but as shown in Figure 7.13 the application of current produces higher changes of ethanol conversion at low temperatures due to the higher polarization of the Pt/YSZ interface. Indeed, current application was found to induce a 500% increase of ethanol conversion at 300°C, 400% increase at 325°C and 150% increase at 350°C.

3.3 Effect of electrochemical promotion on the yield of acetaldehyde.

Ethanol oxidation presents significant interest as a route for the production of acetaldehyde. Considering that acetaldehyde is a product of increased value compared with ethanol it is obvious that the optimization of this production process is of great practical importance. The determination of the optimal conditions (T, I) of electrochemical promotion for the maximization of the amount of acetaldehyde cannot be based on selectivity values because these do not represent quantitative measures of the amounts produced. For this reason, the selection of the optimum conditions can be based on the reaction yield (= selectivity of acetaldehyde x ethanol conversion) to acetaldheyde as summarized in Figure 7.14 which illustrates the distribution of the yield of acetaldehyde in the range of currents and temperatures used in the present study. The yield of acetaldehyde increases as both temperature and applied current increase. At 300°C, the open circuit value of acetaldehyde yield is about 1.2% and may be increased to 8.3-9.1% by applying currents above 40μA. This is an almost 700% increase in the yield of acetaldehyde due to

the electrochemical promotion. The same change can be estimated of the order of 540 and 170% at 325 and 350°C, respectively. Finally, the maximum acetaldehyde yield was about 17.6% at 350°C for I = 80 μA [16].

4. SUMMARY.

The present study was undertaken to examine the existence, the extent and the results of the effect of electrochemical promotion (NEMCA) during the reaction of ethanol oxidation over polycrystalline Pt. It was found that polarization of Pt/YSZ interface is able to dramatically and reversibly enhance the rate of ethanol dehydrogenation into acetaldehyde. The extent of the electrochemical promotion, i.e. the Faradaic efficiency Λ, was found to be of the order of 10^4 at relatively low temperatures (300-325°C) and high oxygen partial pressures (8 kPa). The study focused on the optimization of the effect of the electrochemical promotion to maximize the reaction yield to acetaldehyde. As a result, it was found that the yield of acetaldehyde can increase up to 700% at 300°C and up to 170% at 350 °C due to electrochemical promotion attaining values between 8.3 and 17.6% at high oxygen partial pressures (8 kPa) with application of currents of 80μA. The overall effect has been interpreted in terms of the observed decrease in the catalytic activation energy of ethanol dehydrogenation which was found to be 70-85% lower than the corresponded regular (open circuit) value.

REFERENCES

1. Stoukides, M., *Solid electrolyte membrane reactors: Current experience and future outlook*, Catal. Rev. -Sci. Eng., **42**(1&2), 2000: p. 1.
2. Vayenas, C. G., Jaksic, M. M., Bebelis, S. I., and Neophytides, S. G., *"The electrochemical activation of catalytic reactions"* in *"Modern aspects of electrochemistry"* (J. O'. M. Bockris. et. al., Editors), 1996, Vol. 29, p. 57: Plenum Press, New York.
3. Vayenas, C. G., and Neophytides, S. G., *"Electrochemical activation of catalysis: in situ controlled promotion of catalyst surfaces"* in *"Catalysis"*, 1996, Vol. 12, p.199: Royal Society of Chemistry, Cambridge-UK.
4. Vayenas, C. G., Bebelis, S. I., Yentekakis, I. V., and Neophytides, S. G., in "The CRC handbook of solid state electrochemistry" (Gellings P. J. and Bouwnmeester H. J. M., Editors), 1997, p. 445: The CRC Press Inc..
5. Vayenas C. G., Bebelis S., Pliangos S., Brosda S., and Tsiplakides D., *"Electrochemical activation of catalysis"*, 2001: Kluwer Academic/Plenum Publishers, New York. (and the references therein).
6. Metcalfe, I. S., *Electrochemical promotion of catalysis. I: Thermodynamic considerations.* Journal of Catalysis, **199**, 2001: p. 247-258.
7. Metcalfe, I. S., *Electrochemical promotion of catalysis. II: The role of a stable spillover species and prediction of reaction rate modification.* Journal of Catalysis, **199**, 2001: p. 259-272.
8. Gomez, M. F., Arrua, L. A., and Abello, M. C., *Kinetic studies of partial oxidation of ethanol over VMgO catalyst*, Ind. Eng. Chem. Res., **36**, 1997: p. 3468.
9. McKetta, J. J., in "Encyclopedia of Chemical Processing and Design". 1988, Vol. 1, p. 114: Marcel Dekker Inc., New York
10. Douvartzides, S. and Tsiakaras, P., *Catalytic and electrocatalytic oxidation of ethanol over a $La_{0.6}Sr_{0.4}Co_{0.8}Fe_{0.2}O_3$ pervskite-type catalyst.* Solid State Ionics, **136-137**, 2000: p. 849-855.
11. Vayenas, C. G., Bebelis, S., Yentekakis, I. V., and Lintz H.-G., *Non-Faradaic electrochemical modification of catalytic activity: A status report*, Catalysis Today, **11**(3),1992: p. 303
12. Wang D. Y., and Nowick A. S., *Cathodic and anodic polarization phenomena at platinum electrodes with doped CeO_2 as electrolyte.* J. Electroch. Soc., **126**(7), 1979: p. 1155-1165.
13. Brennan D., Hayward D. O., and Trapnell B. M. W, Proc. R. Soc., **A256**, 1960: p. 81
14. Okamoto H., Kawamura G., and Kudo T., *Study of oxygen adsorption on platinum through observation of exchange current in a solid electrolyte concentration cell*, Electrochemica Acta, **28**(3), 1983: p. 379
15. Cavalca, C., Larsen, G., Vayenas C. G., and Haller, G., *Electrochemical modification of CH_3OH oxidation selectivity and activity on a Pt single-pellet catalytic reactor*, J. Phys. Chem., **97**, 1993: p. 6115
16. Tsiakaras, P. E., Douvartzides, S. L., Sobyanin, V. A., and Demin, A. K., *The oxidation of ethanol over Pt catalyst-electrodes deposited on ZrO_2 (8% mol Y_2O_3)*, Solid State Ionics, **152**, 2002: p. 721-726.

CHAPTER 8

PRELIMINARY STUDY OF A SOLID OXIDE FUEL CELL FUELED BY EXTERNAL ETHANOL DECOMPOSITION

ABSTRACT

In this Chapter the performance of a Pt based anode solid oxide fuel cell (SOFC) fed with a gas mixture containing H_2, CO and CH_4 (molar ratio 1:1:1) produced by external ethanol decomposition was studied. Preliminary experiments were performed at atmospheric pressure in the temperature range 660–800°C and anode potential vs. air -0.78 to -0.23 V. It was shown that at low temperature (660°C), the outlet gas contained the products of complete oxidation of the gas mixture, while high temperature (800°C) facilitated synthesis gas production.

8.1. INTRODUCTION

Ethanol, a product of biochemical conversion of biomass, is seriously considered as a fuel for fuel cells [1,2]. Recently, Pd supported carbon catalysts were found showing high activity and selectivity for ethanol reforming [3]

$$C_2H_5OH \rightarrow CH_4 + CO + H_2 \qquad (1)$$

The gas mixture yielding reaction (1) can be used as a fuel for Solid Oxide Fuel Cell (SOFC). To design an external ethanol reforming SOFC, it is necessary to clarify which reactions occur on an anode fed with ethanol reforming products. The present work reports the performance of a Pt anode SOFC fed with the mixture containing H_2, CO and CH_4 (molar ratio 1:1:1).

8.2. MATERIALS AND METHODS

The experimental apparatus included an electrochemical cell, a potentiostat–galvanostat and a gas chromatograph [4]. The electrochemical cell design was similar to that described elsewhere [5]. It was a tube closed at one end made of yttria stabilized zirconia (YSZ) electrolyte. The electrolyte tube was 100 mm in length, 10 mm in diameter and had a wall thickness of 0.6 mm. The Pt (working) electrode was supported on the inner surfaces of the tube. A reaction mixture of CH_4, CO, H_2 and He (N_2) was fed inside. A Pt electrode containing praseodymium oxide (ca. 2 wt.%) was deposited on the outer surface of the tube and served as the counter and the reference electrode simultaneously. This electrode was blown with air and was practically non-polarized.

Pt electrodes were prepared from a Pt paste containing 5 wt.% of YSZ powder according to the procedure described elsewhere [5]. The geometric area of the electrodes was 3 cm^2, thickness 10–15 μm, Pt content was equal to 10 mg/cm^2. Note that the counter electrode, which at the same time was the reference electrode, contained praseodymium oxide along with the Pt and YSZ. The PrO_2 was added to the Pt electrode by impregnation with a water solution of praseodymium

nitrate. Electric current passing through the cell (oxygen flow through the electrolyte to the reaction zone) was controlled by a potentiostat–galvanostat. Oxygen flow through the electrolyte (rO_2) was calculated by equation

$$rO_2 = I/4F, \quad (2)$$

where I is the current and F is the Faraday constant. The ohmic resistance of the cell was determined by the current interruption method. The measured cell voltage minus ohmic loss was equal to the Pt working electrode potential.

The experiments were carried out at 660–800°C, atmospheric pressure and at a CH_4+CO+H_2+He (N_2) flow rate of 0.4–0.5 cm^3/s. Concentrations of CH_4, CO and H_2 were equal and amounted to ≈5 vol.%. The current passing through the cell was varied from 100 to 600 mA. The composition of inlet and outlet gas mixtures was analyzed by an online gas chromatograph with a molecular sieve and Porapak-Q columns. The concentrations of CH_4, CO, H_2, CO_2 and H_2O were measured with an accuracy of ±5%.

8.3. RESULTS AND DISCUSSION

In the entire range of experimental conditions, the electrochemically pumped oxygen was converted completely, its outlet concentration was below the detection limit (<0.01 vol. %); the outlet gas contained CH_4, CO, CO_2, H_2 and H_2O.

Mass balances of carbon, oxygen and hydrogen were calculated by the following equations

$$r(CH_4)_{in} + r(CO)_{in} = r(CH_4)_{out} + r(CO)_{out} + r(CO_2)_{out} \quad (3)$$

$$rO_2 + \tfrac{1}{2}\, r(CO)_{in} = \tfrac{1}{2}\, r(CO)_{out} + r(CO_2)_{out} + \tfrac{1}{2}\, r(H_2O)_{out} \quad (4)$$

$$2\, r(CH_4)_{in} + r(H_2)_{in} = 2\, r(CH_4)_{out} + r(H_2)_{out} + r(H_2O)_{out} \quad (5)$$

where $r(CH_4)_{in}$, $r(CO_2)_{in}$, $r(H_2)_{in}$ are the inlet fluxes of CH_4, CO_2 and H_2; $r(CH_4)_{out}$, $r(CO)_{out}$, $r(H_2)_{out}$, $r(CO_2)_{out}$, and $r(H_2O)_{out}$ are the outlet fluxes of CH_4, CO, H_2, CO_2 and H_2O; rO_2 is the oxygen flow through the electrolyte to the reaction zone (Eq. (2)). The inlet and outlet flux of each gas was calculated using the volume concentration of each gas and the gas flow rate. No imbalance with respect to carbon (Eq. (3)), oxygen (Eq. (4)) and hydrogen (Eq. (5)) was observed during the experiments (within ±5% accuracy). Moreover, carbon oxides were not detected in the outlet mixture after the experiment had been completed and the mixture of helium and electrochemically pumped oxygen had been fed in the reactor instead of reaction mixture. This proves that no coking on the Pt electrode occurred. Figures 8.1 and 8.2 present typical experimental results for electrochemical oxidation of equimolar mixture of H_2, CO and CH_4 over Pt electrode at 660 and 800°C. They show the outlet gas composition and the Pt electrode potential as functions of the current passing through the cell. Obviously, the outlet gas composition at 660°C is essentially different from that at 800°C. In the experiments at 660°C, only the products of complete oxidation were detected, while at 800°C the outlet mixture contained CO and H_2 together with the complete oxidation products. Note also that in the entire range of experimental conditions, the outlet gas composition differed considerably from the thermodynamic equilibrium composition.

As Figure 8.1 shows, at 660°C the increase of anodic current from 100 to 400 mA or the increase of electrode potential from -0.64 to -0.23 V resulted in the lower outlet concentrations of H_2, CO and CH_4 with respect to their inlet concentrations, and in the increasing outlet concentrations of H_2O and CO_2. Analysis of these results suggests that the electrochemically pumped oxygen in the reaction zone was entirely used for the electrochemical oxidation of H_2, CO and CH_4 via reactions

$$H_2 + O^{2-} = H_2O + 2e^- \quad (6)$$

$$CO + O^{2-} = CO_2 + 2e^- \quad (7)$$

$$CH_4 + 4O^{2-} = CO^2 + 2H_2O + 8e^- \quad (8)$$

At I=100mA that corresponded to the rate of electrochemical pumping of oxygen rO_2 =15.6 μmol/min only the electrochemical oxidation of hydrogen proceeded (reaction (6)). At this current, $[H_2]_{out}$ was lower than $[H_2]_{in}$ and water was detected in the exit gas; $[CO]_{out}$ and $[CH_4]_{out}$ was practically the same as the respective inlet concentrations; CO_2 was not detected in the exit gas. Moreover, the rate of hydrogen consumption (rH_2=$r(H_2)_{in}$ - $r(H2)_{out}$ =30.2 μmol H_2/min) were close to the flux of O^{2-} ions (rO^{2-}= 2rO_2 =31.2 μmol O^{2-}/min) and to the rate of water formation ($r(H_2O)_{out}$ =29.6 μmol H2O/min). The difference may be attributed to measurement error.

At higher current (Figure 8.1), reactions (6)–(8) proceeded simultaneously, since $[H_2]_{out}$, $[CO]_{out}$ and $[CH_4]_{out}$ were lower than the respective inlet concentrations, and H_2O and CO_2 was detected in the exit gas. As mentioned above, no imbalance with respect to carbon, oxygen and hydrogen (Eqs. (3)–(5)) was observed during the experiments. Thus, electrochemical oxidation of H_2+CO+CH_4 gas mixture at the temperature of 660°C and electrode potential within -0.64 to -0.23 V leads to the formation of CO_2 and H_2O by electrochemical oxidation of H_2, CO and CH_4.

As seen from Figure 8.2, at 800°C the increase of anodic current from 100 to 400 mA or the increase of the electrode potential from -0.78 to -0.61 V resulted in the

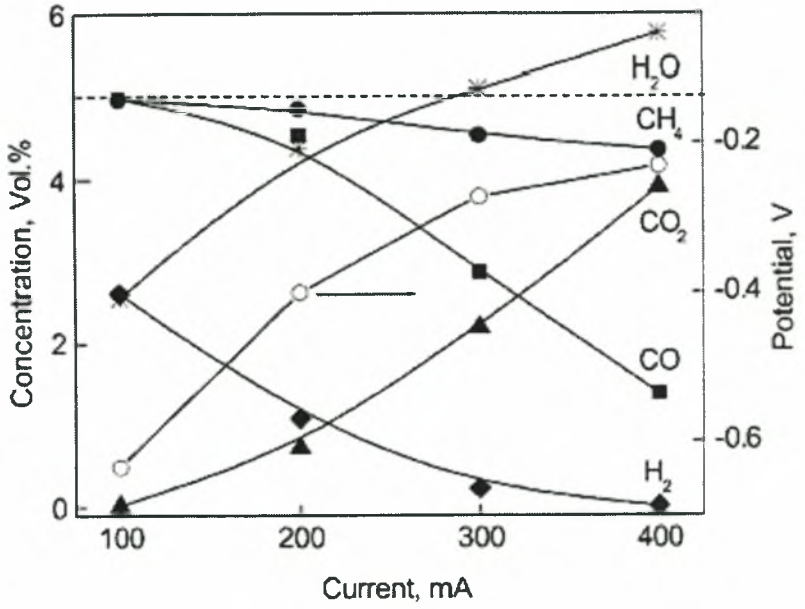

Figure 8.1. Effect of current on the outlet composition and potential of Pt electrode. Experimental conditions: T=660°C, flow rate 0.47 cm^3/s, $[H_2]_{in}=[CH_4]_{in}=[CO]_{in}=5$ vol.%. Dotted line shows the inlet concentrations of H_2, CH_4 and CO.

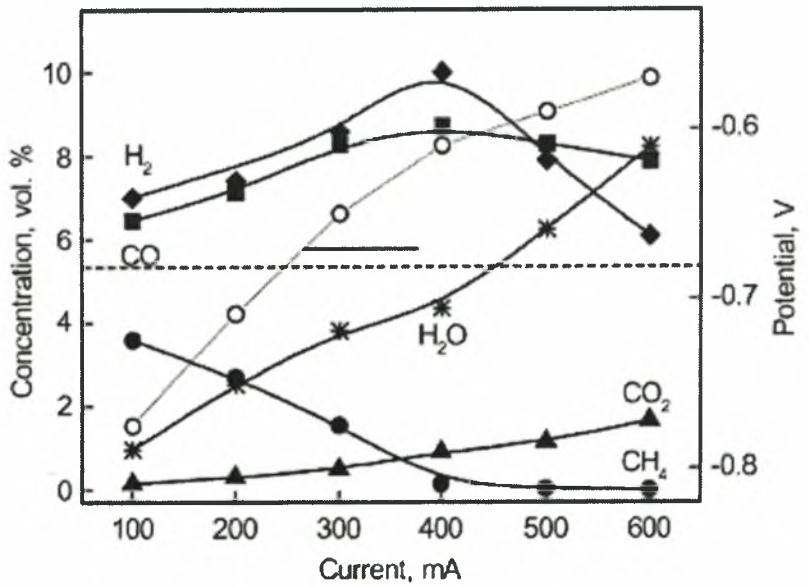

Figure 8.2. Effect of current on the outlet composition and potential of Pt electrode. Experimental conditions: T=800°C, flow rate 0.46 cm^3/s, $[H_2]_{in}=[CH_4]_{in}=[CO]_{in}=5.3$ vol.%. Dotted line shows the inlet concentrations of H_2, CH_4 and CO.

increase of $[H_2]_{out}$ and $[CO]_{out}$ compared to respective inlet concentrations. Besides, $[CO_2]_{out}$ and $[H_2O]_{out}$ increased, while $[CH_4]_{out}$ decreased as compared to respective inlet concentrations. This suggests that methane is converted to the products of partial oxidation of CO and H_2 by reaction:

$$CH_4 + O^{2-} = CO + 2H_2 + 2e^- \quad (9)$$

At 400 mA, no methane was detected in the exit gas; $[CO]_{out}$ and $[H_2]_{out}$ attained the maximum values. As the current increased above 400 mA, $[CO]_{out}$ and $[H_2]_{out}$ decreased, while $[H_2O]_{out}$ and $[CO_2]_{out}$ increased. This most likely may be attributed to the electrochemical

oxidation of H_2 and CO by reactions (6) and (7). Recall, no imbalance with respect to carbon, oxygen and hydrogen (Eqs. (3)–(5)) was observed during the experiments. Thus, the electrochemical oxidation of H_2+CO+CH_4 gas mixture over Pt electrode at 800°C results in the formation of CO_2 and H_2O, as well as H_2 and CO. Most likely, the electrochemical oxidation of H_2 and CO reactions (6) and (7) and selective electrochemical oxidation of CH_4 to H_2 and CO (reaction (9)) occur on the anode at 800°C.

The realization of reaction (9) at 800°C and reaction (8) at 660°C during electrochemical oxidation of H_2+CO+CH_4 gas mixture over Pt electrode agrees with the results reported previously [5–8] on the electrochemical oxidation of CH_4 over Pt electrode in a SOFC reactor. In these works, the products of complete CH_4 oxidation reaction (8) were observed mainly at 660°C, while the products of partial oxidation of CH_4 reaction (9) were detected at 800°C. This phenomenon may be explained by different mechanisms of methane activation at 660 and 800°C. The authors of the references [9,10] suggested that methane activation may proceed both with and without the participation of adsorbed oxygen atoms by the following stages:

$$CH4 \rightarrow CH_{x,s} + (4-x)H_s \qquad (10)$$

$$CH_{x,s} + O_s \rightarrow CH_{x-1,s} + OH_s \qquad (11)$$

where index "*s*" designates surface species.

Stage (11) facilitates complete oxidation of methane, while stage (10)—partial oxidation of methane. Within the framework of this hypothesis, one may suggest that at increasing temperature the surface becomes more and more depleted of oxygen adatoms that leads to the deceleration of H_2O and CO_2 formation and to the acceleration of H_2 and CO formation. Exactly this situation seems to occur at the electrochemical oxidation of H2+CO+CH4 gas mixture over Pt electrode.

It is known that anodic potential correlates with the activity of oxygen adatoms on the anode surface: the higher is the anodic potential, the lower is the activity of O_s. As shown in Figures 8.1 and 8.2, the anodic potential at 800°C is considerably less than that at 660°C. In other words, at 800°C the surface of Pt electrode is more depleted of oxygen adatoms than at 660°C, that facilitates complete oxidation of CH_4 at 660°C and partial oxidation of CH_4 at 800°C.

REFERENCES

1. Design News, June 22, 1998: p. 88.
2. Maggio G., Freni S., and Cavallaro S., *Light alcohols/methane fuelled molten carbonate fuel cells: a comparative study*, J. Power Sources **74**, 1998: p. 17.
3. Galvita V.V., et al., *Synthesis gas production by steam reforming of ethanol*, Applied Catalysis A: General, **220,** 2001: p. 125.
4. Galvita V.V., et. al., *Electrocatalytic conversion of methane to syngas over Ni electrode in a solid oxide electrolyte cell*, Applied Catalysis A: General, **165,** 1997: p. 301.
5. Galvita V.V., et. al., *Conversion of methane to synthesis gas over Pt electrode in a cell with solid oxide electrolyte*, Catalysis Letters, **39**, 1996: p. 209.
6. Semin G. L., et. al., *Methane conversion to syngas over Pt-based electrode in a solid oxide fuel cell reactor*, Applied Catalysis A: General, **181**, 1999: p. 131.
7. Sobyanin V. A., and Belyaev V. D., *Gas phase electrocatalysis: methane oxidation to syngas in a solid oxide fuel cell reactor*. Solid State Ionics **136,** 2000: p. 747.
8. Galvita V.V., Belyaev V. D., and Sobyanin V. A., *Electrochemical methane oxidation to syngas on the Pt electrode in a cell with a solid oxygen-conducting electrolyte*, Kinet. Katal. **38**, 1997: p. 736.
9. Hickman D. A., Haupfear A. E., and Schmidt L. D., *Synthesis gas formation by direct oxidation of methane over Rh monoliths*, Catalysis Letters, **17**, 1993: p. 223.
10. Hickman D. A., and Schmidt L. D., *Production of syngas by direct catalytic oxidation of methane*, Science, **259,** 1993: p. 343.

APPENDIX A

EXTERNAL REFORMER – SOFC STACK: A THERMODYNAMIC ANALYSIS PROGRAM

A.1. INTRODUCTION

Appendix A provides a program for the thermodynamic analysis of a steam reformer-SOFC stack system according to the methodology described in Chapter 4 of this thesis. The program operates in the environment of "Visual Fortran 6.1" and may run assuming methane, methanol, ethanol or gasoline (n-octane) as fuel. The equilibtrium composition of the steam reforming of each fuel is provided according to the method of direct minimization of Gibbs free energy. Internal reforming of carbon monoxide and methane in the dimensionless SOFC stack is taken under consideration by following the same method under the assumption of uniform suplly of O^{2-} anions at the SOFC anode. The thermodynamic efficiency of the reformer-SOFC system, the distribution of chemical species along the SOFC stack, the distribution of the electromotive force of the stack and its average value, are results of the program which are automatically saved after run in a file entitled "fulldata.txt". Results are displayed for the temperature range of 800-1200 K with step of 50 K and for reforming factors above the boundary of carbonization of each fuel. The program is provided to verify results presented in Chapter 4 of this thesis.

A.2. THE THERMODYNAMIC ANALYSIS PROGRAM LIST

```
PROGRAM SOFC_all


! case3 Y2_initial=Y5_initial=0.000001, Y6_initial=0.959
!RECOMMENDED INITIAL GUESSES


IMPLICIT NONE
! ----------------------INITIAL DEFINITION OF PARAMETERS-------------------------
      REAL(8):: &
            Y1,Y2,Y3,Y4,Y5,Y6,LH,LC,LO,NI, M_Min(4,18),                          &
            PLITHOS_C(4),PLITHOS_O(4),PLITHOS_H(4),M,emf(22),                    &
            ALFA,BETA,GAMMA,DELTA,EPSILON,KAPPA,LAMDA,MI,                        &
            X1=0.,X2=0.,X3=0.,D,DX1,DX2,DX3,B1,B2,B3,                            &
            DF1DX1,DF1DX2,DF1DX3,DF2DX1,DF2DX2,DF2DX3,DF3DX1,DF3DX2,DF3DX3,      &
            tol=1.d-8,pos(22),UF(4),Q(4),DEHA(4),efficiency,                     &
            R,T(21)=0,se,meso_emf,                                               &
            B_H, B_C, B_O,                                                       &
            Eth_DG(21)=0,H2O_DG(21)=0,CO_DG(21)=0,CO2_DG(21)=0,CH4_DG(21)=0
      !Gibbs

      INTEGER :: i, M_ax=100, fuel_index=0, k, kk,m_index, is_ok
      CHARACTER(10) What_Fuel(4)



open (unit=25, file='fulldata.txt', status='unknown')
!---------------------------------- PROPERTIES ----------------------------------
      R=8.314

      T(1)=800;T(2)=850;T(3)=900;T(4)=950;T(5)=1000
      T(6)=1050;T(7)=1100;T(8)=1150;T(9)=1200

      CH4_DG(1)=-2038.070888
      CH4_DG(2)=3262.935868
      CH4_DG(3)=8605.288179
      CH4_DG(4)=13982.67502
      CH4_DG(5)=19389.65218
      CH4_DG(6)=24821.51861
      CH4_DG(7)=30274.21492
      CH4_DG(8)=35744.2393
      CH4_DG(9)=41228.57739

      H2O_DG(1)=-203465.8471
      H2O_DG(2)=-200767.4264
      H2O_DG(3)=-198046.5179
      H2O_DG(4)=-195305.2157
      H2O_DG(5)=-192545.4005
      H2O_DG(6)=-189768.7706
      H2O_DG(7)=-186976.8671
      H2O_DG(8)=-184171.0943
      H2O_DG(9)=-181352.737
```

```
CO2_DG(1)=-395567.4867
CO2_DG(2)=-395666.3515
CO2_DG(3)=-395761.3301
CO2_DG(4)=-395852.3925
CO2_DG(5)=-395939.5083
CO2_DG(6)=-396022.6481
CO2_DG(7)=-396101.7831
CO2_DG(8)=-396176.8858
CO2_DG(9)=-396247.9298

CO_DG(1)=-182449.7677
CO_DG(2)=-186920.3575
CO_DG(3)=-191379.2173
CO_DG(4)=-195826.1298
CO_DG(5)=-200260.9487
CO_DG(6)=-204683.5792
CO_DG(7)=-209093.9641
CO_DG(8)=-213492.0738
CO_DG(9)=-217877.8989

!----------------------DIMENSIONLESS SEGREGATION OF THE SOFC STACK----------------

pos(1)=0;          pos(2)=0.02;       pos(3)=0.04;       pos(4)=0.07
pos(5)=0.1;        pos(6)=0.17 ;      pos(7)=0.27;       pos(8)=0.4
pos(9)=0.6;        pos(10)=0.73;      pos(11)=0.82;      pos(12)=0.88
pos(13)=0.91;      pos(14)=0.94;      pos(15)=0.96;      pos(16)=0.975
pos(17)=0.985;     pos(18)=0.993;     pos(19)=0.996;     pos(20)=0.998
pos(21)=0.999;     pos(22)=0.999999


!----------------------DEFINITION OF REFORMING FACTORS, M (fuel,T)-----------------

M_Min(1,1)=0.988; M_Min(4,1)=0.00245;     M_Min(3,1)=1.004; M_Min(2,9)=14.3
M_Min(1,2)=0.991; M_Min(4,2)= 0.0117;     M_Min(3,2)=1.024; M_Min(2,8)= 13.9
M_Min(1,3)=1.004; M_Min(4,3)= 0.0358;     M_Min(3,3)= 1.072;M_Min(2,7)= 12.6
M_Min(1,4)=1.04;  M_Min(4,4)= 0.09;       M_Min(3,4)= 1.179;M_Min(2,6)= 10.92
M_Min(1,5)=1.118; M_Min(4,5)= 0.204;      M_Min(3,5)= 1.398;M_Min(2,5)= 9.52
M_Min(1,6)=1.25;  M_Min(4,6)= 0.3855;     M_Min(3,6)= 1.76; M_Min(2,4)= 8.67
M_Min(1,7)=1.396; M_Min(4,7)= 0.599;      M_Min(3,7)= 2.196;M_Min(2,3)=8.256
M_Min(1,8)=1.455; M_Min(4,8)= 0.771;      M_Min(3,8)= 2.534;M_Min(2,2)= 8.076
M_Min(1,9)=1.486; M_Min(4,9)= 0.825;      M_Min(3,9)= 2.68; M_Min(2,1)= 8.004
M_Min(1,10)=2.;   M_Min(4,10)=1.;         M_Min(3,10)=3.;   M_Min(2,10)=15.
M_Min(1,11)=2.5;  M_Min(4,11)=1.5;        M_Min(3,11)=3.5;  M_Min(2,11)=15.5
M_Min(1,12)=3.;   M_Min(4,12)=2.;         M_Min(3,12)=4.;   M_Min(2,12)=16.
M_Min(1,13)=3.5;  M_Min(4,13)=2.5;        M_Min(3,13)=4.5;  M_Min(2,13)=16.5
M_Min(1,14)=4.;   M_Min(4,14)=3.;         M_Min(3,14)=5;    M_Min(2,14)=17.
M_Min(1,15)=4.5;  M_Min(4,15)=3.5;        M_Min(3,15)=5.5;  M_Min(2,15)=17.5
M_Min(1,16)=5.;   M_Min(4,16)=4.;         M_Min(3,16)=6.;   M_Min(2,16)=18.
M_Min(1,17)=5.5;  M_Min(4,17)=4.5;        M_Min(3,17)=6.5;  M_Min(2,17)=18.5
M_Min(1,18)=6.;   M_Min(4,18)=5.;         M_Min(3,18)=7.;   M_Min(2,18)=19.
```

```
!--------------------------------FUEL SELECTION-------------------------------------

!Methane
            UF(1)=1.9999
            Q(1)=8*96.485
            DEHA(1)=802645.
            What_Fuel(1)='METHANE'
            PLITHOS_O(1)=0
            PLITHOS_H(1)=4
            PLITHOS_C(1)=1

!Gasoline (n-octane)
            UF(2)=12.4999
            Q(2)=50*96.485
            DEHA(2)=5074200.
            What_Fuel(2)='GASOLINE'
            PLITHOS_O(2)=0
            PLITHOS_H(2)=18
            PLITHOS_C(2)=8
!Ethanol
            UF(3)=2.9999
            Q(3)=12*96.485
            DEHA(3)=1235000.
            What_Fuel(3)='ETHANOL'
            PLITHOS_O(3)=1
            PLITHOS_H(3)=6
            PLITHOS_C(3)=2

!Methanol
            UF(4)=1.4999
            Q(4)=6*96.485
            DEHA(4)=638485.
            What_Fuel(4)='METHANOL'
            PLITHOS_O(4)=1
            PLITHOS_H(4)=4
            PLITHOS_C(4)=1

fuel:DO fuel_index=1,4

      WRITE(25,*)'FUEL : ',What_Fuel(fuel_index)

      IF (fuel_index .EQ. 1) THEN
            Eth_DG(1)=-2038.070888;Eth_DG(2)=3262.935868;Eth_DG(3)=8605.288179
            Eth_DG(4)=13982.67502;Eth_DG(5)=19389.65218;Eth_DG(6)=24821.51861
            Eth_DG(7)=30274.21492;Eth_DG(8)=35744.2393;Eth_DG(9)=41228.57739
      ELSE IF (fuel_index .EQ. 2) THEN
            Eth_DG(1)=417590.7707;Eth_DG(2)=458437.5196;Eth_DG(3)=499258.3742
            Eth_DG(4)=540031.7728;Eth_DG(5)=580740.5456;Eth_DG(6)=621371.3133
            Eth_DG(7)=661913.9872;Eth_DG(8)=702361.3512;Eth_DG(9)=742708.7108
      ELSE IF (fuel_index .EQ. 3) THEN
            Eth_DG(1)=-45713.85944;Eth_DG(2)=-32931.92199;Eth_DG(3)=-20118.07408
            Eth_DG(4)=-7280.992402;Eth_DG(5)=5572.137508;Eth_DG(6)=18435.41224
            Eth_DG(7)=31304.03803;Eth_DG(8)=44174.18744;Eth_DG(9)=57042.87921
      ELSE IF (fuel_index .EQ. 4) THEN
            Eth_DG(1)=-35820.95013;Eth_DG(2)=-22349.09233;Eth_DG(3)=-8841.392651
            Eth_DG(4)=4695.451992;Eth_DG(5)=18255.78732;Eth_DG(6)=31834.85266
```

```
            Eth_DG(7)=45428.65871;Eth_DG(8)=59033.88633;Eth_DG(9)=72647.80216
      END IF


temperature:DO k=1,9
      WRITE(25,*)'TEMPERATURE : ',T(k)

analogy:DO m_index=1,18

      M=M_Min(fuel_index,m_index)
      WRITE(25,*)
      WRITE(25,*)' m = ',M
      WRITE(25,1)



position:DO kk=1,1
      Y1=0.;Y2=0.01;Y3=0.;Y4=0.;Y5=0.01;Y6=0.959;is_ok=0

      se=pos(kk)*UF(fuel_index)

      B_O=PLITHOS_O(fuel_index)+M+2.*se
      B_C=PLITHOS_C(fuel_index)
      B_H=PLITHOS_H(fuel_index)+2.*M

!---------------------------------------CONSTANTS---------------------------------
      ALFA=Eth_DG(k)/(R*T(k))
      BETA=H2O_DG(k)/(R*T(k))
      GAMMA=CO_DG(k)/(R*T(k))
      DELTA=CO2_DG(k)/(R*T(k))
      EPSILON=CH4_DG(k)/(R*T(k))

      KAPPA=EXP(-ALFA+PLITHOS_O(fuel_index)*BETA+PLITHOS_C(fuel_index)*EPSILON)
      LAMDA=EXP(BETA-GAMMA+EPSILON)
      MI=EXP(2.*BETA-DELTA+EPSILON)


!********************************* NEWTON STARTS HERE ****************************
  999         DO i=1,M_ax

                B1=     (PLITHOS_C(fuel_index)                                    &
     -PLITHOS_O(fuel_index)*(B_C/B_O))*KAPPA*(Y2**PLITHOS_O(fuel_index))          &
     *(Y5**PLITHOS_C(fuel_index))*(Y6**(4.-PLITHOS_O(fuel_index)                  &
           +.5*PLITHOS_H(fuel_index)-2.*PLITHOS_C(fuel_index)))                   &
                     -(B_C/B_O)*Y2*(Y6**4)                                  &
                     +(1.-(B_C/B_O))*LAMDA*Y2*Y5*Y6                         &
                     +(1.-2*(B_C/B_O))*MI*(Y2**2)*Y5                        &
                     +Y5*(Y6**4)
                B1=-B1

           B2=  (PLITHOS_H(fuel_index)                                             &
     -PLITHOS_O(fuel_index)*(B_H/B_O))*KAPPA*(Y2**PLITHOS_O(fuel_index))          &
     *(Y5**PLITHOS_C(fuel_index))*(Y6**(4.-PLITHOS_O(fuel_index)                  &
           +.5*PLITHOS_H(fuel_index)-2.*PLITHOS_C(fuel_index)))                   &
               +(2.-(B_H/B_O))*Y2*(Y6**4)                                  &
               -(B_H/B_O)*LAMDA*Y2*Y5*Y6                                   &
```

```
     -2.*(B_H/B_O)*MI*(Y2**2)*Y5                                    &
     +4.*Y5*(Y6**4)+2.*(Y6**5)

    B2=-B2

B3=KAPPA*(Y2**PLITHOS_O(fuel_index))*(Y5**PLITHOS_C(fuel_index))*      &
   (Y6**(4.-PLITHOS_O(fuel_index)+.5*PLITHOS_H(fuel_index)             &
             -2.*PLITHOS_C(fuel_index)))                               &
             +Y2*(Y6**4)                                               &
             +LAMDA*Y2*Y5*Y6 +MI*(Y2**2)*Y5 +Y5*(Y6**4)                &
             -(Y6**4) +(Y6**5)
        B3=-B3

!====================Jacobian (=coefficients of the linear system)=================
      DF1DX1= PLITHOS_O(fuel_index)                                    &
      *(PLITHOS_C(fuel_index)-PLITHOS_O(fuel_index)*(B_C/B_O))         &
      *KAPPA*(Y2**(PLITHOS_O(fuel_index)-1))                           &
      *(Y5**PLITHOS_C(fuel_index))*(Y6**(4.-PLITHOS_O(fuel_index)      &
      +.5*PLITHOS_H(fuel_index)-2.*PLITHOS_C(fuel_index)))             &
             -(B_C/B_O)*(Y6**4)                                        &
             +(1.-(B_C/B_O))*LAMDA*Y5*Y6                               &
             +2.*(1.-2*(B_C/B_O))*MI*Y2*Y5

      DF1DX2=PLITHOS_C(fuel_index)                                     &
      *(PLITHOS_C(fuel_index)-PLITHOS_O(fuel_index)*(B_C/B_O))         &
      *KAPPA*(Y2**PLITHOS_O(fuel_index))                               &
      *(Y5**(PLITHOS_C(fuel_index)-1))*(Y6**(4.-PLITHOS_O(fuel_index)  &
      +.5*PLITHOS_H(fuel_index)-2.*PLITHOS_C(fuel_index)))             &
             +(1.-(B_C/B_O))*LAMDA*Y2*Y6                               &
             +(1.-2*(B_C/B_O))*MI*(Y2**2)+(Y6**4)

      DF1DX3=(4.-PLITHOS_O(fuel_index)+.5*PLITHOS_H(fuel_index)        &
      -2.*PLITHOS_C(fuel_index))*(PLITHOS_C(fuel_index)                &
      -PLITHOS_O(fuel_index)*(B_C/B_O))                                &
      *KAPPA*(Y2**PLITHOS_O(fuel_index))*(Y5**PLITHOS_C(fuel_index))   &
      *(Y6**(3.-PLITHOS_O(fuel_index)+.5*PLITHOS_H(fuel_index)         &
      -2.*PLITHOS_C(fuel_index)))-4.*(B_C/B_O)*Y2*(Y6**3)              &
             +(1.-(B_C/B_O))*LAMDA*Y2*Y5+4.*Y5*(Y6**3)


      DF2DX1=PLITHOS_O(fuel_index)*(PLITHOS_H(fuel_index)              &
      -PLITHOS_O(fuel_index)*(B_H/B_O))                                &
      *KAPPA*(Y2**(PLITHOS_O(fuel_index)-1))                           &
      *(Y5**PLITHOS_C(fuel_index))*(Y6**(4.-PLITHOS_O(fuel_index)      &
      +.5*PLITHOS_H(fuel_index)-2.*PLITHOS_C(fuel_index)))             &
              +(2.-(B_H/B_O))*(Y6**4)                                  &
              -(B_H/B_O)*LAMDA*Y5*Y6-4.*(B_H/B_O)*MI*Y2*Y5

      DF2DX2=PLITHOS_C(fuel_index)*(PLITHOS_H(fuel_index)              &
      -PLITHOS_O(fuel_index)*(B_H/B_O))*KAPPA*(Y2**PLITHOS_O(fuel_index))&
      *(Y5**(PLITHOS_C(fuel_index)-1))*(Y6**(4.-PLITHOS_O(fuel_index)  &
      +.5*PLITHOS_H(fuel_index)-2.*PLITHOS_C(fuel_index)))             &
              -(B_H/B_O)*LAMDA*Y2*Y6                                   &
              -2.*(B_H/B_O)*MI*(Y2**2)+4.*(Y6**4)
```

```
      DF2DX3=(4.-PLITHOS_O(fuel_index)+.5*PLITHOS_H(fuel_index)          &
      -2.*PLITHOS_C(fuel_index))*(PLITHOS_H(fuel_index)                  &
      -PLITHOS_O(fuel_index)*(B_H/B_O))*KAPPA*(Y2**PLITHOS_O(fuel_index))&
      *(Y5**PLITHOS_C(fuel_index))*(Y6**(3.-PLITHOS_O(fuel_index)        &
      +.5*PLITHOS_H(fuel_index)-2.*PLITHOS_C(fuel_index)))               &
                  +4.*(2.-(B_H/B_O))*Y2*(Y6**3)                          &
                  -(B_H/B_O)*LAMDA*Y2*Y5                                 &
                  +16.*Y5*(Y6**3)+10.*(Y6**4)

      DF3DX1=PLITHOS_O(fuel_index)*KAPPA*(Y2**(PLITHOS_O(fuel_index)-1)) &
      *(Y5**PLITHOS_C (fuel_index))*(Y6**(4.-PLITHOS_O(fuel_index)       &
      +.5*PLITHOS_H(fuel_index)-2.*PLITHOS_C(fuel_index)))               &
                  +(Y6**4)+LAMDA*Y5*Y6 +2.*MI*Y2*Y5

      DF3DX2=PLITHOS_C(fuel_index)*KAPPA*(Y2**PLITHOS_O(fuel_index))     &
      *(Y5**(PLITHOS_C(fuel_index)-1))*(Y6**(4.-PLITHOS_O(fuel_index)    &
      +.5*PLITHOS_H(fuel_index)-2.*PLITHOS_C(fuel_index)))               &
                  +LAMDA*Y2*Y6 +MI*(Y2**2) +(Y6**4)

      DF3DX3=(4.-PLITHOS_O(fuel_index)+.5*PLITHOS_H(fuel_index)          &
      -2.*PLITHOS_C(fuel_index))*KAPPA*(Y2**PLITHOS_O(fuel_index))       &
      *(Y5**PLITHOS_C(fuel_index))* (Y6**(3.-PLITHOS_O(fuel_index)       &
      +.5*PLITHOS_H(fuel_index)-2.*PLITHOS_C(fuel_index)))               &
                  +4.*Y2*(Y6**3)+LAMDA*Y2*Y5 +4.*Y5*(Y6**3)              &
                  -4.*(Y6**3) +5.*(Y6**4)

!^^^^^^^^^^^^^^^^^^^^^^^^^^^^^solution of the linear system^^^^^^^^^^^^^^^^^^^^^^^^^
            D=     DF1DX1*(DF2DX2*DF3DX3-DF2DX3*DF3DX2) &
                  -DF1DX2*(DF2DX1*DF3DX3-DF2DX3*DF3DX1) &
                  +DF1DX3*(DF2DX1*DF3DX2-DF2DX2*DF3DX1)

            DX1= B1*(DF2DX2*DF3DX3-DF2DX3*DF3DX2) &
                  -DF1DX2*(B2*DF3DX3-DF2DX3*B3)+DF1DX3*(B2*DF3DX2-DF2DX2*B3)

            DX2= DF1DX1*(B2*DF3DX3-DF2DX3*B3) &
                  -B1*(DF2DX1*DF3DX3-DF2DX3*DF3DX1) &
                  +DF1DX3*(DF2DX1*B3-B2*DF3DX1)

            DX3= DF1DX1*(DF2DX2*B3-B2*DF3DX2)-DF1DX2*(DF2DX1*B3-B2*DF3DX1) &
                  +B1*(DF2DX1*DF3DX2-DF2DX2*DF3DX1)

            X1=DX1/D
            X2=DX2/D
            X3=DX3/D

!================================the essence of Newton-Raphson=====================

            Y2=Y2+X1
            Y5=Y5+X2
            Y6=Y6+X3

            IF (ABS(Y2) < tol .AND. ABS(Y5) < tol .AND. ABS(Y6) < tol ) EXIT

      END DO

      Y1=KAPPA*(Y2**PLITHOS_O(fuel_index))                               &
```

```
            *(Y5**PLITHOS_C(fuel_index))/(Y6**(PLITHOS_O(fuel_index)     &
            -.5*PLITHOS_H(fuel_index)+2.*PLITHOS_C(fuel_index)))
            Y3=LAMDA*Y2*Y5/(Y6**3)
            Y4=MI*Y5*(Y2**2)/(Y6**4)


emf(kk)=-R*T(k)*(LOG(ABS(Y2)/ABS(Y6))-(29837./T(k)-6.688)-LOG(0.209)/2)/2/96.485

!           PRINT*, ' Y_fuel =', Y1
!           PRINT*, ' Y_H2O =', Y2
!           PRINT*, ' Y_CO =', Y3
!           PRINT*, ' Y_CO2 =', Y4
!           PRINT*, ' Y_CH4 =', Y5
!           PRINT*, ' Y_H2 =', Y6

IF (Y1.GT.0 .AND. Y2.GT.0 .AND. Y3.GT.0 .AND. Y4.GT.0 .AND. Y5.GT.0 .AND. Y6.GT.0)
THEN
                  WRITE(25,2)pos(kk),Y1,Y2,Y3,Y4,Y5,Y6,emf(kk)
                  CYCLE position
            ELSE
                  Y2=0.000001;Y5=0.000001;Y6=0.959;is_ok=is_ok+1
                  if (is_ok .LE. 1) then
                        GOTO 999
                  else
                        WRITE(25,2)pos(kk),Y1,Y2,Y3,Y4,Y5,Y6,emf(kk)
                  end if
            END IF

      end do position

!================================INTEGRATION OF emf==============================
      meso_emf=0.
      do kk=1,21
            meso_emf=meso_emf+.5*(pos(kk+1)-pos(kk))*(emf(kk+1)+emf(kk))
      end do
      efficiency=Q(fuel_index)*meso_emf/DEHA(fuel_index)
      write(25,*)
      write(25,*) ' E_meso = ', meso_emf
      write(25,*) ' n = ', efficiency
      write(25,*)
      write(25,*)

END DO analogy
END DO temperature
END DO fuel

1
      FORMAT(3x,'X',5x,'Y_fuel',4x,'Y_H2O',5x,'Y_CO',6x,'Y_CO2',4x,'Y_CH4',5x,'Y_H2
',5x,'emf')
2     FORMAT(1x,f7.5,2x,f7.6,2x,f7.6,2x,f7.6,2x,f7.6,2x,f7.6,2x,f7.6,2x,f8.3)


close(25)

END PROGRAM SOFC_all
```

APPENDIX B

SIMULATION PROGRAM OF A SOFC POWER PLANT

B.1. INTRODUCTION

In this Appendix, a simulation program for the SOFC plant of Figure B.1 is listed, assuming that it is fueled by ethanol. The program operates in the environment of "Visual Fortran 6.1" and is capable of estimating the fisrt and second law efficiencies of the plant, mass flow rates, uknown temperatures (T_6, T_{10}, T_{11}) , energy and exergy contents in each stream line (as percentages of the LHV and chemical exergy of ethanol, respectively) and exergy destruction rates in the indivindual devices. The program assumes the knowledge of the exact temperatures of the preheated air (T_4) and the reformate (T_7) and is therefore valid only for adiabatic-SOFC operation. All known temperatures may change in the routine entilted "TEMPERATURES". Input parameters are the feforming factor (steam/fuel molar ratio for reforming reaction), air excess (%), the extend of the reforming reaction (%) and hydrogen utilization in the SOFC device (%) which are requested after running the program. The program is provided to verify results presented in Chapter 5 of this thesis.

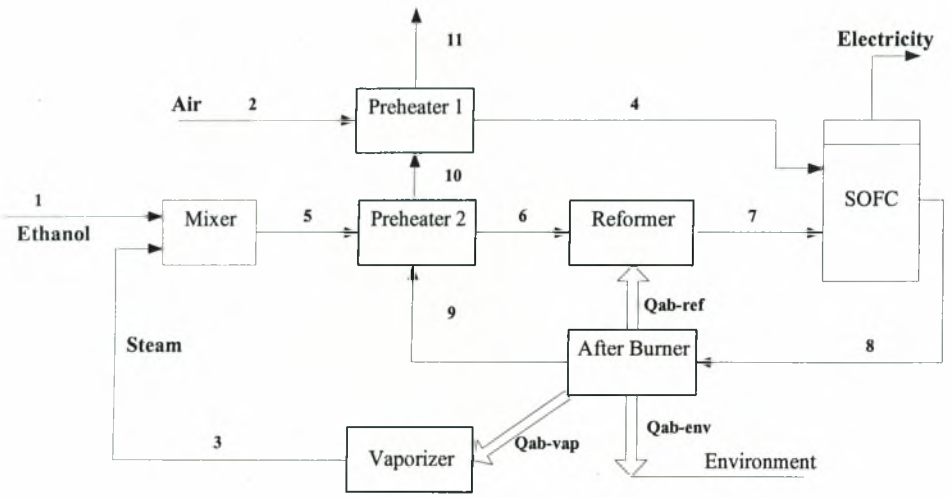

Figure B.1. Definition of positions and heat transfers used in the program list

B.2. THE EXERGY PROGRAM LIST

```
PROGRAM generalXRG
IMPLICIT NONE

!------------------------ INITIAL DEFINITION OF PARAMETERS-------------------------
REAL::      SCE=29.9065, DHS=1235000, MMB=46,                                    &
            SC_O2=3, SC_CO2=2,SC_H2O=3, RC_f=1, RC_H2O=3, RC_CO2=2, RC_H2=6,     &
            DH=173536, SCXRG=1357700, h0=-234950, s0=280.64,                     &
            Ah=3.518,Bh=0.0100005,Ch=0.000001000667,                             &
            As=3.518,Bs=0.020001,Cs=-0.000006002,m,axc,e,uf,                     &
            T1,T2,T3,T4,T5,T6,T7,T8,T9,T10,T11,                                  &
            mdot1,mdot2,mdot3,mdot4,mdot5,mdot6,mdot7,mdot8,mdot9,mdot10,mdot11,&
            N2_1,N2_2,N2_3,N2_4,N2_5,N2_6,N2_7,N2_8,N2_9,N2_10,N2_11,           &
            O2_1,O2_2,O2_3,O2_4,O2_5,O2_6,O2_7,O2_8,O2_9,O2_10,O2_11,           &
            CO2_1,CO2_2,CO2_3,CO2_4,CO2_5,CO2_6,CO2_7,CO2_8,CO2_9,CO2_10,CO2_11,&
            H2O_1,H2O_2,H2O_3,H2O_4,H2O_5,H2O_6,H2O_7,H2O_8,H2O_9,H2O_10,H2O_11,&
            f_1,f_2,f_3,f_4,f_5,f_6,f_7,f_8,f_9,f_10,f_11,                        &
            CH4_1,CH4_2,CH4_3,CH4_4,CH4_5,CH4_6,CH4_7,CH4_8,CH4_9,CH4_10,CH4_11,&
            CO_1,CO_2,CO_3,CO_4,CO_5,CO_6,CO_7,CO_8,CO_9,CO_10,CO_11,           &
            H2_1,H2_2,H2_3,H2_4,H2_5,H2_6,H2_7,H2_8,H2_9,H2_10,H2_11,           &
            Tmean,Told, MMB1,nom,Q,Q24,Q56,QAB,QABR,QABE,QABV,XQABV,XQABE,XQABR,&
            nof,noH2O,noCO2,noH2,noO2,noN2,nofa,noH2Oa,noCO2a,noH2a,noO2a,noN2a,&
            CP_N2,CP_O2,CP_CO2,CP_H2O,CP_fuel,CP_CH4,CP_CO,CP_H2,CP_mix,         &
            hmix,smix,h00,s00,Wel,CHen,Qen,nI,nII,                               &
            EN1,ENper1,EXPH1,EXCH1,EXper1,EX1,EN2,ENper2,EXPH2,EXCH2,EXper2,EX2,&
            EN3,ENper3,EXPH3,EXCH3,EXper3,EX3,EN4,ENper4,EXPH4,EXCH4,EXper4,EX4,&
            EN5,ENper5,EXPH5,EXCH5,EXper5,EX5,EN6,ENper6,EXPH6,EXCH6,EXper6,EX6,&
            EN7,ENper7,EXPH7,EXCH7,EXper7,EX7,EN8,ENper8,EXPH8,EXCH8,EXper8,EX8,&
            EN9,ENper9,EXPH9,EXCH9,EXper9,EX9,EN10,ENper10,EXPH10,EXCH10,EXper10,&
            EX10,EN11,ENper11,EXPH11,EXCH11,EXper11,EX11,P1,P2,MX,RF,FC,AB,      &
            K36, L36, J36, lnk

!---------------------------DEFINITIONS of fuel parameteres ----------------------
!
!     SCE = Chemical Exergy = 29.9065MW
!     DHS = ΔH standard = 1235000 Joule/mol
!     MMB = MB = 46
!     SC_O2 = Stoichiometric oxidation coeff of O2 = 3
!     SC_CO2 = Stoichiometric oxidation coeff of CO2 = 2
!     SC_H2O = Stoichiometric oxidation coeff of H2O = 3
!     RC_f = coeff in oxidation reaction_fuel = 1
!     RC_H2O = coeff in reforming reaction_water = 3
!     RC_CO2 = coeff in reforming reaction_CO2 = 2
!     RC_H2 = coeff in reforming reaction_H2 = 6
!     DH = ΔH = 173536 Joule/mol
!     SCXRG = Standard chemical XRG = 1357700
!     h0 = -234950
!     s0 = 280.64
!     Ah = 3.518
!     Bh = 0.0100005
!     Ch = 0.000001000667
!     As = 3.518
!     Bs = 0.020001
```

```
!     Cs = -0.000006002


!-----------------------------DEFINITIONS of input parameteres --------------------
!m                !     reforming factor
!axc              !     air excess, %
!e                !     extemd of reforming, %
!uf               !     fuel utilization, %

print*,'Give reformig factor, m : ';read(*,*),m
print*,'Give air excess, % : ';read(*,*),axc
print*,'Give extend of reforming, % : ';read(*,*),e
print*,'Give fuel utilization, % : ';read(*,*),uf

!-------------------------------------FLOWS ----------------------------------------
mdot1 = 1
mdot2 = (axc/100.)*(SC_O2/MMB*28.6/0.2035)
mdot3 = m*18/MMB
mdot4 = mdot2
mdot5 = mdot1+mdot3
mdot6 = mdot5
mdot7 = mdot6
mdot8 = mdot4+mdot7
mdot9 = mdot8
mdot10 = mdot9
mdot11 = mdot10


!-----------------------------MOLAR FRACTIONS ------------------------------------

!position1
N2_1=1e-13;O2_1=1e-13;CO2_1=1e-13;H2O_1=1e-13;f_1=1.;CH4_1=1e-13
CO_1=1e-3;H2_1=1e-13

!position2
N2_2=0.7567;O2_2=0.2035;CO2_2=0.0003;H2O_2=0.0303;f_2=1e-13;CH4_2=1e-13
CO_2=1e-13;H2_2=1e-13

!position3
N2_3=1e-13;O2_3=1e-13;CO2_3=1e-13;H2O_3=1.;f_3=1e-13;CH4_3=1e-13
CO_3=1e-13;H2_3=1e-13

!position4
N2_4=0.7567;O2_4=0.2035;CO2_4=0.0003;H2O_4=0.0303;f_4=1e-13;CH4_4=1e-13
CO_4=1e-13;H2_4=1e-13

!position5
N2_5=1e-13;O2_5=1e-13;CO2_5=1e-13;H2O_5=m/(1+m);f_5=1./(1+m);CH4_5=1e-13
CO_5=1e-13;H2_5=1e-13

!position6
N2_6=1e-13;O2_6=1e-13;CO2_6=1e-13;H2O_6=H2O_5;f_6=f_5;CH4_6=1e-13
CO_6=1e-13;H2_6=1e-13
```

```
!position7                    =========   REFORMING   =========
nof      =   RC_f*(1-e/100)*1000/MMB
noH2O =      (mdot3*1000/18)-(RC_H2O*e/100)*(1000/MMB)
noCO2 =      RC_CO2*(e/100)*(1000/MMB)
noH2  =      RC_H2*(e/100)*(1000/MMB)

N2_7=1e-13;O2_7=1e-13;CH4_7=1e-13;CO_7=1e-13;

CO2_7=noCO2/(nof+noH2O+noCO2+noH2)
H2O_7=noH2O/(nof+noH2O+noCO2+noH2)
f_7=nof/(nof+noH2O+noCO2+noH2)
H2_7=noH2/(nof+noH2O+noCO2+noH2)


!position8              ========= FUEL CELL ==================
nofa  =      nof
noN2a =      (mdot2*1000/28.6)*N2_2
noH2Oa       =      (mdot2*1000/28.6)*H2O_2+noH2O+(uf/100.)*noH2
noCO2a       =      (mdot2*1000/28.6)*CO2_2+noCO2
noO2a =      (mdot2*1000/28.6)*O2_2-0.5*(uf/100)*noH2
noH2a =      (1-(uf/100))*noH2

N2_8  =      noN2a/(nofa+noH2Oa+noCO2a+noO2a+noN2a+noH2a)
CO2_8 =      noCO2a/(nofa+noH2Oa+noCO2a+noO2a+noN2a+noH2a)
H2O_8 =      noH2Oa/(nofa+noH2Oa+noCO2a+noO2a+noN2a+noH2a)
f_8           =      nofa/(nofa+noH2Oa+noCO2a+noO2a+noN2a+noH2a)
O2_8  =      noO2a/(nofa+noH2Oa+noCO2a+noO2a+noN2a+noH2a)
H2_8  =      noH2a/(nofa+noH2Oa+noCO2a+noO2a+noN2a+noH2a)

CO_8=1e-13;CH4_8=1e-13

!position9              ========= AFTERBURNER ==================


noN2  =      noN2a
noO2  =      noO2a-SC_O2*nofa-0.5*noH2a
noCO2 =      noCO2a+SC_CO2*nofa
noH2O =      noH2Oa+SC_H2O*nofa+noH2a

N2_9  =      noN2/(noH2O+noCO2+noO2+noN2)
O2_9  =      noO2/(noH2O+noCO2+noO2+noN2)
CO2_9 =      noCO2/(noH2O+noCO2+noO2+noN2)
H2O_9 =      noH2O/(noH2O+noCO2+noO2+noN2)

CO_9=1e-13;CH4_9=1e-13;H2_9=1e-13;f_9=1e-13

!position10
N2_10=N2_9;       O2_10=O2_9;       CO2_10=CO2_9;     H2O_10=H2O_9
CH4_10=CH4_9;     CO_10=CO_9;       H2_10=H2_9;       f_10=f_9

!position11
N2_11=N2_10;      O2_11=O2_10;      CO2_11=CO2_10;    H2O_11=H2O_10
CH4_11=CH4_10;    CO_11=CO_10;      H2_11=H2_10;      f_11=f_10
```

```
!----------------------------TEMPERATURES ----------------------------------------
T1    = 298
T2    = 298
T3    = 298
T4    = 625
T5    = 298
T7    = 1112
T8    = 1200
T9    = 1200

!--T6--
T6 = 800
MMB1=28*N2_6+32*O2_6+44*CO2_6+18*H2O_6+ MMB*f_6+16*CH4_6+28*CO_6+2*H2_6
nom=  1000*mdot6/MMB1
Q=    e*DH/100.

      DO
            Told=T6
            Tmean=0.5*(T6+T7)
      CP_N2 =8.314*(3.28+((0.593/1000)*Tmean)+((0.04*100000)/(Tmean**2)))
      CP_O2 =8.314*(3.639+((0.506/1000)*Tmean)+((-0.227*100000)/(Tmean**2)))
      CP_CO2=8.314*(5.457+((1.045/1000)*Tmean)+((-1.157*100000)/(Tmean**2)))
      CP_H2O=8.314*(3.47+((1.45/1000)*Tmean)+((0.121*100000)/(Tmean**2)))
      CP_fuel=8.314*(As+(Bs*Tmean)+(Cs*(Tmean**2)))
      CP_CH4=8.314*(1.702+((9.081/1000)*Tmean)+((-2.164/1000000)*(Tmean**2)))
      CP_CO =8.314*(3.376+((0.557/1000)*Tmean)+((-0.031*100000)/(Tmean**2)))
      CP_H2 =8.314*(3.249+((0.422/1000)*Tmean)+((0.083*100000)/(Tmean**2)))
      CP_mix=CP_N2*N2_6 + CP_O2*O2_6 + CP_CO2*CO2_6 + CP_H2O*H2O_6 + CP_fuel*f_6 +&
             CP_CH4*CH4_6 + CP_CO*CO_6 + CP_H2*H2_6

      T6=T7 + Q/nom/CP_mix

      IF (ABS(T6-Told).LT.0.1) EXIT

      END DO


!--T10--
MMB1=       28*N2_5+32*O2_5+44*CO2_5+18*H2O_5+MMB*f_5+16*CH4_5+28*CO_5+2*H2_5
nom=        1000*mdot5/MMB1
Tmean =     0.5*(T6+T5)
CP_N2 =     8.314*(3.28+((0.593/1000)*Tmean)+((0.04*100000)/(Tmean**2)))
CP_O2 =     8.314*(3.639+((0.506/1000)*Tmean)+((-0.227*100000)/(Tmean**2)))
CP_CO2=     8.314*(5.457+((1.045/1000)*Tmean)+((-1.157*100000)/(Tmean**2)))
CP_H2O=     8.314*(3.47+((1.45/1000)*Tmean)+((0.121*100000)/(Tmean**2)))
CP_fuel=    8.314*(As+(Bs*Tmean)+(Cs*(Tmean**2)))
CP_CH4=     8.314*(1.702+((9.081/1000)*Tmean)+((-2.164/1000000)*(Tmean**2)))
CP_CO =     8.314*(3.376+((0.557/1000)*Tmean)+((-0.031*100000)/(Tmean**2)))
CP_H2 =     8.314*(3.249+((0.422/1000)*Tmean)+((0.083*100000)/(Tmean**2)))
CP_mix=     CP_N2*N2_5 + CP_O2*O2_5 + CP_CO2*CO2_5 + CP_H2O*H2O_5 + CP_fuel*f_5 +&
            CP_CH4*CH4_5 + CP_CO*CO_5 + CP_H2*H2_5

Q56=  nom*CP_mix*(T6-T5)
```

```
T10 = 800
MMB1 =28*N2_9+2*O2_9+44*CO2_9+18*H2O_9+ MMB*f_9+16*CH4_9+28*CO_9+2*H2_9
nom=  1000*mdot9/MMB1

      DO
            Told=T10
            Tmean=0.5*(T9+T10)
            CP_N2 =8.314*(3.28+((0.593/1000)*Tmean)+((0.04*100000)/(Tmean**2)))
            CP_O2 =8.314*(3.639+((0.506/1000)*Tmean)+((-0.227*100000)/(Tmean**2)))
            CP_CO2=8.314*(5.457+((1.045/1000)*Tmean)+((-1.157*100000)/(Tmean**2)))
            CP_H2O=8.314*(3.47+((1.45/1000)*Tmean)+((0.121*100000)/(Tmean**2)))
            CP_fuel=8.314*(As+(Bs*Tmean)+(Cs*(Tmean**2)))
            CP_CH4=8.314*(1.702+((9.081/1000)*Tmean)+((-2.164/1000000)*(Tmean**2)))
            CP_CO =8.314*(3.376+((0.557/1000)*Tmean)+((-0.031*100000)/(Tmean**2)))
            CP_H2 =8.314*(3.249+((0.422/1000)*Tmean)+((0.083*100000)/(Tmean**2)))
            CP_mix=CP_N2*N2_9+CP_O2*O2_9+CP_CO2*CO2_9+CP_H2O*H2O_9+CP_fuel*f_9+&
                              CP_CH4*CH4_9+CP_CO*CO_9+CP_H2*H2_9

            T10=T9 - Q56/nom/CP_mix

            IF (ABS(T10-Told).LT.0.1) EXIT

      END DO


!--T11--
MMB1= 28*N2_2+32*O2_2+44*CO2_2+18*H2O_2+MMB*f_2+16*CH4_2+28*CO_2+2*H2_2
nom   =     1000*mdot2/MMB1
Tmean =     0.5*(T4+T2)
CP_N2 =     8.314*(3.28+((0.593/1000)*Tmean)+((0.04*100000)/(Tmean**2)))
CP_O2 =     8.314*(3.639+((0.506/1000)*Tmean)+((-0.227*100000)/(Tmean**2)))
CP_CO2=     8.314*(5.457+((1.045/1000)*Tmean)+((-1.157*100000)/(Tmean**2)))
CP_H2O=     8.314*(3.47+((1.45/1000)*Tmean)+((0.121*100000)/(Tmean**2)))
CP_fuel=    8.314*(As+(Bs*Tmean)+(Cs*(Tmean**2)))
CP_CH4=     8.314*(1.702+((9.081/1000)*Tmean)+((-2.164/1000000)*(Tmean**2)))
CP_CO =     8.314*(3.376+((0.557/1000)*Tmean)+((-0.031*100000)/(Tmean**2)))
CP_H2 =     8.314*(3.249+((0.422/1000)*Tmean)+((0.083*100000)/(Tmean**2)))
CP_mix=     CP_N2*N2_2+CP_O2*O2_2+CP_CO2*CO2_2+CP_H2O*H2O_+ CP_fuel*f_2 +&
                  CP_CH4*CH4_2+CP_CO*CO_2+CP_H2*H2_2

Q24=  nom*CP_mix*(T4-T2)

T11 = 800
MMB1 =28*N2_10+32*O2_10+44*CO2_10+18*H2O_10+MMB*f_10+16*CH4_10+28*CO_10+2*H2_10
nom=  1000*mdot10/MMB1

      DO
            Told=T11
            Tmean=0.5*(T11+T10)
            CP_N2 =8.314*(3.28+((0.593/1000)*Tmean)+((0.04*100000)/(Tmean**2)))
            CP_O2 =8.314*(3.639+((0.506/1000)*Tmean)+((-0.227*100000)/(Tmean**2)))
            CP_CO2=8.314*(5.457+((1.045/1000)*Tmean)+((-1.157*100000)/(Tmean**2)))
            CP_H2O=8.314*(3.47+((1.45/1000)*Tmean)+((0.121*100000)/(Tmean**2)))
            CP_fuel=8.314*(As+(Bs*Tmean)+(Cs*(Tmean**2)))
            CP_CH4=8.314*(1.702+((9.081/1000)*Tmean)+((-2.164/1000000)*(Tmean**2)))
```

```
      CP_CO =8.314*(3.376+((0.557/1000)*Tmean)+((-0.031*100000)/(Tmean**2)))
      CP_H2 =8.314*(3.249+((0.422/1000)*Tmean)+((0.083*100000)/(Tmean**2)))
CP_mix=CP_N2*N2_10+CP_O2*O2_10+CP_CO2*CO2_10+CP_H2O*H2O_10+CP_fuel*f_10+&
       CP_CH4*CH4_10+CP_CO*CO_1+ CP_H2*H2_10

      T11=  T10 - Q24/nom/CP_mix

      IF (ABS(T11-Told).LT.0.1) EXIT

END DO


!*****************************  test   ****************************************
!print*,T1,T2,T3,T4,T5,T6,T7,T8,T9,T10,T11
!print*,'------------------';pause
!print*,mdot1,mdot2,mdot3,mdot4,mdot5,mdot6,mdot7,mdot8,mdot9,mdot10,mdot11
!print*,'------------------';pause
!print '(8F8.3)', N2_1,O2_1,CO2_1,H2O_1,f_1,CH4_1,CO_1,H2_1;pause
!print '(8F8.3)', N2_2,O2_2,CO2_2,H2O_2,f_2,CH4_2,CO_2,H2_2;pause
!print '(8F8.3)', N2_3,O2_3,CO2_3,H2O_3,f_3,CH4_3,CO_3,H2_3;pause
!print '(8F8.3)', N2_4,O2_4,CO2_4,H2O_4,f_4,CH4_4,CO_4,H2_4;pause
!print '(8F8.3)', N2_5,O2_5,CO2_5,H2O_5,f_5,CH4_5,CO_5,H2_5;pause
!print '(8F8.3)', N2_6,O2_6,CO2_6,H2O_6,f_6,CH4_6,CO_6,H2_6;pause
!print '(8F8.3)', N2_7,O2_7,CO2_7,H2O_7,f_7,CH4_7,CO_7,H2_7;pause
!print '(8F8.3)', N2_8,O2_8,CO2_8,H2O_8,f_8,CH4_8,CO_8,H2_8;pause
!print '(8F8.3)', N2_9,O2_9,CO2_9,H2O_9,f_9,CH4_9,CO_9,H2_9;pause
!print '(8F8.3)', N2_10,O2_10,CO2_10,H2O_10,f_10,CH4_10,CO_10,H2_10;pause
!print '(8F8.3)', N2_11,O2_11,CO2_11,H2O_11,f_11,CH4_11,CO_11,H2_11


!--------------------------CALCULATION of nrgs and xrgs --------------------

!-- energy@pos1 --
EN1=DHS*mdot1*1000/(28*N2_1+32*O2_1+44*CO2_1+18*H2O_1+MMB*f_1+16*CH4_1+ &
                    28*CO_1+2*H2_1)
ENper1=100.*EN1/EN1

!-- exergy@pos1 --
hmix=       N2_1*1000*(-7.069+24.229*(T1/1000)+(10.521/2)*((T1/1000)**2)      &
                    -(0.18/(T1/1000))-(2.315/3)*((T1/1000)**3))
hmix= hmix +O2_1*1000*(-9.589+29.154*(T1/1000)+(6.477/2)*((T1/1000)**2)       &
                    +0.184/(T1/1000)-(1.017/3)*((T1/1000)**3))
hmix= hmix +CO2_1*1000*(-413.886+51.128*(T1/1000)+(4.368/2)*((T1/1000)**2)    &
                    +1.469/(T1/1000))
hmix= hmix +H2O_1*1000*(-253.871+34.376*(T1/1000)+(7.841/2)*((T1/1000)**2)    &
                    +0.423/(T1/1000))
hmix= hmix +f_1*8.314*(Ah*298*((T1/298)-1)+Bh*298**2*((T1/298)**2-1)          &
                    -Ch*298**3*((T1/298)**3-1))+h0
hmix= hmix +CH4_1*1000*(-81.942+11.933*(T1/1000)+(77.642/2)*((T1/1000)**2)    &
                    -0.142/(T1/1000)-(18.414/3)*((T1/1000)**3))
hmix= hmix +CO_1*1000*(-120.809+30.962*(T1/1000)+(2.439/2)*((T1/1000)**2)     &
                    +0.28/(T1/1000))
hmix= hmix +H2_1*1000*(-7.823+26.882*(T1/1000)+(3.586/2)*((T1/1000)**2)       &
                    -0.105/(T1/1000))
```

```
h00=  N2_1*0
h00=  h00 + O2_1*0
h00=h00 +CO2_1*1000*(-413.886+51.128*0.29815+(4.368/2)*(0.29815**2)+1.469/0.29815)
h00=h00 +H2O_1*1000*(-253.871+34.376*0.29815+(7.841/2)*(0.29815**2)+0.423/0.29815)
h00         =     h00 + f_1*h0
h00=h00 +CH4_1*1000*(-81.942+11.933*0.29815+(77.642/2)*(0.29815**2)-0.142/0.29815&
                  -(18.414/3)*(0.29815**3))
h00=h00 +CO_1*1000*(-120.809+30.962*0.29815+(2.439/2)*(0.29815**2)+0.28/0.29815)
h00=  h00 + H2_1*0


smix= N2_1*((51.539+24.229*LOG(T1) + 10.521*0.29815 - (0.18/2)/(0.29815**2)   &
                  -(2.315/3)*(0.29815**2)) - 8.314*(LOG(1e-13 + N2_1)))
smix= smix +O2_1*((36.116+29.154*LOG(T1) + 6.477*0.29815 + (0.184/2)/(0.29815**2)&
                  -(1.017/3)*(0.29815**2)) - 8.314*(LOG(1e-13 + O2_1)))
smix= smix +CO2_1*((-87.078+51.128*LOG(T1)+4.368*0.29815+(1.469/2)/(0.29815**2))&
                  -8.314*(LOG(1e-13 + CO2_1)))
smix= smix +H2O_1*((-11.75+34.736*LOG(T1)+7.841*0.29815+(0.423/2)/(0.29815**2))&
                  -8.314*(LOG(1e-13 + H2O_1)))
smix  =smix +f_1*(8.314*(As*LOG(T1-298+1)+Bs*(T1-298)+0.5*(Cs*(T1**2-298**2)))+s0)
smix  =smix +CH4_1*((96.731+11.933*LOG(T1)+77.647*0.29815-(0.142/2)/(0.29815**2)&
                  -(18.414/2)*(0.29815**2))-8.314*(LOG(1e-13 + CH4_1)))
smix  =smix +CO_1*((18.937+30.962*LOG(T1)+2.439*0.29815+(0.28/2)/(0.29815**2))&
                  -8.314*(LOG(1e-13 + CO_1)))
smix  =smix +H2_1*((-22.966+26.882*LOG(T1)+3.586*0.29815-(0.105/2)/(0.29815**2))&
                  -8.314*(LOG(1e-13 + H2_1)))

s00 =191.61*N2_1+205.146*O2_1+213.794*CO2_1+188.824*H2O_1+s0*f_1+186.251*CH4_1&
                  +197.648*CO_1+130.679*H2_1

EXPH1 =mdot1/(28*N2_1+32*O2_1+44*CO2_1+18*H2O_1+MMB*f_1+16*CH4_1+28*CO_1+2*H2_1)
EXPH1 =EXPH1*( hmix - h00 -   298*( smix - s00 ) )/1000
EXCH1 =mdot1/(28*N2_1+32*O2_1+44*CO2_1+18*H2O_1+MMB*f_1+16*CH4_1+28*CO_1+2*H2_1)
EXCH1 =EXCH1*(720*N2_1+3970*O2_1+19870*CO2_1+9500*H2O_1+                          &
      SCXRG*f_1+831650*CH4_1+275100*CO_1+236100*H2_1)/1000

EX1=EXPH1 + EXCH1
EXper1=100.*EX1/EX1

!-- energy@pos2 --
EN2   =     0
ENper2=100.*EN2/EN1

!-- exergy@pos2 --
EXPH2 =     0
EXCH2 =     0

EX2=EXPH2 + EXCH2
EXper2=100.*EX2/EX1

!-- energy@pos3 --
EN3   =     0
ENper3=100.*EN3/EN1

!-- exergy@pos3 --
hmix  =N2_3*(1000*(-7.069+24.229*(T3/1000)+(10.521/2)*((T3/1000)**2)          &
```

```
                  -(0.18/(T3/1000))-(2.315/3)*((T3/1000)**3)))
hmix= hmix +O2_3*(1000*(-9.589+29.154*(T3/1000)+(6.477/2)*((T3/1000)**2)      &
                  +0.184/(T3/1000)-(1.017/3)*((T3/1000)**3)))
hmix= hmix +CO2_3*(1000*(-413.886+51.128*(T3/1000)+(4.368/2)*((T3/1000)**2)   &
                  +1.469/(T3/1000)))
hmix= hmix +H2O_3*(1000*(-253.871+34.376*(T3/1000)+(7.841/2)*((T3/1000)**2)   &
                  +0.423/(T3/1000)))
hmix= hmix +f_3*(8.314*(Ah*298*((T3/298)-1)+Bh*298**2*((T3/298)**2-1)         &
                  -Ch*298**3*((T3/298)**3-1))+h0)
hmix= hmix +CH4_3*(1000*(-81.942+11.933*(T3/1000)+(77.642/2)*((T3/1000)**2)   &
                  -0.142/(T3/1000)-(18.414/3)*((T3/1000)**3)))
hmix= hmix +CO_3*(1000*(-120.809+30.962*(T3/1000)+(2.439/2)*((T3/1000)**2)    &
                  +0.28/(T3/1000)))
hmix= hmix +H2_3*(1000*(-7.823+26.882*(T3/1000)+(3.586/2)*((T3/1000)**2)      &
                  -0.105/(T3/1000)))

h00=  N2_3*0
h00=  h00 + O2_3*0
h00=h00+CO2_3*1000*(-413.886+51.128*0.29815+(4.368/2)*(0.29815**2)+1.469/0.29815)
h00=h00+H2O_3*1000*(-253.871+34.376*0.29815+(7.841/2)*(0.29815**2)+0.423/0.29815)
h00=  h00 + f_3*h0
h00=h00+CH4_3*1000*(-81.942+11.933*0.29815+(77.642/2)*(0.29815**2)-0.142/0.29815&
           -(18.414/3)*(0.29815**3))
h00=h00+CO_3*1000*(-120.809+30.962*0.29815+(2.439/2)*(0.29815**2)+0.28/0.29815)
h00=  h00 + H2_3*0

smix= N2_3*((51.539+24.229*LOG(T3) + 10.521*0.29815 - (0.18/2)/(0.29815**2)   &
                              -(2.315/3)*(0.29815**2)) - 8.314*(LOG(1e-13 + N2_3)))
smix= smix+O2_3*((36.116+29.154*LOG(T3) + 6.477*0.29815 + (0.184/2)/(0.29815**2)&
                              -(1.017/3)*(0.29815**2)) - 8.314*(LOG(1e-13 + O2_3)))
smix= smix+CO2_3*((-87.078+51.128*LOG(T3)+4.368*0.29815+(1.469/2)/(0.29815**2))&
                              -8.314*(LOG(1e-13 + CO2_3)))
smix= smix+H2O_3*((-11.75+34.736*LOG(T3)+7.841*(T3/1000)+(0.423/2)/((T3/1000)**2))&
                              -8.314*(LOG(1e-13+H2O_3*1013/1013)))
smix= smix+f_3*(8.314*(As*LOG(T3-298+1)+Bs*(T3-298)+0.5*(Cs*(T3**2-298**2)))+s0)
smix= smix +CH4_3*((96.731+11.933*LOG(T3)+77.647*0.29815-(0.142/2)/(0.29815**2)&
                              -(18.414/2)*(0.29815**2))-8.314*(LOG(1e-13 + CH4_3)))
smix= smix +CO_3*((18.937+30.962*LOG(T3)+2.439*0.29815+(0.28/2)/(0.29815**2)) &
                              -8.314*(LOG(1e-13 + CO_3)))
smix= smix+H2_3*((-22.966+26.882*LOG(T3)+3.586*0.29815-(0.105/2)/(0.29815**2))&
                              -8.314*(LOG(1e-13 + H2_3)))

s00=  191.61*N2_3+205.146*O2_3+213.794*CO2_3+188.824*H2O_3+s0*f_3+186.251*CH4_3&
                              +197.648*CO_3+130.679*H2_3

EXPH3=mdot3/(28*N2_3+32*O2_3+44*CO2_3+18*H2O_3+MMB*f_3+16*CH4_3+28*CO_3+2*H2_3)
EXPH3 =EXPH3*( hmix - h00 -   298*( smix - s00 ) )/1000

EXCH3 =mdot3/(28*N2_3+32*O2_3+44*CO2_3+18*H2O_3+MMB*f_3+16*CH4_3+28*CO_3+2*H2_3)
EXCH3=EXCH3*(720*N2_3+3970*O2_3+19870*CO2_3+9500*H2O_3+SCXRG*f_3  &
           +831650*CH4_3+275100*CO_3+236100*H2_3)/1000

EX3=EXPH3 + EXCH3
EXper3=100.*EX3/EX1
```

```
!-- energy@pos4 --
EN4    =      EN2+Q24
ENper4=100.*EN4/EN1

!-- exergy@pos4 --
hmix= N2_4*(1000*(-7.069+24.229*(T4/1000)+(10.521/2)*((T4/1000)**2)            &
                  -(0.18/(T4/1000))-(2.315/3)*((T4/1000)**3)))
hmix= hmix+O2_4*(1000*(-9.589+29.154*(T4/1000)+(6.477/2)*((T4/1000)**2)        &
                  +0.184/(T4/1000)-(1.017/3)*((T4/1000)**3)))
hmix= hmix +CO2_4*(1000*(-413.886+51.128*(T4/1000)+(4.368/2)*((T4/1000)**2)   &
                  +1.469/(T4/1000)))
hmix= hmix +H2O_4*(1000*(-253.871+34.376*(T4/1000)+(7.841/2)*((T4/1000)**2)   &
                  +0.423/(T4/1000)))
hmix= hmix +f_4*(8.314*(Ah*298*((T4/298)-1)+Bh*298**2*((T4/298)**2-1)          &
                  -Ch*298**3*((T4/298)**3-1))+h0)
hmix= hmix +CH4_4*(1000*(-81.942+11.933*(T4/1000)+(77.642/2)*((T4/1000)**2)   &
                  -0.142/(T4/1000)-(18.414/3)*((T4/1000)**3)))
hmix= hmix +CO_4*(1000*(-120.809+30.962*(T4/1000)+(2.439/2)*((T4/1000)**2)    &
                  +0.28/(T4/1000)))
hmix= hmix +H2_4*(1000*(-7.823+26.882*(T4/1000)+(3.586/2)*((T4/1000)**2)      &
                  -0.105/(T4/1000)))

h00= N2_4*0
h00=  h00 + O2_4*0
h00=h00+CO2_4*1000*(-413.886+51.128*0.29815+(4.368/2)*(0.29815**2)+1.469/0.29815)
h00=h00+H2O_4*1000*(-253.871+34.376*0.29815+(7.841/2)*(0.29815**2)+0.423/0.29815)
h00=  h00 + f_4*h0
h00=h00+CH4_4*1000*(-81.942+11.933*0.29815+(77.642/2)*(0.29815**2)-0.142/0.29815&
                  -(18.414/3)*(0.29815**3))
h00=h00+CO_4*1000*(-120.809+30.962*0.29815+(2.439/2)*(0.29815**2)+0.28/0.29815)
h00=  h00 + H2_4*0

smix= N2_4*((51.539+24.229*LOG(T4)+10.521*(T4/1000) - (0.18/2)/((T4/1000)**2) &
                        -(2.315/3)*((T4/1000)**2)) - 8.314*(LOG(1e-13 + N2_4)))
smix= smix+O2_4*((36.116+29.154*LOG(T4)+6.477*(T4/1000)+(0.184/2)/((T4/1000)**2)&
                        -(1.017/3)*((T4/1000)**2)) - 8.314*(LOG(1e-13 + O2_4)))
smix=smix+CO2_4*((-87.078+51.128*LOG(T4)+4.368*(T4/1000)+(1.469/2)/((T4/1000)**2))&
                        -8.314*(LOG(1e-13 + CO2_4)))
smix=smix+H2O_4*((-11.75+34.736*LOG(T4)+7.841*(T4/1000)+(0.423/2)/((T4/1000)**2))&
                        -8.314*(LOG(1e-13+H2O_4*1013/1013)))
smix=smix+f_4*(8.314*(As*LOG(T4-298+1)+Bs*(T4-298)+0.5*(Cs*(T4**2-298**2)))+s0)
smix=smix+CH4_4*((96.731+11.933*LOG(T4)+77.647*(T4/1000)-(0.142/2)/((T4/1000)**2)&
                        -(18.414/2)*((T4/1000)**2))-8.314*(LOG(1e-13 + CH4_4)))
smix= smix+CO_4*((18.937+30.962*LOG(T4)+2.439*(T4/1000)+(0.28/2)/((T4/1000)**2))&
                        -8.314*(LOG(1e-13 + CO_4)))
smix= smix+H2_4*((-22.966+26.882*LOG(T4)+3.586*(T4/1000)-(0.105/2)/((T4/1000)**2))&
                        -8.314*(LOG(1e-13 + H2_4)))

s00=191.61*N2_4+205.146*O2_4+213.794*CO2_4+188.824*H2O_4+s0*f_4+186.251*CH4_4 &
                  +197.648*CO_4+130.679*H2_4

EXPH4=mdot4/(28*N2_4+32*O2_4+44*CO2_4+18*H2O_4+MMB*f_4+16*CH4_4+28*CO_4+2*H2_4)
EXPH4 =EXPH4*( hmix - h00 -   298*( smix - s00 ) )/1000

EXCH4=mdot4/(28*N2_4+32*O2_4+44*CO2_4+18*H2O_4+MMB*f_4+16*CH4_4+28*CO_4+2*H2_4)
```

```
EXCH4=EXCH4*(720*N2_4+3970*O2_4+19870*CO2_4+9500*H2O_4+SCXRG*f_4          &
           +831650*CH4_4+275100*CO_4+236100*H2_4)/1000
EX4=EXPH4 + EXCH4
EXper4=100.*EX4/EX1

!-- energy@pos5 --
EN5   =     EN1+EN3
ENper5=100.*EN5/EN1

!-- exergy@pos5 --
hmix=       N2_5*(1000*(-7.069+24.229*(T5/1000)+(10.521/2)*((T5/1000)**2)     &
                  -(0.18/(T5/1000))-(2.315/3)*((T5/1000)**3)))
hmix= hmix +O2_5*(1000*(-9.589+29.154*(T5/1000)+(6.477/2)*((T5/1000)**2)      &
                  +0.184/(T5/1000)-(1.017/3)*((T5/1000)**3)))
hmix= hmix +CO2_5*(1000*(-413.886+51.128*(T5/1000)+(4.368/2)*((T5/1000)**2)   &
                  +1.469/(T5/1000)))
hmix= hmix +H2O_5*(1000*(-253.871+34.376*(T5/1000)+(7.841/2)*((T5/1000)**2)   &
                  +0.423/(T5/1000)))
hmix= hmix +f_5*(8.314*(Ah*298*((T5/298)-1)+Bh*298**2*((T5/298)**2-1)         &
                  -Ch*298**3*((T5/298)**3-1))+h0)
hmix= hmix +CH4_5*(1000*(-81.942+11.933*(T5/1000)+(77.642/2)*((T5/1000)**2)   &
                  -0.142/(T5/1000)-(18.414/3)*((T5/1000)**3)))
hmix= hmix +CO_5*(1000*(-120.809+30.962*(T5/1000)+(2.439/2)*((T5/1000)**2)    &
                  +0.28/(T5/1000)))
hmix= hmix +H2_5*(1000*(-7.823+26.882*(T5/1000)+(3.586/2)*((T5/1000)**2)      &
                  -0.105/(T5/1000)))

h00=  N2_5*0
h00=  h00 + O2_5*0
h00=h00+CO2_5*1000*(-413.886+51.128*0.29815+(4.368/2)*(0.29815**2)+1.469/0.29815)
h00=h00+H2O_5*1000*(-253.871+34.376*0.29815+(7.841/2)*(0.29815**2)+0.423/0.29815)
h00=  h00 + f_5*h0
h00=h00+CH4_5*1000*(-81.942+11.933*0.29815+(77.642/2)*(0.29815**2)-0.142/0.29815&
                  -(18.414/3)*(0.29815**3))
h00=h00+CO_5*1000*(-120.809+30.962*0.29815+(2.439/2)*(0.29815**2)+0.28/0.29815)
h00=  h00 + H2_5*0

smix=N2_5*((51.539+24.229*LOG(T5)+10.521*(T5/1000) - (0.18/2)/((T5/1000)**2)  &
                        -(2.315/3)*((T5/1000)**2)) - 8.314*(LOG(1e-13 + N2_5)))
smix=smix+O2_5*((36.116+29.154*LOG(T5)+6.477*(T5/1000)+(0.184/2)/((T5/1000)**2)&
                        -(1.017/3)*((T5/1000)**2)) - 8.314*(LOG(1e-13 + O2_5)))
smix=smix+CO2_5*((-87.078+51.128*LOG(T5)+4.368*(T5/1000)+(1.469/2)/((T5/1000)**2))&
                        -8.314*(LOG(1e-13 + CO2_5)))
smix=smix+H2O_5*((-11.75+34.736*LOG(T5)+7.841*(T5/1000)+(0.423/2)/((T5/1000)**2))&
                        -8.314*(LOG(1e-13+H2O_5*1013/1013)))
smix= smix+f_5*(8.314*(As*LOG(T5-298+1)+Bs*(T5-298)+0.5*(Cs*(T5**2-298**2)))+s0)
smix= smix+CH4_5*((96.731+11.933*LOG(T5)+77.647*(T5/1000)-(0.142/2)/((T5/1000)**2)&
                        -(18.414/2)*((T5/1000)**2))-8.314*(LOG(1e-13 + CH4_5)))
smix= smix+CO_5*((18.937+30.962*LOG(T5)+2.439*(T5/1000)+(0.28/2)/((T5/1000)**2))&
                        -8.314*(LOG(1e-13 + CO_5)))
smix= smix+H2_5*((-22.966+26.882*LOG(T5)+3.586*(T5/1000)-(0.105/2)/((T5/1000)**2))&
                        -8.314*(LOG(1e-13 + H2_5)))

s00=191.61*N2_5+205.146*O2_5+213.794*CO2_5+188.824*H2O_5+s0*f_5+186.251*CH4_5 &
                  +197.648*CO_5+130.679*H2_5
```

```
EXPH5=mdot5/(28*N2_5+32*O2_5+44*CO2_5+18*H2O_5+MMB*f_5+16*CH4_5+28*CO_5+2*H2_5)
EXPH5=EXPH5*( hmix - h00 -    298*( smix - s00 ) )/1000

EXCH5=mdot5/(28*N2_5+32*O2_5+44*CO2_5+18*H2O_5+MMB*f_5+16*CH4_5+28*CO_5+2*H2_5)
EXCH5=EXCH5*(720*N2_5+3970*O2_5+19870*CO2_5+9500*H2O_5+SCXRG*f_5        &
           +831650*CH4_5+275100*CO_5+236100*H2_5)/1000
EX5=EXPH5 + EXCH5
EXper5=100.*EX5/EX1

!-- energy@pos6 --
EN6=EN5+Q56
ENper6=100.*EN6/EN1

!-- exergy@pos6 --
hmix  = N2_6*(1000*(-7.069+24.229*(T6/1000)+(10.521/2)*((T6/1000)**2)          &
                  -(0.18/(T6/1000))-(2.315/3)*((T6/1000)**3)))
hmix  =hmix+O2_6*(1000*(-9.589+29.154*(T6/1000)+(6.477/2)*((T6/1000)**2)       &
                  +0.184/(T6/1000)-(1.017/3)*((T6/1000)**3)))
hmix  =hmix+CO2_6*(1000*(-413.886+51.128*(T6/1000)+(4.368/2)*((T6/1000)**2)    &
                  +1.469/(T6/1000)))
hmix  =hmix +H2O_6*(1000*(-253.871+34.376*(T6/1000)+(7.841/2)*((T6/1000)**2)   &
                  +0.423/(T6/1000)))
hmix  =hmix +f_6*(8.314*(Ah*298*((T6/298)-1)+Bh*298**2*((T6/298)**2-1)         &
                  -Ch*298**3*((T6/298)**3-1))+h0)
hmix  =hmix +CH4_6*(1000*(-81.942+11.933*(T6/1000)+(77.642/2)*((T6/1000)**2)   &
                  -0.142/(T6/1000)-(18.414/3)*((T6/1000)**3)))
hmix  =hmix +CO_6*(1000*(-120.809+30.962*(T6/1000)+(2.439/2)*((T6/1000)**2)    &
                  +0.28/(T6/1000)))
hmix  =hmix +H2_6*(1000*(-7.823+26.882*(T6/1000)+(3.586/2)*((T6/1000)**2)      &
                  -0.105/(T6/1000)))

h00=  N2_6*0
h00=  h00 + O2_6*0
h00=h00+CO2_6*1000*(-413.886+51.128*0.29815+(4.368/2)*(0.29815**2)+1.469/0.29815)
h00=h00+H2O_6*1000*(-253.871+34.376*0.29815+(7.841/2)*(0.29815**2)+0.423/0.29815)
h00=  h00 + f_6*h0
h00h00+CH4_6*1000*(-81.942+11.933*0.29815+(77.642/2)*(0.29815**2)-0.142/0.29815&
                  -(18.414/3)*(0.29815**3))
h00=h00+CO_6*1000*(-120.809+30.962*0.29815+(2.439/2)*(0.29815**2)+0.28/0.29815)
h00=  h00 + H2_6*0

smix=N2_6*((51.539+24.229*LOG(T6)+10.521*(T6/1000) - (0.18/2)/((T6/1000)**2)  &
                        -(2.315/3)*((T6/1000)**2)) - 8.314*(LOG(1e-13 + N2_6)))
smix=smix+O2_6*((36.116+29.154*LOG(T6)+6.477*(T6/1000)+(0.184/2)/((T6/1000)**2)&
                        -(1.017/3)*((T6/1000)**2)) - 8.314*(LOG(1e-13 + O2_6)))
smix=smix+CO2_6*((-87.078+51.128*LOG(T6)+4.368*(T6/1000)+(1.469/2)/((T6/1000)**2))&
                        -8.314*(LOG(1e-13 + CO2_6)))
smix=smix+H2O_6*((-11.75+34.736*LOG(T6)+7.841*(T6/1000)+(0.423/2)/((T6/1000)**2))&
                        -8.314*(LOG(1e-13+H2O_6*1013/1013)))
smix=smix+f_6*(8.314*(As*LOG(T6-298+1)+Bs*(T6-298)+0.5*(Cs*(T6**2-298**2)))+s0)
smix=smix+CH4_6*((96.731+11.933*LOG(T6)+77.647*(T6/1000)-(0.142/2)/((T6/1000)**2)&
                        -(18.414/2)*((T6/1000)**2))-8.314*(LOG(1e-13 + CH4_6)))
smix= smix+CO_6*((18.937+30.962*LOG(T6)+2.439*(T6/1000)+(0.28/2)/((T6/1000)**2))&
                        -8.314*(LOG(1e-13 + CO_6)))
smix=smix+H2_6*((-22.966+26.882*LOG(T6)+3.586*(T6/1000)-(0.105/2)/((T6/1000)**2))&
                        -8.314*(LOG(1e-13 + H2_6)))
```

```
s00=191.61*N2_6+205.146*O2_6+213.794*CO2_6+188.824*H2O_6+s0*f_6+186.251*CH4_6 &
                +197.648*CO_6+130.679*H2_6

EXPH6=mdot6/(28*N2_6+32*O2_6+44*CO2_6+18*H2O_6+MMB*f_6+16*CH4_6+28*CO_6+2*H2_6)
EXPH= EXPH6*( hmix - h00 -    298*( smix - s00 ) )/1000

EXCH6=mdot6/(28*N2_6+32*O2_6+44*CO2_6+18*H2O_6+MMB*f_6+16*CH4_6+28*CO_6+2*H2_6)
EXCH6=EXCH6*(720*N2_6+3970*O2_6+19870*CO2_6+9500*H2O_6+SCXRG*f_6        &
                +831650*CH4_6+275100*CO_6+236100*H2_6)/1000
EX6=EXPH6 + EXCH6
EXper6=100.*EX6/EX1


!-- energy@pos7 --
QABR=f_6*mdot6*10*DH*e/(28*N2_6+32*O2_6+44*CO2_6+18*H2O_6         &
                        +MMB*f_6+16*CH4_6+28*CO_6+2*H2_6)
XQABR=100*QABR*(1-(298/T8))/(EX1*1000000)
EN7   =     EN6+QABR
ENper7=100.*EN7/EN1

!-- exergy@pos7 --
hmix= N2_7*(1000*(-7.069+24.229*(T7/1000)+(10.521/2)*((T7/1000)**2)           &
                -(0.18/(T7/1000))-(2.315/3)*((T7/1000)**3)))
hmix= hmix+O2_7*(1000*(-9.589+29.154*(T7/1000)+(6.477/2)*((T7/1000)**2)       &
                +0.184/(T7/1000)-(1.017/3)*((T7/1000)**3)))
hmix= hmix+CO2_7*(1000*(-413.886+51.128*(T7/1000)+(4.368/2)*((T7/1000)**2)    &
                +1.469/(T7/1000)))
hmix= hmix+H2O_7*(1000*(-253.871+34.376*(T7/1000)+(7.841/2)*((T7/1000)**2)    &
                +0.423/(T7/1000)))
hmix= hmix+f_7*(8.314*(Ah*298*((T7/298)-1)+Bh*298**2*((T7/298)**2-1)           &
                -Ch*298**3*((T7/298)**3-1))+h0)
hmix= hmix+CH4_7*(1000*(-81.942+11.933*(T7/1000)+(77.642/2)*((T7/1000)**2)    &
                -0.142/(T7/1000)-(18.414/3)*((T7/1000)**3)))
hmix= hmix+CO_7*(1000*(-120.809+30.962*(T7/1000)+(2.439/2)*((T7/1000)**2)     &
                +0.28/(T7/1000)))
hmix= hmix+H2_7*(1000*(-7.823+26.882*(T7/1000)+(3.586/2)*((T7/1000)**2)       &
                -0.105/(T7/1000)))

h00=  N2_7*0
h00=  h00 + O2_7*0
h00=h00+CO2_7*1000*(-413.886+51.128*0.29815+(4.368/2)*(0.29815**2)+1.469/0.29815)
h00=h00+H2O_7*1000*(-253.871+34.376*0.29815+(7.841/2)*(0.29815**2)+0.423/0.29815)
h00=  h00 + f_7*h0
h00=h00+CH4_7*1000*(-81.942+11.933*0.29815+(77.642/2)*(0.29815**2)-0.142/0.29815&
                -(18.414/3)*(0.29815**3))
h00=h00+CO_7*1000*(-120.809+30.962*0.29815+(2.439/2)*(0.29815**2)+0.28/0.29815)
h00=  h00 + H2_7*0

smix= N2_7*((51.539+24.229*LOG(T7)+10.521*(T7/1000)-(0.18/2)/((T7/1000)**2)   &
                        -(2.315/3)*((T7/1000)**2)) - 8.314*(LOG(1e-13 + N2_7)))
smix= smix+O2_7*((36.116+29.154*LOG(T7)+6.477*(T7/1000)+(0.184/2)/((T7/1000)**2)&
                        -(1.017/3)*((T7/1000)**2)) - 8.314*(LOG(1e-13 + O2_7)))
smix=smix+CO2_7*((-87.078+51.128*LOG(T7)+4.368*(T7/1000)+(1.469/2)/((T7/1000)**2))&
                        -8.314*(LOG(1e-13 + CO2_7)))
smix=smix+H2O_7*((-11.75+34.736*LOG(T7)+7.841*(T7/1000)+(0.423/2)/((T7/1000)**2))&
```

```
                        -8.314*(LOG(1e-13+H2O_7*1013/1013)))
smix= smix+f_7*(8.314*(As*LOG(T7-298+1)+Bs*(T7-298)+0.5*(Cs*(T7**2-298**2)))+s0)
smix=smix +CH4_7*((96.731+11.933*LOG(T7)+77.647*(T7/1000)-(0.142/2)/((T7/1000)**2)&
                        -(18.414/2)*((T7/1000)**2))-8.314*(LOG(1e-13 + CH4_7)))
smix= smix+CO_7*((18.937+30.962*LOG(T7)+2.439*(T7/1000)+(0.28/2)/((T7/1000)**2))&
                        -8.314*(LOG(1e-13 + CO_7)))
smix= smix+H2_7*((-22.966+26.882*LOG(T7)+3.586*(T7/1000)-(0.105/2)/((T7/1000)**2))&
                        -8.314*(LOG(1e-13 + H2_7)))

s00=191.61*N2_7+205.146*O2_7+213.794*CO2_7+188.824*H2O_7+s0*f_7+186.251*CH4_7 &
                  + 197.648*CO_7 + 130.679*H2_7

EXPH7=mdot7/(28*N2_7+32*O2_7+44*CO2_7+18*H2O_7+MMB*f_7+16*CH4_7+28*CO_7+2*H2_7)
EXPH7=EXPH7*( hmix - h00 -    298*( smix - s00 ) )/1000

EXCH7=mdot7/(28*N2_7+32*O2_7+44*CO2_7+18*H2O_7+MMB*f_7+16*CH4_7+28*CO_7+2*H2_7)
EXCH7=EXCH7*(720*N2_7+3970*O2_7+19870*CO2_7+9500*H2O_7+SCXRG*f_7        &
            +831650*CH4_7+275100*CO_7+236100*H2_7)/1000
EX7=EXPH7 + EXCH7
EXper7=100.*EX7/EX1

!-- energy@pos8 --
QAB=nofa*DHS+noH2a*241818
QABV=mdot3*2442310
QABE=QAB-QABV-QABR
XQABV=100*QABV*(1-(298/T8))/(EX1*1000000)-EXper3
XQABE=100*QABE*(1-(298/T8))/(EX1*1000000)

CHen=H2_7*mdot7*10*241818*Uf
CHen=CHen/(28*N2_7+32*O2_7+44*CO2_7+18*H2O_7+MMB*f_7+16*CH4_7+28*CO_7+2*H2_7)


MMB1=28*N2_8+32*O2_8+44*CO2_8+18*H2O_8+MMB*f_8+16*CH4_8+28*CO_8+2*H2_8
nom    =      1000*mdot8/MMB1
Tmean  =      0.5*(T8+0.5*(T4+T7))
CP_N2  =      8.314*(3.28+((0.593/1000)*Tmean)+((0.04*100000)/(Tmean**2)))
CP_O2  =      8.314*(3.639+((0.506/1000)*Tmean)+((-0.227*100000)/(Tmean**2)))
CP_CO2=       8.314*(5.457+((1.045/1000)*Tmean)+((-1.157*100000)/(Tmean**2)))
CP_H2O=       8.314*(3.47+((1.45/1000)*Tmean)+((0.121*100000)/(Tmean**2)))
CP_fuel=      8.314*(As+(Bs*Tmean)+(Cs*(Tmean**2)))
CP_CH4=       8.314*(1.702+((9.081/1000)*Tmean)+((-2.164/1000000)*(Tmean**2)))
CP_CO  =      8.314*(3.376+((0.557/1000)*Tmean)+((-0.031*100000)/(Tmean**2)))
CP_H2  =      8.314*(3.249+((0.422/1000)*Tmean)+((0.083*100000)/(Tmean**2)))
CP_mix=       CP_N2*N2_8+CP_O2*O2_8+CP_CO2*CO2_8+CP_H2O*H2O_8+CP_fuel*f_8+      &
                              CP_CH4*CH4_8+CP_CO*CO_8+CP_H2*H2_8

Qen=  nom*CP_mix*(T8-0.5*(T4+T7))

J36=228572./(8.314*298)
K36=-241818/8.314+1.5985*298-(0.00078/2)*298**2+15150/298
L36=J36+K36/298+1.5985*LOG(298.)-(0.00078/2)*298-15150/(2*298**2)

lnk=-K36/Tmean-1.5985*LOG(Tmean)+(0.00078/2)*Tmean+15150/(2*Tmean**2)+L36

Wel=RC_H2*E*Uf*1000*mdot1/10000.
Wel=Wel/(28*N2_1+32*O2_1+44*CO2_1+18*H2O_1+MMB*f_1+16*CH4_1+28*CO_1+2*H2_1)
```

```
Wel=Wel*(8.314*Tmean*lnk)

nI = 100.*Wel/EN1
nII= 100.*Wel/EX1/1000000

EN8=EN4+EN7-Wel
ENper8=100.*EN8/EN1

!-- exergy@pos8 --
hmix= N2_8*(1000*(-7.069+24.229*(T8/1000)+(10.521/2)*((T8/1000)**2)     &
                              -(0.18/(T8/1000))-(2.315/3)*((T8/1000)**3)))
hmix= hmix +O2_8*(1000*(-9.589+29.154*(T8/1000)+(6.477/2)*((T8/1000)**2)      &
                              +0.184/(T8/1000)-(1.017/3)*((T8/1000)**3)))
hmix= hmix +CO2_8*(1000*(-413.886+51.128*(T8/1000)+(4.368/2)*((T8/1000)**2)   &
                              +1.469/(T8/1000)))
hmix  =hmix +H2O_8*(1000*(-253.871+34.376*(T8/1000)+(7.841/2)*((T8/1000)**2)  &
                              +0.423/(T8/1000)))
hmix  =hmix +f_8*(8.314*(Ah*298*((T8/298)-1)+Bh*298**2*((T8/298)**2-1)        &
                              -Ch*298**3*((T8/298)**3-1))+h0)
hmix  =hmix +CH4_8*(1000*(-81.942+11.933*(T8/1000)+(77.642/2)*((T8/1000)**2)  &
                              -0.142/(T8/1000)-(18.414/3)*((T8/1000)**3)))
hmix  =hmix +CO_8*(1000*(-120.809+30.962*(T8/1000)+(2.439/2)*((T8/1000)**2)   &
                              +0.28/(T8/1000)))
hmix  =hmix +H2_8*(1000*(-7.823+26.882*(T8/1000)+(3.586/2)*((T8/1000)**2)     &
                              -0.105/(T8/1000)))


h00=  N2_8*0
h00=  h00 + O2_8*0
h00=  h00+CO2_8*1000*(-413.886+51.128*0.29815+(4.368/2)*(0.29815**2)+1.469/0.29815)
h00=  h00+H2O_8*1000*(-253.871+34.376*0.29815+(7.841/2)*(0.29815**2)+0.423/0.29815)
h00=  h00+f_8*h0
h00=h00+CH4_8*1000*(-81.942+11.933*0.29815+(77.642/2)*(0.29815**2)-0.142/0.29815&
                              -(18.414/3)*(0.29815**3))
h00=  h00+CO_8*1000*(-120.809+30.962*0.29815+(2.439/2)*(0.29815**2)+0.28/0.29815)
h00=  h00 + H2_8*0

smix= N2_8*((51.539+24.229*LOG(T8)+10.521*(T8/1000)-(0.18/2)/((T8/1000)**2)   &
                           -(2.315/3)*((T8/1000)**2)) - 8.314*(LOG(1e-13 + N2_8)))
smix= smix+O2_8*((36.116+29.154*LOG(T8)+6.477*(T8/1000)+(0.184/2)/((T8/1000)**2)&
                           -(1.017/3)*((T8/1000)**2)) - 8.314*(LOG(1e-13 + O2_8)))
smix=smix+CO2_8*((-87.078+51.128*LOG(T8)+4.368*(T8/1000)+(1.469/2)/((T8/1000)**2))&
                           -8.314*(LOG(1e-13 + CO2_8)))
smix= smix+H2O_8*((-11.75+34.736*LOG(T8)+7.841*(T8/1000)+(0.423/2)/((T8/1000)**2))&
                           -8.314*(LOG(1e-13+H2O_8*1013/1013)))
smix= smix+f_8*(8.314*(As*LOG(T8-298+1)+Bs*(T8-298)+0.5*(Cs*(T8**2-298**2)))+s0)
smix= smix+CH4_8*((96.731+11.933*LOG(T8)+77.647*(T8/1000)-(0.142/2)/((T8/1000)**2)&
                           -(18.414/2)*((T8/1000)**2))-8.314*(LOG(1e-13 + CH4_8)))
smix= smix+CO_8*((18.937+30.962*LOG(T8)+2.439*(T8/1000)+(0.28/2)/((T8/1000)**2))&
                           -8.314*(LOG(1e-13 + CO_8)))
smix= smix+H2_8*((-22.966+26.882*LOG(T8)+3.586*(T8/1000)-(0.105/2)/((T8/1000)**2))&
                           -8.314*(LOG(1e-13 + H2_8)))

s00   =191.61*N2_8+205.146*O2_8+213.794*CO2_8+188.824*H2O_8+s0*f_8+186.251*CH4_8&
                + 197.648*CO_8 + 130.679*H2_8
```

```
EXPH8=mdot8/(28*N2_8+32*O2_8+44*CO2_8+18*H2O_8+MMB*f_8+16*CH4_8+28*CO_8+2*H2_8)
EXPH8=EXPH8*( hmix - h00 -    298*( smix - s00 ) )/1000

EXCH8=mdot8/(28*N2_8+32*O2_8+44*CO2_8+18*H2O_8+MMB*f_8+16*CH4_8+28*CO_8+2*H2_8)
EXCH8=EXCH8*(720*N2_8+3970*O2_8+19870*CO2_8+9500*H2O_8+SCXRG*f_8  &
           +831650*CH4_8+275100*CO_8+236100*H2_8)/1000
EX8=EXPH8 + EXCH8
EXper8=100.*EX8/EX1

!-- energy@pos9 --
EN9   =EN8-QABR-QABE-QABV
ENper9=100.*EN9/EN1

!-- exergy@pos9 --
hmix= N2_9*(1000*(-7.069+24.229*(T9/1000)+(10.521/2)*((T9/1000)**2)           &
                  -(0.18/(T9/1000))-(2.315/3)*((T9/1000)**3)))
hmix= hmix+O2_9*(1000*(-9.589+29.154*(T9/1000)+(6.477/2)*((T9/1000)**2)       &
                  +0.184/(T9/1000)-(1.017/3)*((T9/1000)**3)))
hmix= hmix+CO2_9*(1000*(-413.886+51.128*(T9/1000)+(4.368/2)*((T9/1000)**2)    &
                  +1.469/(T9/1000)))
hmix= hmix+H2O_9*(1000*(-253.871+34.376*(T9/1000)+(7.841/2)*((T9/1000)**2)    &
                  +0.423/(T9/1000)))
hmix= hmix+f_9*(8.314*(Ah*298*((T9/298)-1)+Bh*298**2*((T9/298)**2-1)          &
                  -Ch*298**3*((T9/298)**3-1))+h0)
hmix= hmix+CH4_9*(1000*(-81.942+11.933*(T9/1000)+(77.642/2)*((T9/1000)**2)    &
                  -0.142/(T9/1000)-(18.414/3)*((T9/1000)**3)))
hmix= hmix+CO_9*(1000*(-120.809+30.962*(T9/1000)+(2.439/2)*((T9/1000)**2)     &
                  +0.28/(T9/1000)))
hmix= hmix+H2_9*(1000*(-7.823+26.882*(T9/1000)+(3.586/2)*((T9/1000)**2)       &
                  -0.105/(T9/1000)))

h00=  N2_9*0
h00=  h00 + O2_9*0
h00=  h00+CO2_9*1000*(-413.886+51.128*0.29815+(4.368/2)*(0.29815**2)+1.469/0.29815)
h00=  h00+H2O_9*1000*(-253.871+34.376*0.29815+(7.841/2)*(0.29815**2)+0.423/0.29815)
h00=  h00 + f_9*h0
h00=  h00+CH4_9*1000*(-81.942+11.933*0.29815+(77.642/2)*(0.29815**2)-0.142/0.29815&
                  -(18.414/3)*(0.29815**3))
h00=  h00+CO_9*1000*(-120.809+30.962*0.29815+(2.439/2)*(0.29815**2)+0.28/0.29815)
h00=  h00 + H2_9*0

smix= N2_9*((51.539+24.229*LOG(T9)+10.521*(T9/1000)-(0.18/2)/((T9/1000)**2)   &
                        -(2.315/3)*((T9/1000)**2)) - 8.314*(LOG(1e-13 + N2_9)))
smix= smix+O2_9*((36.116+29.154*LOG(T9)+6.477*(T9/1000)+(0.184/2)/((T9/1000)**2)&
                        -(1.017/3)*((T9/1000)**2)) - 8.314*(LOG(1e-13 + O2_9)))
smix=smix+CO2_9*((-87.078+51.128*LOG(T9)+4.368*(T9/1000)+(1.469/2)/((T9/1000)**2))&
                        -8.314*(LOG(1e-13 + CO2_9)))
smix= smix+H2O_9*((-11.75+34.736*LOG(T9)+7.841*(T9/1000)+(0.423/2)/((T9/1000)**2))&
                        -8.314*(LOG(1e-13+H2O_9*1013/1013)))
smix= smix+f_9*(8.314*(As*LOG(T9-298+1)+Bs*(T9-298)+0.5*(Cs*(T9**2-298**2)))+s0)
smix= smix+CH4_9*((96.731+11.933*LOG(T9)+77.647*(T9/1000)-(0.142/2)/((T9/1000)**2)&
                        -(18.414/2)*((T9/1000)**2))-8.314*(LOG(1e-13 + CH4_9)))
smix= smix+CO_9*((18.937+30.962*LOG(T9)+2.439*(T9/1000)+(0.28/2)/((T9/1000)**2))&
                        -8.314*(LOG(1e-13 + CO_9)))
smix= smix+H2_9*((-22.966+26.882*LOG(T9)+3.586*(T9/1000)-(0.105/2)/((T9/1000)**2))&
                        -8.314*(LOG(1e-13 + H2_9)))
```

```
s00=  191.61*N2_9+205.146*O2_9+213.794*CO2_9+188.824*H2O_9+s0*f_9+ 86.251*CH4_9&
                +197.648*CO_9+130.679*H2_9

EXPH9=mdot9/(28*N2_9+32*O2_9+44*CO2_9+18*H2O_9+MMB*f_9+16*CH4_9+28*CO_9+2*H2_9)
EXPH9=EXPH9*( hmix - h00 -    298*( smix - s00 ) )/1000

EXCH9=mdot9/(28*N2_9+32*O2_9+44*CO2_9+18*H2O_9+MMB*f_9+16*CH4_9+28*CO_9+2*H2_9)
EXCH9=EXCH9*(720*N2_9+3970*O2_9+19870*CO2_9+9500*H2O_9+SCXRG*f_9        &
           +831650*CH4_9+275100*CO_9+236100*H2_9)/1000
EX9=EXPH9 + EXCH9
EXper9=100.*EX9/EX1

!-- energy@pos10 --
EN10  =     EN9-Q56
ENper10=100.*EN10/EN1

!-- exergy@pos10 --
hmix= N2_10*(1000*(-7.069+24.229*(T10/1000)+(10.521/2)*((T10/1000)**2)        &
                -(0.18/(T10/1000))-(2.315/3)*((T10/1000)**3)))
hmix= hmix+O2_10*(1000*(-9.589+29.154*(T10/1000)+(6.477/2)*((T10/1000)**2)    &
                +0.184/(T10/1000)-(1.017/3)*((T10/1000)**3)))
hmix= hmix+CO2_10*(1000*(-413.886+51.128*(T10/1000)+(4.368/2)*((T10/1000)**2) &
                +1.469/(T10/1000)))
hmix= hmix+H2O_10*(1000*(-253.871+34.376*(T10/1000)+(7.841/2)*((T10/1000)**2) &
                +0.423/(T10/1000)))
hmix= hmix+f_10*(8.314*(Ah*298*((T10/298)-1)+Bh*298**2*((T10/298)**2-1)        &
                -Ch*298**3*((T10/298)**3-1))+h0)
hmix= hmix+CH4_10*(1000*(-81.942+11.933*(T10/1000)+(77.642/2)*((T10/1000)**2) &
                -0.142/(T10/1000)-(18.414/3)*((T10/1000)**3)))
hmix= hmix+CO_10*(1000*(-120.809+30.962*(T10/1000)+(2.439/2)*((T10/1000)**2)  &
                +0.28/(T10/1000)))
hmix= hmix+H2_10*(1000*(-7.823+26.882*(T10/1000)+(3.586/2)*((T10/1000)**2)    &
                -0.105/(T10/1000)))

h00=  N2_10*0
h00=  h00 + O2_10*0
h00=h00+CO2_10*1000*(-413.886+51.128*0.29815+(4.368/2)*(0.29815**2)+1.469/0.29815)
h00=h00+H2O_10*1000*(-253.871+34.376*0.29815+(7.841/2)*(0.29815**2)+0.423/0.29815)
h00=  h00 + f_10*h0
h00=h00+CH4_10*1000*(-81.942+11.933*0.29815+(77.642/2)*(0.29815**2)-0.142/0.29815&
                -(18.414/3)*(0.29815**3))
h00=h00+CO_10*1000*(-120.809+30.962*0.29815+(2.439/2)*(0.29815**2)+0.28/0.29815)
h00=  h00 + H2_10*0

smix= N2_10*((51.539+24.229*LOG(T10)+10.521*(T10/1000)-(0.18/2)/((T10/1000)**2)&
                        -(2.315/3)*((T10/1000)**2)) - 8.314*(LOG(1e-13 + N2_10)))
smix= smix+O2_10*((36.116+29.154*LOG(T10)+6.477*(T10/1000)&
+(0.184/2)/((T10/1000)**2)-(1.017/3)*((T10/1000)**2))-8.314*(LOG(1e-13+ O2_10)))

smix=smix+CO2_10*((-87.078+51.128*LOG(T10)+4.368*(T10/1000)&
                        +(1.469/2)/((T10/1000)**2))-8.314*(LOG(1e-13 + CO2_10)))
smix= smix+H2O_10*((-11.75+34.736*LOG(T10)+7.841*(T10/1000)&
                +(0.423/2)/((T10/1000)**2))-8.314*(LOG(1e-13+H2O_10*1013/1013)))
smix=smix+f_10*(8.314*(As*LOG(T10-298+1)+Bs*(T10-298)+0.5*(Cs*(T10**2-298**2)))+s0)
smix= smix+CH4_10*((96.731+11.933*LOG(T10)+77.647*(T10/1000)             &
```

```
            -(0.142/2)/((T10/1000)**2)                                    &
            -(18.414/2)*((T10/1000)**2))-8.314*(LOG(1e-13 + CH4_10)))
smix= smix+ CO_10*((18.937+30.962*LOG(T10)+2.439*(T10/1000)               &
            +(0.28/2)/((T10/1000)**2))-8.314*(LOG(1e-13 + CO_10)))
smix= smix+H2_10*((-22.966+26.882*LOG(T10)                                &
      +3.586*(T10/1000)-(0.105/2)/((T10/1000)**2))-8.314*(LOG(1e-13 + H2_10)))

s00=191.61*N2_10+205.146*O2_10+213.794*CO2_10+188.824*H2O_10              &
            +s0*f_10+186.251*CH4_10+ 197.648*CO_10 + 130.679*H2_10

EXPH10=mdot10/(28*N2_10+32*O2_10+44*CO2_10+18*H2O_10+MMB*f_10+16*CH4_10 &
            +28*CO_10+2*H2_10)
EXPH10=     EXPH10*( hmix - h00 -   298*( smix - s00 ) )/1000

EXCH10=mdot10/(28*N2_10+32*O2_10+44*CO2_10+18*H2O_10+MMB*f_10+16*CH4_10 &
            +28*CO_10+2*H2_10)
EXCH10=EXCH10*(720*N2_10+3970*O2_10+19870*CO2_10+9500*H2O_10+SCXRG*f_10 &
            +831650*CH4_10+275100*CO_10+236100*H2_10)/1000
EX10=EXPH10 + EXCH10
EXper10=100.*EX10/EX1

!-- energy@pos11 --
EN11  =     EN10-Q24
ENper11=100.*EN11/EN1

!-- exergy@pos11 --
hmix= N2_11*(1000*(-7.069+24.229*(T11/1000)+(10.521/2)*((T11/1000)**2)        &
                  -(0.18/(T11/1000))-(2.315/3)*((T11/1000)**3)))
hmix= hmix+O2_11*(1000*(-9.589+29.154*(T11/1000)+(6.477/2)*((T11/1000)**2)    &
                  +0.184/(T11/1000)-(1.017/3)*((T11/1000)**3)))
hmix= hmix+CO2_11*(1000*(-413.886+51.128*(T11/1000)+(4.368/2)*((T11/1000)**2) &
                  +1.469/(T11/1000)))
hmix= hmix+H2O_11*(1000*(-253.871+34.376*(T11/1000)+(7.841/2)*((T11/1000)**2) &
                  +0.423/(T11/1000)))
hmix= hmix+f_11*(8.314*(Ah*298*((T11/298)-1)+Bh*298**2*((T11/298)**2-1)        &
                  -Ch*298**3*((T11/298)**3-1))+h0)
hmix= hmix+CH4_11*(1000*(-81.942+11.933*(T11/1000)+(77.642/2)*((T11/1000)**2) &
                  -0.142/(T11/1000)-(18.414/3)*((T11/1000)**3)))
hmix= hmix+CO_11*(1000*(-120.809+30.962*(T11/1000)+(2.439/2)*((T11/1000)**2)  &
                  +0.28/(T11/1000)))
hmix= hmix+H2_11*(1000*(-7.823+26.882*(T11/1000)+(3.586/2)*((T11/1000)**2)    &
                  -0.105/(T11/1000)))

h00=  N2_11*0
h00=  h00 + O2_11*0
h00=  h00 + CO2_11*1000*(-
413.886+51.128*0.29815+(4.368/2)*(0.29815**2)+1.469/0.29815)
h00=h00+H2O_11*1000*(-253.871+34.376*0.29815+(7.841/2)*(0.29815**2)+0.423/0.29815)
h00=  h00 + f_11*h0
h00=h00+CH4_11*1000*(-81.942+11.933*0.29815+(77.642/2)*(0.29815**2)-0.142/0.29815&
                  -(18.414/3)*(0.29815**3))
h00=h00+CO_11*1000*(-120.809+30.962*0.29815+(2.439/2)*(0.29815**2)+0.28/0.29815)
h00=  h00 + H2_11*0


smix= N2_11*((51.539+24.229*LOG(T11)+10.521*(T11/1000)-(0.18/2)/((T11/1000)**2)&
```

```
                        -(2.315/3)*((T11/1000)**2)) - 8.314*(LOG(1e-13 + N2_11)))
smix= smix+O2_11*((36.116+29.154*LOG(T11)+6.477*(T11/1000)  &
+(0.184/2)/((T11/1000)**2)-(1.017/3)*((T11/1000)**2)) - 8.314*(LOG(1e-13 + O2_11)))

smix=smix+CO2_11*((-87.078+51.128*LOG(T11)+4.368*(T11/1000) &
                        +(1.469/2)/((T11/1000)**2))-8.314*(LOG(1e-13 + CO2_11)))
smix= smix+H2O_11*((-11.75+34.736*LOG(T11)+7.841*(T11/1000) &
                  +(0.423/2)/((T11/1000)**2))-8.314*(LOG(1e-13+H2O_11*1013/1013)))
smix=smix+f_11*(8.314*(As*LOG(T11-298+1)+Bs*(T11-298)+0.5*(Cs*(T11**2-298**2)))+s0)
smix=smix+CH4_11*((96.731+11.933*LOG(T11)+77.647*(T11/1000) &
-(0.142/2)/((T11/1000)**2)-(18.414/2)*((T11/1000)**2))-8.314*(LOG(1e-13 + CH4_11)))

smix=smix+CO_11*((18.937+30.962*LOG(T11)+2.439*(T11/1000)   &
                  +(0.28/2)/((T11/1000)**2))-8.314*(LOG(1e-13 + CO_11)))
smix=smix+H2_11*((-22.966+26.882*LOG(T11)+3.586*(T11/1000)  &
                  -(0.105/2)/((T11/1000)**2))-8.314*(LOG(1e-13 + H2_11)))

s00=191.61*N2_11+205.146*O2_11+213.794*CO2_11+188.824*H2O_11+s0*f_11    &
          +186.251*CH4_11+ 197.648*CO_11 + 130.679*H2_11

EXPH11=mdot11/(28*N2_11+32*O2_11+44*CO2_11+18*H2O_11        &
                        +MMB*f_11+16*CH4_11+28*CO_11+2*H2_11)
EXPH11=EXPH11*( hmix - h00 -  298*( smix - s00 ) )/1000

EXCH11=mdot11/(28*N2_11+32*O2_11+44*CO2_11+18*H2O_11  &
                        +MMB*f_11+16*CH4_11+28*CO_11+2*H2_11)
EXCH11=EXCH11*(720*N2_11+3970*O2_11+19870*CO2_11+9500*H2O_11      &
                        +SCXRG*f_11+831650*CH4_11+275100*CO_11+236100*H2_11)/1000
EX11=EXPH11 + EXCH11
EXper11=100.*EX11/EX1

!---------------------------------- EQUILIBRIA -----------------------------------
P1=EXper2+EXper10-EXper4-EXper11
P2=EXper5+EXper9-EXper10-EXper6
MX=EXper1+EXper3-EXper5
RF=EXper6+XQABR-EXper7
FC=EXper4+EXper7-EXper8-nII
AB=EXper8-XQABR-XQABE-XQABV-EXper9

print*,'pos    T     mdot        en       en%           ex      ex%'
print*,'-------------------------------------------------------------'
print   '(a5,f6.1,f7.2,3x,f11.0,2x,f6.1,f15.6,f6.1)',   '  1        ',T1,mdot1,EN1,
ENper1,EX1, EXper1
print   '(a5,f6.1,f7.2,3x,f11.0,2x,f6.1,f15.6,f6.1)',   '  2        ',T2,mdot2,EN2,
ENper2,EX2, EXper2
print   '(a5,f6.1,f7.2,3x,f11.0,2x,f6.1,f15.6,f6.1)',   '  3        ',T3,mdot3,EN3,
ENper3,EX3, EXper3
print   '(a5,f6.1,f7.2,3x,f11.0,2x,f6.1,f15.6,f6.1)',   '  4        ',T4,mdot4,EN4,
ENper4,EX4, EXper4
print   '(a5,f6.1,f7.2,3x,f11.0,2x,f6.1,f15.6,f6.1)',   '  5        ',T5,mdot5,EN5,
ENper5,EX5, EXper5
print   '(a5,f6.1,f7.2,3x,f11.0,2x,f6.1,f15.6,f6.1)',   '  6        ',T6,mdot6,EN6,
ENper6,EX6, EXper6
print   '(a5,f6.1,f7.2,3x,f11.0,2x,f6.1,f15.6,f6.1)',   '  7        ',T7,mdot7,EN7,
ENper7,EX7, EXper7
```

```
print   '(a5,f6.1,f7.2,3x,f11.0,2x,f6.1,f15.6,f6.1)',   '   8         ',T8,mdot8,EN8,
ENper8,EX8, EXper8
print   '(a5,f6.1,f7.2,3x,f11.0,2x,f6.1,f15.6,f6.1)',   '   9         ',T9,mdot9,EN9,
ENper9,EX9, EXper9
print   '(a5,f6.1,f7.2,3x,f11.0,2x,f6.1,f15.6,f6.1)',   '   10      ',T10,mdot10,EN10,
ENper10,EX10, EXper10
print   '(a5,f6.1,f7.2,3x,f11.0,2x,f6.1,f15.6,f6.1)',   '   11      ',T11,mdot11,EN11,
ENper11,EX11, EXper11
print*,' '
print '(a11,2f6.1)', ' Qab->ref ',100.*QABR/EN1,XQABR
print '(a11,2f6.1)', ' Qab->vap ',100.*QABV/EN1,XQABV
print '(a11,2f6.1)', ' Qab->env ',100.*QABE/EN1,XQABE
print*,' '
print '(3(a19,f3.1))', ' Preheater1 : ',P1,'    Preheater2 : ',P2,' Mixer : ',MX
print '(3(a19,f3.1))', ' Reformer  : ',RF,'    Fuel Cell  : ',FC,'Afterburner: ',AB
print*,' '
print '(2(a7,f6.1))', ' nI : ',nI,' nII : ',nII


END PROGRAM generalXRG
```